# INFN - LNGS

## Laboratori Nazionali del Gran Sasso

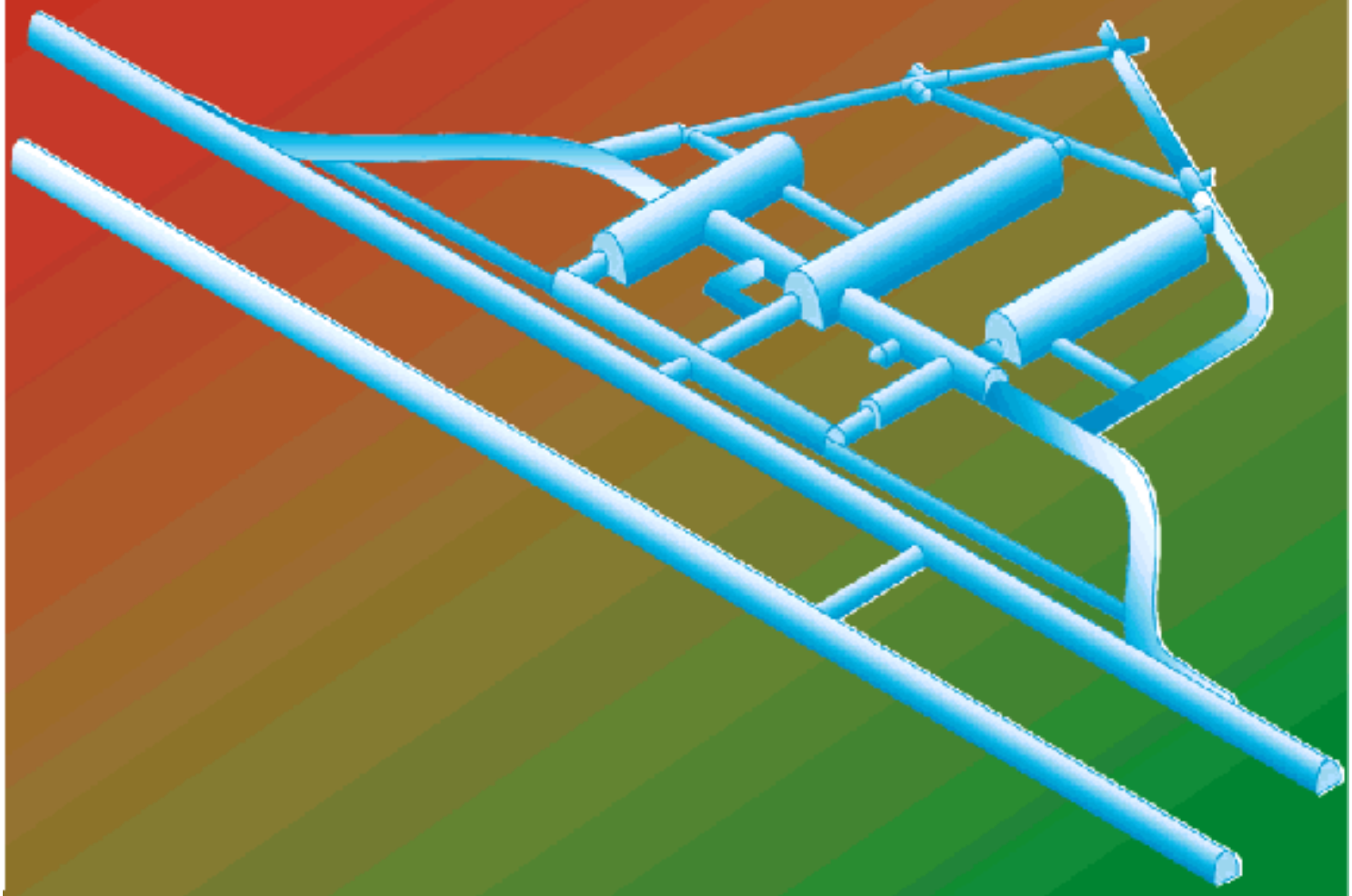

# Annual Report 1999

# The Gran Sasso National Laboratory

The Gran Sasso National Laboratory (LNGS) is one of four INFN National Laboratories. It is the largest underground laboratory in the world for experiments in particle and nuclear astrophysics and it is used as a world-wide facility by scientists (presently 450 in number) from 18 countries and 84 institutions.
Its location is close to the town of L'Aquila, about 120 km from Rome. The underground facilities are near the ten kilometre long freeway tunnel crossing the Gran Sasso mountain. They consist of three large experimental halls, each about 100 m long, 20 m wide and 20 m high and service tunnels for a total volume of about 180,000 cubic metres. The average 1400 m rock coverage (corresponding to 4,000 m.w.e.) gives a reduction factor of one million in the cosmic ray flux; moreover the neutron flux is particularly low due to the small content of Uranium and Thorium in the dolomite rocks of the mountain.
The mission of the Laboratory is to host experiments that require a low background environment in the field of particle and nuclear astrophysics. Their purpose are the following:
- study of the basic constituents of matter and their interactions by non-accelerator and accelerator means;
- study of nuclear and particle properties and processes of astrophysical interest in the Universe;
- study of the sources, acceleration mechanism and propagation of high energy particles in the Universe.
The Laboratory hosts experiments in other disciplines too, mainly geology and biology, that can profit from its characteristics and its infrastructures.
Main research topics of the present program are: solar neutrino physics, neutrino oscillations with solar neutrinos, neutrino oscillations with atmospheric neutrinos, neutrino oscillations with a beam from CERN, search for neutrinos from stellar collapses, double beta decays (search for Majorana electron-neutrino mass), dark matter search, small cross section nuclear reactions of astrophysical interest, high energy cosmic rays, search for exotics (monopoles, wimps, etc.).
A complementary facility at Campo Imperatore, 2,000 m a.s.l., hosts an extensive air shower experiment (EAS-TOP) aimed toward the study of the cosmic radiation especially around the "knee" of the energy spectrum both in its own and in coincidence with two large underground detectors, LVD and MACRO.
Solar neutrino physics is one of the main research sectors of the laboratory. The GALLEX experiment, completed in 1997, has already given fundamental results in particle physics and astrophysics, proving that thermonuclear fusion is the mechanism producing the energy in the Sun and showing a relevant deficit in the solar neutrino flux at low energy. It is extremely difficult now, after the GALLEX results, to avoid the conclusion that neutrinos

oscillate, and as a consequence have non-zero masses. If confirmed, this will be the first evidence of physics beyond the standard theory.
GNO uses the Gallex technique and mainly its apparatus to continue the research of Gallex for a long period, gradually improving the resolution. During 1999 GNO ran smoothly, performing extractions for 13 solar runs and one blank run. The publication of the first series of runs is expected for summer 2000.
The results of GALLEX and of the other solar neutrino experiments in the world (Homestake, Kamiokande and Superkamiokande) indicate that the flux of electron-neutrinos from the Be chain might be particularly different from the predictions of the theory and, as a consequence, is particularly sensitive to new physics. Borexino is dedicated mainly to the measurement of the Be line component of the solar neutrino spectrum. In 1999 the large stainless steel sphere that separates the internal and external parts of the detector and that will host the photomultipliers has been assembled and tested, the four storage containers for the inner part scintillator have been built and the production of the sealed photomultipliers units has began. A large fraction of the resources of the laboratory has been dedicated to the construction of this experiment during 1999.
The present solar models are based on data and extrapolations; in particular, the thermonuclear cross sections of the involved reactions are not measured in the relevant energy range but are rather extrapolated from higher energies.
The direct measurements are made very difficult by the very low values of the cross sections; LUNA is continuing its experimental program to cover this field in the low activity environment of the laboratory. The cross section of the reaction D + $^3$He $\rightarrow$ p + $^4$He, relevant for solar physics, has been measured at 4.5 and 15 keV using a 50 kV accelerator. LUNA will complete its physics program in 2000. Its successor, LUNA2, has proceeded in the construction phase: the new 400 kV accelerator has been designed and ordered and work has proceeded on the new BGO detector, on the data acquisition system and the windowless target system.
If electron-neutrinos are massive, part (or all) of their mass might be of the Majorana type; in this case, some well defined nuclides would decay through the neutrinoless double beta channel. The Laboratory hosts experiments searching for these very rare decays, employing different and complementary techniques.
The Heidelberg-Moscow experiment with a sensitive mass of 11 kg of enriched $^{76}$Ge is the most sensitive experiment in the world; the Mibeta experiment has produced an array of 20 thermal detectors, based on $TeO_2$ crystals (340 g natural tellurium each). Both experiments ran continuously and regularly during 1999, improving their sensitivity. They give presently the best and the second best upper limit on the electron-neutrino mass (if Majorana) in the world.
A third experiment, DBA, is searching for two-neutrino and neutrino-less double beta decay in $^{100}$Mo employing a liquid Argon proportional chamber. During 1999 a 1355 h long run was performed. Amongst the physics results is the measurement of the two-neutrino double beta decay half life of $^{100}$Mo.
From astronomical observations, we know that our Galaxy contains matter, globally ten times more than normal matter, that does not emit light. It is called dark matter, for this reason, but its nature is unknown. Very probably, not yet discovered elementary particles constitute a large, or even the dominant, fraction of dark matter. These particle

should be massive, with masses of the order of several tens to hundreds of the proton mass, and should interact only weakly with ordinary matter; otherwise they would have already been observed. They are collectively called WIMPs (Weakly Interacting Massive Particles). The search for WIMPs is very difficult and requires a very low background environment (one must work deep underground) and the development of advanced background reduction techniques. The search is going on in many experiments world wide. At Gran Sasso three experiments, using different techniques, are active.
DAMA employs NaI crystals to detect the WIMPs by means of the flash of light produced in the detector by an Iodine nucleus recoiling after having been hit by a WIMP, a very rare phenomenon. To distinguish these events from the background, DAMA searches for an annual modulation of the rate, a behaviour that has several aspects that are peculiar of the searched for effect and not of the main backgrounds. With its about 100 kg sensitive mass DAMA is the most sensitive experiment world-wide. During 1999 DAMA ran continuously. Data corresponding to a two-year continuous run have been published in January 2000. They show evidence of the annual modulation signal, with all the expected characteristics at four standard deviation significance. To further proceed, DAMA is working on an improved detector that, in particular, will have a 250 kg sensitive mass.
CRESST searches for WIMPs with a cryogenic technique, looking for a very tiny temperature increase in the detector due to the energy deposited by nuclei hit by the WIMPs. To this aim, the detector is kept at a very low temperature, 15 mK. During 1999 the experiment continued the still necessary R&D. It is expected to start and complete the physics runs in the year 2000.
HDMS uses Ge crystals to search for WIMPs, a crystal where the WIMP interaction takes place, fully surrounded by a second crystal that acts as an active screen from the background. A prototype detector was installed in March 1998 and successfully took data for 15 months, until July 1999.
MACRO is a very large, multi-purpose experiment that has continuously collected data for several years. It has steadily improved the limits on the monopole flux, well below the Parker bound and it is producing many interesting results on cosmic ray physics. Particularly relevant are the muons originated by muon-neutrino interactions from below, in other words, from neutrinos produced in the atmosphere that have crossed a large fraction of the earth and have interacted in the rock under the detector or in the detector itself. Evidence for muon-neutrino oscillations has been reported, confirming the results of the SuperKamiokande experiment in Japan. Further analyses, with increasing statistics and systematic accuracy, have been performed in 1999.
LVD has continued towards the completion of the apparatus having now 90% of the final configuration in operation; the experiment would collect a few hundred events from a supernova explosion in the centre of the Galaxy. Interesting data on the penetrating component of the cosmic rays are continuously collected.
ICARUS is a general purpose detector. It was proposed in 1985 based on the novel concept of the liquid Argon time-projection chamber. A first important step was the construction of a 3 t prototype that was used for the necessary R&D program, completed in 1993. The following years have been spent to develop the techniques suitable for industrial production of large scale detectors. A first 600 t module, proposed in 1995 and approved and funded in 1996, is presently being constructed in Pavia, to be later transferred to

Gran Sasso during 2001, according to the latest schedule. A ten cubic metre prototype, industrially built with the same techniques of the 600 t unit, has been transferred to Gran Sasso in an experimental hall on the surface and is being fully instrumented to perform a series of tests.
Experiments in geology.
GIGS is a laser interferometer for geophysical studies operating since 1994. The main results obtained so far are: 1) the recording of coseismic steps during local earthquakes in 1994, 2) the recording of swarms of slow earthquakes, more than 180 in total, after 1997. A new scale law between the seismic moment and the rise time of the slow quakes has been established. A very interesting statistical, not causal, correlation between slow and normal quake sequences has been observed. During 1999 the group further analysed the 1997 data. Till October 1999 the spectrometer worked in an equal arm configuration. In 1999 a new interferometer was built and from October 1999 two independent interferometers are at work.
A dedicated instrumental set-up continued during 1999 its systematic monitoring of the deformation phenomena in the rocks.
Experiments in biology.
The PULEX-2 is a biology experiment that exploits the unique low radiation characteristics of the Laboratory. Mammalian cells where cultured in parallel at LNGS underground laboratory, where a cell culture facility has been set up for this purpose, and at the ISS in Rome in the presence of standard background, both for up to about 360 generations; checks for the onset of metabolic changes and for sensitivity to genotoxic damage caused by different agents were periodically performed. A few first generation experiments at the Gran Sasso Laboratory are approaching their closure and we are defining now the scientific program for the next period on the basis of several experimental proposals in various stages of preparation.
Experiments in underground laboratories, mainly GALLEX and Superkamiokande have, for the first time, shown evidence for physics beyond the Standard Theory. In particular neutrinos seem to have non-zero masses and lepton numbers seem not to be conserved. Gran Sasso Laboratory has a great opportunity to give further revolutionary contributions to the knowledge of the basic forces of nature. In particular, the problem of neutrino masses will be tackled. We must definitively confirm the oscillation phenomenon, we must establish the states amongst which oscillations take place and we must measure the masses and the mixing parameters. The following approaches will be taken:
1) Experiments on a neutrino beam produced at CERN and aimed to detectors at Gran Sasso. A major step forward came in December 1999 when the CERN Council approved the CNGS (Cern Neutrinos to Gran Sasso), the program to build the beam, which will be ready in 2005. In parallel, two proposals for appearance experiments, ICANOE and OPERA, have been submitted. During 1999 both collaborations made important steps forward in the R&D and in the simulation studies necessary to finally focus the experimental proposals.
2) Next generation atmospheric neutrinos experiments. A specific proposal, MONOLITH, was submitted to the Laboratory; during 1999 a series of tests and simulation studies were performed.
3) Solar neutrino spectroscopy experiments. LENS is a proposal for a real time, flavour

sensitive experiment sensitive down to the fusion neutrinos, aiming to a final clarification of the solar neutrino problem and to the measurement of the oscillation parameters. The first R&D studies have been performed.
4) Next generation searches for Majorana neutrino mass. Several proposals, in various stages of elaboration, have been submitted. One of them, Cuoricino, based on a technique similar to MIBETA, has been approved.
All the services and the personnel of the lab have contributed to the planning of the next phases of activity ranging from the decommissioning of some large experiments (EAS-TOP will be decommissioned in 2000, MACRO in 2001), to the preparation of the infrastructures needed for the next experiments and to the rigorous definition of the safety rules, procedures and infrastructures.

Gran Sasso, June 2000.

The Director of the Laboratory
Prof. Alessandro Bettini

# Contents

# BOREXINO. Solar Neutrino Physics

G. Alimonti[a], C. Arpesella[b], M. Balata[b], G. Bellini[a], J. Benziger[c], T. Beau[o], A. de Bellefon[o]
S. Bonetti[a], B. Caccianiga[a], L. Cadonati[d], F.P. Calaprice[d], G. Cecchet[e], M. Chen[d],
M. Deutsch[f], F. Elisei[g], A. Etenko[r], F. von Feilitzsch[h], R. Fernholz[d], R. Ford[b],
B. Freudiger[j], C. Galbiati[d], F. Gatti[i], S. Gazzana[b], M.G. Giammarchi[a], D. Giugni[a],
A. Golubchikov[a], A. Goretti[b], C. Hagner[h], T. Hagner[h], W. Hampel[j], J. Handt[j],
F.X. Hartmann[a], R. von Hentig[h], G. Heusser[j], M. Hult[n], A. Ianni,[d], H. de Kerret[o], J. Kiko[j],
T. Kirsten[j], G. Korschinek[h], D. Kryn[o], V. Lagomarsino[i], P. LaMarche[d], M. Laubenstein[b],
P. Lombardi[a], S. Magni[a], S. Malvezzi[a], J. Maneira[a], I. Manno[k], G. Manuzio[i],
F. Masetti[g], U. Mazzucato[g], E. Meroni[a], P. Musico[i], H. Neder[j], M. Neff[h], L. Oberauer[h],
M. Obolensky[o], M. Pallavicini[i], L. Perasso[a], A. Pocar[d], R.S. Raghavan[l], G. Ranucci[a]
W. Rau[j], A. Razeto[i], E. Resconi[i], C. Salvo[i], R. Scardaoni[a], S. Schönert[h], T. Shutt[d],
N. Skorokhvatov[r], O. Smirnov[m], A. Sonnenschein[d], S. Sukhotin[r], R. Tartaglia,[b], G. Testera[i],
B. Vogelaar[p], S. Vitale[i], D. Vignaud[o], O. Zaimidoroga[m] Y. Zakharov[j], M. Wojcik[q]

[a]Dip. di Fisica dell'Università and Infn Milano - Italy
[b]Laboratori Nazionali del Gran Sasso, Assergi (Aq) - Italy
[c]Dep.t of Chemical Engineering, Princeton University - NJ USA
[d]Dep.t of Physics, Princeton University - NJ USA
[e]Dip. di Fisica dell'Università and Infn Pavia - Italy
[f]Dep.t of Physics, Massachusetts Institute of Technology - MA USA
[g]Dip. di Chimica dell'Università and Infn Perugia - Italy
[h]Technische Universität München - Germany
[i]Dip. di Fisica dell'Università and Infn Genova - Italy
[j]Max Planck Inst. für Kernphysik, Heidelberg - Germany
[k]KFKI-RMKI Research Institute for Particle & Nuclear Physics, Budapest - Hungary
[l]Bell Laboratories, Lucent Technologies, Murray Hill - NJ USA
[m]J.I.N.R. Dubna - Russia
[n]I.R.M.M. European Joint Research Center, Geel - Belgium
[o]Collège de France, Paris - France
[p]Virginia Polytechnic Institute, Blacksburg VA - USA
[q]Institute of Physics, Jagellonian University, Cracow - Poland
[r]Kurchatov Institute, Moscow - Russia

**Abstract**

This report describes the status of the BOREXINO experiment at Laboratori Nazionali del Gran Sasso. An overview of the BOREXINO Counting Test Facility is also given [1] .

# 1 BOREXINO

BOREXINO is a low background real time experiment for low energy (sub-MeV) solar neutrino physics. The main experimental goal is the detection of the 0.862 MeV $^7$Be solar neutrino component through the $\nu e^- \rightarrow \nu e^-$ electroweak scattering reaction. The maximum energy of the recoiling electron is 664 keV and the experimental design threshold will be of 250 keV, so that a solar $^7$Be flux at the Standard Solar Model level will generate 43 events/day.

BOREXINO is an unsegmented liquid detector featuring 300 tonnes of well shielded ultrapure scintillator viewed by 2200 photomultipliers (fig. 1). The detector core is a transparent spherical vessel (Nylon Sphere, 100 $\mu$m thick), 8.5 $m$ of diameter, filled with 300 tonnes of liquid scintillator and surrounded by 1000 tonnes of a high-purity buffer liquid. The scintillator mixture is PC and PPO (1.5 $g/l$) as a fluor, while the buffer liquid will be PC alone (with the addition of a light quencher, DMP). The photomultipliers are supported by a Stainless Steel Sphere (SSS) which also separates the inner part of the detector from the external shielding, provided by 2400 tonnes of pure water (water buffer). An additional containment vessel (Nylon film Radon barrier) is interposed between the Scintillator Nylon Sphere and the photomultipliers, to the goal of reducing Radon diffusion towards the internal part of the detector.

The outer water shield is instrumented with 200 outward-pointing photomultipliers serving as a veto for penetrating muons, the only significant remaining cosmic ray background at the Gran Sasso depth (about 3500 meters of water equivalent). In addition the 2200 photomultipliers viewing the internal part of the detector are divided in two sets: 1800 photomultipliers are equipped with light cones so that they see light only from the Nylon Sphere region, while the remaining 400 PMT's are sensitive to light originated in the whole volume of the Stainless Steel Sphere. This design greatly increases the capability of the system to identify muons crossing the PC buffer (and not the scintillator).

The BOREXINO design is based on the concept of a *graded shield* of progressively lower intrinsic radioactivity as one approaches the sensitive volume of the detector; this culminates in the use of 200 tonnes of the low background scintillator to shield the 100 tonnes innermost Fiducial Volume. In these conditions, the ultimate background will be dominated by the intrinsic contamination of the scintillator, while all backgrounds from the construction materials and external shieldings are negligible.

In addition to the purity of the construction materials and the rejection efficiency of the muon system, the detection of the $^7$Be solar signal in the 100 tonnes of the BOREXINO Fiducial Volume requires that the intrinsic radiopurity of the target scintillator be below $\sim 5 \times 10^{-16}$ $g/g$ of U,Th equivalent.

[1]Corresponding Author: Marco G. Giammarchi (giammarchi@mi.infn.it).

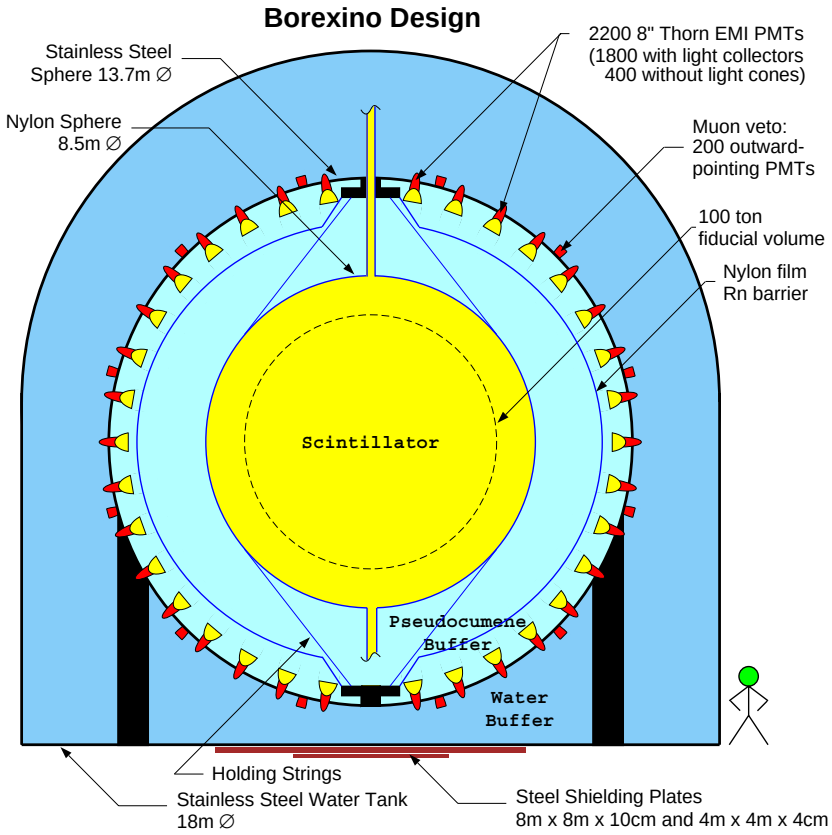


Figure 1: *Schematics of the BOREXINO detector. See text.*

BOREXINO also features several external systems and apparatuses conceived to purify the experimental fluids (water, nitrogen and scintillator) and to keep clean conditions during the installation of the detector (clean rooms).

During the year 1999, the BOREXINO Collaboration has proceeded with the construction and installation of the main apparatus and correlated facilities. The External Water Tank and the Stainless Steel Sphere have been completed and tested (Hydrostatic test). In the same period, the two structures called Big Building West (BBW) and Big Building East (BBE) have been completed, too. In the BBW the following facilities will be installed: - the BOREXINO Counting Room; - the devices needed for the radon measurements in the fluids (water, gases); - the CTF Counting Room; this electronic facility has been completed installed and is currently operating. In the BBE the facility called MOD-0 has also been installed: it consists of a part of the Fluid Handling System and of a scintillator filtering device which uses a purification column made of Silicagel. In the same period the storage area has been completed; it consists of 4 storage vessels (113 $m^3$ each), in electro-polished stainless steel (AISI 304L), confined in a concrete basin. The CTF has been started up again (CTF-2 Phase), with some minor change to the detector device and fully integrated electronic system and Fluid Handling System.

The BOREXINO detector is currently under construction in the LNGS Hall C. The

beginning of the data taking is scheduled for the year 2002.

# 2 The BOREXINO Counting Test Facility

The Counting Test Facility is a (smaller scale) BOREXINO-like device. It features 4.3 tonnes of liquid scintillator shieldied by 1000 tonnes of high purity water and viewed by 100 photomultipliers located on a support steel structure (see fig. 2). The scintillator is contained in a 0.5 *mm* thick nylon balloon. The detector is also equipped with a muon-tagging system.

The first phase of the CTF data taking (called CTF1) took place from 1994 to 1997. It was mainly devoted to the study of the radiopurity needed to operate at the experimental threshold of 250 keV, required for the detection of the $^{7}$Be solar neutrinos . The CTF1 summary results in terms of Uranium, Thorium and Carbon-14 radioactive contamination of the scintillator were [1],[2],[3]:

- Uranium chain contamination (more appropriately $^{226}$Ra) has been measured to be at most $3.5 \pm 1.3 \times 10^{-16}$ $g/g$.
- Thorium contamination was found to be $4.4^{+1.5}_{-1.2} \times 10^{-16}$ $g/g$.
- Carbon-14 contamination was measured to be $1.94 \pm 0.09 \times 10^{-18}$ ($^{14}$C/$^{12}$C).

These results indicated that the radiopurity goals for BOREXINO can be reached in a large-scale scintillation detector.

The Counting Test Facility is being upgraded to begin a second phase, called CTF2. In the CTF2 a new PMT assembly is used and a Radon-blocking nylon barrier (not shown in fig. 2) will be installed between the PMT system and the scintillator containment vessel. In addition, an entirely new muon-tagging system has been installed. The CTF2 is scheduled to be restarted in 2000 with the main goal of quality-testing the scintillator during the BOREXINO filling.

More information can be obtained through the references, or on the Borexino website http://almime.mi.infn.it and links therein.

# 3 List of 1999 publications and presentations

- G. Alimonti et al. (BOREXINO Collaboration). Light propagation in a large volume liquid scintillator. In publication on *Nuclear Instruments and Methods*.
- G. Heusser et al. $^{222}$Rn detection at the $\mu Bq/m^3$ range in Nitrogen gas and a new Rn purification technique for Liquid Nitrogen. In publication on *Appl. Rad. Isot.* and presented at the *Conference on Radionuclide Metrology and its Applications, Prague, June 1999.*

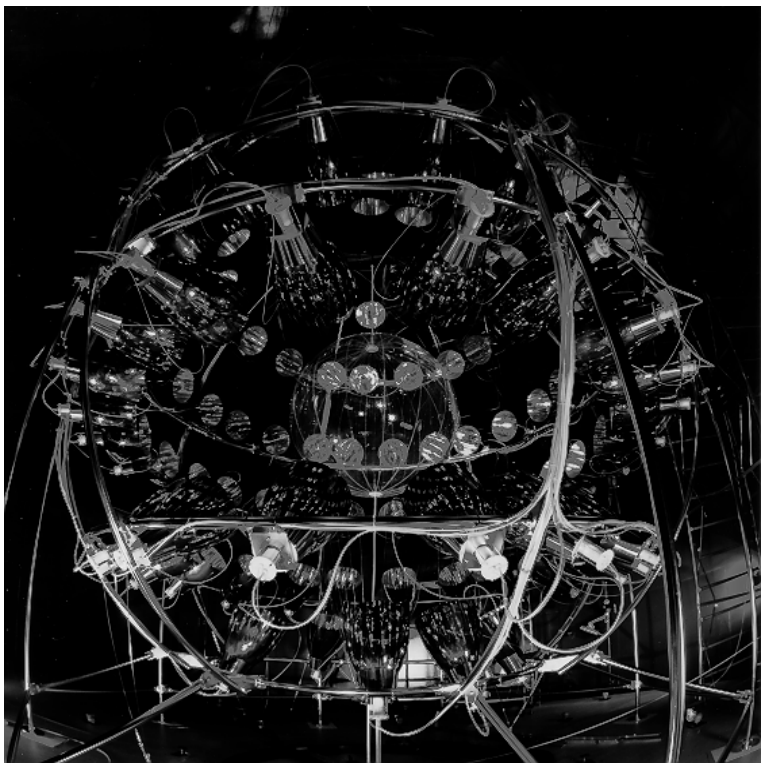

Figure 2: *The Counting Test Facility experimental setup viewed from inside the water tank. The scintillator is contained in the (1.05 m radius) nylon balloon at the center.*

- F. Elisei. The choice of a scintillator mixture for the Solar Neutrino detector of BOREXINO experiment. *American Chemical Society National Meeting, Anheim, CA USA, March 1999.*
- B. Caccianiga. Future Solar Neutrino Projects: BOREXINO. *WIN 99 International Conference, Capetown, January 1999.*
- A. Ianni. Status of the BOREXINO experiment. *Panic 99 International Conference, Uppsala, June 1999.*
- J.C. Maneira. BOREXINO: a new Calorimeter for Low Energy Solar Neutrinos. *CALOR99 International Conference, Lisbon, June 1999.*
- F.P. Calaprice. The BOREXINO experiment - A status report. *TAUP99 International Conference, Paris, September 1999.*
- F. Elisei. Optical properties of scintillator mixtures for the large-scale detector of Solar Neutrinos in the BOREXINO experiment. *Congresso Nazionale di Chimica-Fisica, Firenze, 1999.*

# References


[1] G. Alimonti et al. (BOREXINO Collaboration). A Large Scale Low Background Liquid Scintillation Detector: the Counting Test Facility at Gran Sasso, *Nuclear Instruments & Methods*, A406 (1998) 411.

[2] G. Alimonti et al. (BOREXINO Collaboration). Ultralow background measurements in a large volume underground detector, *Astroparticle Physics*, 8 (1998) 141.

[3] G. Alimonti et al. (BOREXINO Collaboration). Measurement of the $^{14}$C abundance in a low-background liquid scintillator, *Phys. Lett. B*, 422 (1998) 349.

# CRESST. Dark Matter Search

M. Bruckmayer[a], C. Bucci[d], S. Cooper[c], C. Cozzini[a],
P. Di Stefano[a], F. v. Feilitzsch[b], T. Frank[a], J. Jochum[b],
R. Keeling[c], H. Kraus[c], J. Macallister[c], J. Marchese[c],
F. Pröbst[a], Y. Ramachers[c], J. Schnagl[b], W. Seidel[a,*],
I. Sergeyev[a], L. Stodolsky[a], H. Wulandari[b]

[a] Max–Planck–Institut für Physik, Föhringer Ring 6, D-80805 Munich - Germany
[b] Technische Universität München, Physik Department, D-85747 Munich - Germany
[c] University of Oxford, NAPL, Keble Road, Oxford OX1 3RH - UK
[d] Laboratori Nazionali del Gran Sasso, 67010 Assergi (AQ) - Italy

**Abstract**

We report about the progress achieved in 1999 for the CRESST (Cryogenic Rare Event Search with Superconducting Thermometers) experiment to search for dark matter WIMPs (weakly interacting massive particles) using cryogenic detectors.

*spokesman

# 1 Introduction

The goal of the CRESST project is the direct detection of elementary particle dark matter and the elucidation of its nature. The search for dark matter and the understanding of its nature remains one of the central and most fascinating problems of our time in physics, astronomy and cosmology. There is strong evidence for it on all scales, ranging from dwarf galaxies through spiral galaxies like our own to large scale structures. The history of the universe is difficult to be consistently reconstructed without it, be it primordial nucleosynthesis [1] or the formation of structure [2].

The importance of the search for dark matter in the form of elementary particles, created in the early stages of the universe, is underlined by the recent weakening of the case for other forms such as MACHOs, faint stars and black holes [3]. Particle Physics provides some independently motivated candidates for dark matter; the favourite one, called the neutralino, originates from the assumption that the lightest supersymmetric particle should be stable. Apart from solving numerous particle physics problems, supersymmetry would provide an excellent dark matter WIMP candidate with the neutralino fulfilling all known particle physics and cosmological constraints for a large set of solutions. These solutions originate from the many parameters of supersymmetric models and additional simplifying assumptions which can be relaxed yielding candidates in a wide mass range, i.e. from some GeV up to TeV for neutralinos [4]. The experimental approach to detect these WIMPs would be by elastic scattering on nuclei and the resulting energy deposition. All direct detection schemes have focused on this possibility.

Conventional methods for direct detection rely on the ionization or scintillation caused by the recoiling nucleus. This leads to certain limitations connected with the relatively high energy needed for ionization and the sharply decreasing efficiency of ionization by slow nuclei. Cryogenic detectors use much lower energy excitations, such as phonons, and while conventional methods are probably close to their limits, cryogenic technology can still make great improvements. Since the principal physical effect of a WIMP nuclear recoil is the generation of phonons, cryogenic calorimeters are well suited for WIMP detection and, indeed, the first proposal to search for dark matter particles were inspired by early work on cryogenic detectors [5]. Furthermore, when this technology is combined with charge or light collection the resulting background suppression leads to a powerful technique to search for rare nuclear recoils due to WIMP scattering.

# 2 CRESST Detectors

The detector developed by the CRESST collaboration consists of a dielectric crystal in which the particle interaction takes place, and a small superconducting film evaporated onto the surface, serving as a thermometer. The device is operated within the superconducting–to–normal transition of the thermometer, where a small temperature rise $\triangle$T of the thermometer leads to a relatively large rise $\triangle$R of its resistance. The $\triangle$T induced by a particle is usually much smaller than the width of the transition which yields an approximately linear relation between $\triangle$T and $\triangle$R. The resistance of the film (0.1 $\Omega$) is measured by passing a constant current through a circuit in which the strip is

in parallel with a small (0.05 Ω) resistor and the pickup coil of a SQUID. A rise in the film resistance is then measured via the current rise through the SQUID input coil.

To a good approximation, the high frequency phonons created by an event do not thermalize in the crystal before being directly absorbed in the superconducting film [6]. Thus the energy resolution is only moderately dependent on the size of the crystal and scaling up to large detectors is feasible. The detectors presently employed in Gran Sasso use tungsten films and 262 g sapphire ($Al_2O_3$) absorbers, running near 15 mK and during the year 1999 we further developed detectors based on a scintillating crystal ($CaWO_4$) of about 300 g for simultaneous phonon–light detection for background suppression [7].

The 262 g sapphire detectors were developed by scaling up a 32 g sapphire detector [8]. Due to optimised design, and because of the non-thermalization of the phonons, this scaling could be achieved without loss of sensitivity. Present CRESST detectors have the best energy resolution per unit mass of any cryogenic device presently in use. Fig. 1 shows the spectrum of an X-ray fluorescence source measured with a 262 g CRESST sapphire detector with an energy resolution of 133 eV at 1.5 keV.

Fig. 2 shows a 262 g sapphire detector mounted in its low background copper housing. The 4×4×4.1 $cm^3$ crystal rests thermally insulated on sapphire balls. Some of the balls are loaded with plastic springs. Thermal contact between the holder and the detector is provided by 20 $\mu$m Au wires bonded between a Au pad in the middle of the W thermometer and the Cu holder. The electrical connection is established by superconducting Al wires bonded from Al pads on both ends of the thermometer to isolated contact pads on the holder. To avoid radioactive solder joints the superconducting wires connecting the thermometer to the readout circuit are screwed to the contact pads. Narrow Au films extend on both sides from the central Au pad of the thermometer and serve to inject electrical heater pulses for monitoring the long term stability of the energy calibration without a source installed inside the cryostat.

# 3 CRESST Installation and Status at Gran Sasso

The central part of the CRESST low background facility at the LNGS is the cryostat. The design of this cryostat had to combine the requirements of low temperatures with those of low background. Since a standard dilution refrigerator is made of various materials which are by far too radioactive, we have separated the dilution refrigerator from the detectors, as shown in Fig. 3. The experimental volume, the cold box, can house up to 100 kg of target mass. The cold box is made of low background selected copper with high purity lead used for the vacuum seals. It is surrounded by shielding consisting of 14 cm of low background copper and 20 cm of lead. Special consideration was given to the space between the dilution refrigerator and the cold box. The separation was chosen large enough so that the neck of the external shielding, together with the internal shields, eliminates any direct line of sight from the outside world into the cold box. The low temperature of the dilution refrigerator is transferred to the cold box by a 1.5 m long cold finger protected by thermal radiation shields, all of low background copper. A 20 cm thick lead shield inside a copper can is placed between the mixing chamber and the cold finger with the low temperature transmitted here by the copper can. This internal

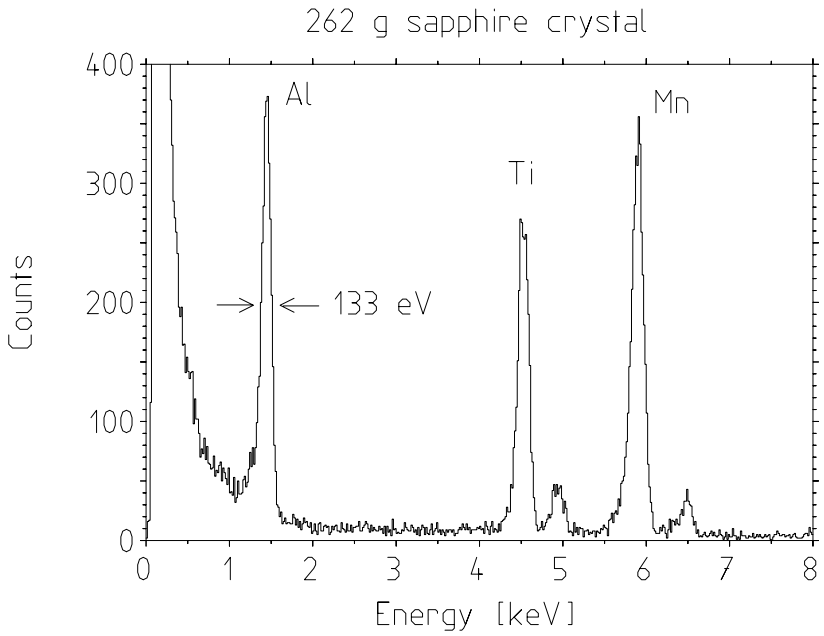


Figure 1: Pulse height spectrum of a 262 g detector with an X-ray fluorescence source installed inside the cold box to provide the X-ray lines of Al, Ti, and Mn. The large background towards lower energies, which was not present in earlier spectra, is attributed to damage later noticed to the thin Al sheet meant to absorb Auger electrons from the source.

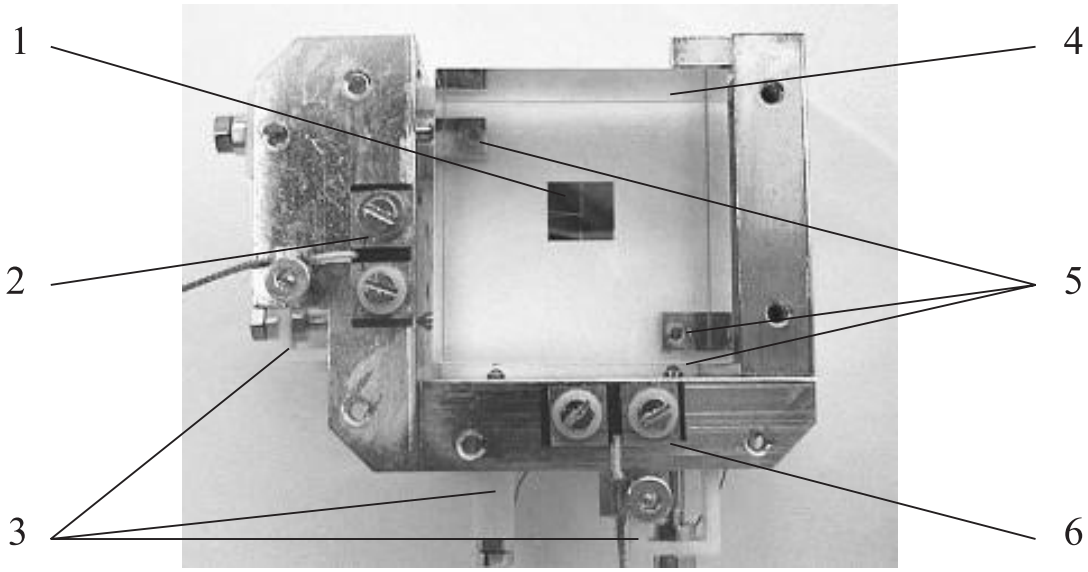


Figure 2: Picture of a 262 g sapphire detector. (1) Tungsten thermometer. (2) Holder pads with screw contacts for connecting to the heater circuit. (3) Plastic springs. (4) Sapphire crystal. (5) Sapphire balls. (6) Holder pads with screw contacts for connecting to the SQUID read-out circuit.

shield combined with another one surrounding the cold finger serves to block any line of sight for radiation coming from the dilution refrigerator into the experimental volume. All of our copper has been carefully stored in the cellar of a beer brewery near Munich in order to avoid cosmogenic activation. The total above–ground exposure of the copper was about 10 weeks.

It is not sufficient to use high-purity materials. Their surfaces must also be kept clean during use, and we have taken care to design our facilities in Gran Sasso to make this possible. The Faraday cage which surrounds the experiment was chosen large enough so that all work on the low-background components of the experiment can be performed inside the cage. The cage is divided into two levels. The lower level is equipped as a clean room with a measured clean room class of 100 to protect the low-background components. The external lead and copper shields are in two closely fitting halves, each supported on a "wagon" so that the shielding can be opened without handling the individual pieces. The entire shielding is enclosed in a gas-tight Radon box that is flushed with $N_2$ and maintained at a small overpressure. In its retracted position (shown in Fig. 4) the shielding is outside the dilution refrigerator support structure but still inside the clean room and sufficient room is then available to disassemble the cold box .

Entrance to the clean room is through a changing room external to the Faraday cage (not shown in Fig. 4). The upper level of the Faraday cage is outside the clean room and allows access to the top of the cryostat for servicing and to the electronics. To save on floor space in Gran Sasso, the counting room and a laminar flow work space for handling the detectors is placed on top of the Faraday cage. All of this equipment is inside a building in Hall B.

The installation was completed at the end of 1998, when the prototype cold box of normal copper was replaced by a radio-pure version of the same design. The purpose of the prototype cold box was to test the cryogenic functioning of the design and to provide a well shielded environment for completing the development of the 262 g detectors. After machining, the new low background cold box was cleaned by electro-polishing and subsequent rinsing with high purity water. The pieces were then brought to Gran Sasso in gas tight transport containers made of PE and flushed with nitrogen.

During 1999, a series of first measurements with four 262 g detectors under low background conditions was performed in the new cold box. The measured rate was of the order of a few 10 counts/ (kg keV day) above 30 keV and below 1 count/(kg keV day) above 100 keV. This is much larger than expected and most likely not caused by radioactivity. The detectors are mounted facing each other with no material in between. The complete absence of any events in true time coincidence between any pair of the detectors excludes surface contaminations of the crystal with $\beta$ emitters and contaminations with $\gamma$ emitters in the crystals and the surrounding. Also, $\beta$ emitters within the crystal are most likely excluded by the shape of the measured energy spectra. Moreover, the rate has a non-Poissonian character in time, which can not be caused by radioactivity.

Sources of vibrations inside the cryostat have been investigated and eliminated; for example a needle valve needed for a 1 K cooling stage has been replaced by a capillary. In addition, the detectors have been insulated from external vibrations by mounting them on a spring- suspended platform ( horizontal and vertical resonance frequencies of 1.5 Hz and 3 Hz). These steps have dramatically improved the immunity of the base line signal

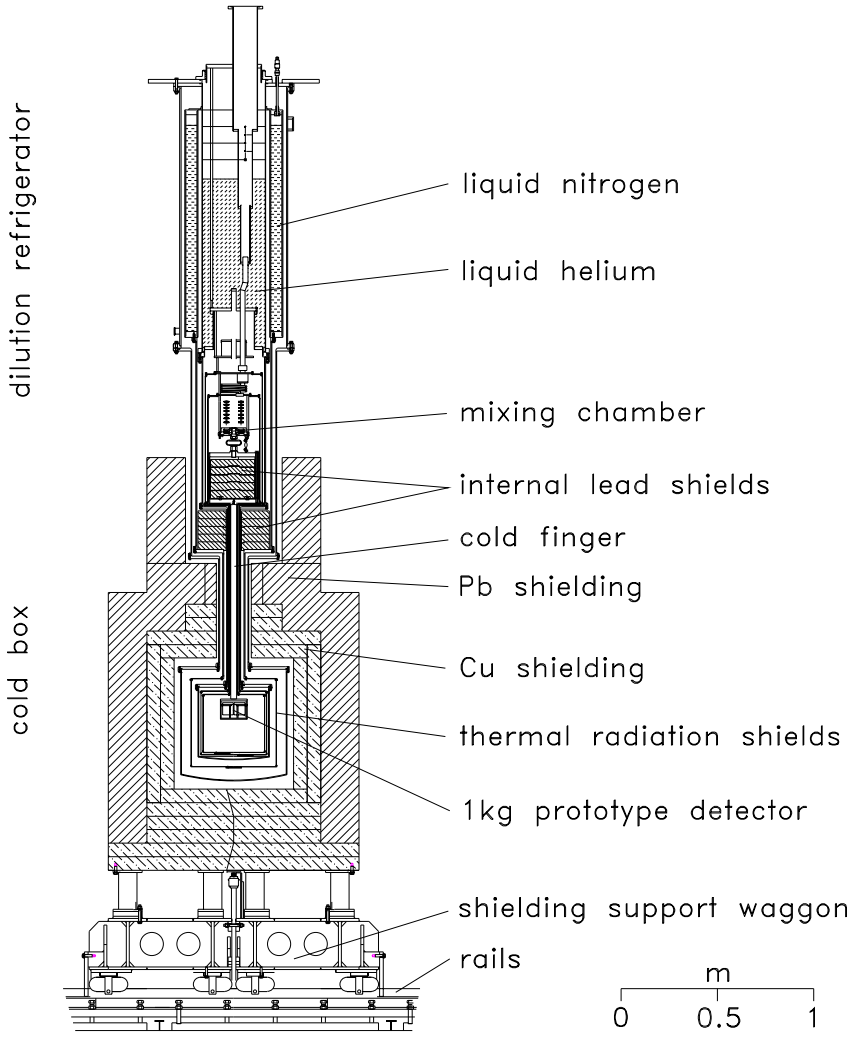


Figure 3: Layout of dilution refrigerator and cold box.

against vibrations, as was found in tests where external vibrations were applied to the cryostat. Nevertheless the rate remained the same. This excludes vibrations as the origin of the background.

We also investigated the possibility that electromagnetic interferences with a duration too short to be seen directly by the SQUID might heat the W-thermometer and cause thermal signals with a shape very similar to particle pulses. A modification of the readout circuit of one detector in order to suppress the heating effect of interference pulses made the system completely immune to any external electromagnetic interferences, such as those created for test purposes inside the Faraday cage. However, the background rate did not decrease and we can exclude electromagnetic interferences as the source of our background.

In the present run as a further diagnostic tool we have installed a 262 g sapphire detector carrying two W thermometers. We find that the signals from both thermometers are strictly coincident in time, with a constant ratio of the pulse heights, and again with the same shape as particle pulses. As in previous runs, the signals of different

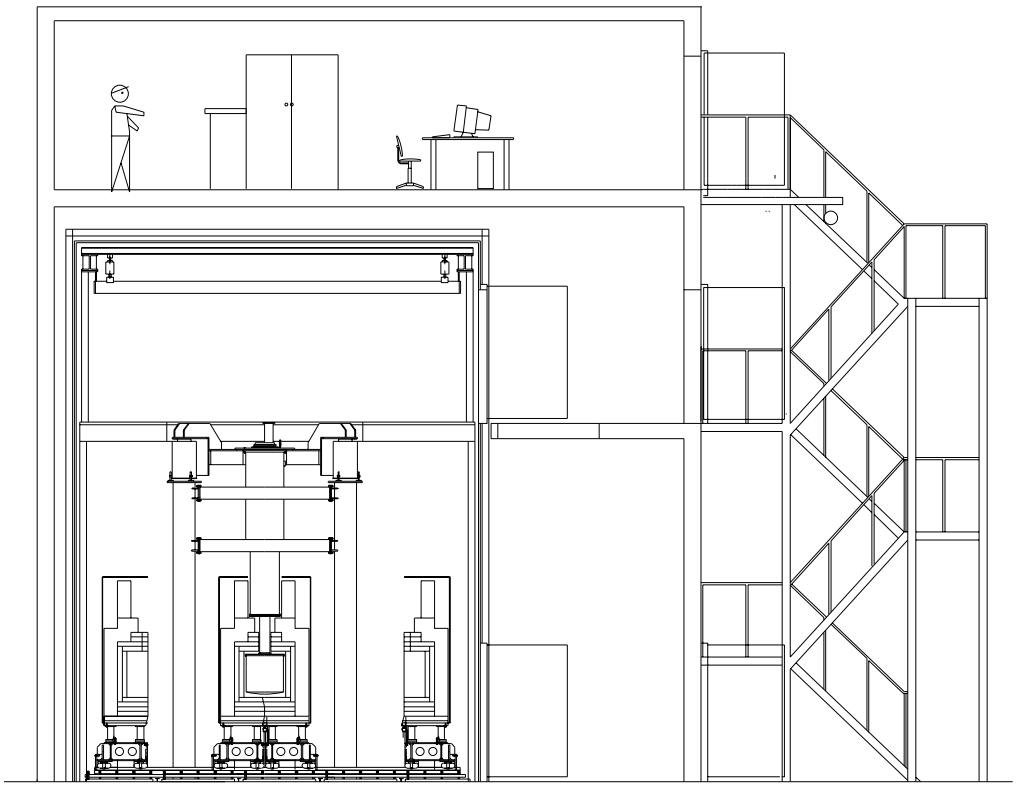

Figure 4: Cross section of CRESST building in Hall B.

detectors are not coincident. This clearly demonstrates that all signals originate from energy depositions which create high frequency phonons in the sapphire and confirms that the background is not due to electrical interferences. Our present hypothesis is that the energy depositions in the crystals are due to random structural relaxations in the supporting structure of the crystal. In the next run we will investigate this possibility. These various tests have allowed us to very much pin down the possible sources of the spurious signals. We are confident of solving the problem early in 2000 and then will continue with a physics run with the 262 g sapphire detectors.

# 4 List of Publications


1. M. Bravin et al., "The CRESST Dark Matter Search", Astropart. Phys. **12** (1999) 107

2. P. Meunier et al., "Discrimination between Nuclear Recoils and Electron Recoils by Simultaneous Detection of Phonons and Scintillation Light", Appl. Phys. Lett. **75** (1999) 1335

3. M. Bruckmayer et al., "Superconducting Phase Transition Thermometers for X-ray

Calorimeters", to be published in Nucl. Instr. Meth. (LTD-8 proceedings)

4. M. Sisti et al., "The CRESST Dark Matter Experiment: Status and Perspectives", to be published in Nucl. Instr. Meth. (LTD-8 proceedings)

5. M. Bravin et al., Simultaneous measurement of phonons and scintillation light for active background rejection in the CRESST experiment", to be published in Nucl. Instr. Meth. (LTD-8 proceedings)

# References


[1] J. Audouze, Nucl. Phys. News **8** (1998) No.2, 22

[2] S. Dodelson, E.I. Gates and M. Turner, Science **274** (1996) 69

[3] Proc. Workshop on Dark Matter in Astro- and Particle Physics, Heidelberg, 20-25 July 1998, Eds. H.V. Klapdor–Kleingrothaus, L. Baudis; Proc. Workshop on the Identification of Dark Matter, Buxton, England, 7-11 Sept. 1998, Ed. N. Spooner

[4] A. Gabutti et al., Astropart. Phys. 6 (1996) 1

[5] M. Goodman and E. Witten, Phys. Rev. D**23** (1985) 3059

[6] F. Pröbst et al., J. Low Temp. Phys. **100** (1995) 69

[7] M. Bravin et al., Astropart. Phys. **12** (1999) 107

[8] P. Colling et al., NIM **354** (1995) 408

# DAMA. Dark Matter Search

M.Amato[b,c], P. Belli[a], R. Bernabei[a], R. Cerulli[a], C.J. Dai[d], H. L. He[d], G. Ignesti[b,c], A. Incicchitti[b], H.H. Kuang[d], J.M. Ma[d] F. Montecchia[a] D. Prosperi[b]

*and*

*in the neutron measurements:* M.Angelone[e], P.Batistoni[e], M.Pillon[e]

*in $\beta\beta$ decay searches and CNC quests:* V.V. Kobychev[f], O.A. Ponkratenko[f], V.I. Tretyak[f], Yu.G. Zdesenko[f]

*in studies for possible future experiments by using low radioactive NaI(Tl):* I.R. Barabanov[g] and collaborators

*+ technical staff:* A. Bussolotti[a], A. Mattei[b]

[a]Dip. di Fisica, Università di Roma "Tor Vergata" and INFN, sez. Roma2, Italy; [b]Dip. di Fisica, Università di Roma "La Sapienza" and INFN, sez. Roma, Italy; [c]Laboratorio Nazionale del Gran Sasso, INFN, Assergi(Aq), Italy; [d]IHEP, Chinese Academy, P.O. Box 918/3, Beijing 100039, China; [e]ENEA - C. R. Frascati, P.O. Box 65, I-00044 Frascati, Italy; [f]Institute for Nuclear Research, 252650 Kiev, Ukraine; [g]Institute for Nuclear Research, Moscow, Russia.

**Abstract**

DAMA is searching for rare processes — mainly for Dark Matter particle elastic scattering on target nuclei — by developing and using several kinds of radiopure scintillators. The main set-ups are: i) the $\simeq$ 100 kg highly radiopure NaI(Tl) set-up (which, in particular, allows to effectively investigate the WIMP annual modulation signature); ii) the $\simeq$ 6.5 l liquid Xenon (LXe) scintillator; iii) the R&D installation for measurements with $CaF_2$(Eu) and NaI(Tl) radiopure prototypes and for small scale experiments. Moreover, sample measurements are realized with Ge detector deep underground and in Ispra, in the framework of devoted R&D for higher radiopure detectors. Several rare event searches have been performed during 1999; only the major results are summarized in the following.

# 1 Introduction

DAMA is devoted to rare events searches by developing and using low radioactive scintillators; its main aim is the search for relic particles embedded in the galactic halo. Many experimental observations suggest the existence of a large amount of non luminous Matter (Dark Matter) in our Universe. In fact, gravitational fields much stronger than those accounted only by the luminous matter are required to explain the observed motion of the astrophysical objects. A full description in terms of known physical laws requires that more than about 90% of the mass in the Universe should be dark. This conclusion is further supported by current cosmological models that point out the necessity of the existence of a large amount of relic particles - named WIMPs (Weakly Interacting Massive Particles) - from the early Universe. This scenario implies that our Galaxy should be completely embedded in a large WIMP halo; thus our solar system, which is moving with a velocity of about 232 km/s with respect to the galactic system, is continuously hit by a WIMP "wind". The quantitative study of this "wind" allows to obtain information on the Universe evolution and on Physics beyond the Standard Model, being the more credited candidate for WIMP the lightest neutral stable particle, the neutralino, expected by supersymmetric extension of the Standard Model. The DAMA esperiments are searching for these particles mainly by investigating their elastic scattering on target nuclei, which constitute scintillation detectors. The scintillators are a well known technology, allowing to reach reliable results. In the DAMA experiments both solid and liquid scintillators are used, in particular: NaI(Tl), liquid Xenon and $CaF_2$(Eu).

The success of this kind of search depends on the possibility to build large mass detectors with high intrinsic radiopurity in order to reduce at maximum the background contribution. Large mass detectors are needed both to search for candidates with extremely reduced rate (such as the neutralino) and to exploit the main peculiarity of the WIMP "wind": the so-called "annual modulation signature" to unambiguously select a signal from the background. In fact, since the Earth rotates around the Sun, it would be crossed by a larger WIMP flux in June (when its rotational velocity is summed to the one of the solar system with respect to the Galaxy) and by a smaller one in December (when the two velocities are subtracted). The fractional difference between the maximum and the minimum of the rate is of order of $\simeq 7\%$. The relevance of performing experiments with a proper clear signature results evident; it also allows to overcome the intrinsic uncertainties which exist in the comparison of exclusion plots at given C.L.in the WIMP cross-section on proton ($\sigma_p$) versus WIMP mass ($M_W$) plane achieved by different experiments, mainly when different techniques are used.

Furthermore, profiting by the high radiopurity achieved in the detectors and in the set-ups, several other searches for rare events have also been performed, such as for: i) $\beta\beta$ processes; ii) charge-non-conserving (CNC) processes; iii) Pauli exclusion principle (PEP) violating processes. Also in these cases competitive results have been achieved.

An R&D activity to develop higher radiopure detectors is continuously carried out toward the creation of ultimate radiopure detectors as well as studies on their possible new applications, such as e.g. in neutrino magnetic moment measurements and right boson search.

In the following we will summarize the main DAMA activity during 1999 and we will

give the corresponding references.

# 2 The $\simeq$ 100 kg highly radiopure NaI(Tl) set-up

## 2.1 Introduction

The main goal of the $\simeq$ 100 kg low-radioactive DAMA NaI(Tl) set-up is to search for WIMPs by the annual modulation signature [1, 2, 3] over several years.

Parts of the experimental set-up are the NaI(Tl) detectors, the Cu box containing the detectors, the shield and the glove-box for calibrations. The detectors are enclosed in a sealed low radioactive OFHC Cu box fluxed with HP $N_2$ long stored deep underground; the Cu box is maintained at small overpressure with respect to the environment, such as also the glove-box. All the used materials have been selected for low radioactivity by measuring with Ge detector deep underground in the Gran Sasso National Laboratory (LNGS), with AAS and MS in the Rome University "La Sapienza" and in Ispra; results on their residual radioactivity have been given in the devoted paper published on 1999. There also the detailed description of the whole set-up, of its main perfomances and operating procedures have been discussed.

The experiment is taking data from single photoelectron threshold to several MeV (being the optimization done for the lowest energy region: 2-20 keV); it is equipped also with additional triggers to achieve some "by-product" results.

Efforts are in progress to increase the experimental sensitivity by preparing several upgradings. In particular, we plan to fulfil in incoming years the present installation up to 250 kg thanks to the success of the new R&D for further radiopurification of the NaI(Tl).

## 2.2 Status of the search for the WIMP annual modulation signature

During 1999 the results achieved by investigating the DAMA/NaI-2 data set and those obtained by combining it with the DAMA/NaI-1 have been published. The results – obtained when standard assumptions are considered for the astrophysical, nuclear and particle physics parameters – are summarized in table 1. In this table and in the following the quantity $\xi$ represents the local neutralino matter density in units of 0.3 GeV cm$^{-3}$. These results have been obtained comparing by a maximum likelihood method the number of events in each *ijk* cell[1] with the expectation from the standard WIMP model[3]. For the sake of completeness we recall that independent analyses performed by using a $\chi^2$ strategy or the Feldman and Cousins approach[4] give substancially the same results.

As regards possible systematics they have been quantitatively investigated (see papers and proceedings); moreover, the only ones which could play a significant role are those able to fullfil contemporaneously all the requirements which should be satisfied by the data to credit the possible presence of a relic particle in a WIMP annual modulation search: 1) modulated rate according to cosine function; 2) only in a defined low energy

[1]The data are grouped in cells of 1 day ($i$) and 1 keV ($k$) for each detector ($j$).

Table 1: Summary of the DAMA results on the annual modulation signature as published up to 1999. Standard assumptions for astrophysical, nuclear and particle physics parameters have been considered there.

| running period | statistics (kg · d) | $M_W$ (GeV) | $\xi\sigma_p$ (pb) | C.L. m.l.ratio |
|---|---|---|---|---|
| DAMA/NaI-1 | 3363.8 winter + 1185.2 summer | $(59^{+36}_{-19})$ | $(1.0^{+0.1}_{-0.4})10^{-5}$ | 90% |
| DAMA/NaI-2 | 14962 from middle November to the subsequent end of July | $(59^{+22}_{-14})$ | $(7.0^{+0.4}_{-1.7})10^{-6}$ | 98.5% |
| DAMA/NaI-1+2 | 19511 | $(59^{+17}_{-14})$ | $(7.0^{+0.4}_{-1.2})10^{-6}$ | 99.6% |

range; 3) with proper period (1 year); 4) with proper phase (about 2 june); 5) for single "hit" events (when searching for Dark Matter particles by a multi-detector set-up – as the $\simeq$ 100 kg NaI(Tl) DAMA set-up – the quoted low energy rate is always referred to events where only one detector is firing, being negligible the probability that a WIMPs will interact in more than one of them); 6) with modulated amplitude in region of maximal sensitivity $\lesssim 7\%$.

During 1999 some of us – in collaboration with A. Bottino, F. Donato, N. Fornengo, S. Scopel – have carried out a detailed investigation on the effect of the uncertainties in the local ($v_0$) and escape velocities ($v_{esc}$) on the DAMA allowed region. The result is shown in fig. 1. It enlarges the allowed mass region: from 30 GeV to 130 GeV (1 $\sigma$ C.L.). This interval is further extended from 30 GeV to 180 GeV (1 $\sigma$ C.L.) when including possible dark halo rotation. It has been found that a number of supersymmetric configurations singled out by the DAMA/NaI results have cosmological properties compatible with a relic neutralino as a dominant component of cold dark matter. The potential discovery for the relevant supersymmetric configurations at accelerators of present generation has also been discussed.

During 1999 the DAMA collaboration has continued the data taking; moreover, the data of two further yearly cycles (up to roughly the second half of August 1999) have been analysed. The data realease has been the beginning of 2000 and, therefore, the achieved results are not described here.

The next plans for the experiments are the installation of a new electronics and DAQ to investigate further peculiarities of the effect and, as mentioned above, the increase of the exposed mass.

## 2.3 Search for the WIMP diurnal rate variation signature

The lowest energy rate measured during the DAMA/NaI-2 running period (already analysed in terms of annual modulation signature) has been investigated in terms of rate

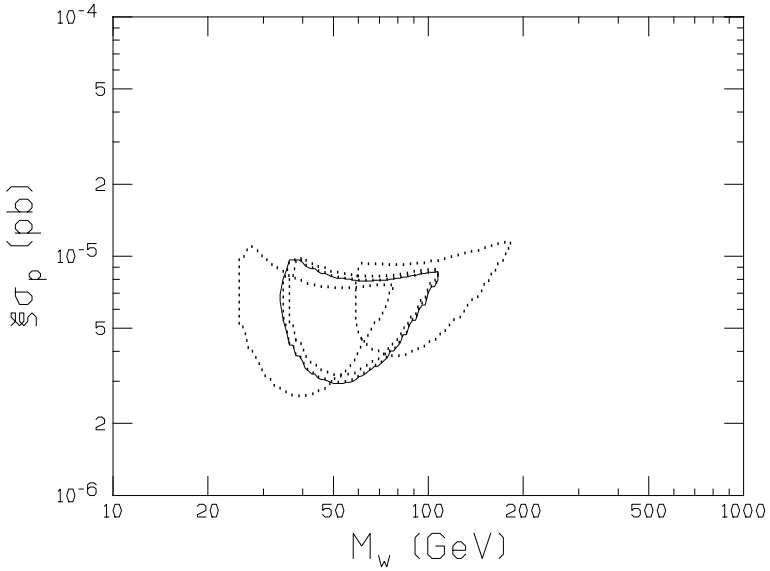


Figure 1: Effect of the uncertainties in the local ($v_0$) and escape velocities ($v_{esc}$) on the DAMA allowed region is shown; the solid contour represents the region at $2\sigma$ C.L. for a SI coupled candidate with $v_0 = 220$ km/s and $v_{esc} = 650$ km/s. The dotted ones are the obtained extensions when considering $v_0$ varying between 170 and 270 km/s and $v_{esc}$ varying between 450 and 650 km/s.

diurnal variation with respect to both the sidereal and the solar time. In the first case effects induced by spin - independent (SI) coupled WIMPs can be investigated to test the possible presence of a high cross section relic component with small halo fraction ($\lesssim 10^{-3}$), while in the second case the possible presence of unknown effects in the data can be verified.

A diurnal variation of the low energy rate with sidereal time in WIMP direct searches could be expected because of the Earth's daily rotation [5]. In fact, during the sidereal day the Earth shields a given detector with a variable thickness, eclipsing the wind of Dark Matter particles. The induced effect should be a daily variation of the WIMP velocity distribution, therefore of their flux and, of course, of the signal rate measured deep underground. However, this effect results very small and would be appreciable only in case of high cross section SI coupled candidates.

Let us now introduce the angle, $\theta$, defined by the Earth velocity in the galactic frame with the vector joining the center of the Earth to the position of the laboratory. Because of the Earth's rotational motion, it varies with the diurnal sidereal time between a minimum and a maximum which depend on the laboratory position on the Earth: the larger the allowed range of $\theta$ would be, the larger the effect would result[2].

The degrading of the WIMPs velocity due to their interactions with the nuclei of

[2]We note that the diurnal variation signature for WIMPs should satisfy the following peculiarities: sidereal daily variation of the rate (1) for single "hit" events (2) with minimum around 9:00 h sidereal time (3), with maximum around 21:00 h sidereal time (4), only in the lowest energy region (5). Unfortunately, as already mentioned, this signature results effective only in case of high cross section candidates.

the Earth and of the over standing mountain has been evaluated by MonteCarlo code. Standard assumptions have been considered for the WIMP model. In particular, the behaviour of the signal rate as a function of $\theta$ – in the cumulative 2-6 keV energy interval – has been evaluated by the MonteCarlo code for various $M_W$ varying $\sigma_p$; it has been found that it can be successfully fitted by the empirical parabolic formula:

$$S_0 - B\,(\theta^2 - <\theta^2>) + C\,(\theta - <\theta>)$$

where: i) $<\theta^2> = 1.1427$ rad$^2$ and $<\theta> = 0.9651$ rad in our case; ii) $S_0$ is the unmodulated part of the signal rate; iii) B and C are parameters which quantitatively describe the presence of diurnal variation in the counting rate. It should be noted that the ratios $(\frac{S_0}{\xi\sigma_p})$, $(\frac{B}{\xi\sigma_p})$ and $(\frac{C}{\xi\sigma_p})$ do not depend on $\theta$ and $\xi$, but vary as a function of $\sigma_p$ and $M_W$. The behaviours of these ratios can be calculated by fitting according to the formula given above the expected signal rate for each given $M_W$ when varying $\sigma_p$.

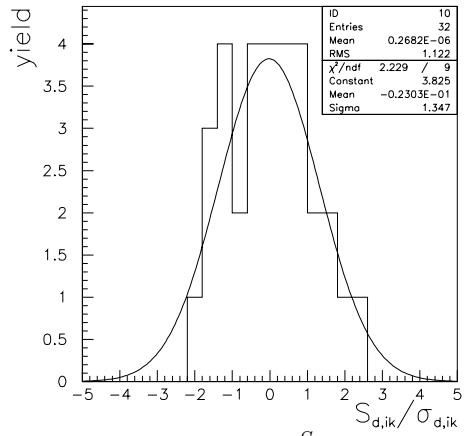


Figure 2: Distribution of the experimental $\frac{S_{d,ik}}{\sigma_{d,ik}}$ values, which should be distributed as a standardized gaussian variable in case of absence of rate diurnal variation. The obtained gaussian best fit is shown.

The energy and time correlation analysis of the DAMA/NaI-2 data has been performed by applying the standard maximum likelihood method, grouping the events in $i'jk$ cells ($i'$ identifies the sidereal time interval over the whole DAMA/NaI-2 period, $j$ the crystal of mass $M_j$ and $k$ the considered energy interval). The number of events in each cell, $N_{i'jk}$, will follow a Poissonian distribution with expected value: $\mu_{i'jk} = (b_{jk} + S_{0,k} + S_{d,ik})M_j\Delta t_{i'}\Delta E\epsilon_{jk}$. There $S_{0,k}$ is the constant part of the signal in the $k$-th energy interval and $S_{d,ik}$ is its periodical component in the $i$-th time interval in the sidereal day (the $S_{d,ik}$ are defined in order to have the mean value over one sidereal day equal to zero). Let us note that the modulated part of the signal $S_{d,ik}$ is periodical and it repeats itself every eight temporal intervals, three hours each one, that is every sideral day; the relation which ties $i$ to $i'$ is: $i = Mod(i' - 1, 8) + 1$. Moreover, $\Delta t_{i'}$ is the running time during the $i'$-th sidereal time interval during the DAMA/NaI-2 period, $\epsilon_{jk}$ is the efficiency for the $j$-th detector in the considered $k$-th energy interval and $b_{jk}$ is the background contribution, which depends on the detector and can be considered constant with time due to the results

of the stability controls on the DAMA/NaI-2 data; this is also further supported by the results obtained investigating the diurnal rate in the region just above the first pole of the Iodine form factor.

The full compatibility of the $S_{d,ik}$ values (obtained by analysing the sidereal time correlation of the DAMA/NaI-2 data in the energy intervals 2-3 keV, 3-4 keV, 4-5 keV, 5-6 keV) with zero is shown in fig. 2 where the histogram of the $\frac{S_{d,ik}}{\sigma_{d,ik}}$ ratios is presented. The data have been further analysed in terms of rate dependence on $\theta$, considering the 2-6 keV as a cumulative energy interval; obtainining for the $B$ and $C$ parameters the following upper limits at 90% C.L.: $B < 0.031$ cpd/kg/keV and $C < 0.043$ cpd/kg/keV. ¿From these experimental limits and from the knowledge of the $(\frac{B}{\xi\sigma_p})$ and $(\frac{C}{\xi\sigma_p})$ dependence on $M_W$ and $\sigma_p$, exclusion plots in the plane $\xi$ versus $\sigma_p$ have been evaluated as reported in fig. 3.

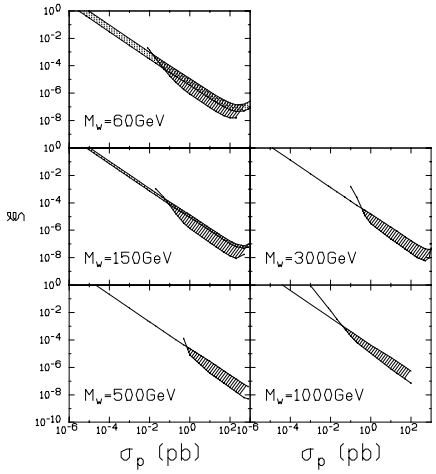


Figure 3: Exclusion plots at 90% C.L. in the ($\xi$, $\sigma_p$) plane for SI coupled candidates with the given $M_W$ values. The regions excluded at 90% C.L. by the present analysis for masses of 60 and 150 GeV (dashed areas) are compared with those allowed for them in the 1999 paper where the effect of the $v_0$ uncertainties have been discussed (dotted areas). The regions excluded at 90% C.L. by the present analysis for masses of 300, 500 and 1000 GeV (dashed areas) are shown together with those (above the slant lines) already excluded at 90% C.L. by the best existing limits on $\xi\sigma_p$ [6, 7].

In conclusion, this investigation of possible diurnal variation of the rate with sidereal time has allowed to exclude – at 90% C.L. – new regions for high cross section candidates (to which very small halo fraction would correspond). Moreover, in particular, this result supports that the possible signal pointed out by the studies on the WIMP annual modulation signature could account for a halo fraction greater than $10^{-3}$.

A corollary experimental results has been obtained repeating the same analysis as a function of the solar time to verify the possible presence in the data of a rate diurnal variation of unknown origin. The hypothesis of absence of this modulation is fully supported by the data.

## 2.4 Search for neutral SIMPs and nuclearites

A new search for neutral Strongly Interacting Massive Particles (SIMPs) - both with coherent and spin-dependent coupling - has been performed. These particles could be formed e.g. by the "neutralization" of exotic particles, having electromagnetic and/or nuclear charge, with ordinary matter during the primordial nucleosynthesis. They could be embedded in the galactic halo ($\beta \simeq 10^{-3}$) and have masses ($M_S$) from the GeV range up to the GUT scale with cross sections on protons up to $\simeq 10^{-22} cm^2$. It has been suggested that they could be the sources of UHE cosmic rays [8], while in some models of supersymmetry breaking they could appear as e.g. gluino LSP [9]. The overlaying rock degrades the SIMPs energy and reduces the set-up sensitivity to large cross sections, but the low background technique and the $\mu$ flux reduction allow to extend the SIMPs search to lower fluxes and higher masses.

We searched for delayed coincidences from SIMP elastic scattering on Sodium and/or Iodine nuclei using two "planes" (23.2 cm — center to center — distance; three detectors each one) of the $\simeq$ 100 kg NaI(Tl) DAMA set-up during 350.05 days. The measured quantities are the recoil energies. Both "downward-" and "upward-"going events have been collected, that is events in which a signal due to a nuclear recoil in one detector of a "plane" is followed - within 350 to 3000 ns - by another signal in one detector of the other "plane". The total exposition resulted 1.1 $\cdot 10^6$ cm$^2$ sr days. A particular attention has been devoted to minimize the possible sources of background events as coincidences from uncorrelated processes and those deriving from nuclear processes occurring both in the detectors and in the environment. Two energy regions have been considered: 4 to 60 keV electron equivalent for mainly single scattering events and above 60 keV electron equivalent for multiple scatterings inside the crystals, giving pulses with multi-bumps/long time structure.

Table 2: Energies released in the two "planes" and time delay of the delayed coincidences measured in the mainly single scattering region.

| $E_1$ (keV) | $E_2$ (keV) | $\Delta t$ (ns) |
|---|---|---|
| 18.3 | 45.9 | 1975 |
| 13.4 | 53.4 | 362.5 |

In table 2 the released energies and the time delay of the delayed coincidences measured in the mainly single scattering region are summarized; both had a downward direction giving an oblique pattern in the two "planes" between first close detectors. In this energy region only 0.2 coincidences were expected from random and correlated background during 350.05 days. The upper limit on the number of events both of upward and downward delayed coincidences in this energy region has been, therefore, derived by considering a Poissonian distribution with 0.2 expected events having observed 2. The limit is $< 5.12$ events at 90% C.L. No delayed coincidence with multi-bump/long time structure has

been detected in the 350.05 days; therefore, also for the multiple scattering region the upper limit on the number of events has been calculated with a similar approach both for downward and upward delayed coincidences. It resulted $< 2.3$ events at 90% C.L. having never observed a multi-bump/long time structure event.

To achieve the final result we also considered the data we previously collected at Gran Sasso with another of our set-ups, the one named "F" in ref. [10] (exposure: 132980 cm$^2$ sr days); the different features have been properly taken into account.

A MonteCarlo code has been used to evaluate the effect of the crossed matter (mainly a degrading of the SIMP velocity) accounting for the chemical composition of the overstanding mountain in case of downward coincidences and for the mean composition of the different regions inside the Earth in case of upward coincidences, together with the different SIMP cross sections on the involved nuclei. Standard astrophysical assumptions have been considered to calculate the exclusion plots at 90% C.L. in the $\sigma_p$ versus $M_S$ plane both for spin-dependent and spin-independent interactions. This analysis has improved the excluded regions up to $M_S \simeq 4 \cdot 10^{16}$ GeV.

The result obtained in the multiple scattering region has been also used to calculate a model independent upper limit on the neutral nuclearities, which may constitute a new form of matter with roughly equal number of up, down and strange quarks. In fact, considering that in the multiple scattering region the rate of neutral nuclearities depends only on geometrical factors (being the cross section large enough to induce always a total detected energy above 60 keV), the model independent upper limit on their flux ($\Phi$) is: $\Phi < 1.9 \cdot 10^{-11} s^{-1} cm^{-2} sr^{-1}$ at 90% C.L. when $\beta \simeq 10^{-3}$. Moreover, the model independent 90% C.L. limit contours on the flux of neutral nuclearities have also been calculated for various other cases.

## 2.5 Search for charge-non-conserving (CNC) processes

The conservation of the electric charge is one of the fundamental laws of the standard quantum electrodynamics based on the underlying principle of gauge invariance. Nevertheless, the possibility that charge conservation may be broken in future unified gauge theories and the implications of such a violation have been extensively discussed in literature [11] and experimental efforts to test this basic feature of nature in direct measurements are continuing since the pioneering search by G. Feinberg and M. Goldhaber [12].

### 2.5.1 New experimental limit on the electron stability and non-paulian transitions in Iodine atoms

The idea was to use the features of the NaI(Tl) DAMA set-up to look for signals from X-ray and Auger electron cascade, which would follow the decay of a K (energy released 33.2 keV) or of an L electron (energy release of about 5 keV) in a Iodine atom of the NaI(Tl). Each Iodine atom contains 8 electrons on L-shell (2 on L1-, 2 on L2-, and 4 on L3-subshell), while only 2 are available on K-shell; thus, the possibility to investigate the energy region corresponding to L-shell electron decays increases the source strength by a factor 4 with respect to the standard procedure searching for K-electron decay. In particular, in this case we have considered only L-shell electron decays, because the K-

shell will contribute to the overall sensitivity on $\tau_e$ only at $\simeq 1\%$, when — as in our case — the counting rates in two energy intervals are similar. The statistics considered in the analysis was 19511 kg·day (DAMA/NaI-1&2 running periods).

The possible decay of L-electrons in Iodine atoms inside the NaI(Tl) detectors would be visible as a peak at the energy of about 5 keV (5.19 keV for L1-shell, 4.85 keV for L2-shell and 4.56 keV for L3-shell [13]). The absence of such a peak in the collected data was evident. Thus, we have determined the limit on the electron life time fitting the experimental energy distribution in the energy interval 3.5 - 6.0 keV by the sum of two functions: the background and the effect being searched for. As simplified background model, suitable for the purposes, a linear function has been assumed, while the effect has been represented by the sum of three gaussians, centered at 4.56, 4.85 and 5.19 keV respectively. The amplitudes of the gaussians have been normalized for two electrons on L1-, two electrons on L2-, and four electrons on L3-shell, requiring therefore only one free parameter for the effect amplitude. ¿From the fit this amplitude was found to be $(-0.0029 \pm 0.0240)$ cpd/kg, giving no statistical evidence for it ($\chi^2/d.o.f. = 1.2$). Therefore, we obtained: $\tau_e(e^- \to \nu_e\bar{\nu}_e\nu_e) > 4.2(2.4) \cdot 10^{24}$ years at 68% (90%) C.L.; this result is one order of magnitude higher than the best limit previously available [14].

The searches for "disappearance" of electrons on the atomic shells allow interesting considerations also on possible violation of the Pauli exclusion principle (PEP) and on the limit on photon mass. Quantitative estimates on these topics have been also carried out.

### 2.5.2 New limits on the nuclear level excitation of $^{127}$I and $^{23}$Na during charge-non-conservation

We followed the S. Holjevic et al. [15] approach searching for the electron's disappearance in atomic shells involving the excitation of nuclear levels. The idea was to consider the process, analogous to the electron capture, which does not change the nucleon charge but leaves the nucleus in an excited state:

$$(A, Z) + e^- \to (A, Z)^* + \nu_e. \tag{1}$$

The CNC nuclear excitation can involve both the weak boson (W) and the photon ($\gamma$) mediating processes[16]; therefore, while the electron decay is concerned with the CNC process at the lepton sector, the nuclear excitation (and the nuclear beta decay) is concerned with the CNC process at both the lepton and quark (nucleon) sectors.

The CNC electron capture (1) can feed the excited states of the nucleus with energies $E_{exc}$ up to $m_e c^2 - E_B$ with $E_B$ binding energy of the electron; in the de-excitation process the nucleus returns to the ground state emitting $\gamma$ quanta and conversion electrons which could be observed by the detector. If the electron capture takes place in the detector itself, the observed energies will be shifted up to the $E_{exc} + E_B$ value due to the absorption of X rays and Auger electrons emitted in the relaxation of the atomic shells. It is supposed that CNC excitations feed preferably the lowest levels with difference in spin between ground and excited states $\Delta J = 0, 1$ and that K electrons are most probably involved in the process, being the closest to the nucleus.

The data collected by the nine 9.7 kg NaI(Tl) detectors during $\simeq$ 400 days (34866 kg·day statistics) have been analysed searching for $\gamma$ rays from the possible de-excitation processes in $^{127}$I and $^{23}$Na nuclei which could follow the CNC electron captures. In accordance with the low energy level schemes of $^{127}$I and $^{23}$Na four levels could be excited in $^{127}$I ($E_{exc}$ = 57.6; 202.9; 375.0 and 418.0 keV) and one in $^{23}$Na ($E_{exc}$ = 440.0 keV) [13]. Thus, taking into account the binding energies of Iodine ($E_B^K$ = 33.2 keV) and Sodium ($E_B^K$ = 1.1 keV) K atomic shells, the energies of the possible peaks to be searched for in the experimental energy distribution should be: 90.8, 236.1, 408.2 and 451.2 keV for Iodine and 441.1 keV for Sodium. These peaks have not been found in our experimental data; therefore, limits for the probabilities of CNC nuclear excitations of $^{127}$I and $^{23}$Na nuclei have been set and the new experimental lifetime limits on the CNC electron capture involving nuclear levels excitation of $^{127}$I and $^{23}$Na (reported in table 3) have been obtained.

Table 3: Experimental lifetime limits on the CNC electron capture involving nuclear levels excitation of $^{127}$I and $^{23}$Na.

| Nucleus, $E_{exc}$ | Lifetime limits $\tau$, year | | |
|---|---|---|---|
| | this work | [15] | [16] |
| | 90% C.L. | 90% C.L. | 68% C.L. |
| $^{127}$I | | | |
| 57.6 keV | $2.4 \cdot 10^{23}$ | $2.1 \cdot 10^{21}$ | $5.8 \cdot 10^{22}$ |
| 202.9 keV | $2.0 \cdot 10^{23}$ | $1.9 \cdot 10^{21}$ | $5.6 \cdot 10^{22}$ |
| 375.0 keV | $1.8 \cdot 10^{23}$ | $2.4 \cdot 10^{21}$ | – |
| 418.0 keV | $1.6 \cdot 10^{23}$ | $2.4 \cdot 10^{21}$ | – |
| $^{23}$Na | | | |
| 440.0 keV | $1.5 \cdot 10^{23}$ | – | – |

According to Bahcall [17], we have used as a suitable CNC parameter the relative strength ($\varepsilon^2$) of the studied CNC process with respect to that of a suitably selected charge conserving (CC) process. To derive restrictions on $\varepsilon^2$ from the lifetime limits on the CNC electron capture with the excitation of $^{127}$I nuclear levels, the CNC nuclear excitation of $^{127}$I was compared with the usual K electron capture and the CNC nuclear matrix elements were derived from the analogous M1 $\gamma$ decay matrix elements experimentally measured [16]. The most stringent limit has been obtained for the $7/2^+$ level (57.6 keV) of $^{127}$I. In fact, in this case: $\varepsilon_W^2 = 2.3 \cdot 10^{-2}/\tau^{CNC}$ ($\tau^{CNC}$ given in years) and, substituting there our experimental limit for this level, we obtain: $\varepsilon_W^2 < 9.6 \cdot 10^{-26}$ (90% C.L.), which is one order of magnitude more severe than the one previously available[16].

The CNC nuclear excitation process of $^{127}$I through photon exchange was also considered. The analogous CC process is the standard internal electron conversion (IC). Properly developing the calculation, we have obtained for the $7/2^+$ level (57.6 keV) of $^{127}$I: $\varepsilon_\gamma^2 < 1.2 \cdot 10^{-40}$ (90% C.L.), also a condition more severe than the previously available one[16].

Finally, the present restriction on $\varepsilon_W^2$ has been compared with the one derived from the best $\tau$ limit for the electron disappearance we have set in the previous subsection. Let us take into account the possible disappearance channel $e^- \rightarrow \nu_e + \bar{\nu}_e + \nu_e$, for which we can

write: $\tau_{e3\nu} > 2.4(4.2) \cdot 10^{24}$ y at 90(68)% C.L. and use the calculation of Ref. [16] where this channel was evaluated by comparing it with $\mu$ decay, obtaining: $\varepsilon^2_{e3\nu} = 2.6 \cdot 10^{-2}/\tau_{e3\nu}$ ($\tau_{e3\nu}$ given in years). Our quoted limit leads to the bound $\varepsilon^2_{e3\nu} < 11(6.2) \cdot 10^{-27}$ at 90(68)% C.L., which is the most stringent restriction on the CNC admixture to the lepton current at present.

# 3 The LXe set-up

## 3.1 Introduction

The LXe detector is filled with about 2 l ($\simeq$ 6.5 kg) liquid Kr-free Xenon enriched at 99.5% in $^{129}$Xe by ISOTEC company. Its features have been described in details elsewhere; we recall here only its main characteristics. It was measured that U/Th contamination does not exceed $\approx$ 2 ppt at 90% C.L. The vessel for the LXe is made by the OFHC and low radioactive copper ($\leq$100 $\mu$Bq/kg for U/Th and $\leq$310 $\mu$Bq/kg for potassium). The scintillation light collection is assured by three EMI photomultipliers (PMT) with $MgF_2$ windows working in coincidence. The quantum efficiency of the PMT's photocathodes is ranging between 18 and 32%. The PMT-s collect light through three windows (3" in diameter) made of special cultured crystal quartz (total transmission of the LXe scintillation light $\approx$ 80%, including the reflection losses). A low radioactive copper shield inside the thermo-insulation vacuum cell surrounds the PMT-s; then, 2 cm of steel (insulation vessel thickness), 5 $-$ 10 cm of low radioactive copper, 15 cm of low radioactive lead, $\approx$1 mm of cadmium and $\approx$10 cm of polyethylene are used as outer hard shielding. The environmental Radon nearby the detector is removed by continuous flushing of a high purity Nitrogen gas from bottles stored underground since time. An external envelop made by Supronyl (now replaced by a plexiglass box) offers an additional Radon protection. Each PMT is connected with a low noise preamplifier, whose outputs are fed to the data acquisition system. For every event the following information are recorded: amplitudes of each single PMT pulse, amplitude and shape of the sum pulse (recorded with the help of a Lecroy transient digitizer). The energy dependence of the detector resolution was measured to be: $\sigma/E = 0.056 + 1.19/\sqrt{E[keV]}$.

## 3.2 New limits on the nuclear level excitation of $^{129}$Xe during charge-non-conservation

We have pursued the same kind of investigation as for the NaI(Tl) data in sect. 2.5.2, establishing for the first time lifetime limits on the charge non-conserving (CNC) electron capture with nuclear levels excitation of $^{129}$Xe.

For this purpose we have analysed a statistics of 823.1 kg·day collected by the $\simeq$ 6.5 kg liquid Xenon DAMA scintillator deep underground. In accordance with the nuclear level scheme, five levels of $^{129}$Xe could be excited due to the process (1) searched for ($E_{exc} = 39.6; 236.1; 318.2; 321.7$ and 411.5 keV) [13]. The first one is the most interesting due to the difference in spin $\Delta J = 1$ between ground ($1/2^+$) and excited level ($3/2^+$) and to the very low energy (39.6 keV) which is favorable to derive restrictions on the

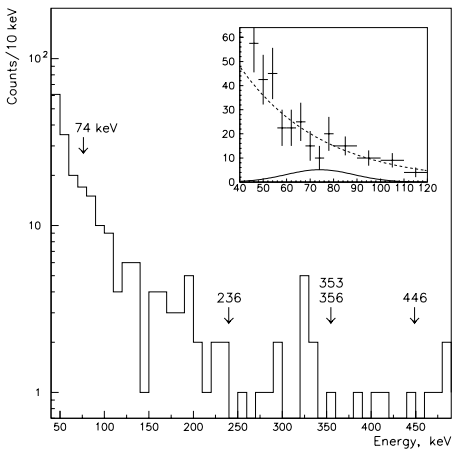


Figure 4: Energy spectrum measured by the LXe scintillator in the energy region $40-500$ keV with total statistics of 823.1 kg·day. In the insert the low energy part is shown in linear scale together with the fitting curve and excluded peak ($\tau = 1.1 \cdot 10^{24}$ y) for the first excited level of $^{129}$Xe.

CNC parameters of the theory from the experimental $\tau$ limits. The energy distribution measured by the DAMA LXe set-up has been analysed to search for $\gamma$ rays from the possible de-excitation processes in $^{129}$Xe which could follow the CNC electron captures. Taking into account the binding energy of the Xe K atomic shell ($E_B^K = 34.6$ keV), the energies of the possible peaks in the background spectra should be: 74.2; 236.1[3]; 352.8, 356.3 and 446.1 keV. The experimental spectrum of the LXe scintillator in the energy region $40 - 500$ keV with total statistics of 823.1 kg·day is shown in fig. 4, where the absence of these peaks is evident. Therefore, limits have been set for the probabilities of CNC nuclear excitations of $^{129}$Xe nuclei. The derived experimental life time limits on the CNC electron capture involving nuclear levels excitation of $^{129}Xe$ are given in table 4.

Table 4: Experimental life time limits on the CNC electron capture involving nuclear levels excitation of $^{129}$Xe.

| $E_{exc}$ | $\tau$ limits, year 90(68)% C.L. |
|---|---|
| 39.6 keV | $1.1(2.0) \cdot 10^{24}$ |
| 236.1 keV | $3.7(6.4) \cdot 10^{24}$ |
| 318.2 keV | $2.2(3.9) \cdot 10^{24}$ |
| 321.7 keV | $2.5(4.4) \cdot 10^{24}$ |
| 411.5 keV | $2.3(4.2) \cdot 10^{24}$ |

Also in this case, according to Bahcall [17], we have used as a suitable CNC parameter the relative strength ($\varepsilon^2$) of the studied CNC process with respect to that of a suitably

[3]Because the second excited level is long-lived ($t_{1/2} = 8.89$ d) the energy of peak searched for is equal to $E_{exc} = 236.1$ keV.

selected charge conserving (CC) process. With proper calculations the following relations have been derived: $\varepsilon_W^2 = 2.4 \cdot 10^{-2}/\tau^{CNC}$ and $\varepsilon_\gamma^2 = 1.4 \cdot 10^{-18}/\tau^{CNC}$ ($\tau^{CNC}$ in years). By substituting into the equations given above the experimental limit obtained for the first excited level of $^{129}$Xe we get $\varepsilon_W^2 < 2.2 \cdot 10^{-26}$ and $\varepsilon_\gamma^2 < 1.3 \cdot 10^{-42}$ (both at 90% C.L.), more severe than those achieved in sect. 2.5.2 for $^{127}$I.

# 4 R&D developments and by products

In the barrack, where the $\simeq$ 100 kg NaI(Tl) set-up is installed, another set-up (mainly devoted to test new scintillator prototypes and to perform small scale experiments) is also running. There a sealed low radioactive copper box to house detectors is installed inside a multi-component low radioactive shield, which is enclosed in an external sealed plexiglass box. The boxes are maintained in high purity Nitrogen atmosphere.

## 4.1 Results on $\beta\beta$ and WIMP searches with $CaF_2$(Eu)

The development of highly radiopure $CaF_2$(Eu) crystal scintillators has been performed by an R&D program with the Bicron company, aiming at a substantial sensitivity enhancement of the $2\beta$ decay investigation and of the search for dark matter particles with spin-dependent (SD) interaction. In fact, these detectors can be usefully utilized to search for the $2\beta$ decays of $^{46}$Ca (natural abundance: $\delta = 0.004\%$; $Q_{\beta\beta} = 990.4$ keV) and of $^{48}$Ca ($\delta = 0.187\%$; $Q_{\beta\beta} = 4272$ keV) besides the double electron capture of $^{40}$Ca ($\delta$ =96.941%; $Q_{2EC} = 193.8$ keV). Moreover, they can be promising detectors for the direct search of Dark Matter particles with SD coupling [19, 20], containing the $^{19}$F nuclei ($\delta = 100\%$) with non zero spin (J=1/2) for which a relatively large cross section for SD coupled WIMPs has been calculated [21].

Two $CaF_2$(Eu) crystals, 3" diameter by 1" length (370 g mass) each one, have been used; they will be labelled as Bicron-1 and Bicron-2 in the following.

The main features of the apparatus for the measurements performed with Bicron-2 as well as the used procedures have been described in the paper. The background spectrum of the Bicron-2 crystal was measured in this apparatus during 1906.3 h in the three energy regions: 4 - 20 keV, 40 - 230 keV and 200 - 4000 keV. Data previously collected with Bicron-1 were also available for analysis; in this case the measuring time was 631.4 h for the energy interval 4 - 24 keV and 260.9 h for the energy region 200 - 3300 keV [19]. During the measurement, the energy scale and resolution of the detector were calibrated periodically with various sources, while – in addition – background peaks ($E_\gamma$ = 128 and 169 keV) from $^{152}$Eu contamination in the Bicron-2 crystal were used for calibration in the energy region 40 - 230 keV. Three peaks at the energies of about 0.81, 1.01 and 1.15 MeV were present and – considering the typical $\alpha/\beta$ ratio for the light output of the $CaF_2$(Eu) crystals – they can be attributed to $\alpha$-particles from $^{232}$Th and $^{238}$U internal impurities. Moreover, in the lower energy region, three clear peaks at energies $\simeq$ 47 keV, $\simeq$ 129 keV and $\simeq$ 169 keV were also present; the simulations have shown that they could be explained by $^{152}$Eu ($T_{1/2}$ =13 y) activity created in the $CaF_2$(Eu) crystal by the neutron activation at Earth surface. The locations and amounts of the radioactive contaminations

have been estimated by simulating the background spectra of the $CaF_2$(Eu) crystal by the GEANT3.21 package and the event generator DECAY4.

The simulated response functions of $CaF_2$(Eu) crystals and the calculated values of efficiencies for the different $2\beta$ decay processes were used together with the corresponding background rates, the measuring times and the numbers of $^{40}$Ca and $^{46}$Ca nuclei in order to estimate half-life limits for the effects under investigation; the latters are summarized in table 5.

Table 5: Half-life limits for different $2\beta$ processes of $^{40}$Ca and $^{46}$Ca.

| $2\beta$ process (Peak energy) | $T_{1/2}$ limit, y 68% (90%) C.L. (Combined from Bicron-1+Bicron-2) |
|---|---|
| $0\nu$2EC of $^{40}$Ca (6.4 keV) | $4.9(3.0) \cdot 10^{21}$ |
| $0\nu$2EC of $^{40}$Ca (193.8 keV) | $3.4(1.8) \cdot 10^{20}$ |
| $2\nu$2EC of $^{40}$Ca (6.4 keV) | $9.8(5.9) \cdot 10^{21}$ |
| $0\nu2\beta$ of $^{46}$Ca (990 keV) | $1.7(1.0) \cdot 10^{17}$ |

The $T_{1/2}$ limit obtained for $0\nu2\beta$ decay of $^{46}$Ca is higher than the best result previously available. Restriction for the two neutrino 2EC of $^{40}$Ca is also improved from value $4.6 \cdot 10^{21}$ y [19] to $\simeq 10^{22}$ y. It should be stressed that the latter is the highest half-life limit obtained up-to-date for the $2\beta^+$ decay processes and, in particular, for the double electron capture. The same is true for the neutrinoless 2EC of $^{40}$Ca, which $T_{1/2}$ limit is established for the first time.

Finally, the exclusion plot at 90% C.L. in the WIMP-nucleon cross section versus WIMP mass has been derived for WIMP-$^{19}$F elastic scattering combining the Bicron-1 and Bicron-2 data (OR-ed) according to the astrophysical and nuclear physics considerations and to the parameters' values given in ref. [19]. It slightly improve the DAMA/$CaF_2$-1 result of ref. [19].

At present a 3-rd prototype is at hand; new measurements are foreseen in 2000.

## 4.2 Status of the new R&D for further radiopurification of the NaI(Tl)

The R&D for further radiopurification of NaI(Tl) is at conclusion; the chemical/physical purification of the NaI and TlI powders has been satisfactory. Measurements on full detector prototypes are in progress.

# 5 Conclusions

Interesting results have been achieved by the DAMA experiments during 1999 on various rare events searches. Upgradings of the set-ups are in preparation.

# 6 List of Publications during 1999


1. R. Bernabei, P. Belli, F. Montecchia, W. Di Nicolantonio, A. Incicchitti, D. Prosperi, C. Bacci, C.J. Dai , L.K. Ding, H.H. Kuang, J.M. Ma, "WIMPs search by scintillators: possible strategy for annual modulation search with large-mass highly-radiopure NaI(Tl)", *Nucl.Phys.* **B (Proc. Sup.) 70** (1999), 79.

2. P. Belli, R. Bernabei, C. J. Dai, L.K. Ding, W. Di Nicolantonio, G. Ignesti, A. Incicchitti, H.H. Kuang, J. M. Ma, F. Montecchia, D. Prosperi, M. Angelone, P. Batistoni, M. Pillon, "The DAMA experiments: status report", in the volume *Dark Matter in Astrophysics and particle Physics 1998*, IOP pub, Phyladelphia (1999), 711.

3. P. Belli, R. Bernabei, A. Incicchitti, C. Arpesella, V.V. Kobychev, O.A. Ponkratenko, V.I. Tretyak, Yu.G. Zdesenko, "New limits on $2\beta^+$ decay processes in $^{106}$Cd", *Astroparticle Phys.* **10** (1999), 115.

4. I. Barabanov, R. Bernabei, P. Belli, V. I. Gurentsov, V. N. Kornukhov, O. G. Miranda, V. B. Semikoz, J. W. F. Valle, "Testing for New Physics with Low-Energy Anti-Neutrino Sources: LAMA as a Case Study", *Nucl. Phys.* **B546** (1999), 19.

5. R. Bernabei, P. Belli, F. Montecchia, W. Di Nicolantonio, G. Ignesti, A. Incicchitti, D. Prosperi, C.J. Dai, L.K. Ding, H.H. Kuang, J.M. Ma, "Performances of the $\simeq$ 100 kg NaI(Tl) set-up of the DAMA experiment at Gran Sasso", *Il Nuovo Cim.* **A112** (1999), 545.

6. R. Bernabei, P. Belli, F. Montecchia, W. Di Nicolantonio, G. Ignesti, A. Incicchitti, D. Prosperi, C.J. Dai, L.K. Ding, H.H. Kuang, J.M. Ma, "On a further search for a yearly modulation of the rate in particle Dark Matter direct search", *Phys. Lett.* **B450** (1999), 448.

7. P. Belli, R. Bernabei, F. Montecchia, W. Di Nicolantonio, G. Ignesti, A. Incicchitti, D. Prosperi, C.J. Dai, L.K. Ding, H.H. Kuang, J.M. Ma, "New DAMA results on annual modulation searches", in the volume *Proc. of the II Int. Workshop on "The identification of Dark Matter"*, World Scie. ed. (1999), 299.

8. P. Belli, R. Bernabei, C.J. Dai, W. Di Nicolantonio, L.K. Ding, G. Ignesti, A. Incicchitti, H.H. Kuang, J.M. Ma, F. Montecchia, D. Prosperi, "Direct search for Dark Matter particles deep underground", in the volume *3K-Cosmology*, AIP pub. (1999), 65.

9. P. Belli, R. Bernabei, A. Bottino, F. Donato, N. Fornengo, D. Prosperi, S. Scopel, *Extending the DAMA annual modulation region by inclusion of the uncertainties in astrophysical velocities*, hep-ph/9903501 and *Phys. Rev.* **D61** (2000), 023512.

10. P. Belli, R. Bernabei, C.J. Dai, H.L. He, G. Ignesti, A. Incicchitti, H.H. Kuang, J.M. Ma, F. Montecchia, O.A. Ponkratenko, D. Prosperi, V.I. Tretyak, Yu.G. Zdesenko, "New experimental limit on the electron stability and non-paulian transitions in Iodine atoms", *Phys. Lett.* **B460** (1999), 235.

11. P. Belli, R. Bernabei, C.J. Dai, F. Grianti, H.L. He, G. Ignesti, A. Incicchitti, H.H. Kuang, J.M. Ma, F. Montecchia, O.A. Ponkratenko, D. Prosperi, V.I. Tretyak, Yu.G. Zdesenko, "New limits on spin-dependent coupled WIMPs and on $2\beta$ processes in $^{40}$Ca and $^{46}$Ca by using low radioactive $CaF_2$(Eu) crystal scintillators", *Nucl. Phys.* **B563** (1999), 97.

12. R. Bernabei, P. Belli, R. Cerulli, F. Montecchia, M. Amato, G. Ignesti, A. Incicchitti, D. Prosperi, C.J. Dai, H.L. He, H.H. Kuang, J.M. Ma, G.X. Sun, Z. Ye, "Extended limits on neutral SIMPs and nuclearities from NaI(Tl) scintillators", *Phys. Rev. Lett.* **83** (1999), 4918.

13. R. Bernabei, "Dark matter searches", in the volume *Proceed. of the 8-th Int. Workshop on Neutrino Telescopes*, edited by M. Baldo-Ceolin, Papergraf ed., vol. II (1999),239.

14. P. Belli, R. Bernabei, C.J. Dai, W. Di Nicolantonio, L.K. Ding, G. Ignesti, A. Incicchitti, H.H. Kuang, J.M. Ma, F. Montecchia, D. Prosperi, "Searching for the Dark Universe by the DAMA experiments", to appear in the volume *Proc. of II Int. Conf. Beyond the desert '99*, Castle Ringberg, June 1999.

15. P. Belli, R. Bernabei, C.J. Dai, H.L. He, G.Ignesti, A. Incicchitti, H.H. Kuang, J.M. Ma, F. Montecchia, O.A. Ponkratenko, D. Prosperi, V.I. Tretyak, Yu.G. Zdesenko, "New limits on the nuclear level excitation of $^{127}$I and $^{23}$Na during charge nonconservation", *Phys. Rev.* **C60** (1999), 065501.

16. R. Bernabei, P. Belli, R. Cerulli, F. Montecchia M. Amato, G. Ignesti, A. Incicchitti, D. Prosperi, C.J. Dai, H.L. He, H.H. Kuang, J.M. Ma, "Investigation on possible diurnal effects induced by Dark Matter particles", ROM2F/99/26 to appear on Il Nuovo Cimento.

17. P. Belli, R. Bernabei, C.J. Dai, G. Ignesti, A. Incicchitti, F. Montecchia, O.A. Ponkratenko, D. Prosperi, V.I. Tretyak, Yu.G. Zdesenko, "Charge non-conservation restrictions from the nuclear levels excitation of $^{129}$Xe induced by the electron's decay on the atomic shell", *Phys. Lett.* **B465** (1999), 315.

# References


[1] K. Freese et al., *Phys. Rev.* **D37** (1988), 3388; Drukier, et al., *Phys. Rev.* **D33** (1986), 3495.

[2] R. Bernabei, *La Rivista del Nuovo Cimento*, n. **5** (1995).

[3] R. Bernabei et al., *Phys. Lett.* **B424** (1998), 195.

[4] R. Bernabei, seminar given at CERN, Geneva, April 13, 1999.

[5] J.I. Collar e F.T. Avignone III, *Phys. Lett.* **B275** (1992), 181; J.I. Collar e F.T. Avignone III, *Phys. Rev.* **D47** (1993), 5238.

[6] R. Bernabei et al., *Phys. Lett.* **B389** (1996), 757.

[7] R. Bernabei et al., *Phys. Lett.* **B436** (1998), 379.

[8] D. Chung, G. Farrar and E.W. Kolb, *FERMILAB-pub-97/187*; C. Albuquerque, G. Farrar and E.W. Kolb, *astro-ph/9805288*. V. Berezinsky and M. Kalcheries, *hep-ph/9709485*; V. Berezinsky and B.L. Ioffe, *Sov. Phys. JETP* **63** (1986), 920.

[9] R. N. Mohapatra and S. Nandi, *Phys. Rev. Lett.* **79** (1997), 181; S. Raby, *Phys. Rev.* **D56** (1997), 2852.

[10] C. Bacci et al., *Astroparticle Phys.* **4** (1996), 195.

[11] L.B. Okun and Ya.B. Zeldovich, *Phys. Lett.* **B78** (1978), 597; M.B. Voloshin and L.B. Okun, *JETP Lett.* **32** (1978), 145; R.N. Mohapatra, *Phys. Rev. Lett.* **59** (1987), 1510; L.B. Okun, *Leptons and Quarks* (North-Holland, Amsterdam, 1982), p. 181; L.B. Okun, *Sov. Phys. Usp.* **32** (1989), 543; *Comments Nucl. Part. Phys.* **19** (1989), 99; *Phys. Rev.* **D45**, No. 11 (1992) VI.10.

[12] G. Feinberg and M. Goldhaber, *Proc. Nat. Acad. Sci. U.S.A.* **45** (1959), 1301.

[13] R.B. Firestone, *Table of Isotopes*, 8-th ed. (Wiley, New York, 1996).

[14] Y. Aharonov et al., *Phys. Lett.* **B353** (1995), 168; *Phys. Rev.* **D52**, 3785 (1995).

[15] S. Holjevic et al., *Phys. Rev.* **C35** (1987), 341.

[16] H. Ejiri et al., *Phys. Rev.* **C44** (1991), 502.

[17] J.N. Bahcall, *Rev. Mod. Phys.* **50** (1978), 881; in *Neutrino Astrophysics* (Cambridge University, Cambridge, 1993), p. 360.

[18] P. Belli et al., *Astroparticle Phys.* **5** (1996), 217.

[19] R. Bernabei et al., *Astroparticle Phys.* **7** (1997), 73.

[20] C. Bacci et al., *Astroparticle Phys.* **2** (1994), 13.

[21] J. Ellis and R.A. Flores, *Phys. Lett.* **B263** (1991), 259.

# DBA. Search for double beta decay of $^{100}$Mo with liquid argon ionization chamber.

V.D. Ashitkov[1], A.S. Barabash[1], S.G. Belogurov[1], G. Carugno[2], S.I. Konovalov[1], F.Massera[4], G. Puglierin[2], R.R. Saakyan[1,3], V.N. Stekhanov[1], V.I. Umatov[1],

[1]Institute of Theoretical and Experimental Physics, B. Cheremushkinskaya 25, 117259 Moscow, Russia

[2]Dipartimento di Fisica e INFN, Universita di Padova, via Marzolo 8, I-35131 Padova, Italy

[3]Laboratori Nazionali del Gran Sasso dell'INFN, I-67010 Assergi (L'Aquila), Italy

[4]INFN, Sezione di Bologna, 40126, via Berti Pichat, 6/2 (Bologna), Italy

**Abstract**

The experiment is located in the Gran Sasso Underground Laboratory (3500 m w.e.). Full weight of $^{100}$Mo under investigation is 306 g. New measurement run was done (1355 h). As a result the limits on half-lives for $0\nu$- and $0\nu\chi^0$-decays of $^{100}$Mo were obtained as $3.4 \cdot 10^{21}$ y and $2.2 \cdot 10^{20}$ y, respectively, at 90% CL. The $2\nu\beta\beta$ decay of $^{100}$Mo was firmly detected ($> 6\sigma$ of effect) and its half-life was measured, $[6.8 \pm 1.1(stat) \pm 0.7(syst)] \cdot 10^{18}$ y.

## 1 Introduction

At present time the neutrinoless double beta decay is one of the best probe for physics beyond the standard model of electroweak interactions providing the unique information about the lepton number non-conservation, existence and nature of neutrino mass and many other fundamental aspects of particle physics. In connection with $0\nu\beta\beta$-decay the detection of double beta decay with the emission of two neutrinos is also of great importance since it enables the experimental determination of nuclear matrix elements involved in double beta decay processes.

In order to search for double beta decay of $^{100}$Mo with a novel technique a multisectional liquid argon ionization chamber was suggested [1]. The experiment was installed in Gran Sasso Underground Laboratory in 1996.

The experimental setup consists of a liquid argon ionization chamber placed in passive shielding (15cm of lead), gas system, electronics and data acquisition system. The active detection portion of the chamber is composed of alternating circular planes of anodes and

cathodes with screen grids placed between them. The cathodes are made of molybdenum foil approximately 50 mg/cm$^2$ thick. The chamber contains 14 cathodes, 15 anodes and 28 screening grids. The grid anode distance is 5.5 mm and the grid-cathode is 14.5 mm. The sensitive volume's diameter is 30 cm and its height is 56 cm. Each anode is connected to a charge-sensitive preamplifier, followed by an amplifier and a shaper. Shaped and unshaped signals are digitized by two 8-bit flash ADC with the 50 ns sampling time. Unshaped pulse analysis gives the space information of events. The trigger for data collection requires that at least one anode signal exceeds the threshold ( 700 keV). Each trigger causes digitized signals from all anodes to be written to a data tape. The more detailed description of the experimental setup can be found in previous Annual Reports [2, 3, 4].

# 2 Collaboration activity in 1999

In the last year DBA collaboration has made a notable progress in the detector hardware upgrade as well as in data taking and analysis. The main features of the experimental activity in 1999 are listed below.

- Total mass of $^{100}$Mo has been increased up to 306 grammes. The measurements have been done with this mass of enriched isotope which is more than double of the isotope mass used before.

- Heating system maintaining the temperature of liquid argon has been redone so as to get rid of the electronic noise due to this system. This made it possible to reduce significantly detector dead time.

- Remote slow control facilities for the most essential detector parameters such as pressure in the fiducial volume and liquid nitrogen level in the detector's cryostat have been included in experimental setup.

- Liquid nitrogen refilling system (LN2) has been also modified. The very low continuous flux of LN2 going through the pipe-line in the detector cryostat was used instead of batch operation mode with periodical filling. It reduces the manpower needed to maintain the detector during the measurements and improves the measurement/maintenance time ratio.

- Neutron passive shielding has been developed and is being constructed. It will consist of 25 cm of water for neutron thermalisation and 1 cm of boron acid ($H_3BO_3$) to capture the thermal neutrons. The resulting gamma radiation will be captured by passive shielding of lead. Preliminary calculations show that this shielding can reduce the background due to the (n,$\gamma$) reactions in the fiducial volume in two orders of magnitude.

- 1355 hours of data taking were done. The results have been analysed and they are presented below.

# 3 Experimental results

The chamber has been assembled with eight cathodes containing enriched $^{100}$Mo and six cathodes with natural molybdenum. This configuration is optimal to provide background subtraction for two-neutrino double beta decay measurement. Experimental run have

been performed with electric fields of 1.93 kV/cm for the cathode-grid gap and 3.64 kV/cm for the anode-grid gap. The chamber filled with liquid Ar has been calibrated by $^{22}$Na (1275 keV) and $^{88}$Y (1836 keV) radioactive sources. Extrapolation gives the energy resolution (FWHM) of 6% at the energy of $^{100}$Mo double beta decay transition (3033 keV). The total measurement time was 1355 hours. The single electron spectrum used to explore $^{42}$Ar content is shown in figure 1.

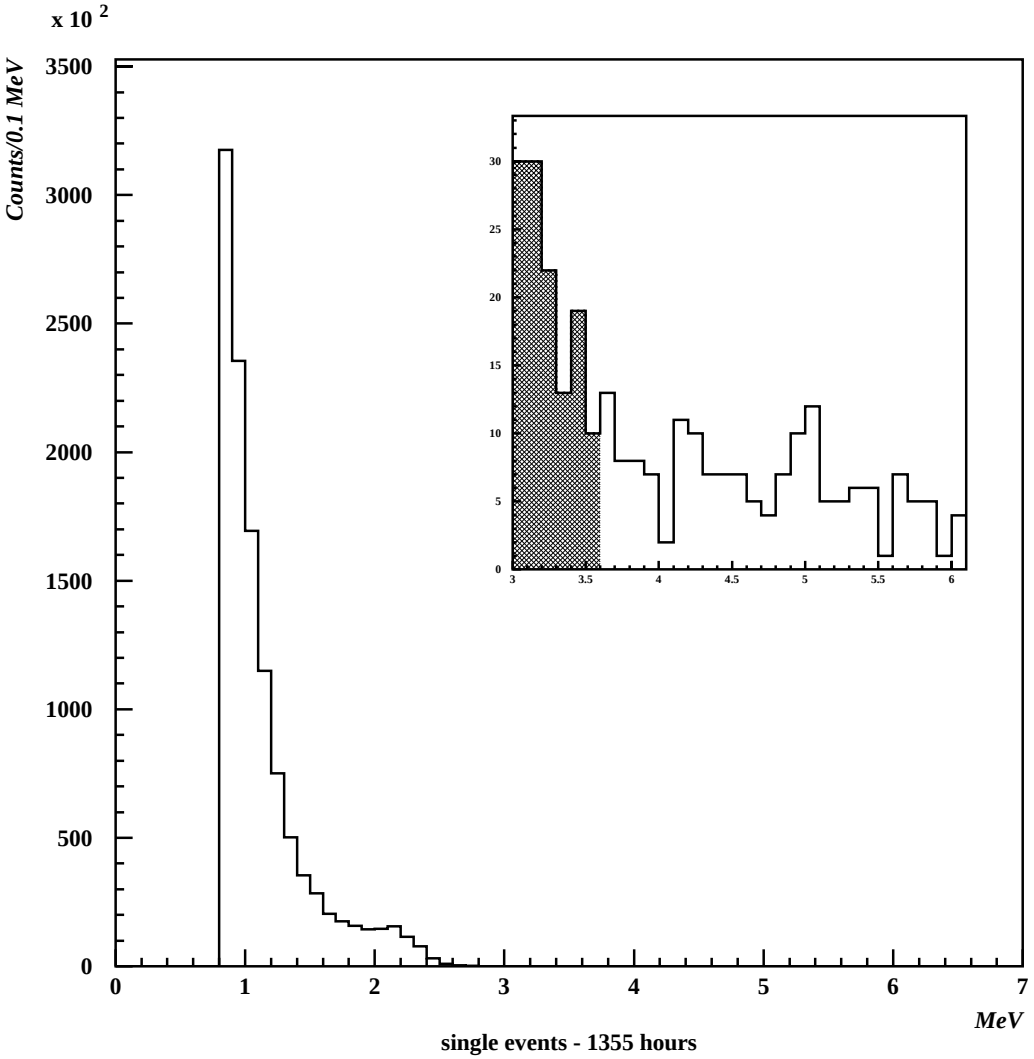


Figure 1: The single electron spectrum.

To search for double beta decay we select so called "double" events when signals appear in two neighbouring channels and when there are no signals in other 13 channels. In addition, we choose the time difference between the maxima of the pulses $< 0.6\mu$s. The detection efficiency for each decay mode was calculated in a GEANT-based MC program. In the off-line analysis we used the combined results from the last and previous (1998) experimental runs. This corresponds to the 458 kg*hours and 303 kg*hours of

measurements with enriched and natural molybdenum respectively (fig. 2). Considered individually below are various types of the decay processes under study.

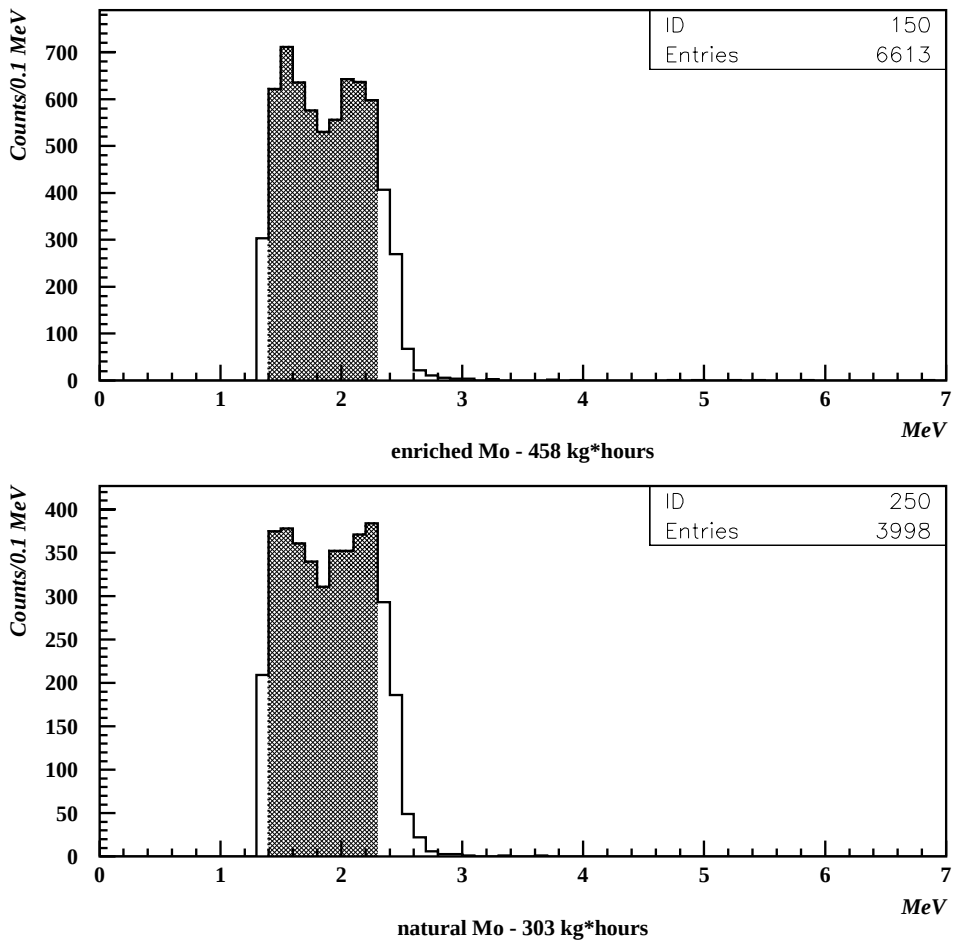


Figure 2: Spectra of double electron events

## 3.1 $0\nu$-decay

A loss of the detection efficiency due to pulse shape analysis applied to the high energy events and software cuts of 1 MeV for single electrons are well compensated by the background reduction factor in the $^{100}$Mo $0\nu\beta\beta$ energy region. Three events in the enriched foils and three events in the natural ones were detected in the energy interval of $2.8 - 3.1$ MeV. Taking into account the efficiency of 6.9% and assuming Poisson distributions for the numbers of true, observed and estimated background counts, one can obtain a limit on the $0\nu$ decay of $^{100}$Mo, $T_{1/2} > 6.4(3.4) \cdot 10^{21}$ y at 68%(90%) C.L.

### 3.2 $0\nu\chi^0$-decay

The energy interval of $2.3 - 3.0$ MeV was investigated. 783 events were recorded for enriched Mo foils. Taking into account the difference of masses natural Mo foils gave 843 events, i.e. there was no excess of double events in the enriched foils. Using the efficiency value of 5.7% we obtained the limit, $T_{1/2} > 2.8(2.2) \cdot 10^{20}$ y at 68%(90%) C.L.

### 3.3 $2\nu$-decay

The best signal-to-background ratio according to MC calculations was found in the energy interval of $1.4 - 2.3$ MeV. The off-line analysis applied to this energy region (figure 2) gives more than $6.2\sigma$ of effect due to the $2\nu$ decay of $^{100}$Mo. Background subtraction leads to the final value of the effect, $636 \pm 102$ events. Using the calculated detection efficiency of the $2\nu\beta\beta$ decay of $^{100}$Mo (2.2%) one gets the half-life:

$T_{1/2} = [0.68 \pm 0.11(stat) \pm 0.07(syst)] \cdot 10^{19}$ y.

### 3.4 $^{42}$Ar content

The spectrum of single electrons (figure 1) was used to obtain the limit on radioactive $^{42}$Ar contamination of natural argon contained in the operating volume. During 1355 hours of counting 124 events were obtained in the energy range of 3 to 3.6 MeV to be compared with 41 events collected for 440 hours in the previous measurements [5]. The values are in good agreement and lead to the same limit, $^{42}\mathrm{Ar}/^{nat}\mathrm{Ar} < 6 \cdot 10^{-21}$. According to the MC simulations the main contributions in counting above 3 MeV can be due to $^{42}$Ar, (n,$\gamma$) reactions from external neutron background or $\beta$-decay of $^{214}$Bi in the fiducial volume of the detector. In particular, the neutron background is clearly seen now at the high energy edge of spectrum. Passive shielding of water and boron acid installed around the lead shielding will strongly reduce this type of background and will allow to reach the higher sensitivity to $^{42}$Ar.

## 4 Discussions and prospects

Two neutrino double beta decay of $^{100}$Mo has been firmly detected ($> 6\sigma$ of effect). It was demonstrated that only 3 months of data taking will allow to measure $2\nu\beta\beta$-decay of $^{100}$Mo with accuracy of 10-12%.

In [6] it was proposed that the difference in the decay rate in $2\nu\beta\beta$ process at "present" (direct counter experiments) and in the "past" (geochemical experiments) can be explained by the time variation of the weak interaction constant. It was pointed out that $^{100}$Mo is one of the best candidate to check this hypothesis because it has the maximum rate of decay and quite high concentration of the $^{100}$Mo (9.6%) in the natural molybdenum. Besides, the $^{100}$Ru arised due to the $2\beta$-decay of $^{100}$Mo will be kept in minerals. Therefore measuring the half-life of the $2\nu\beta\beta$ decay of $^{100}$Mo with accuracy down to 10% or better is of great interest and importance given also that two most accurate modern results for $^{100}$Mo give the different values of its half-life [7, 8].

It is expected that $H_2O/H_3BO_3$ passive shielding will reduce the neutron background in two orders of magnitude. If the count rates in the $0\nu$ energy range are mainly due to neutron background, 4 months of counting with this shielding will make it possible to reach the sensitivity to $0\nu$ decay at the level of the best present experiments with $^{100}$Mo. In this case one year of measurements will increase the sensitivity to $0\nu$- and $0\nu\chi^0$-modes to the level of $(1-2)\cdot 10^{23}$ y and $(1-2)\cdot 10^{22}$ y respectively. However, if $^{42}$Ar content in the Earth's atmosphere is more than $10^{-21}$ g/g it will limit the sensitivity of the experiment to $0\nu$ decay. At the same time the $^{42}$Ar content will be carefully investigated and determined. Furthermore $^{42}$Ar production mechanism in the atmosphere will be understood. We plan also to develop a method for identifying the background from $^{42}$Ar in the future argon-based low background detectors operating at low energy.

# 5 Acknowledgements

We would like to thank M. Balata for providing the liquid nitrogen system and fruitfil discussions. We are also very grateful to L. Marrelli, B. Romualdi, A. Rotilio and E. Tatananni for frequent technical support. The portion of this work was supported by the INFN (Italy) and the Russian Foundation for Basic Research under grant 97-02-17344.

# 6 Publications and Conferences in 1999

1. V.D. Ashitkov et al., Yadernaya Fisika 62 (1999) 2217.

# References

[1] A.S. Barabash et al., preprint ITEP-154 (1986).

[2] V.D. Ashitkov et al., INFN-LNGS Annual report 1996, 143

[3] V.D. Ashitkov et al., INFN-LNGS Annual report 1997, 23

[4] V.D. Ashitkov et al., INFN-LNGS Annual report 1998, 29

[5] V.D. Ashitkov et al., Nucl. Instr. Meth. A416 (1998) 179.

[6] A.S. Barabash, JETP Lett., 68 (1998) 1.

[7] D. Dassie et al., Phys. Rev. D 51 (1995) 2090.

[8] A. De Silva et al., Phys. Rev. C 56 (1997) 2451.

# EAS-TOP. Cosmic Rays Experiment

M. Aglietta[a,b], B. Alessandro[b], P. Antonioli[c], F. Arneodo[d], L. Bergamasco[b,e], M. Bertaina[b,e], C. Castagnoli[a,b], A. Castellina[a,b], A. Chiavassa[b,e], G. Cini Castagnoli[b,e], B. D'Ettorre Piazzoli[f], G. Di Sciascio[f], W. Fulgione[a,b], P. Galeotti[b,e], P.L. Ghia[a,b], M. Iacovacci[f], G. Mannocchi[a,b], C. Morello[a,b], G. Navarra[b,e], O. Saavedra[b,e], G. C. Trinchero[a,b], P. Vallania[a,b], S. Vernetto[a,b], C. Vigorito[b,e], S. Valchierotti[b,e]

[a] Istituto di Cosmo-Geofisica del CNR, Torino, Italy
[b] Istituto Nazionale di Fisica Nucleare, Sezione di Torino, Italy
[c] Istituto Nazionale di Fisica Nucleare, Sezione di Bologna, Italy
[d] Istituto Nazionale di Fisica Nucleare, LNGS, Assergi, L'Aquila, Italy
[e] Dipartimento di Fisica Generale dell'Università di Torino, Italy
[f] Dipartimento di Scienze Fisiche dell' Università and INFN, Sezione di Napoli, Italy

**Abstract**

The status of the EAS-TOP experiment, the activity of the collaboration, and the main results obtained in 1999 are summarized. For a more complete view of the experiment refer also to the previous Annual Reports.

## 1 Introduction

The EAS-TOP array (Campo Imperatore, 2000 m a.s.l., $30^0$ with respect to the vertical of the underground Gran Sasso Laboratories) is operating with:

- the e.m. detector: 35 modules of scintillators, 10 $m^2$ each (8 of them equipped with vertical scintillators, to improve the response to Horizontal Air Showers), fully efficient for $N_e > 10^5$;

- the muon-hadron detector: 140 $m^2$ calorimeter with 9 layers of 13 cm iron absorbers and streamer tubes as active elements, operating for hadron calorimetry at $E_h > 50$ GeV, and for muon counting at $E_\mu > 1$ GeV (two vertical walls made of streamer tubes operate at the North and South sides of the detector; 130 $m^2$ scintillator muon detectors are distributed in the field ), and 40 $m^2$ RPC muon detector below the bottom layer, for timing measurements (to test the "Time Track Compatibilty" method for reconstructing the EAS longitudinal profile [1] );

[1] *Collaboration with: M. Ambrosio, C. Aramo, G. Battistoni, R. Fonte, A. Grillo.*

Figure 1: *Aerial view of part of the EAS-TOP array during winter time. The e.m. modules are visible out of the snow; the muon detector is located inside the shed on top of the picture.*

- the Cherenkov light detector: 8 telescopes with tracking capabilities equipped with imaging photomultipliers and wide angle optics, with full opening angles: 15 and 60 degrees (QUASAR, in cooperation with the TUNKA group of Institute for Nuclear Physics of Moscow State University [2] );

- three radio antennas for EAS radio emission measurements;

- moreover it operates in coincidence with the underground MACRO and LVD muon detectors ($E_\mu > 1.3$ TeV; full area $A_\mu^{TeV} \approx 1000$ m$^2$).

An aerial view of part of the array is shown in fig. 1.

The display of an event as observed in the muon tracking and scintillator detectors is shown in figs. 2 and 3 respectively (in fact this is a peculiar event, at a zenith angle $\theta \approx 75^o$, see the HAS section).

Main aims of the experiment are of:

- contributing to construct the experimental knowledge of cosmic radiation in the energy range $10^{13} - 10^{17}$ eV (i.e. around the "knee" of the primary spectrum), through all the available observables: spectra, composition, anisotropies, gamma-ray primaries;

- performing multiparametric analysis, also exploiting the unique possibility of surface and deep underground measurements, which is essential for the debugging of the "interaction-composition-fluctuation" problem in the understanding of EAS data, through the interpretation of a subset of individual events;

- checking the main features of the high energy hadron interactions relevant for the interpretation, and the extrapolation to higher energies of the models elaborated from the accelerator data;

- providing significant informations to interpret the deep underground data.

[2] *Collaboration with: A.M. Hillas, H. Korosteleva, L. Kuzmichev, B. Lubsandorjev, V. Prosin.*

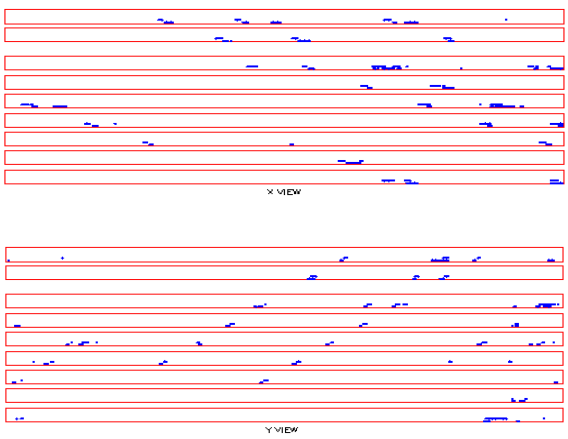


Figure 2: *Muon detector: hits from muon tracks seen on orthogonal projections. The drawing is not on scale: dimensions are 12 m in lengths, 3 m in height.*

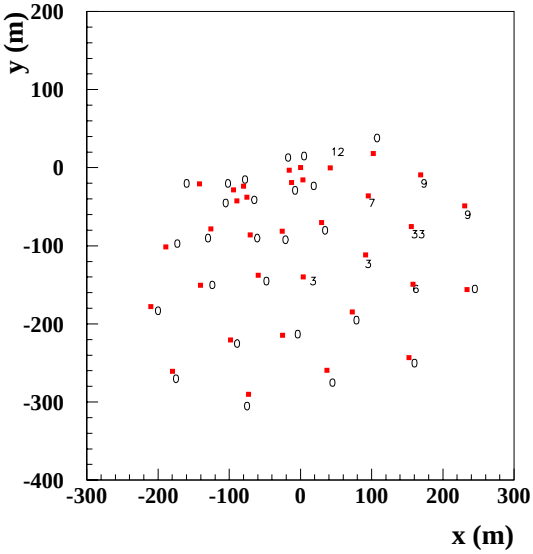


Figure 3: *Scintillator detector: number of equivalent vertical m.i.p.s in each module.*

EAS-TOP has reported results on:

- the characteristics of Extansive Air Showers in their different components: e.m., muon, atmospheric Cherenkov light;

- the structure of the e.m., and muon size spectrum in the region of the knee, with derivation of information on the primary energy spectrum and composition;

- the hadron flux and spectrum ($0.05 < E_0 < 5$ TeV) at mountain altitudes;

- some features of hadronic interactions (proton-nucleus) at energies $E_0 > 10^{15}$ eV that can be measured through the EAS data (inelastic cross section, large $P_t$ jet production);

- hadronic interactions and primary composition from the e.m. observations and the GeV and TeV muon data (in collaboration with MACRO and LVD);

- gamma ray and anisotropies at $E_0 = 5.10^{13} - 10^{14}$ eV;

- the nature of the Extensive Air Showers observed in very inclined directions ($\theta > 75^0$, HAS), and upper limits to the UHE cosmic neutrino flux.

Most of these measurements have been discussed in previous issues of these Reports, in the present one we will summarize the main results achieved in 1999 or on which significant developments have been obtained. On other items the statistics does not allow conclusions or significant progresses at the moment. They will be concluded when full experimental statistics will be available.

The experiment results from a collaboration between INFN and CNR (Istituto di Cosmo-Geofisica, Torino).

## 2 The studies of the *knee*

The shower size and muon size spectra around the knee are shown in figs. 4 and 5.

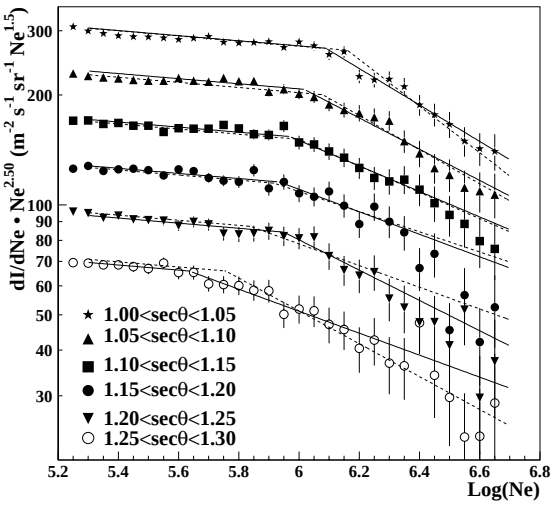


Figure 4: *Differential shower size spectra measured at different zenith angles (i.e. atmospheric depths).*

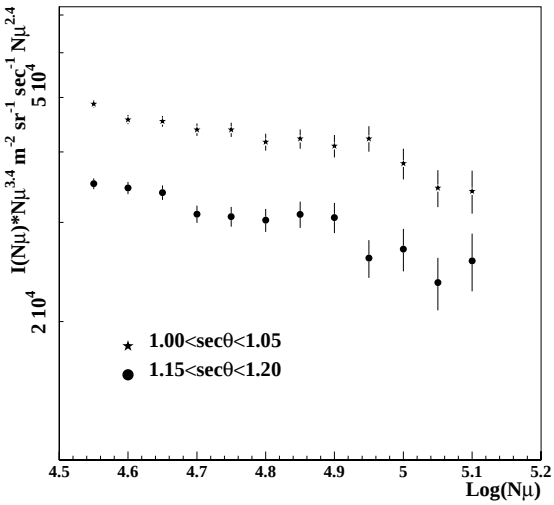


Figure 5: *$N_\mu$ spectra measured in two different intervals of zenith angles (i.e. atmospheric depths).*

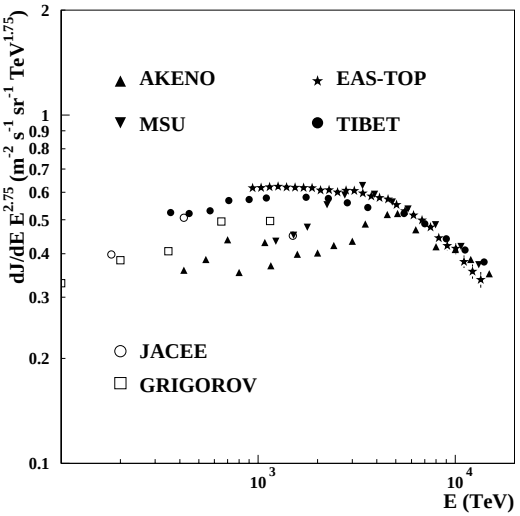


Figure 6: *The all particle energy spectrum obtained from the EAS-TOP shower size data, compared with the results of other experiments operating outside the atmosphere or at ground level.*

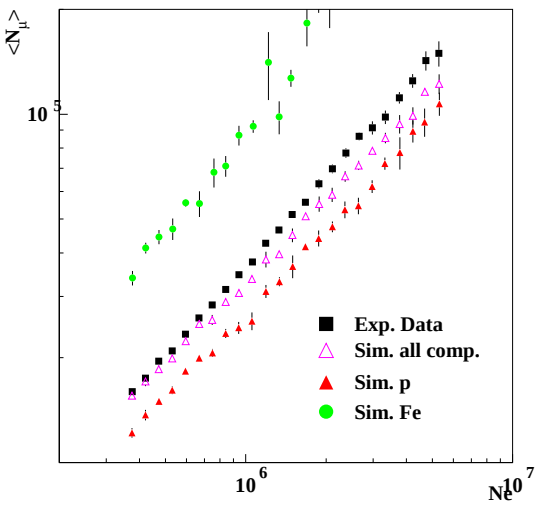


Figure 7: *$N\mu$ vs $Ne$ relation for experimental data and a composition with the same slope ($\gamma = 2.75$) for all components. Pure proton and pure iron simulated data are also plotted.*

A paper on the $N_e$ spectrum has been published in Astroparticle Physics, reporting the first observation of the dependence of the shower size at the knee on the atmospheric

depth (i.e. zenith angle), and thus proving that the observed spectral break is a real effect characterized by a given primary energy.

Table 1: *Parameters of the Ne spectra in different intervals of zenith angles.*

| $\Delta \sec\theta$ | $\gamma_1$ | $\gamma_2$ | $I(>Ne_k)\times 10^7$ $\mathrm{m^{-2}\ s^{-1}\ sr^{-1}}$ | $Log(Ne_k)$ |
|---|---|---|---|---|
| $1.00-1.05$ | $2.56\pm0.02$ | $2.99\pm0.09$ | $0.99\pm0.2$ | $6.09\pm0.05$ |
| $1.05-1.10$ | $2.55\pm0.02$ | $2.93\pm0.11$ | $1.01\pm0.3$ | $6.02\pm0.07$ |
| $1.10-1.15$ | $2.55\pm0.03$ | $2.85\pm0.12$ | $0.93\pm0.4$ | $5.97\pm0.08$ |
| $1.15-1.20$ | $2.56\pm0.03$ | $2.81\pm0.16$ | $0.80\pm0.4$ | $5.93\pm0.14$ |
| $1.20-1.25$ | $2.59\pm0.03$ | $2.91\pm0.26$ | $0.52\pm0.3$ | $5.95\pm0.11$ |
| $1.25-1.30$ | $2.55\pm0.07$ | $2.80\pm0.11$ | $1.30\pm0.6$ | $5.63\pm0.12$ |

Table 2: *Parameters of the $N\mu$ spectra in different intervals of zenith angles (the analysis is performed in terms of $\rho_\mu^{r=150m}$; here $N_\mu$ is given for easier comparison, by using the average l.d.f.).*

| $\Delta \sec\theta$ | $\gamma_1$ | $\gamma_2$ | $I(>N\mu_k)\times 10^7$ $\mathrm{m^{-2}\ s^{-1}\ sr^{-1}}$ | $Log(N\mu_k)$ |
|---|---|---|---|---|
| $1.00-1.05$ | $3.18\pm0.07$ | $3.44\pm0.10$ | $1.32\pm0.3$ | $4.66\pm0.10$ |
| $1.05-1.10$ | $3.23\pm0.15$ | $3.40\pm0.12$ | $1.03\pm0.3$ | $4.62\pm0.10$ |
| $1.10-1.15$ | $3.20\pm0.07$ | $3.34\pm0.12$ | $1.09\pm0.3$ | $4.65\pm0.12$ |
| $1.15-1.20$ | $3.12\pm0.10$ | $3.45\pm0.15$ | $1.28\pm0.3$ | $4.60\pm0.10$ |

The characteristics of the two spectra, below and above the knee, are shown in tables 1 and 2, demonstrating the consistency: i) of the observed intensities at $E_k$ (again proving the reality of the break) and ii) of the spectral slopes (the expected relation between $\gamma_e$ and $\gamma_\mu$ is: $\frac{\gamma_e-1}{\gamma_\mu-1}=\alpha$, where $\alpha$, exponent of relation $N_\mu \propto N_e^\alpha$, is measured and predicted from interaction models: $\alpha\approx 0.8$).

In figs. 6 and 7 the primary energy spectrum and the $N_e-N_\mu$ relation in the knee region, providing information on the primary composition, are shown. Following the main interaction models (CORSIKA-HDPM in fig. 7) the $N_e-N_\mu$ relation leads to a composition becoming heavier in the energy range $E_0=10^{15}-10^{16}$ eV. The sensitivity of the $N_e-N_\mu$ measurement to primary composition and the reliability of the interaction models have been checked by correlated measurements with the underground detectors. A better statistics is necessary to improve the confidence level of such consistency check. All data will be upgrated when the full statistics of the experiment will be available.

# 3 Gamma-ray Astronomy

A search for possible gamma-ray transient sources has been completed over the whole visible sky, also in coincidence with the Baksan Air Shower Array, which is located at similar latitude, and shifted in longitude of about $30^o$. The search is motivated by the

observation of the transient from the Crab Nebula on February 23, 1989 by the Baksan, KGF and EAS-TOP arrays, and the recent detection of flaring activities of AGNs by atmospheric Cerenkov Light detectors. The excellent operation of the detectors (at a statistical level of fluctuations) has been proved. No statistically significant excess has been found. An interesting episode from Mrk421 has been pointed out: the second most significant daily excess observed from Baksan coincides with the most significant one in EAS-TOP. The chance imitation rate of the effect is 0.01, still not stringent enough to derive firm conclusions.

The EAS-TOP analysis has been extended to Supernova Remnants: to check the hypothesis that they can be responsible of the acceleration of galactic cosmic rays. A limit to the power law spectrum in the energy range between a few GeV (EGRET data) and 50 TeV: $\gamma > 2.1$ is obtained.

## 3.1 EHE clusters of events

UHE gamma-ray astronomy can be a powerful tool for the study of EHE cosmic ray origin.

47 EHE cosmic rays above $4 \cdot 10^{19}$ eV (i.e. GKZ cutoff) have been observed by the AGASA experiment (Takeda et al., 1999). A clustering effect has been probably detected, into one triplet and three doublets. The corresponding directions have been searched for UHE $\gamma$-ray emission in two data sets (fourfold: L.E. triggers, and sevenfold internal events: H.E. triggers, see tab. 3).

| Source | $E_{typ}$ [TeV] | $N_{ON}$ | $N_{<OFF>}$ | S | $\Phi_{d.c.}$ [cm$^{-2}$ s$^{-1}$] |
|---|---|---|---|---|---|
| doublet (a) | 25 | 8481683 | 8478596 | +1.0 | $2.6 \cdot 10^{-13}$ |
| $<\delta>=20.6°$, $<\alpha>=18.6°$ | 120 | 202364 | 203041 | -1.4 | $4.2 \cdot 10^{-14}$ |
| doublet (b) | 25 | 15684665 | 15684431 | +0.1 | $1.4 \cdot 10^{-13}$ |
| $<\delta>=48.1°$, $<\alpha>=283.°$ | 90 | 301275 | 301750 | -0.8 | $3.3 \cdot 10^{-14}$ |
| doublet (c) | 25 | 12364070 | 12357264 | +1.8 | $2.6 \cdot 10^{-13}$ |
| $<\delta>=30.0°$, $<\alpha>=69.9°$ | 100 | 192058 | 191307 | +1.6 | $5.8 \cdot 10^{-14}$ |
| triplet | 25 | 14562977 | 14570775 | -1.9 | $1.1 \cdot 10^{-13}$ |
| $<\delta>=56.9°$, $<\alpha>=169.7°$ | 100 | 334472 | 334471 | 0. | $4.0 \cdot 10^{-14}$ |
| $\Sigma$ | 25 | 51093396 | 51091068 | +0.3 | $8.5 \cdot 10^{-14}$ |
| | 100 | 1030169 | 1030569 | -0.4 | $1.9 \cdot 10^{-14}$ |

Table 3: *Summary of the search for emission from EHE clusters: coordinates, typical primary energies, number of observed events on- and off-source, d.c. excess significances, 90% c.l. upper limits to the d.c. flux are given for L.E. and H.E. triggers.*

As shown in tab. 3 (where the mean directions are given), from none of them a significant excess is observed: 90% c.l. upper limits to the flux are given for each observed position and for the sum of all of them.
The lack of $\gamma$-ray signals at UHE provides constraints to the mechanisms of acceleration of EHE cosmic rays, both in the frame of "bottom-up" models and of "top-down" ones.

Concerning the latter, we consider the model of Blasi, 1999, in which the flux of UHE $\gamma$-rays is calculated from the decay of super-heavy relic particles clustered in the galactic

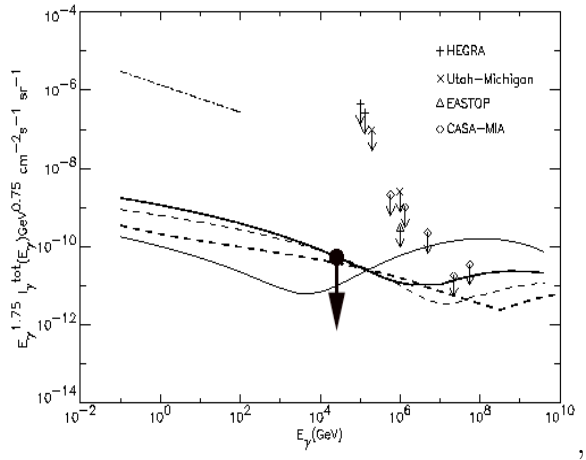


Figure 8: *Expected intensity of $\gamma$-rays from Blasi, 1999, for $m_X = 10^{14}$ GeV (thick lines) and $m_X = 10^{13}$ GeV (thin lines). The solid lines refer to SUSY-QCD fragmentation function and the dashed lines to ordinary QCD one. Crosses, triangles and diamonds indicate experimental upper limits to diffuse emission. Full dot and arrow represent the result of the present analysis.*

halo. If these particles cluster at the positions corresponding to the arrival directions of cosmic rays with energy $> 4\cdot 10^{19}$ eV, the diffuse intensity $I_\gamma$ would be concentrated in point-like $\gamma$-ray sources. We convert the upper limit $\Phi_\Sigma$ to $I_\gamma$ through expression: $I_\gamma = \Phi_\Sigma \cdot \frac{1}{4\pi} \cdot \frac{9}{47}$ cm$^{-2}$ s$^{-1}$ sr$^{-1}$. The limit obtained through L.E. triggers (not affected by absorption on low energy photons in space) is shown in fig. 8. In this frame, X-masses $m_X > 10^{14}$ GeV are excluded for ordinary QCD fragmentation function in hadron production.

Concerning conventional EHE cosmic ray acceleration, the clustering effect suggests the possibility of " nearby" sources ($D$ <30 Mpc) (Medina Tanco, 1999). The cosmic ray interactions in the source lead to a $\gamma$-ray flux (at $E_0 \approx 100$ TeV: $\frac{I_\gamma}{I_p} \approx 6\cdot 10^{-4} \times x$, where $x$ in g cm$^{-2}$ is the target thickness (1)). For our case, using as $I_p$ the extrapolation back to the 100 TeV region of the suggested and measured power law spectrum ($\gamma$=3), for the 3 events (over 47) of the AGASA triplet, from the limit of tab. 3 we obtain $\frac{I_\gamma}{I_p} < 3.3\cdot 10^{-7}$, i.e. comparing with expression (1), $x_{matter}^{source} < 5\cdot 10^{-4}$ g cm$^{-2}$. Concerning photons, from $\pi_0$ photoproduction we obtain: $x_{photon}^{source} < 1.5\cdot 10^{23}$ ph cm$^{-2}$ for $E_{ph} \approx$ KeV. The upper limit on matter column density sets a constraint to the dimension (d) of the proposed sources: $d < 1$ Mpc also for intergalactic matter density (excluding e.g. acceleration in sites as the core of Virgo cluster).

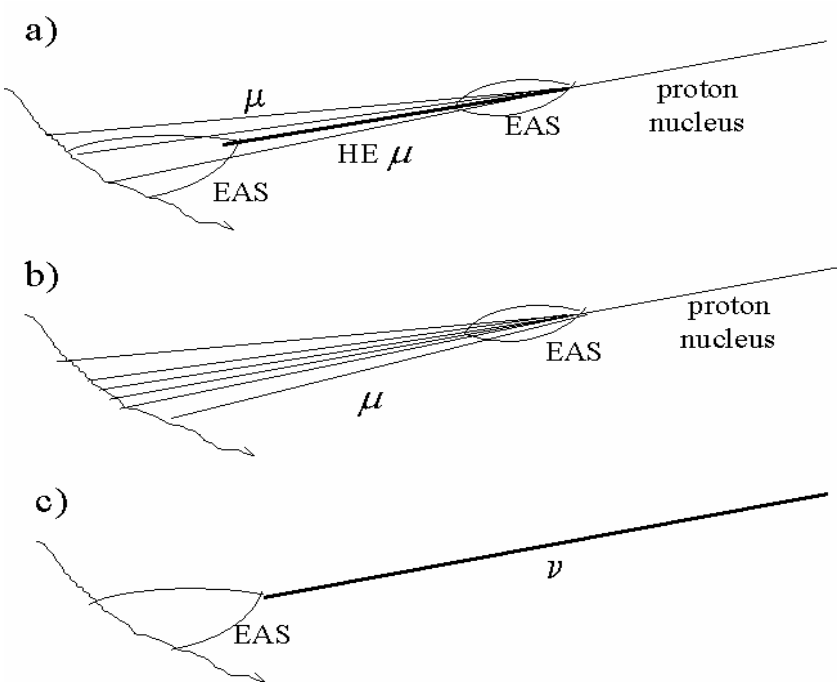


Figure 9: *Possible sources of Horizontal Air Showers: a) "local" high energy muon interactions, b) muon dominated showers, residuals from an UHE cosmic ray interaction at very large distance, c) neutrino events.*

# 4 The studies of HAS

The detection of EAS at very large zenith angles (HAS) can be a tool for the search of UHE neutrinos from cosmic ray sources. In fact such technique has been eploited by the EAS-TOP group and upper limits to the UHE $\nu - flux$ have been set. The events observed at zenith angles $\theta > 75^o$ constitute a background to such experiments and have never been fully understood, due to the difficulties of explaining their muon content (an example of such events is shown in figs. 2 and 3). We report here the main results of the related analysis at EAS-TOP.

Possible sources of such events are atmospheric muons and their interactions.

(a) High energy single muons can interact through bremmstrahlung (which dominate 10:1) or deep inelastic scattering and initiate showers at the appropriate depth for detection. Such showers are essentially electromagnetic, since the remnant muons from the initial shower (whose typical primary energy is not much larger than the muon one) are dispersed over a very large area (see fig. 9a).

(b) Ultra high energy cosmic rays interacting at the top of the atmosphere, at very large zenith angles (and therefore distances from the detector $l_d \approx 100$ km), produce a 'large' amount of muons, through the pion decays (favoured, at large angles, with respect to pion interactions due to the low atmospheric density at the interaction altitude). Such showers are therefore composed essentially of muons since the e.m. component is fully absorbed (see fig. 9b).

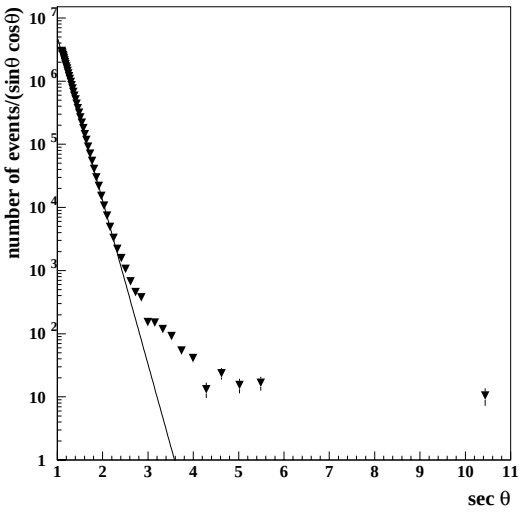


Figure 10: *The zenith angle distribution of a sample of EAS as measured by the EAS-TOP e.m. array.*

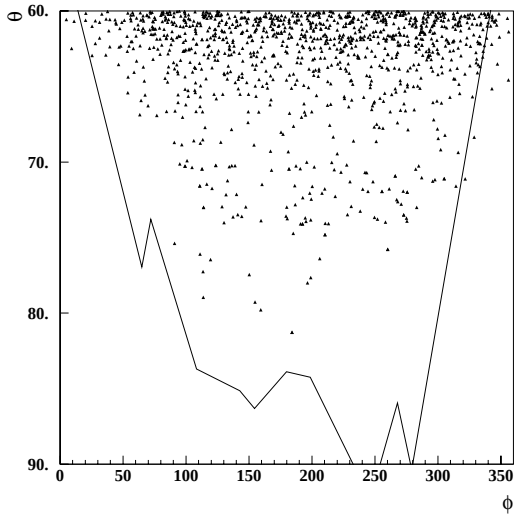


Figure 11: *Arrival directions of EAS and the mountain profile seen by EAS-TOP.*

Neutrino induced showers (fig. 9c) have some intermediate typology, being more similar to conventional Extensive Air Showers or to events (a), when a large amount of their energy is transferred to the electromagnetic cascade. Arrays must therefore have the possibility of discriminating between the different typologies of events through $\mu/e$ identification.

## 4.1 HAS: angular distribution and muon content

At zenith angles $\theta > 65°$ an excess of events (HAS) is observed above the rate of EAS as expected from their attenuation length in the atmosphere (see fig. 10).

The physical nature of the anomalous arrival directions of HAS is confirmed by the absence of events from the direction of the sky shaded by the top of the mountain on which the array is located (see fig. 11).

Moreover, the dependence of the barometric effect on zenith angle, shown in fig. 12. [3], clearly shows a deviation from the $sec\theta$ behaviour for $sec\theta > 2$. This can be explained by the presence of a "non-attenuated" EAS component that amounts to about 30% of the total EAS flux at 70°, and dominates at larger zenith angles.

The comparison of the zenith angle measurements of the scintillator and muon detectors is shown in fig. 13 (for such analysis, as well as in the following, a cut in the e.m. reconstruction $\chi^2 \leq 1$/d.f., introducing an efficiency $\epsilon \geq 85\%$ has been applied). The agreement of the two measurements is quite good, and the presence of events with $\theta \geq 75°$, which cannot be explained by errors in the angular reconstruction, is confirmed.

[3] *The barometric coefficient* $\beta = \frac{1}{n}\frac{dn}{dx}$ *( n = counting rate, x = atmospheric pressure) is related to zenith angle* $\theta$ *as:* $\beta(\theta) = \beta(0^0)sec\theta$.

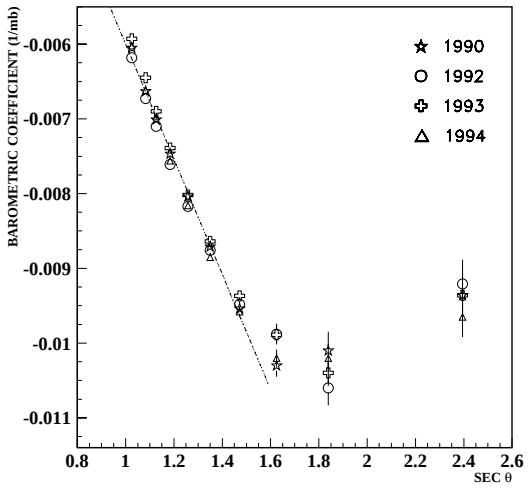


Figure 12: *Barometric coefficient for different zenith angles measured by* EAS-TOP.

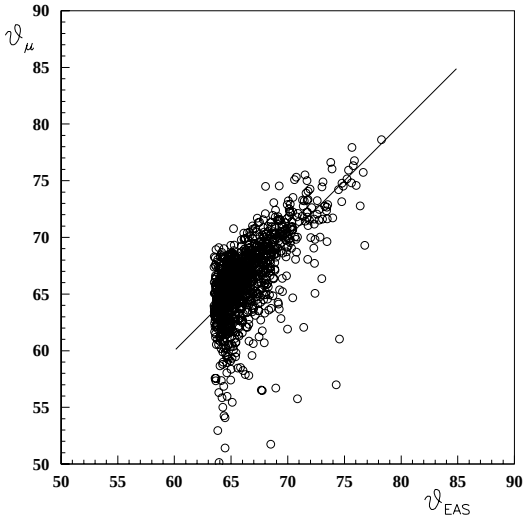


Figure 13: *Scatter plot of the event directions obtained by the e.m. and muon detectors.*

In 575 common observation days of the two detector, 37 events have been recorded with $\theta \geq 75°$. Very few of such showers have a negligible content of muons (2 over 37 have zero muons in the $\mu$-detector) i.e. could be $\mu$-poor as expected for $\mu$ induced showers in the atmosphere (events quoted (a)). In fact they correspond to events with rather low energy losses in the scintillators, compatible with the absence of muons in the tracking module respectively at 1. and 3.5 s.d.. For all other events, the muon density ($\rho_\mu \approx \bar{n}_\mu / A_\mu \approx 0.3$ muons m$^{-2}$) is comparable with the total density of charged particles measured by the scintillator modules (comparison is done by using the data of scintillators located at the same distance as the muon detector from the module with highest recorded number of particles, assumed as approximate shower core location). The charged particle density as measured by the scintillator detector ($\Delta E / \Delta E_{m.i.p.}$) and the muon density measured by the tracking detector at the same distances from the shower axis are compared in fig. 14: all experimental points lay inside a $\pm 2$ s.d. interval around the 1 to 1 correlation line. This is expected from "pure" muon showers, indicating a marginal content of electrons.

## 4.2 Horizontal Muon Bundles (HMB)

HMB ($N_\mu \geq 3$ and $\theta \geq 75°$, selected through the trigger provided by the "vertical walls" on the South and North sides of the muon-hadron detector) have been detected during 474 observation days at a rate of 8.4 events day$^{-1}$. Their frequency distribution for different muon multiplicities is shown in fig. 15. These events can be easily interpreted as EAS originated at large distances in the atmosphere, in which the e.m. component has been completely absorbed and the remnant muons are observed.

The expected rate of such events has been calculated by using a simulation code to

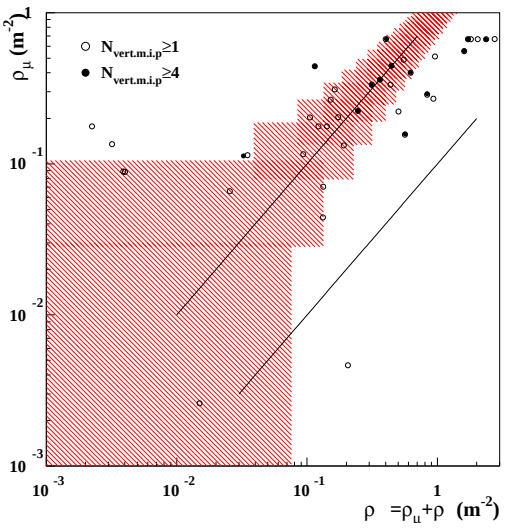


Figure 14: *Particle density as measured by the scintillator and tracking detectors. 1 s.d. error boxes are shown. $\rho_\mu$ is "saturated" at 0.7 m$^{-2}$. Empty (full) symbols represent events at 1 (4) vertical m.i.p. level. The $\rho_\mu = 0.1\rho_{ch}$ line is also shown: hadron and neutrino initiated showers are expected to populate the region at the right of such line.*

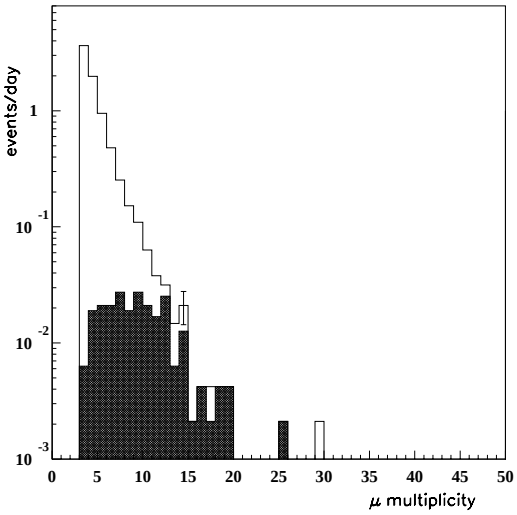


Figure 15: *Rate of Horizontal Muon Bundles of different multiplicities. The shaded area corresponds to events in coincidence with the e.m. detector.*

propagate very inclined Extensive Air Showers in the atmosphere (CORSIKA-QGSJET). Inside the uncertainties on the primary spectrum and composition, the experimental event rate and multiplicity distribution can thus be fairly well explained. It appears that events with detected muon multiplicities $N_\mu \geq 10$ are due to primaries with typical energy $E_0 \approx 10^{17}$ eV, detected at core distances $r \approx 500$ m, the total muon number for such events being $N_\mu \geq 10^4$.

The dashed istogram of fig. 15 represents the events which fire the scintillator trigger too. It is interesting to notice that, as the muon multiplicity increases, the two experiments (HAS and HMB) coincide. For $N_\mu \geq 10$ about 50% of HMBs could be as well considered HASs: the muon triggers include the scintillator triggers. This means that very large zenith angle muon bundles are mostly responsable for the excess of events in the EAS angular distribution (HAS). For smaller muon multiplicities the density threshold in the individual scintillator ($\rho_{th} \approx 0.2$ m$^{-2}$) reduces, as expected, the scintillator trigger rate.

The muon content of scintillator triggered events (showing that the muon density includes the total density of the ionizing components), and the rate of muon bundle triggers (that for large enough muon densities correspond to the scintillator triggers) lead to the conclusion that HAS are largely dominated by muon showers, i.e. events quoted (b) in fig. 9. The e.m. component in such case is essentially due to local muon interactions with small energy losses (delta rays, direct pairs).

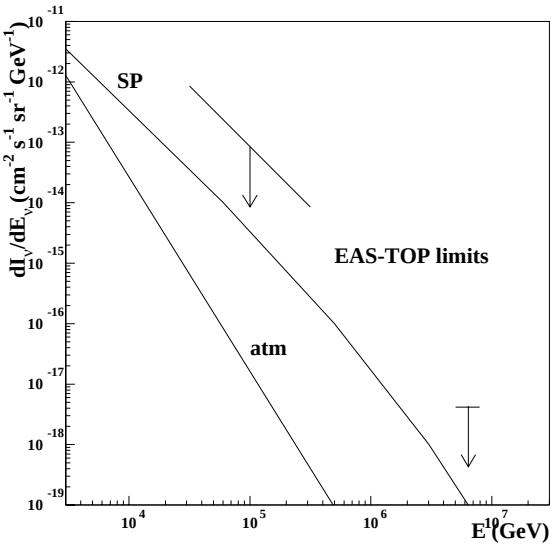


Figure 16: *Upper limits to the intensity of the cosmic neutrino flux obtained from the EAS-TOP HAS analysis. 'SP' represents the expected flux from Szabo and Protheroe, 'atm' the flux of neutrinos produced by cosmic ray interactions in the atmosphere.*

UHE cosmic neutrinos produce showers with muon content "lower" or "similar" to ordinary cosmic ray showers. In fig. 14 a $\rho_\mu = 0.1\rho_{\mu+e}$ line is drawn, as an upper limit to the muon content of cosmic ray hadron, and therefore neutrino induced showers. Also in fig. 14 the muon density vs. (muon+electron) density is shown for events with energy losses triggering the scintillators above the 1 effective particle level at $\theta \geq 75^0$. For none of such events the quoted limit is exceeded, i.e. the e.m. component is 10 times larger than the muon one, as would be expected also for neutrino induced events. From such upper limit in the 575 days of common operation of the muon and e.m. detectors, we derive as upper limit to the diffuse neutrino intensity (at 90 % c.l.):

$$I_\nu(E_\nu > 10^5 GeV) < 8.5 \times 10^{-9} cm^{-2} s^{-1} sr^{-1}. \quad (1)$$

For the differential flux in the energy range $E_0 \approx 10^5$ GeV, and for a spectrum $S(E_\nu) \propto E_\nu^{-2}$ we obtain the upper limits shown in fig. 16:

$$\frac{dI_\nu}{dE_\nu} < 8.5 \times 10^{-14} (\frac{10^5}{E_\nu})^2 cm^{-2} s^{-1} sr^{-1} GeV^{-1} \quad (2)$$

and for resonant events (for $E_{\bar{\nu}_e} = 6.4 10^6$ GeV):

$$\frac{dI_{\bar{\nu}_e}}{dE_{\bar{\nu}_e}} < 4.3 \times 10^{-18} cm^{-2} s^{-1} sr^{-1} GeV^{-1}. \quad (3)$$

# 5 High energy interaction data in p-N collisions

The study of the two aspects on p-N collisions discussed in the previous Report has been pursued:

i) concerning the p-Air total inelastic cross section, improved statistics of the simulations still provide better agreement of experimental data with models predicting longer attenuation length in the atmosphere (HDPM and VENUS), and, at $2.10^6 < E_0 < 4.10^6$ GeV, a value of $\sigma_{in}^{p-Air} < 400$ mb, i.e. lower than would be expected from previous EAS experiments (Akeno, Fly's Eye);

ii) concerning large $P_t$ jet production, the analysis has been completed, and the value of $\alpha$ of relation: $(\frac{d\sigma}{dp_t})_{pN}^{jet} = A^{\alpha}(\frac{d\sigma}{dp_t})_{pp}^{jet}$, $\alpha = 1.55 \pm 0.07$ (representing the entity of the *Cronin effect*) is confirmed to be constant between $\sqrt{s} \approx 30$ GeV and $\sqrt{s} \approx 500$ GeV. A paper has been published in Physics Letters B.

# 6 Gamma-rays and ionizing component during thunderstorms

A monitoring measurement of the temporal variations of environmental airborne radionuclides and secondary cosmic rays due to atmospheric effects has been performed in collaboration with SAO and TESRE CNR Institutes (Bologna) [4]. In order to study a wide energy range both a NaI scintillator detector, sensitive to gamma-rays of energy $E >$100 KeV, and the EAS-TOP air shower array, operating in single particle mode and in coincidence mode (i.e. EAS mode) have been used. In the following we will mainly discuss a peculiar event, occurred during conditions of perturbed weather on July 11, 1996.

The NaI detector consists of a cylindrical NaI(Tl) monocrystal (10×20⊘ cm) with sides and bottom shielded by 1.0 cm Pb, 0.2 mm Cu and 0.3 mm Al. The following data sets have been obtained:

*a)* Counting rate per minute in the energy range 0.4 - 20 MeV (referred here as "Ratemeter", and including both radioactivity and secondary cosmic rays);

*b)* Counting rate per hour in the energy range 0.1-2.8 MeV (radioactivity + secondary cosmic rays);

*c)* Counting rate per hour in the energy range 3-10 MeV (secondary cosmic rays); these data being corrected for the atmospheric pressure effect, the barometric coefficient being $\beta = -(0.50 \pm 0.04)\%$/mbar.

In a few occasions of perturbed weather significant increases in the counting rates have been observed in all data sets. In fig. 17 the event under discussion is shown. The Ratemeter (data *a*) shows a fast increase, lastings about 10 minutes, of magnitude exceeding 20%, superimposed to a slower and smoother one, lasting a few hours. It is interesting to note the different behaviours of the hourly counting rates in the two different energy ranges: between 0.1 and 2.8 MeV (data *b*) it follows the Ratemeter curves, while in the 3-10 MeV range (data *c*) the increase occurs only at the time of the first peak,

[4] *M. Brunetti, D. Cattani, S. Cecchini, M. Galli, G. Giovannini, A. Pagliarin.*

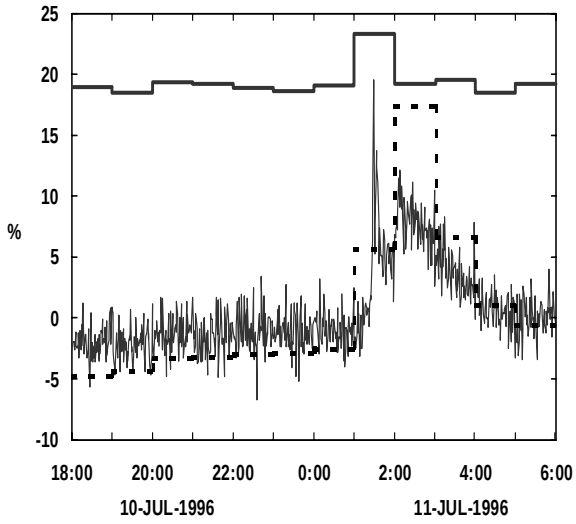


Figure 17: *NaI scintillator data during the July 11 event. Thin line: percent increase of the counts per minute at energy $E > 0.4$ MeV (ratemeter); thick dashed line: hourly counting rates in the energy range 0.1-2.8 MeV; thick countinuous line: hourly counting rate in the energy range 3-10 MeV.*

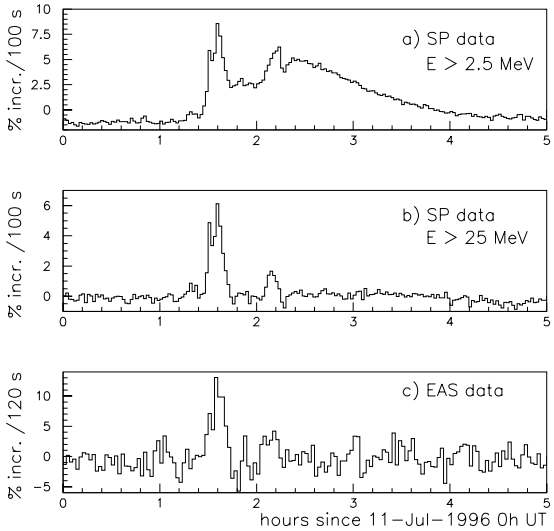


Figure 18: *EAS-TOP data during the July 11 event: a) percent increase of the single particle counting rate for detector energy E >2.5 MeV; b) single particle counting rate at E >25 MeV; c) Extensive Air Shower rate.*

showing that effects at different energies have different durations, and therefore can be of different origin.

The EAS-TOP data considered here are:

1) SP data: the single particle counting rate of individual scintillators;

2) EAS data: Extensive Air Showers generated by cosmic rays of energy $E \geq 50$ TeV, at trigger rate about 28 $s^{-1}$.

Each detector operates at an energy threshold $E_{th} = 3.0 \pm 0.5$ MeV. Ten out of the 35 detectors have an additional wooden cover that increases the energy threshold of charged particles to $E_{th} \sim 25$ MeV. The average SP counting rate is $n_c \sim 500$ and 400 $m^{-2}$ $s^{-1}$ respectively for "external" and "covered" detectors.

1) The SP counting rate is mostly due to secondary particles (muons and electrons) generated in the atmosphere by low energy primary cosmic rays.

In fig.18 (curves *a* and *b*), the SP counting rate of two EAS-TOP detectors are shown during the episode under discussion. Plot *a*, corresponding to an "external" detector, shows the same temporal behaviour as the Ratemeter, while plot *b* corresponding to a "covered" detector only shows two short duration peaks. These observations agree with the NaI detector data and confirm the difference in the energy range between long duration

and short duration increases.

2) Concerning EAS data, a significant excess in the air shower counting rate is observed in coincidence with the short duration peaks (see fig. 18c). During the first peak the increase reaches a magnitude of more than 10% and lasts about 10 minutes. All events recorded during the increase consist of well reconstructed air showers and show no unusual characteristics.

As possible explanations:

i) the "low energy" events could be related to the gamma ray emission from radioactive aerosols transported to the ground by the rain, as Radon daughters (that constitute condensation nuclei for raindrops);

ii) the "high energy" ones could be due to the effect of strong atmospheric electric fields on the propagation of the secondary cosmic rays particles.

The electric field could affect both the single muon and the electron component of EAS, and possibly modify the air shower counting rate: the EAS electrons can be accelerated by electric fields of magnitude $E_c >$ 1-2 KV cm$^{-1}$ and initiate an "avalanche" process producing more and more fast electrons by collisions with air molecules (Gurevich et al., 1999). This would increase the size of air showers and consequently increase the rate of events observed above a given detection threshold.

# 7 Collaborators and Institutions

M. Aglietta, B. Alessandro, V.V. Alexeenko, P. Antonioli, F. Arneodo, V.S. Berezinsky, L. Bergamasco, M. Bertaina, A. Campos Fauth, A. Castellina, C. Castagnoli, A. Chiavassa, G. Cini Castagnoli, B. D'Ettorre Piazzoli, G. Di Sciascio, W. Fulgione, P. Galeotti, A. Gazizov, P. L. Ghia, R. Granella, M. Iacovacci, L. B. Konstantinovich, L. Kuzmichev, A.S. Lidvansky, A. Lima de Godoi, G. Mannocchi, C. Melagrana, N. Mengotti Silva, C. Morello, G. Navarra, H. Nogima, L. Periale, P. Picchi, V.V. Prosin, L. Riccati, O. Saavedra, M. Serio, G. C. Trinchero, A. Turtelli, P. Vallania, S. Vernetto, C.Vigorito, S. Valchierotti

Technical staff: G. Giuliani, A. Giuliano, F. Gomez, G. Pirali

*Istituto Nazionale di Fisica Nucleare, Sezione di Torino, Torino, Italy*
*Istituto di Cosmo-Geofisica del CNR, Torino, Italy*
*Dipartimento di Fisica Generale dell' Università di Torino, Torino, Italy*
*INFN, Laboratori Nazionali del Gran Sasso, Assergi (AQ), Italy*
*Dipartimento di Scienze Fisiche dell' Università and INFN, Napoli, Italy*
*Istituto Nazionale di Fisica Nucleare, Sezione di Bologna, Bologna, Italy*
*Instituto di Fisica, Universidade Estadual, de Campinas, Campinas (SP), Brazil*
*Institute of Physics, National Academy of Sciences of Belarus, Minsk, Belarus*
*Institute for Nuclear Research, Russian Academy of Sciences, Moscow, Russia*
*Institute for Nuclear Physics, Moscow State University, Moscow, Russia*
*Universidade de Sao Paulo, Sao Paulo (SP), Brazil*

# 8 List of Publications

1. "The EAS Size Spectrum and the Cosmic Ray Energy Spectrum in the Region $10^{15} - 10^{16}$ eV"
   *Astroparticle Physics*, **10**, 1 (1999)

2. "Study of jet production in $p$-N interactions at $\sqrt{s} \approx 500$ GeV in EAS multicore events"
   *Physics Letters B*, **460**, 474 (1999)

3. "Search for high energy GRBs with EASTOP"
   *Astronomy and Astrophysics Suppl. Ser.*, **138**, 595 (1999)

4. "The cosmic ray anisotropy at $E_0 > 100$ TeV"
   *Adv. Space Res.*, **23**, 603 (1999)

5. "The observed mean free path and the $p$-air inelastic cross section of proton primaries at $E_0 = (2-4)10^{15}$ eV"
   *Proc 26th International Cosmic Ray Conference*, **1**, 143 (Salt Lake City, 1999)

6. "Gamma-rays and ionizing component during thunderstor;s at Gran Sasso"
   *Proc 26th International Cosmic Ray Conference*, **7**, 351 (Salt Lake City, 1999)
   (EASTOP Coll. and M. Brunetti, D. Cattani, S. Cecchini, M. Galli, G. Giovannini, A. Pagliarin)

7. "Study of jet production in $p$-N interactions at $\sqrt{s} \approx 500$ GeV in EAS multicore events"
   *Proc 26th International Cosmic Ray Conference*, **1**, 139 (Salt Lake City, 1999)

8. "Search for $\approx 10^{14}$ eV $\gamma$-ray transients through the BAKSAN and EASTOP correlated data"
   *Proc 26th International Cosmic Ray Conference*, **3**, 398 (Salt Lake City, 1999)
   (EAS-TOP and BAKSAN Collaborations)

9. "Search for $\approx 10^{14}$ eV $\gamma$-ray sources from a full sky survey at EAS-TOP"
   *Proc 26th International Cosmic Ray Conference*, **4**, 68 (Salt Lake City, 1999)

10. "Study of Horizontal Air Showers at EAS-TOP"
    *Proc 26th International Cosmic Ray Conference*, **2**, 24 (Salt Lake City, 1999)

11. "Study of the knee structure in the EAS electron and muon components"
    *Proc 26th International Cosmic Ray Conference*, **1**, 230 (Salt Lake City, 1999)

12. "Study of jet production in $p$-N interactions at $\sqrt{s} \approx 500$ GeV in EAS multicore events"
    *Nuclear Physics B*, **75A**, 225 (1999)

13. "The proton attenuation length and the p-air inelastic cross section at $\sqrt{s} \approx 2$ TeV from EAS-TOP"
    *Nuclear Physics B*, **75A**, 220 (1999)

14. "Study of the knee in the electron and muon components of Extensive Air Showers at EAS-TOP"
*Nuclear Physics B*, **75A**, 251 (1999)

15. "High Energy muons and atmospheric Cerenkov light in EAS"
*Nuclear Physics B*, **75A**, 259 (1999)
(EAS-TOP and LVD Coll.)

16. "Cosmic ray composition and interactions: measurements at the "knee""
*Nuclear Physics B*, **75A**, 72 (1999)

# GNO. Gallium Neutrino Observatory

M. Altmann[a], M. Balata[b], P. Belli[c], E. Bellotti[d], R. Bernabei[c], C. Cattadori[d], G. Cerichelli[e], M. Chiarini[e], S. d'Angelo[c], G. Del Re[e], K. Ebert[g], F. von Feilitzsch[a], N. Ferrari[a], W. Hampel[f], J. Handt[f], E. Henrich[g], G. Heusser[f], J. Kiko[f], T. Kirsten[f], M. Laubenstein[b], D. Motta[d], T. Lachenmaier[a], J. Lanfranchi[a], H. Richter[f], F. Veglio[e], R. Volpe[e], S. Wänninger[a], L. Zanotti[d]

[a] Physik Department E15, Technische Universität München (TUM), James-Franck Straße, D-85747 Garching b. München, Germany

[b] INFN, Laboratori Nazionali del Gran Sasso (LNGS), S.S. 17/bis Km 18+910, I-67010 L'Aquila - Italy

[c] Dip. di Fisica, Università di Roma "Tor Vergata" and INFN, Sezione di Roma II, Via della Ricerca Scientifica, I-0133 Roma - Italy

[d] Dip. di Fisica, Università di Milano "La Bicocca", and INFN Sezione di Milano

[e] Dip. di Ingegneria Chimica e Materiali, Università dell'Aquila.

[f] Max Plank Institut für Kernphysik (MPIK), Postfach 103980, D-69029 Heidelberg, Germany

[g] Institut für Technische Chemie, Forschungszentrum Karlsruhe (FZK), Postfach 3640, D-76021 Karlsruhe, Germany

**Abstract**

GNO (Gallium Neutrino Observatory) is monitoring the low energy solar neutrino flux with a 30 tons gallium detector at LNGS. From January 1999 to January 2000 13 solar runs and 1 blank run were successfully done. Together with extractions performed in 1998, GNO has accumulated about 650 days live time. During 1999 the counting system was enlarged to accomodate 16 independent lines. A new X-ray calibration system for the proportional counters was installed and is now in operation.

# 1 Introduction

The gallium solar neutrino experiment at Laboratori Nazionali del Gran Sasso detects solar neutrinos via the reaction $^{71}Ga\,(\nu_e, e\,)^{71}Ge$, which has a threshold of 233 keV. The detector is sensitive mainly to pp-neutrinos (53%for standard solar model fluxes [1]), with smaller contributions to the signal from $^7$Be $\nu$ (27%), $^8$B $\nu$ (12%), and CNO $\nu$ (8%).

The target consists of 101 tons solution of $GaCl_3$ in water and HCl, containing 30.3 tons of natural gallium; this amount corresponds to $\sim 10^{29}\,^{71}Ga$ nuclei.

The $^{71}$Ge atoms produced by solar neutrinos (at a rate of about 0.7 per day, one half of the amount predicted by solar models) are chemically extracted from the gallium tank every 4 weeks [3] and introduced in low-background gas proportional counters [2] as germane gas ($GeH_4$). The decay of $^{71}$Ge (e.c., $\tau$=16.5 days) produces a signal in the counters consisting of a point-like ionization at 10.4 keV, or 1.1 keV. The signal is recorded by fast digitizers to allow background reduction by pulse shape analysis. The solar neutrino interaction rate on $^{71}$Ga is deduced from the number of $^{71}$Ge atoms observed. For a complete description of the experimental procedure see [4].

The gallium detector was operated between 1991 and 1997 by the GALLEX collaboration: 65 'solar runs' were performed. The solar neutrino capture rate on $^{71}$Ga was measured with a global uncertainty of 10 % as: 77.5 $\pm$ 6.2 (stat.) $^{+4.3}_{-4.7}(sys.)$ SNU [1] ($1\sigma$) [5]. This result has important physical implications both for astrophysics and for particle physics (for discussion see [5] and [6]).

After maintenance of the chemical plants and renovation of the DAQ and electronics, a new series of measurements was started in April 1998, within the GNO (Gallium Neutrino Observatory) project [7]. The experiment is presently running with 30 tons of gallium (GNO30).

The goals of GNO are:
- measurement of the interaction rate of low energy solar neutrinos on gallium, with an accuracy of 4-5% (half of the error achieved in GALLEX);
- monitoring of the neutrino flux over a complete solar cycle.

The importance of these goals is evident when one considers that the only experiments sensitive to the main component of the solar neutrino flux (the pp neutrinos) which can operate in the next decade are those based on the use of gallium. The $^8B$ neutrino flux has been measured with high accuracy by the Superkamiokande experiment; the $^7Be$ is going to be directly measured by the Borexino experiment. Therefore, the achievement of a good precision in the measurement of the neutrino interaction rate on gallium represents a unique possibility to probe the pp component in the solar neutrino flux within a few percent.
The long-term time schedule for the GNO project is organized as follows (see figure 1):

1. Solar neutrino observations will be carried on regularly with the present 30 tons of gallium; by R&D on several items (see Table 1) the systematic error is planned to be reduced at the level of about 4%

2. depending on the cost and availability of gallium, the target mass can be increased

[1] 1 SNU (Solar Neutrino Unit) = $10^{-36}$ captures per second and per absorber nucleus

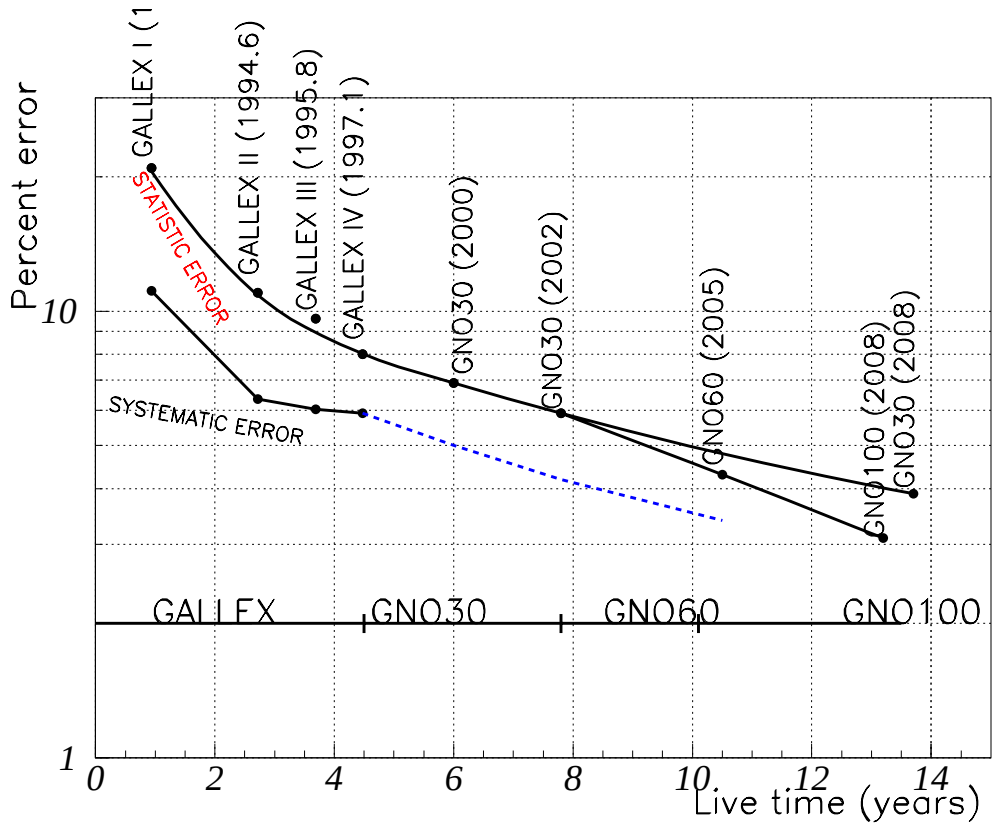


Figure 1: Evolution of the statistic and systematic errors in GALLEX, and expectations for GNO. The evolution of the statistical error is shown both in the hypothesis that the detector will continue with 30 tons of gallium, or with an increase of the mass as described in the text. The evolution of the systematic error in GNO is indicative.

to about 66 tons, the maximum amount that can be accomodated in the two tanks available in the underground lab (GNO66);

3. Further on, it is foreseen to increase the mass to about 100 tons, with the last 35 tons possibly in metallic form (GNO100).

Figure 1 shows the evolution of the experimental error on the solar neutrino capture rate in GALLEX and the expected evolution in GNO.

Together with the increase of the target mass, the crucial point in the GNO project is to obtain a substantial reduction of systematic error. Thus presently a R&D is carried on with the aim to reduce the most relevant components of the systematic error (see table 1); for a deeper discussion see [8].

Table 1: Systematic errors (%) in GALLEX and GNO. The reduction on the Rn cut component is expected to come from the Rn test presently under way; the uncertainty on the counting efficiency will be reduced in GNO30 using information from direct counter calibrations performed at the end of GALLEX. Further decrease in GNO66 will be achieved employing new standardized proportional counters. For details on the separate items see text and [8].

| Source | GALLEX | GNO30 expected | GNO66 expected |
|---|---|---|---|
| Background from side reactions ( muons, Actinides, $^{69}Ge$) | 1.6 | 1.6 | 1.6 |
| Backgound from $^{68}Ge$ | $^{+0.9}_{-2.6}$ | 0 | 0 |
| Background from Rn in the counter | 1.5 | 1.0 | 0.5 |
| $^{71}$Ge Counting efficiency | 4.5 | 3.0 | 2.0 |
| Chemical yield and target Size | 2.2 | 2.2 | 2.2 |
| Total | 5.9 | 4.2 | 3.4 |

# 2 Experimental activity during 1999

## 2.1 Solar neutrino observations

The GNO detector was continuously operated in 1999; 13 solar runs and 1 blank run were performed between January 1999 and January 2000. One of the solar extractions (A12) was lost during the $GeH_4$synthesis. Together with the extractions performed in 1998, the situation at 1-Feb-2000 is the following (see Table 1):
- counting is completed for 14 solar runs;
- other 5 solar runs are still counting;
In the first seven runs (A1 to A7) the conditions during counting were not completely stable, and special care is needed to analyze these data. The release of the first set of the GNO data is foreseen for summer 2000.

## 2.2 Extraction system and synthesis line

The activity at the extraction plant and synthesis line in 1999 can be summarized as follows:

1. maintenance of the main building itself: care of the structure, of the electrical plant, water disribution piping etc; maintenance of gallium tank, absorber plant, auxiliary plants; maitnenace of the building safety equipments: building ventilation system, tank leak sensor, and HCl leak detector.

2. preparation and carrying out of 13 Solar neutrino Runs, and 1 blank (from extraction A10 to extraction A23, see table 2); this includes addition and mixing of Ge isotope carrier, $N_2$ Stripping of $^{71}$Ge from Gallium solution, absorption in water of tank outlet flow stream, final acidification and concentration of Ge/water acidic solution.

3. Acidification of the 53 $m^3$ Gallium solution, by addition of 164 kg of pure HCl [2] .

4. Atomic absorption analysis of samples taken at the end of each Ge-extraction , for the determination of the chemical yields.

## 2.3 Counting system

Each counter is contained in a copper box together with a preamplifier; during the 6 months counting time the box is housed in a special Rn-tight shielding [10].

Each pulse from the proportional counters is sent to amplifiers, where it is split in three parts (figure 2):

1. amplification x4, 300 MHz bandwidth; output is sent to a fast transient digitizer (TDF), operated at 0.2 ns/chan, with a depth of 400 ns. The vertical scale (255 channels) is set to observe the 10 keV signals from $^{71}$Ge K captures (figures 3(a) and 3(b)).

[2] About 2.3 Kg HCl are removed at each desorptions by the $N_2$ flow.

Table 2: Summary of GNO runs performed between April 1998 and February 2000. For every extraction the following data are reported: extraction label; extraction date, referred to the end of the extraction (duration 8 hours); exposure time in days; counter type and number used for $^{71}$Ge counting (Fe=Iron cathode, Si=Silicon cathode, SF=Iron shaped cathode, SC=Silicon shaped cathode)[2]; tank to counter yield, measured by non-radioactive Ge carrier. Status at 01-Feb-2000.

| Extraction | Date | Exposure (days) | Counter | Counting (01-Feb-2000) | tank to counter yield (%) (preliminary) |
|---|---|---|---|---|---|
| A1 | 23-apr-98 | | Fe-112 | completed | 94.2 |
| A2 | 20-may-98 | 27 | Si-106 | completed | 96.1 |
| A3 | 17-jun-98 | 28 | SC-138 | completed | 96.1 |
| A4 | 22-jul-98 | 35 | Fe-118 | completed | 93.5 |
| A5 | 26-aug-98 | 35 | Si-114 | completed | 95.1 |
| A6 | 23-sep-98 | 28 | Si-113 | completed | 97.9 |
| A7 | 21-oct-98 | 28 | SF-093 | completed | 94.6 |
| A8 | 18-nov-98 | 28 | Si-108 | completed | 94.5 |
| A9 | 16-dec-98 | 28 | SC-136 | completed | 94.4 |
| A10 | 12-jan-99 | 28 | FC-102 | completed | 96.4 |
| A11 | 09-feb-99 | 28 | SC-135 | completed | 95.8 |
| A12 | 10-mar-99 | 28 | - | - | Ge lost |
| A13 | 14-apr-99 | 35 | SC-139 | completed | 94.6 |
| A14 | 19-may-99 | 35 | Fe-039 | completed | 96.3 |
| A15 | 16-jun-99 | 28 | Fe-112 | completed | 95.7 |
| A16 | 28-jul-99 | 41 | SC-136 | completed | 94.4 |
| A17 | 25-aug-99 | 28 | SF-093 | completed | 96.0 |
| A18 | 22-sep-99 | 28 | SF-102 | ongoing | 97.1 |
| A19 | 20-oct-99 | 28 | Si-113 | ongoing | 95.7 |
| A20 | 17-nov-99 | 28 | SC-139 | ongoing | 95.6 |
| A21 | 14-dec-99 | 27 | Fe-039 | ongoing | 94.7 |
| A22 | 13-jan-00 | 28 | Si-106 | ongoing | 91.5 |
| A23 | 14-jan-00 | 1 | SC-138 | ongoing | |

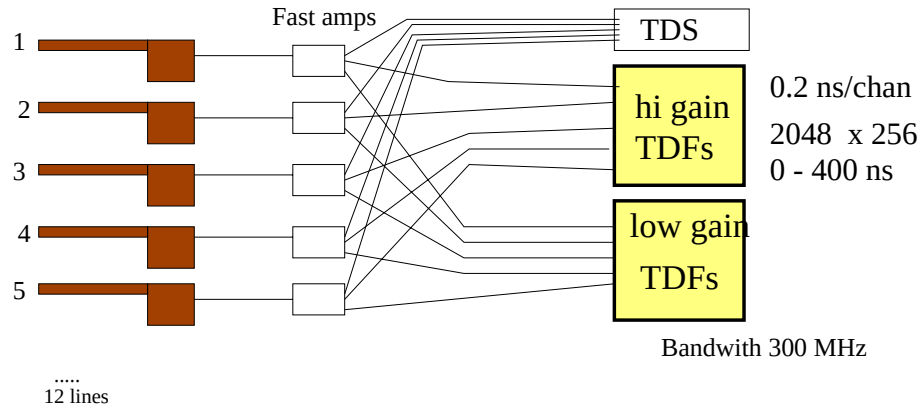


Figure 2: Simplified scheme of the electronics used in GNO for the DAQ of the gas proportional counters.

2. amplification x28, 300 MHz bandwidth; output is sent to a separate channel of TDF; the higher amplification allows to digitize with good resolution the signals at 1 keV from $^{71}$Ge L captures (figures 3(c) and 3(d)) [3].

3. amplification x4, 50Mz bandwidth; output is sent to a slow transient digitizer (TDS), 400 ns/chan, with a depth 800 $\mu$s, which records the complete development of the signal.

The use of the new electronic chain has allowed to reach significantly lower noise levels, compared to GALLEX: this has positive effects in the pulse shape analysis of data (see section 2.6).

During 1999 the electronics necessary to deal with 16 independent lines has been set-up. This allows to perform several tests without interference with the solar neutrino observations. Assuming one extraction per month and 6 months counting time per counter, 6 lines are permanently occupied by the solar runs. Supplementary lines are needed for special tests (e.g. Rn and $^{71}$Ge calibrations), background measurements for new counters, blanks etc.

Further details on the GNO counting system and on the DAQ were discussed in the 1998 annual report [8].

## 2.4 Installation of a new X-ray calibration source.

The energy- and rise-time calibration of the proportional counters was performed in GALLEX and in the first set of the GNO measurements with cerium X-rays, produced by a radioactive $^{153}$Gd source and a Ce target. $^{153}$Gd sources are no longer commercially available at the needed activity (GBq) and purity level; moreover they require frequent replacement, due to the decay of Gd (half-life 239.5 d). This problem was solved by adopting a tunable low power x-ray tube in place of the Gd-source. A system with two stepping motors was built, which allows to move the tube inside the shielding with remote

[3] or K captures where a 9 keV Ga K X-ray escapes the counter

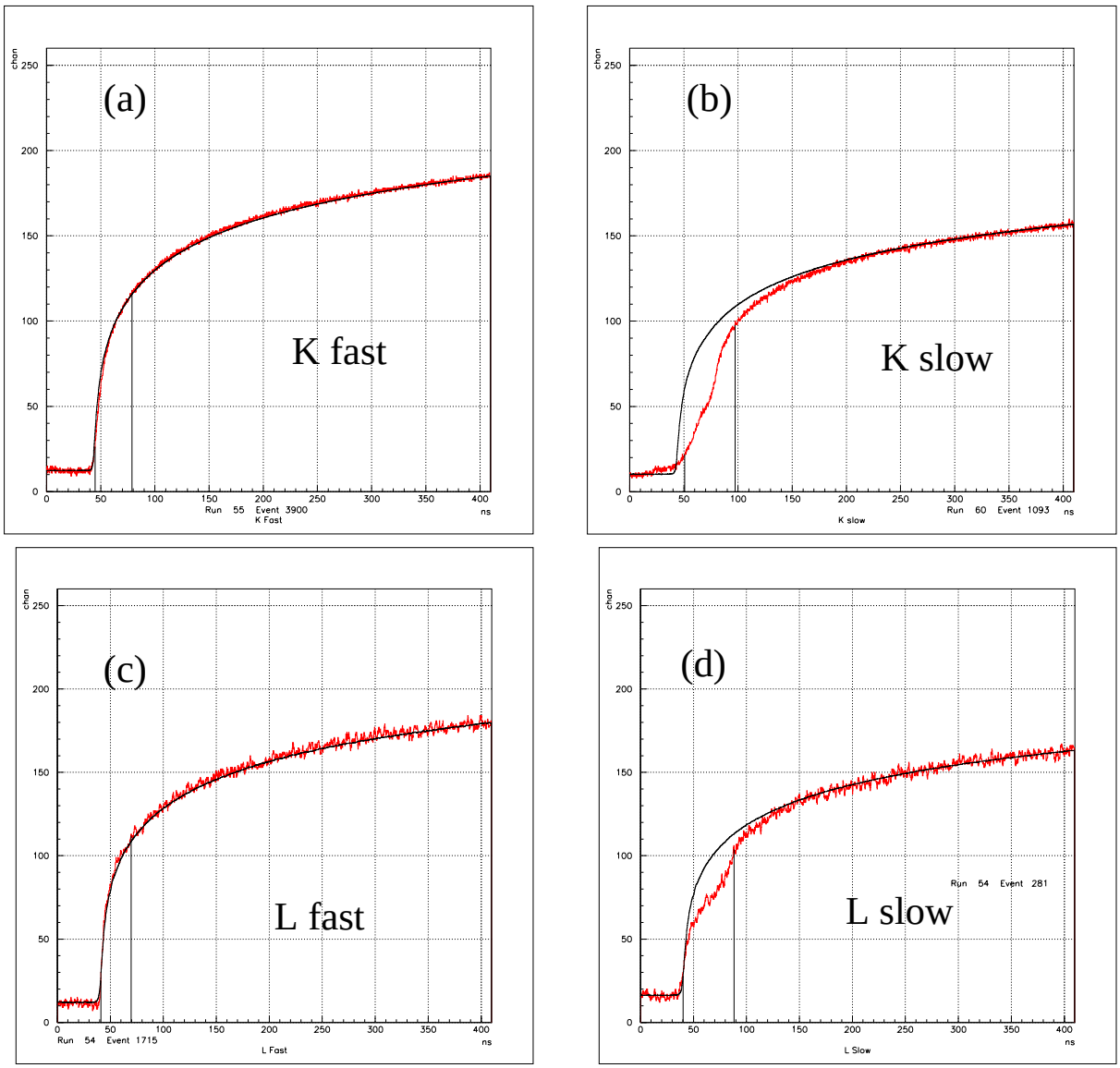


Figure 3: Examples of 4 pulses recorded by the GNO TDFs. $^{71}$Ge e-capture (both from K and L shells) produce fast pulses, while most background events generate slow pulses from diffuse ionization. (a) fast 'K' pulse, (b) slow pulse in the 'K' region, (c) fast 'L' pulse, (d) slow pulse in the 'L' region. The solid lines represent the average fast pulse expected for a $^{71}$Ge signal.

control (see figure 4). The setup was installed in July 1999 with a one week interruption of the normal counting just before the start of counting of run A14. The calibration procedure is fully software controlled; during normal counting periods the system is completely switched off from electric power in order to maintain the low electronic noise level. With the new calibration system, each proportional counter can be calibrated in its counting position on the passive side of the shield. Before, the calibration with the Gd source had required to open the shielding and remove the counter from its counting position; thus, the new procedure allows more frequent calibrations without stresses on cables. This also helps to reduce the systematic error to to calibrations. The new calibration system works as expected, and was employed regularely since july 1999.

## 2.5 Radon test

The experience with GALLEX has shown that a few Rn atoms are sometimes introduced in the counters during the synthesis and counter filling. The decays of Rn and its daughters can produce events which cannot be distinguished from real $^{71}$Ge events, and are concentrated in the first days of counting (the half-life of $^{222}Rn$ is 3.83 days). A 'Rn cut' is introduced in the data analysis, by defining a dead time for each detected Rn decay chain (see [12] for details). The efficiency of this cut was evaluated in GALLEX to be $(91 \pm 5)\%$, and the uncertainty on that number represents a relevant component of the systematic error in the experiment. A Rn test was started in 1999 to lower this error to about 1% or less. A Ra source was introduced in a proportional counter, releasing some Rn atoms per day in the counter gas. The decay of the Rn atoms and its daughters is recorded with the same DAQ used for standard runs. Such measurement requires to be held continuously for a long time (of the order of at least 6 months.) In fact one needs a low Rn activity (of the order of 4-5 Rn chains per day, in order not to overlap subsequent chains, and disentangle the single decays in the chain.

## 2.6 Data analysis

For the selection of the $^{71}$Ge events, we use as a first approach an amplitude/ rise-time discrimination similar to the one used for GALLEX [9]: in that way it is possible to have an immediate cross-check with data collected in GALLEX.

More sophisticated pulse-shape analyses are under development; they extract all the information from the pulse recording, using all the benefits of the new fast electronic chain. As an example in figure 3 we show two fast pulses from $^{71}$Ge decay and two background slow pulses, with superimposed the average 'fast pulse' as observed in the counter calibrations with the X-ray source. The definition of a good test parameter (for example a $\chi^2$) can decide wether or not the observed signal is compatible with the expected fast signal from $^{71}$Ge decay.

## 2.7 Developement of cryogenic detectors

At TUM a project is ongoing to test the feasibility of low temperature calorimeters as detectors for measuring the $^{71}Ge$-decay [11]. With such detectors the $^{71}$Ge extracted from

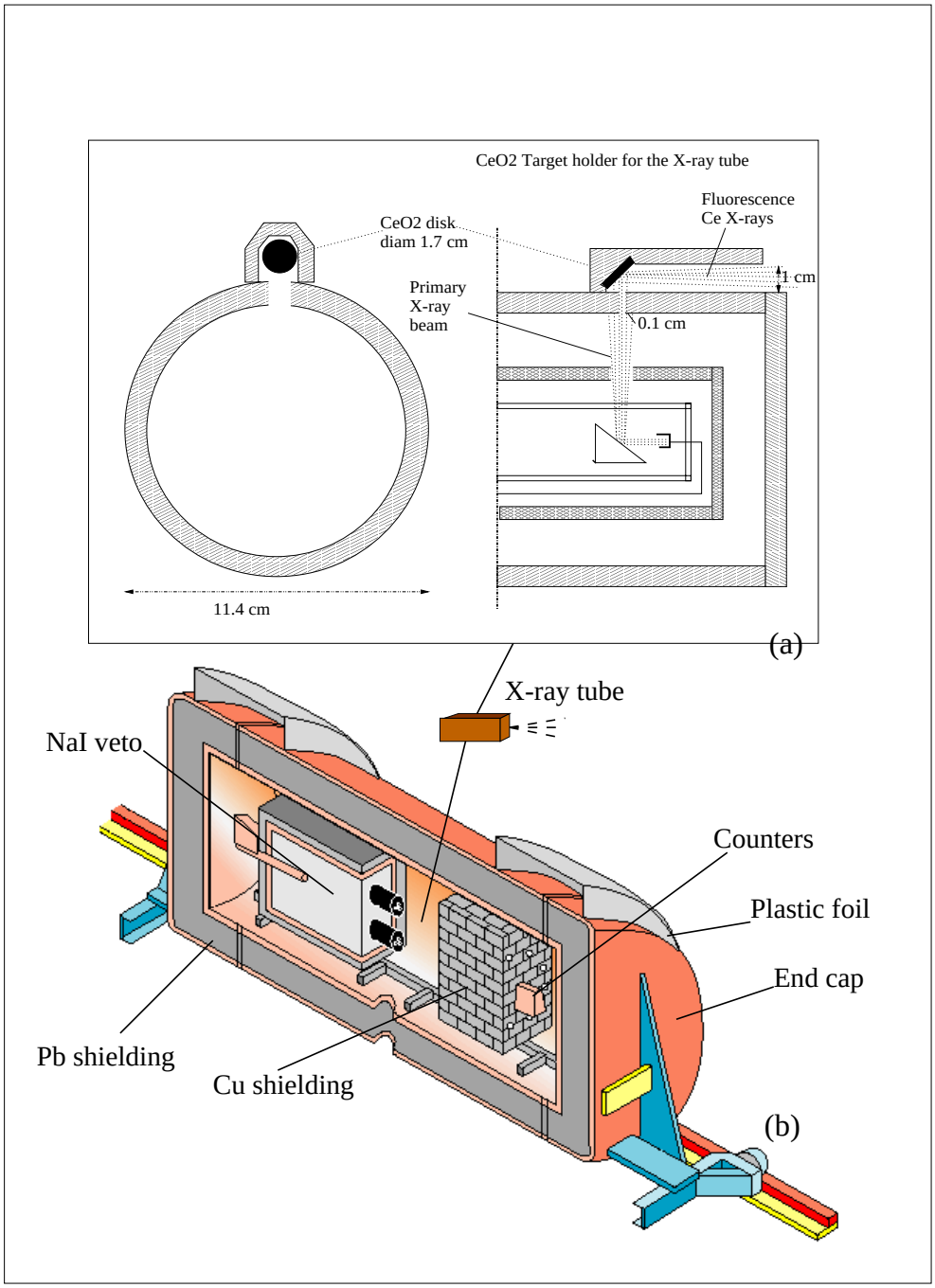


Figure 4: The new X-ray system used for the calibration of the proportional counters in GNO. (a) scheme of the X-ray tube. (b) Location of the X-ray tube inside the shielding.

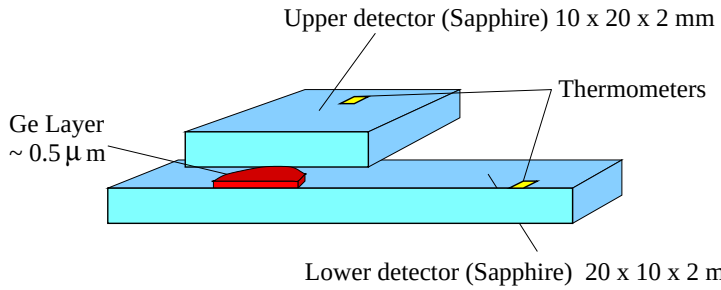


Figure 5: Scheme of the 4 $\pi$ thermal detector under development at TUM. The $^{71}$Ge extracted from the tank is thermally deposited on a sapphire substrate together with the non radioactive carrier germanium substrate. X-rays and Auger electrons from the $^{71}$Ge decay are captured either in the lower or in the upper detector, with an efficiency near 98%.

the gallium tank together with the non-radioactive Germanium, is converted to $GeH_4$, and then thermally deposited on a substrate, which is then put in a cryostat to work as a thermal detector. During 1999 a detector with a $4\pi$ geometry (Figure 5) was built and operated at TUM to detect a $^{71}$Ge activity. The Ge layer was deposited on a sapphire crystal (lower detector); a second sapphire substrate (upper detector) recovers the X-rays eventually produced by the $^{71}$Ge decay, and escaping the Ge layer from above. The $^{71}$Ge calibration showed that the detector can work with the expected energy resolution and counting efficiency, which is near 98%. Significant improvements have also been obtained during 1999 in the Ge-deposition technique.

R&D is under development at TUM to reach a high and reproducible Ge deposition efficiency, and to build a system (cryostat + detectors) capable of a stable and continuous measurement.

# 3 List of Publications

1. GNO collaboration, "GNO progress report for 1998", LNGS annual Report 1998, 55-79., GNO report n.11 (1999)

# References

[1] J.N. Bahcall, S.Basu and M.H.Pinsonneault, Phys.Lett. B433 (1998) 1, V. Castellani et al. Phys. Rep. 281 (1997) 309; V.Castellani et al., preprint astro-ph/9712174, A.S.Brun, S. Turck Chiéze and P.Morel, preprint astro-ph/9806272.

[2] R. Wink et al. Nucl. Inst. and Meth. A329 (1993) 541

[3] E.Henrich, K.H.Ebert, Angew. Chemie Int. Ed. (Engl.) 31 (1992) 1283; E.Henrich et al., 'GALLEX, a challange for chemistry', Proc. IV Int'l. Solar Neutrino Conf., ed. W.Hampel, MPI Kernph., Heidelberg (1997) 151-162.

[4] GALLEX collaboration, Phys.Lett. B285 (1992) 376; Phys.Lett. B314 (1993) 445; Phys.Lett. B327 (1994) 377; Phys.Lett. B342 (1995) 440; Phys.Lett. B357 (1995) 237; Phys.Lett. B388 (1996) 384

[5] W.Hampel et al. GALLEX collaboration Phys.Lett. B447 (1999) 127.

[6] T.Kirsten, Rev.Mod.Phys., 71 (1999) 411.

[7] E.Bellotti et al., GNO collaboration, LNGS report INFN/AE-96-27, also available at http://kosmopc.mpi-hd.mpg.de/gallex.html

[8] W.Hampel et al., GNO collaboration, LNGS annual report 1998, pag. 55-69

[9] M. Sann 'Data acquisition, calibrations, and data analysis for GALLEX', GALLEX internal report GX114 (1997).

[10] G. Heusser, 'Characteristics of the GALLEX Spectrometer', Trends in Astroparticle Physics', ed. P. Ch. Bosetti, (1994) p.33, Teubner, Leibzig

[11] M.Altmann et al., 'Progress in the development of cryogenic detectors for GNO', Proc. Int. Workshop on Topics in Astroparticle and Underground Physics (TAUP97), Nucl. Phys. B (Proc. Suppl.) 70 (1999) 374-376.

[12] H.Lalla, 'Zeitabhängiger Untergrund im GALLEX- Sonnenneutrino-Experiment', thesis, Ruprecht-Karls-Universität Heidelberg (1993).

# HDMS. Dark Matter Search

V. Alexeev[b], L. Baudis[a], A. Dietz[a], H.V. Klapdor–Kleingrothaus[*a], B. Majorovits[a], F. Schwamm[a], H. Strecker[a], S. Zhukov[b]

[a]Max–Planck–Institut für Kernphysik, P.O.Box 10 39 80, D–69029 Heidelberg, Germany

[b]Russian Science Centre Kurchatov Institute, 123 182 Moscow, Russia

[*] Spokesman of the collaboration

**Abstract**

The prototype of a new Dark Matter Experiment for the Gran Sasso underground laboratory has been installed and was taking data for 15 month. Our HDMS (Heidelberg Dark Matter Search) experiment consists of two germanium detectors in a unique configuration. It is specialized to discriminate the already low background obtained in the Heidelberg-Moscow experiment considerably further. The use of anticoincidence between our Ge-detectors reduces the photon background which mainly limits the direct detection of hypothetical dark matter particles (WIMPs). The results of 15 months of measurement are discussed in detail.

## 1 Introduction

Weakly Interacting Massive Particles (WIMPs) are leading candidates for the dominant form of matter in our Galaxy. These relic particles from an early phase of the Universe arise independently from cosmological considerations in supersymmetric particle physics theories as neutralinos - the lightest supersymmetric particles.

Direct WIMP detection experiments exploit the elastic WIMP scattering off nuclei in a terrestrial detector [1]. However, detecting WIMPs is not a simple task. As their name suggests, their interaction with matter is very faible ($\sigma \leq \sigma_{weak}$) and predicted rates in supersymmetric models range from 10 to $10^{-5}$ events per kilogram detector material and day [2]. Moreover, for WIMP masses between a few GeV and 1 Tev, the energy deposited by the recoil nucleus is less then 100 keV. Thus, in order to be able to detect a WIMP, an experiment with a low energy threshold and an extremely low radioactive background is required. Since the reward would be no less than discovering the dark matter in the Universe, a huge effort is put into direct detection experiments. More than 20 experiments are running at present and even more are planned for the future (for recent reviews see [3, 4, 5]).

The focus of this paper is to present first results of the Heidelberg Dark Matter Search (HDMS) experiment [6], which took data over a period of about 15 month in the Gran Sasso Underground Laboratory (LNGS) in Italy. After a description of the experimental setup, its performance is discussed in some detail. The last 100 d of data taking are then analyzed in terms of WIMP-nucleon cross sections and a comparison to other running dark matter experiments is made. Finally conclusions and an outlook are given.

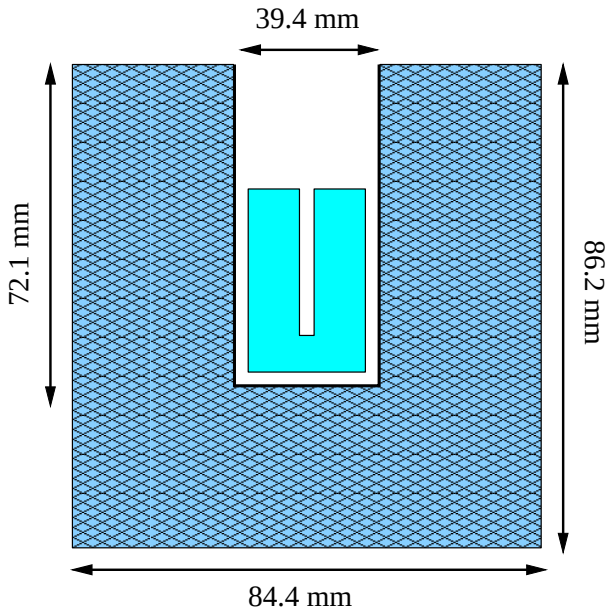


Figure 1: Schematic view of the HDMS experiment. A small Ge crystal is surrounded by a well type Ge-crystal, the anticoincidence between them is used to suppress background created by external photons.

## 2 Description of the experiment

HDMS operates two ionization HPGe detectors in a unique configuration [6]. A small, p-type Ge crystal is surrounded by a well-type Ge crystal, both being mounted into a common cryostat system (see Figure 1 for a schematic view). To shield leakage currents on the surfaces, a 1 mm thin vespel insulator is placed between them. Two effects are expected to reduce the background of the inner target detector with respect to our best measurements with the Heidelberg-Moscow experiment [7]. First, the anticoincidence between the two detectors acts as an effective suppression of multiple scattered photons. Second, we know that the main radioactive background of Ge detectors comes from materials situated in the immediate vicinity of the crystals. In the case of HDMS the inner detector is surrounded (apart from the thin isolation) by a second Ge crystal - one of the radio-purest known materials.

In order to house both Ge crystals and to establish the two HV and two signal contacts, a special design of the copper crystal holder system was required. The cryostat system was built up in Heidelberg and made of low radioactivity copper, all surfaces being electropolished. The FETs are placed 20 cm away from the crystals, their effect on the background is minimized by a small solid angle for viewing the crystals and by 10 cm of copper shielding.

## 3 Detector performance at LNGS

The HDMS prototype was installed at LNGS in March 1998 and successfully took data over a period of about 15 month, until July 1999. Figure 2 shows the detector in its open

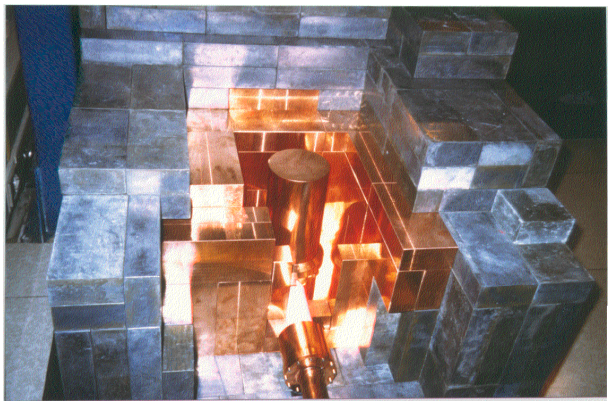

Figure 2: The HDMS detector during its installation at LNGS.

shielding. The inner shield is made of 10 cm of electrolytic copper, the outer one of 20 cm of Boliden lead. The whole setup is enclosed in an air tight steel box and flushed with gaseous nitrogen in order to suppress Radon diffusion from the environment. Finally a 15 cm thick borated polyethylene shield surrounds the steel box in order to minimize the influence of neutrons from the natural radioactivity and muon produced neutrons in the Gran Sasso rock.

The individual runs were about 0.9 d long. Each day the experiment was stopped and parameters like leakage current of the detectors, nitrogen flux, overall trigger rate and count rate of each detector were checked. The experiment was calibrated weakly with a $^{133}$Ba and a $^{152}$Eu-$^{228}$Th source. The energy resolution of both detectors (1.2 keV at 300 keV inner detector and 3.2 keV at 300 keV outer detector) were stable as a function of time. The zero energy resolution is 0.94 keV for the inner detector and 3.3 keV for the outer one.

The energy threshold are 2.5 keV and 7.5 keV for the inner and outer detector, respectively.

After correction for the cross talk and recalibration to standard calibration values (according to the weakly determined calibration parameters), the spectra of the daily runs were summed up. The figure 3 show the sum spectra for the outer and inner detector, respectively (the most important identified lines are labeled).

In the outer detector the lines of the cosmogenic isotopes $^{68}$Ge, $^{57}$Co, $^{58}$Co, $^{54}$Mn, $^{60}$Co, $^{65}$Zn, of the natural decay chains $^{238}$U and $^{232}$Th, of the primordial $^{40}$K, the anthropogenic radionuclide $^{137}$Cs and the annihilation line at 511 keV can be identified. The statistics in the inner detector is not as good, however the $^{68}$Ge $K_\beta$ line at 10.37 keV, the $^{210}$Pb line at 46.5 keV, the external $^{57}$Co line at 122.1 keV and the internal at 143.6 keV, the 511 keV annihilation line, the $^{54}$Mn line at 834 keV, the two $^{60}$Co lines at 1173 keV and 1332 keV and the $^{40}$K line at 1460 keV can be clearly seen. The region below 10 keV is dominated by the X-rays of $^{57}$Co (6.4 keV, 7.1 keV), and $^{54}$Mn (5.41 keV). In addition a structure centered at 32 keV with a FWHM of 2 keV is identified. Its origin is not yet clear and is currently under investigation. The isotope $^{137}$Cs, which would be a good candidate, has a $K_\alpha$ sum line at 32.06 keV, with an emission probability of 5.6 %. The emission probability of the $\gamma$-line with 661.66 keV is with 85.1 % by a factor of 15 higher.

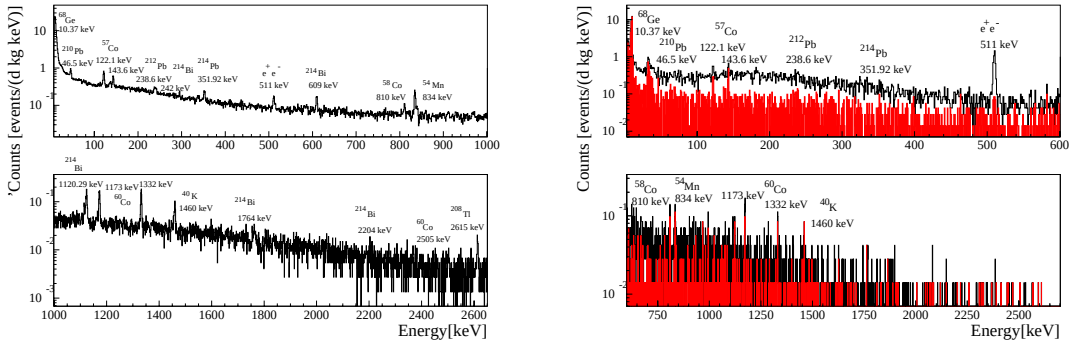


Figure 3: Left: Sum spectrum of the outer detector after a measuring time of 363 days. The most prominent lines are labeled. Right: Sum spectrum of the inner detector after a measuring time of 363 days. The most prominent lines are labeled. The filled histogram is the spectrum after the anticoincidence with the outer detector.

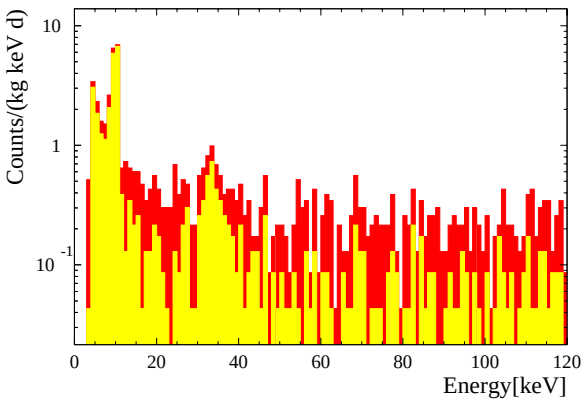


Figure 4: Low energy spectrum of the inner detector before and after the anticoincidence.

This line is however not observed in the spectrum.

After 363 days of pure measuring time the statistics in the inner detector was however high enough in order to estimate the background reduction through the anticoincidence with the outer detector.

Figure 4 shows the low energy spectrum of the inner detector before and after the anticoincidence. The cosmogenic X-rays below 11 keV are preserved, since in this case the decays are occuring in the inner detector itself. The same is valid for the structure at 32 keV, also a $^3$H spectrum with endpoint at 18 keV is presumably present. If the anticoincidence is evaluated in the energy region between 40 keV and 100 keV, the background reduction factor is 4.3. The counting rate after the anticoincidence in this energy region is 0.07 events/(kg d keV), thus very close to the value obtained in the Heidelberg-Moscow experiment with the enriched detector ANG2 [7]. In the energy region between 11 keV and 40 keV the background index is with 0.2 events/(kg d keV) a factor of 3 higher.

# 4 Dark Matter Limits

The evaluation for dark matter limits on the WIMP-nucleon cross section $\sigma_{\mathrm{scalar}}^{\mathrm{W-N}}$ follows the conservative assumption that the whole experimental spectrum consists of WIMP events. Consequently, excess events from calculated WIMP spectra above the experimental spectrum in any energy region with a minimum width of the energy resolution of the detector are forbidden (to a given confidence limit).

The parameters used in the calculation of expected WIMP spectra are summarized in [7]. We use formulas given in the extensive reviews [8, 9] for a truncated Maxwell velocity distribution in an isothermal WIMP–halo model (truncation at the escape velocity, compare also [10]).

After calculating the WIMP spectrum for a given WIMP mass, the scalar cross section is the only free parameter which is then used to fit the expected to the measured spectrum using a one-parameter maximum-likelihood fit algorithm. The minimum of cross section values obtained via these multiple fits of the expected to the measured spectrum gives the limit.

To compute the limit for the HDMS inner detector we took only the last 114.95 d of measurement. We subtracted the 10.37 keV line by setting the energy bins corresponding to 9 keV, 10 keV and 11 keV to the value we see in the 8 keV energy bin. This bin lies between the two X-ray lines of $^{57}$Co at 7.1 keV and $^{68}$Ge at 10.37 keV. Since the expected form of a WIMP-nuclear recoil spectrum is decreasing with energy, this is a conservative assumption. We took an energy threshold of 3 keV. The resulting upper limit exclusion plot in the $\sigma_{\mathrm{scalar}}^{\mathrm{W-N}}$ versus $\mathrm{M_{WIMP}}$ plane is shown in Fig. 5.

At this stage, the limit is not yet competitive with our limit from the Heidelberg-Moscow experiment. However, the sensitivity it is already comparable to the most advanced direct WIMP search experiments.

Also shown in the figure are limits from the Heidelberg-Moscow experiment [7], from the DAMA experiment [11] and the most recent limits from the CDMS experiment [12]. The filled contour represents the $2\sigma$ evidence region of the DAMA experiment [13].

# 5 Conclusion and Outlook

The prototype detector of the HDMS experiment successfully took data at LNGS over a period of about 15 months. Most of the background sources (with exception of the 32 keV structure in the inner detector) were identified. The background reduction factor in the inner detector through anticoincidence is about 4. It is less then previously expected [6], due to the smaller diameter of the veto detector than originally planned. Nevertheless, the background in the low-energy region of the inner detector (with exception of the region still dominated by cosmogenic activities) is already now on the level of the Heidelberg-Moscow experiment.

For the full scale experiment, important changes were made. The crystal holder was replaced by a holder made of extremely low level copper, the soldering of the contacts was hereby omitted. The inner crystal made of natural Germanium in the described prototype was replaced by an enriched $^{73}$Ge crystal. In this way, the $^{70}$Ge isotope (which

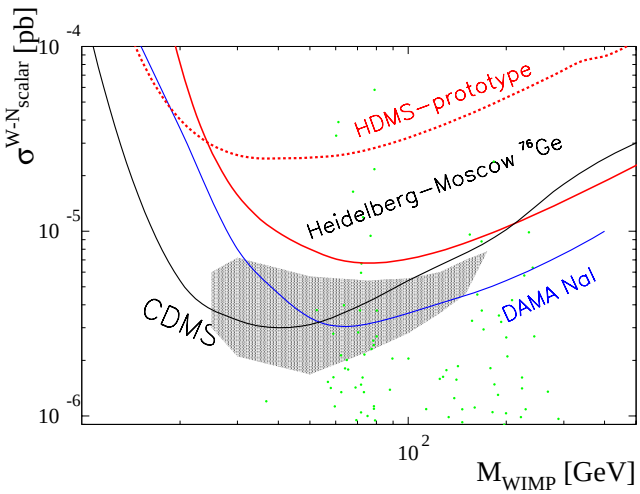


Figure 5: WIMP-nucleon cross section limits as a function of the WIMP mass for spin-independent interactions. The dashed line corresponds to the limit set by the HDMS-prototype detector. The plain curves correspond to the limits given by CDMS [12], DAMA [11] and the Heidelberg-Moscow Experiment [7]. The filled contour represents the $2\sigma$ evidence region of the DAMA experiment [13].

is the source of $^{68}$Ge) is strongly deenriched (the abundance in natural Germanium is 7.8%).

After a period of test measurements in the low-level laboratory in Heidelberg, the full scale experiment will be installed at LNGS in the second part of the 2000.

The aim of HDMS is to test the region singled out by the DAMA experiment [13] in the MSSM parameter space after two years of measurement with raw data and a completely different detection technique.

# References


[1] M. W. Goodman and E. Witten, Phys. Rev. D 31 (1985) 3059.

[2] G. Jungmann, M. Kamionkowski, K. Griest, Phys. Rep. 267 (1996) 195, V. Bednyakov, H.V. Klapdor–Kleingrothaus, S.G. Kovalenko, Y. Ramachers, Z. Phys. A 357 (1997) 339, Bottino et al., hep-ph/0001309.

[3] A. Morales, astro-ph/9912554 and in Proc. of the 6th Int. Workshop "TAUP99", Paris, France 6-10 sept. 1999, Nucl. Phys. (Proc. Suppl.).

[4] Y. Ramachers, astro-ph/9911260 and in Proc. XIth Rencontres de Blois, Frontiers of Matter, France, June 27 - July 3, 1999.

[5] L. Baudis, H.V. Klapdor-Kleingrothaus, astro-ph/0003434 and in Proceedings of Beyond the Desert '99, Second International Conference on Physics beyond the Standard Model, Castle Ringberg, Tegernsee, Germany, 6-12 June 1999.

[6] L. Baudis et al., Nucl. Instrum. Methods A **385**, 265 (1997).

[7] L. Baudis et al., Phys. Rev. D 59 (1998) 022001-1.

[8] R. Bernabei, Riv. Nuovo Cimento **18**, 1 (1995).

[9] J.D. Lewin and P.F. Smith, Astropart. Phys. **6**, 87 (1997).

[10] K. Freese, J. Frieman, and A. Gould, Phys. Rev. D **37**, 3388 (1988).

[11] P. Belli et al., in Proc. of the Second Int. Conference on Dark Matter in Astro– and Particle Physics (DARK98) July 1998, Heidelberg, Eds. H.V. Klapdor–Kleingrothaus and L. Baudis, IOP, Bristol& Philadelphia, 1999, p. 711.

[12] R. Gaitskell, talk at the 4th International Symposium on Sources and Detection of Dark Matter/Energy in the Universe, February 23-25, 2000, Marina del Rey, CA., R. Abusaidi et al. (CDMS Collaboration) astro-ph/0002471.

[13] R. Bernabei et al., Phys. Lett. B 424 (1998) 195, Phys. Lett. B 450 (1999) 448, INFN/AE-00/01, February 2000.

# The Heidelberg - Moscow experiment on $\beta\beta$ decay and GENIUS

V. Alexeev [b], A. Bakalyarov [b], A. Balysh [b], L. Baudis[a], S.T. Belyaev[b], A. Dietz[a], G. Heusser[a] , H.V. Klapdor–Kleingrothaus*[a], S. Kolb[a], I.V. Krivosheina[a], V.I. Lebedev[b], B. Majorovits[a], H. Päs[a], F. Schwamm[a], H. Strecker[a], H. Tu[a], S. Zhukov[b]

[a]Max–Planck–Institut für Kernphysik, P.O.Box 10 39 80, D–69029 Heidelberg, Germany

[b]Russian Science Centre Kurchatov Institute, 123 182 Moscow, Russia

* Spokesman of the collaboration

**Abstract**

The Heidelberg–Moscow experiment gives the most stringent limit on the Majorana neutrino mass. After 31 kg yr of data with pulse shape measurements, we set a lower limit on the half-life of the $0\nu\beta\beta$-decay in $^{76}$Ge of $T^{0\nu}_{1/2} \geq 3.0 \times 10^{25}$ yr at 68% C.L., thus excluding an effective Majorana neutrino mass greater than 0.29 eV (68 % C.L.). New limits have been obtained - using $\sim$ 140.000 events in the spectrum - for $2\nu\beta\beta$ decay and Majoron accompanied $0\nu\beta\beta$ decay. A new pulse-shape analysis method based on neural networks has been developed improving the efficiency of the pulseshape discrimination and confirming the method used so far. The preparational work for the GENIUS project has been continued.

## 1 Introduction

The Heidelberg–Moscow experiment, situated in the Gran Sasso Underground Laboratory, operates five p–type HPGe detectors, made of 86% enriched $^{76}$Ge material. The total active mass of the detectors is 10.96 kg, corresponding to 125.5 mol $^{76}$Ge, the presently largest source strength of all double beta experiments. Four detectors are placed in a common 30 cm thick lead shielding in a radon free nitrogen atmosphere, surrounded by 10 cm of boron-loaded polyethylene and two layers of 1 cm thick scintillators on top. The remaining detector is situated in a separate box with 27 cm electrolytical copper, 20 cm lead shielding and 10 cm of boron-loaded polyethylene below the box, flushed with gaseous nitrogen. A detailed description of the experiment and its background is given in [1]. For a further reduction of the already very low background of the experiment, two pulse shape analysis (PSA) methods were developed [2, 3]. The analysis distinguishes between multiple scattered interaction in the Ge crystal, so called multiple site events (MSE) and pointlike interactions, or single site events (SSE). Since double beta decay events belong to the SSE category, the method allows to effectively reduce the background of multiple Compton scattered photons. The probablity of correct detection for a SSE is 75%, and

74% for a MSE [2] for the old method. The new pulse shape analysis based on neural networks allows for an improvement of the efficiency up to 90% [3].

# 2 Results on neutrinoless double-beta-decay, $2\nu\beta\beta$ decay and Majoron accompanied $0\nu\beta\beta$ decay

For the evaluation of the $0\nu\beta\beta$-decay we consider both data sets, with and without pulse shape analysis. We see in none of them an indication for a peak at the Q-value of the $0\nu\beta\beta$-decay. The total spectrum of the five detectors with a statistical significance of 49.03 kg yr contains all the data with exception of the first 200 d of measurement of each detector (see Fig. 1). The extrapolated energy resolution at the energy of the hypothetical $0\nu\beta\beta$-peak is (3.91±0.13) keV. To estimate the expected background in the $0\nu\beta\beta$ region, we take the energy intervall from 2000 to 2080 keV. The number of expected events in the peak region is (93±3) events, the number of measured events in the $3\sigma$ peak interval centered at 2038.56 keV is 100. With the achieved energy resolution, the number of excluded events in the $3\sigma$ peak region is 23.59 (15.54) with 90% C.L. (68% C.L.), resulting in a half-life limit of:

$$T^{0\nu}_{1/2} \geq 1.1 \times 10^{25} \text{ yr} \quad 90\% \text{ C.L.}$$
$$T^{0\nu}_{1/2} \geq 1.6 \times 10^{25} \text{ yr} \quad 68\% \text{ C.L.}$$

We consider now the data with pulse shape measurements, with a statistical significance of 30.99 kg yr and an energy resolution at 2038.56 keV of (4.06±0.14) keV. The expected number of events from the background left and right of the peak is (17.9±1.5) events, the measured number of events in the $3\sigma$ peak region is 18.33. We can exclude 8.43 (4.98) events with 90% C.L. (68 % C.L.). The limit on the half-life is:

$$T^{0\nu}_{1/2} \geq 1.8 \times 10^{25} \text{ yr} \quad 90\% \text{ C.L.}$$
$$T^{0\nu}_{1/2} \geq 3.0 \times 10^{25} \text{ yr} \quad 68\% \text{ C.L.}$$

Obviously the pulse shape data are now not only competitive with the complete data set, but they deliver more stringent lower limits on the half-life of the $0\nu\beta\beta$-decay. The pulse shape analysis reduces the background in the interesting energy region by a factor of 3 [background index without PSA: (0.18±0.02) events/(kg yr keV), with PSA: (0.06±0.02) events/(kg yr keV)]. This reduction factor is due to the large fraction of multiple Compton scattered events in the $0\nu\beta\beta$-decay region.

Figure 1 shows the combined spectrum of the five detectors after 49.03 kg yr and the SSE spectrum in the $0\nu\beta\beta$-region, corrected for the detection efficiency, after 30.99 kg yr. The solid lines represent the exclusion limits for the two spectra at the 90% C.L.

The sensitivity of the experiment, as defined in [6], is again obtained by setting the measured number of events equal to the expected background. With 7.51 (4.71) excluded events at 90% C.L (68% C.L.), the sensitivity is:

| | $T^{0\nu}_{1/2}$ [yr] | $\langle m \rangle$ [eV] | C.L. [%] |
|---|---|---|---|
| Full data set | $\geq 1.1 \times 10^{25}$ | $\leq 0.43$ | 90 |
| | $\geq 1.6 \times 10^{25}$ | $\leq 0.33$ | 68 |
| SSE data after [4] | $\geq 1.8 \times 10^{25}$ | $\leq 0.36$ | 90 |
| | $\geq 3.0 \times 10^{25}$ | $\leq 0.29$ | 68 |
| Sensitivity | $\geq 1.6 \times 10^{25}$ | $\leq 0.38$ | 90 |
| | $\geq 2.5 \times 10^{25}$ | $\leq 0.30$ | 68 |

Table 1: Limits on the effective Majorana neutrino mass from the $0\nu\beta\beta$-decay of $^{76}$Ge for the matrix elements from [5].

$$T^{0\nu}_{1/2} \geq 1.6 \times 10^{25} \text{ yr} \quad 90\% \text{ C.L.}$$
$$T^{0\nu}_{1/2} \geq 2.5 \times 10^{25} \text{ yr} \quad 68\% \text{ C.L.}$$

With the matrix elements of [5], neglecting RHC's, we can convert the lower half-life limit into an upper limit on the effective Majorana neutrino mass. The obtained limits are shown in Table 1. Already in the present stage the Heidelberg-Moscow experiment is setting the most stringent limit on the Majorana neutrino mass, allowing to test the predictions of degenerate neutrino mass models. In models which try to accomodate the solar and atmospheric neutrino problems while considering the neutrino as a hot dark matter candidate with a few eV, the small angle MSW solution is practically ruled out [7]. For the large angle MSW solution, an effective neutrino mass smaller than 0.36 eV would need an unnatural fine tuning to account for a relevant neutrino mass in a mixed hot and cold dark matter cosmology [8].

For the implications for other physics beyond the standard model, like left-right supersymmetric models, supersymmetry, leptoquarks and compositeness we refer to [9, 10].

For the two-neutrino decay mode we obtain a value of

$$T^{2\nu}_{1/2} = (1.55 \pm 0.01(\text{Stat})^{+0.16}_{-0.13}(\text{Syst})) \times 10^{21}\text{y}.$$

This bases on ∼140.000 counts in the spectrum after subtraction of the background model [11].

A simultanous analysis for Majoron-accompanied $0\nu\beta\beta$ decay yields $T^{1}_{1/2} > 6.76 \times 10^{22}$y for spectral index of n=1 and $T^{3}_{1/2} > 1.40 \times 10^{22}$y for spectral index of n=3.

# 3 The new Pulse Shape Analysis

A large amount of information is neglected with the pulse shape discrimination method used so far since only one parameter serves as the distinguishing criterium. Furthermore the method relies on a statistical correction of the measured SSE pulses since the efficiency of the method is substantially smaller than 100% resulting in a loss of information about the single events. For this reason we developed a new method based on neural networks to

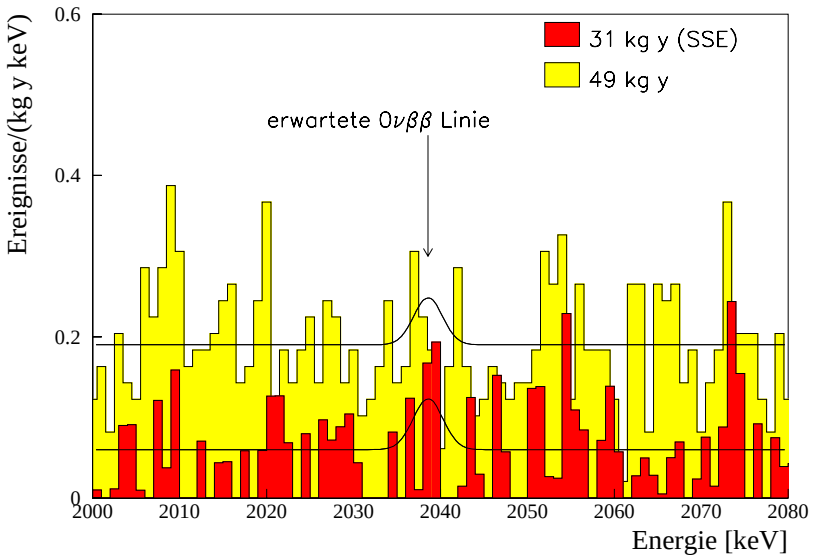


Figure 1: Energy region of the neutrinoless double beta decay. SSE spectrum (dark) after 31 kg y and spectrum containing MSE (light) after 49 kg y of data taking, both analyzed using the procedure given in [4]. Shown is also the excluded peak from these data.

use as much information as possible from the recorded pulse shapes and to avoid statistical treatment of the obtained data.

Neural Networks are nowadays used in a wide variety of applications like pattern-, image- and videoimage-recognition. Since in the case of PSA the discrimination technique relies on a sort of pattern recognition it seemed consequent to base a new PSA-technique on this method. In contrast to the old method, where only one parameter was used as the distinguishing criterium, all the information obtained by the measurement about the time structure of the pulse is fed to the neural networks in order to distinguish between SSE's and MSE's.

The network has to be configured in order to be able to distinguish reasonably between two types of input patterns. This is mostly done by a sort of training process, the backpropagation procedure. If one has a library of input patterns, these can be passed to the network. After the input pattern has been applied and the output has been calculated, the connections between the neurons are adjusted according to the generalized delta rule (see [12] for a detailed description of neural networks). After a certain number of these training procedures the network 'learns' the patterns of the types of input information and the output of the network results in a value close to zero for a pattern of type A) and in a value close to one for a pattern of type B).

For a detailed description of the use of neural networks in the data analysis see [3].

Using libraries of SSE and MSE events, we trained the networks with approximately 400.000 events per network. The resulting seperation of the network is seen in Fig. 2. From this figure it is also visible that for a non-negligible fraction of the pulses an output $y_o$ between 0.1 and 0.9 is returned from the network, i.e. the pulses are not properly attributed to a definite type. The fraction of these pulses is $\sim 20\%$ for all the detectors.

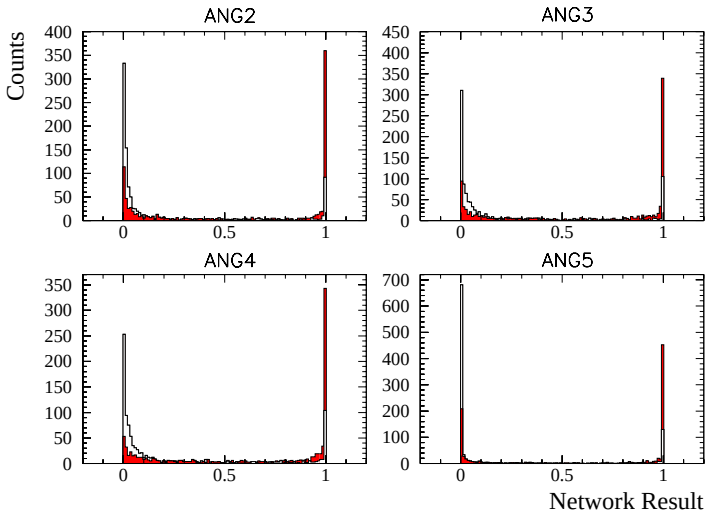


Figure 2: Result of the trained networks tested on independent data, i.e. on pulses which were not used for the training process. The blank histograms correspond to results of events from the SSE-library (expected result: 0), the filled histograms to events from the MSE-library (expected result: 1). Note that the network identifies the contamination with wrong pulses in the refrence libraries correctly.

| **Detector** | **Ratio measured double-escape** | **Ratio simulated Peak 1592 keV** | **Ratio measured 1621 keV** | **Ratio simulated Peak** |
|---|---|---|---|---|
| ANG2 | 70.9±2.7 | 71.7±7.7 | 28.3±1.7 | 18.0±4.8 |
| ANG3 | 72.4±2.7 | 75.1±7.8 | 29.2±1.7 | 17.5±4.7 |
| ANG4 | 72.2±2.7 | 74.8±7.3 | 29.9±1.7 | 18.5±3.4 |
| ANG5 | 76.0±2.8 | 76.4±8.5 | 28.7±1.7 | 17.4±4.5 |

Table 2: Fraction of identified SSE events in the peak areas of the double-escape 1592 keV line and the total absorption 1621 keV peak and their expectations from the simulation.

This quantity can roughly be identified as the efficiency of the separation. However to calculate the exact efficiency, we made detailed Monte Carlo simulations. These provide us with the expected ratio of SSE pulses with respect to the overall spectrum. We use this fact first to adjust the outcome of the networks to the expectations from the simulation.

To compare the results of simulation and measurement directly, the measured and expected ratios of SSE's in the spectrum as a function of energy are shown in Fig. 3 together with the result from the old one-parameter method. It is evident that the result from the neural netwok is satisfactory over the whole energy range above $\sim$ 500 keV. Only below $\sim$1000 keV there is a noticable difference between the neural network method and the old method. Here the old cut yields too many SSE pulses. Note that especially in the energy region interesting for the neutrinoless double beta decay (2000 keV-2080 keV) the agreement of the two techniques is very good.

In Tab. 2 the fraction of identified SSE's in the double-escape peak is listed for the four detectors together with the expected results from the simulation. As evident, the

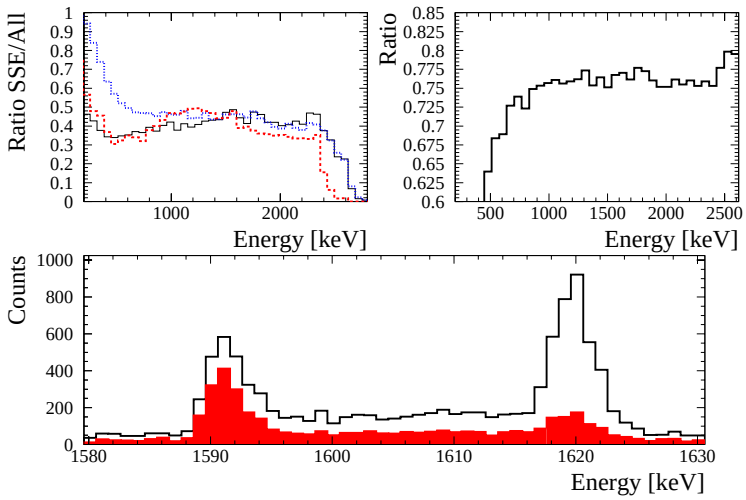


Figure 3: Upper Panel left: Fraction of SSE's in the spectrum obtained using Neural Network (solid line), applying the one-parameter cut (densely dashed line) and the expectation from the simulation (losely dashed line). Upper panel right: Fraction of pulses identified identically by Neural Network and one-parameter cut. Lower panel: Measured spectrum in the energy region of the reference pulses (data independent of the training sample). The filled histogram corresponds to the identified SSE pulses. The open histogram shows the spectrum of all events.

| **Detector** | $e_s$ | $e_m$ | $e_{tot}$ |
|---|---|---|---|
| ANG2 | 0.93±0.27 | 0.86±0.25 | 0.90±0.38 |
| ANG3 | 0.91±0.26 | 0.84±0.24 | 0.87±0.37 |
| ANG4 | 0.91±0.19 | 0.84±0.17 | 0.87±0.27 |
| ANG5 | 0.95±0.27 | 0.85±0.24 | 0.90±0.38 |

Table 3: Efficiencies for correct SSE and MSE identification for the detectors of the Heidelberg–Moscow experiment by neural network.

measured results are in good agreement with the expectation for the double-escape peak. The situation for the measured SSE fraction in the 1621 keV peak is slightly different. Since the efficiency $e_m$ for correct identification of MSE's is not 100%, the actual measured SSE fraction within this peak is somewhat higher than the expected fraction from the simulation. Once the real fraction of SSE's in a certain energy region is known through e.g. a simulation, it is easy to calculate the efficiencies of the recognition (see [3] for details). The total efficiency $e_{tot}$ of the method is then given by the square root of the product of the two single efficiencies. The obtained efficiencies for the four networks in the Heidelberg–Moscow experiment are listed in Tab. 3.

Obviously an efficient separation of MSE and SSE pulses can be accomplished with Neural Networks.

From the ratio of identified SSE pulses in the energy region between 2000 keV and 2080 keV it is expected that the background in the calibration spectrum can be further

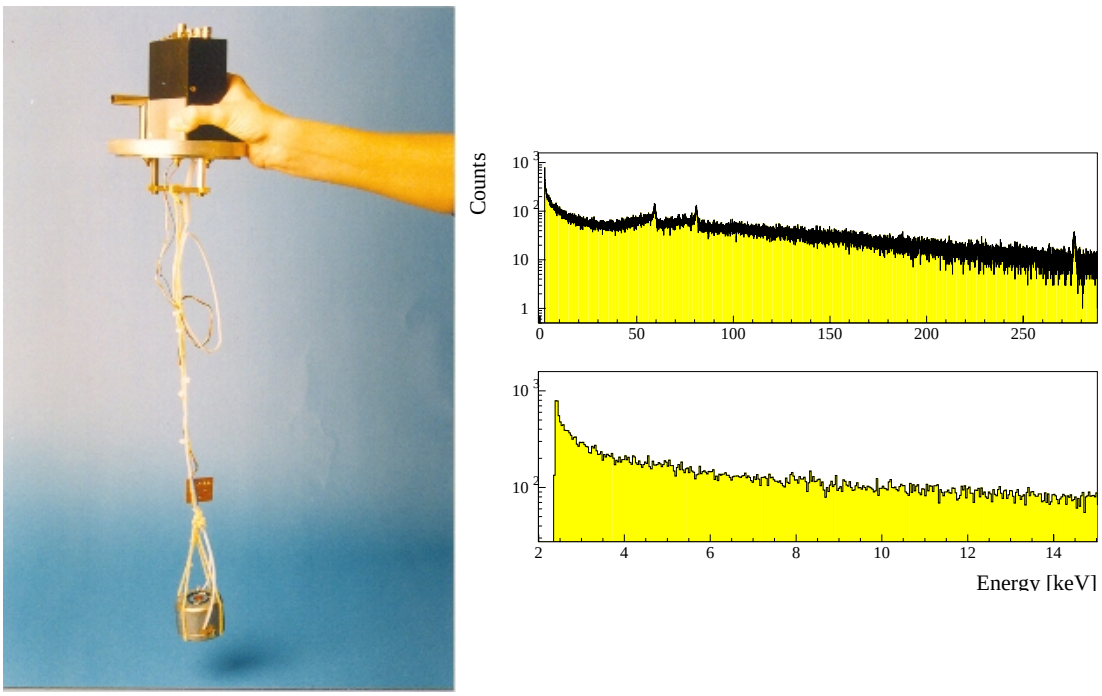


Figure 4: Left: Picture of the detector system including the complete FET circuit (rectangular plate above the knot) and the preamplifier (black box). The HPGe-crystal is hanging on a Kevlar rope. Right: Spectrum obtained with an $^{241}$Am source. Note the logarithmical scale of the spectrum.

reduced by a factor of 2.67±0.05 which is in good agreement with the results obtained from the simulation which yields a reduction factor of 2.78±0.01 and the one parameter-cut, which gives a reduction by a factor of 2.53±0.05. The slightly smaller value in the measurement is the effect of the efficiencies for the recognition. We expect a similar reduction for the Heidelberg–Moscow experiment .

# 4 Preparational work for GENIUS

GENIUS is a project aiming at a very large increase in sensitivity in dark matter and double beta decay search [13, 14].

Several studies have been carried out to demonstrate the possibility of operating 'naked' High-purity Germanium-Detectors in liquid nitrogen [15]. It was shown that the concept of this new detector design works well and seems to be even superior in detector performance compared to conventionally operated High-Purity Germanium-Detectors.

In a further study [16] a detector setup with only 3.5g of contacting materials was developed and succesfully tested (see Fig. 4).

The aim of the GENIUS experiment is to reach the extremely low background level of $\sim$ 0.01 events/(kg y keV) in the energy region below 100 keV and of $\sim 10^{-4}$ events/(kg y keV) in the double beta range around 2 MeV. To show that this is indeed achievable, we performed detailed Monte Carlo simulations and calculations of all the relevant background sources. The sources of background can be divided into external and internal ones. Exter-

nal background is generated by events originating from outside the liquid shielding, such as photons and neutrons from the Gran Sasso rock, muon interactions and muon induced activities. Internal background arises from residual impurities in the liquid nitrogen, in the steel vessel, in the crystal holder system, in the Ge crystals themselves and from activation of both liquid nitrogen and Ge crystals at the Earths surface.

In a first estimation the influence of the components expected to be dominant were studied [17]. In the simulation the setup consisted of a tank with liquid nitrogen, with 288 naked enriched germanium crystals of 3.6 kg each, positioned in its center (this simulation has been performed in view of GENIUS as a neutrinoless double beta decay experiment with 1 ton of enriched $^{76}$Ge). From the background sources mentioned above, only the activities in the liquid nitrogen, steel vessel and muon showers were simulated.

For a more detailed study of the sensitivity of GENIUS in a first experimental phase, further simulations with a new, more accurate geometry have been carried out [15].

The measured photon flux in the Gran Sasso laboratory with photon energies between 0 and 3 MeV was simulated for all the dominant radioisotopes. The influence of neutrons from the natural radioactivity of the rocks was estimated under the conservative assumption that every neutron reaching the liquid shielding is captured leading to excited $^{14}C^*$ and $^{15}N^*$ nuclei. We simulated the radon contamination of the nitrogen and studied the activation of the shielding by muon induced nuclear disintegration and by secondary neutrons from muon interactions. At the same time we calculated the activation of the Ge crystals and of the liquid nitrogen during the period of their exposure at sea level.

The obtained count rates and activation levels confirm the possibility to achieve a background count rate of $\sim 10^{-2}$ counts/(kg keV y) in the energy region below 100 keV and of $\sim 10^{-4}$ counts/(kg keV y) in the energy region interesting for the $0\nu\beta\beta$ decay.

For this, we need only fairly standard arrangements for the setup, like a boron implanted polyethylen foam isolation or a neutron absorption film, an anticoincidence shield for muons (scintillators on top of the setup of a 12m diameter, 12 m height liquid nitrogen tank) and a nitrogen-cleaning device (eventually with nitrogen recycling).

Besides that, we need more sensitive measurements of the contamination level of materials to hold the Ge-crystals and the Rn contamination of liquid nitrogen. Both measurements are underway. Furthermore, surface contamination of the crystals and the supporting structure needs high attention.

Reaching the background level aimed at, the GENIUS project could bring decisive progress in the field of direct dark matter search. It could probe a major part of the SUSY–WIMP parameter space interesting for the detection of neutralinos, thus possibly deciding whether or not neutralinos are the major component of the dark matter in our Galaxy and it is an indispensable experiment to solve the problem of the nature of the neutrino, and of the neutrino mass matrix in connection with the running and future neutrino oscillation experiments [9, 18, 19, 20, 21]

# 5 Acknowledgments

The Heidelberg–Moscow experiment was supported by the Bundesministerium für Forschung und Technologie der Bundesrepublik Deutschland, the State Committee of Atomic Energy

of Russia and the Istituto Nazionale di Fisica Nucleare of Italy. B.M. is supported by the Graduiertenkolleg of the University of Heidelberg.

# References

[1] Heidelberg–Moscow Collaboration, M. Günther *et al.*, Phys. Rev. **D 55** (1997)54.

[2] Heidelberg–Moscow Collaboration, L. Baudis *et al.*, Phys. Lett. **B 407** (1997)219.

[3] B. Majorovits, H.V. Klapdor-Kleingrothaus, Europ. Phys. J. **A 6** (1999)463-469

[4] R.M. Barnett *et al.*, Physical Review **D 54** (1996)1.

[5] K. Muto, A. Staudt, H.V. Klapdor-Kleingrothaus, Europhys. Lett. **13** (1990)31.

[6] G.J. Feldman, R.D. Cousins, Physical Review **D 57** (1998)3873.

[7] H. Minakata and O. Yasuda, Pys. Rev. **D 56** (1997)1692

[8] H. Minakata and O. Yasuda, Nucl. Phys. **B 523** (1998)597

[9] H.V. Klapdor-Kleingrothaus, in Tracts in Modern Physics **163**(2000)69-104, Springer

[10] H.V. Klapdor-Kleingrothaus, H. Päs, Cosmo99, Trieste, Sept. 1999 and hep-ph/0002109

[11] A. Dietz, Diploma thesis, University of Heidelberg, unpublished, 2000

[12] B. Kröse and P. van der Smagt, University of Amsterdam, An Introduction to Neural Networks, 1996

[13] H.V. Klapdor-Kleingrothaus in Proceedings of the First International Conference on Particle Physics Beyond the Standard Model, Castle Ringberg, Germany, 8-14 June 1997, edited by H.V. Klapdor-Kleingrothaus and H. Päs, IoP, Bristol, 1998, 485-531

[14] H.V. Klapdor-Kleingrothaus, L. Baudis, G. Heusser, B. Majorovits, H. Päs, GENIUS - a Supersensitive Germanium Detector System for Rare Events, Proposal, MPI-Report MPI-H-V26-1999 and hep-ph/9910205

[15] L. Baudis, G. Heusser, B. Majorovits,Y. Ramachers, H. Strecker and H.V. Klapdor-Kleingrothaus, NIM A **426**(1999)425 and Preprint hep-ex/981140

[16] B. Majorovits, L. Baudis, G. Heusser, H.V. Klapdor-Kleingrothaus, H. Strecker, submitted to NIM A

[17] H.V. Klapdor-Kleingrothaus, J. Hellmig, M. Hirsch, J. Phys. **G 24** (1998) 483

[18] H.V. Klapdor-Kleingrothaus, Int. J. Mod. Phys **A 13** (1998)3953-3992

[19] H.V. Klapdor-Kleingrothaus, H. Päs, A. Yu. Smirnov, submitted to Phys. Rev. D and hep-ph/0003219

[20] S.M. Bilenky et al., Phys. Lett. **B 465** (1999)193-202

[21] F. Vissani, JHEP 9906 (1999)022 and hep-ph/9906525

# ICARUS. Imaging Cosmic And Rare Underground Signals

F.Arneodo[a], A.Badertscher[b], B.Baiboussinov[c], G.Battistoni[d], P.Benetti[e], E.Bernardini[a], A.Borio di Tigliole[d], R.Brunetti[e], A.Bueno[b], E.Calligarich[e], M.Campanelli[b], C.Carpanese[b], D.Cavalli[d], F.Cavanna[f], P.Cennini[g], S.Centro[c], A.Cesana[d], C.Chen[h], Y.Chen[h], D.Cline[i], I.De Mitri[a], R.Dolfini[e], A.Ferrari[d,g], A.Gigli Berzolari[e], P.Goudsmit[b], K.He[h], X.Huang[h], A.Kruse[b], Z.Li[h], F.Lu[h], J.Ma[h], F.Mauri[e], C.Matthey[i], D.Mazza[f], L.Mazzone[e], G.Meng[c], C.Montanari[e], G.P.Nurzia[f], S.Otwinowski[i], O.Palamara[a], D.Pascoli[d], L.Periale[j], S.Petrera[f], G.Piano Mortari[f], A.Piazzoli[e], P.Picchi[k,l,j], F.Pietropaolo[c], T.Rancati[d], A.Rappoldi[e], G.L.Raselli[e], D.Rebuzzi[e], J.Rico[b], M.Rossella[e], C.Rossi[f], A.Rubbia[b], C.Rubbia[e,g], P.Sala[d,g], D.Scannicchio[e], Y.Seo[i], F.Sergiampietri[m,g], S.Suzuki[l], M.Terrani[d], P.Torre[e], S.Ventura[c], C.Vignoli[e], H.Wang[i], J.Woo[i], G.Xu[h], Z.Xu[e], C.Zhang[h], Q.Zhang[h], S.Zheng[h]

[a] Lab. Naz. del Gran Sasso, S.S. 17 bis Km. 18,910 - Assergi (AQ), Italy
[b] Inst. for Part. Phys. Eidgenössische Tech. Hochschule CH-8093 Zürich, Switzerland
[c] Dip. di Fisica e INFN, Univ. di Padova, via Marzolo 8, Padova, Italy
[d] Dip. di Fisica e INFN, Univ. di Milano, via Celoria, Milano, Italy
[e] Dip. di Fisica Nucleare e Teorica e INFN, Univ. di Pavia, via Bassi 6, Pavia, Italy
[f] Dip. di Fisica e INFN, Univ. di L'Aquila, via Vetoio, L'Aquila, Italy
[g] CERN, CH-1211, Geneva 23, Switzerland
[h] IHEP - Academia Sinica, 19 Yuquan Road, Beijing, People's Republic of China
[i] Dept. of Physics, UCLA, Los Angeles, CA 90024, USA
[j] ICGF del CNR di Torino, corso Fiume 4, Torino, Italy
[k] Dip. di Fisica, Univ. di Torino, via Giuria 1, Torino, Italy
[l] Lab. Naz. di Frascati dell'INFN, via Fermi 40, Frascati (Roma), Italy
[m] INFN Sez. di Pisa, Via Livornese 1291, S. Piero a Grado (Pisa), Italy

**Abstract**

The status of the ICARUS experiment and the main activities of the Collaboration during the year 1999 are summarized. In particular the construction of the 600 ton module, the test of the $10m^3$ prototype, measurements and studies for the optimisation of the working conditions for some critical items of the apparatus and the proposal of the *ICANOE* experiment, which would address the detection of CNGS neutrinos, of atmospheric neutrinos, and searches for nucleon decays, are reported in some details.

# 1 Introduction

The ICARUS technology is a new detector technique, outcome of many years of a graded and careful R&D program developed to provide "bubble-chamber" quality events. It is now a mature technology and a 600 ton ($T600$) module is under construction, in order to study atmospheric and solar neutrinos, and nucleon decay at the LNGS. The $T600$ experiment will stand as a demonstrator that a large scale liquid Argon detector can be built and operated underground.

During the year 1999 the main activities of the ICARUS Collaboration were related to the construction of the $T600$ module. In particular, the construction of the cryostat (the first half-module) is presently being completed, the internal detector mechanics and the high voltage system have been delivered and are being assembled, the production and the test of a first batch of electronics have been completed (Section 2).

The $10m^3$ prototype, already used in 1998, has been widely modified and partly rebuilt in order to reflect the final design of the $T600$. A series of cryogenic tests have been performed in Pavia and, after transportation to the LNGS and installation of the internal detector, the $10m^3$ module is now ready to be used for test of the full detector configuration (Section 3).

Many activities have also been carried out concerning measurements and studies aiming to the optimization of the working conditions for some critical items of the apparatus (Section 4).

The possibility of a long-baseline experiment, based on the ICARUS technique, using the CERN to LNGS neutrino beam facility, has been already discussed in former ICARUS proposals and in recent documents[1]. During 1999, a new detector configuration has been conceived. This consists of an appropriate combination of the ICARUS liquid Argon imaging detector and of the fine grain calorimeter, suitably upgraded to provide also magnetic analysis of muons, developed by $N^{O}E$ [2]. This idea led to the proposal of the *ICANOE* experiment, addressing at the same time to the detection of neutrinos coming from CERN beam, of atmospheric neutrinos, and searches for nucleon decays (Section 5).

# 2 $T600$ Module: status report

The $T600$ module (see Figure 1) consists of two identical, independent liquid Argon (LAr) reservoirs (half-modules), with parallelepiped shape and made of a structure of aluminum honeycomb panels reinforced by aluminum frames. The two half-modules are

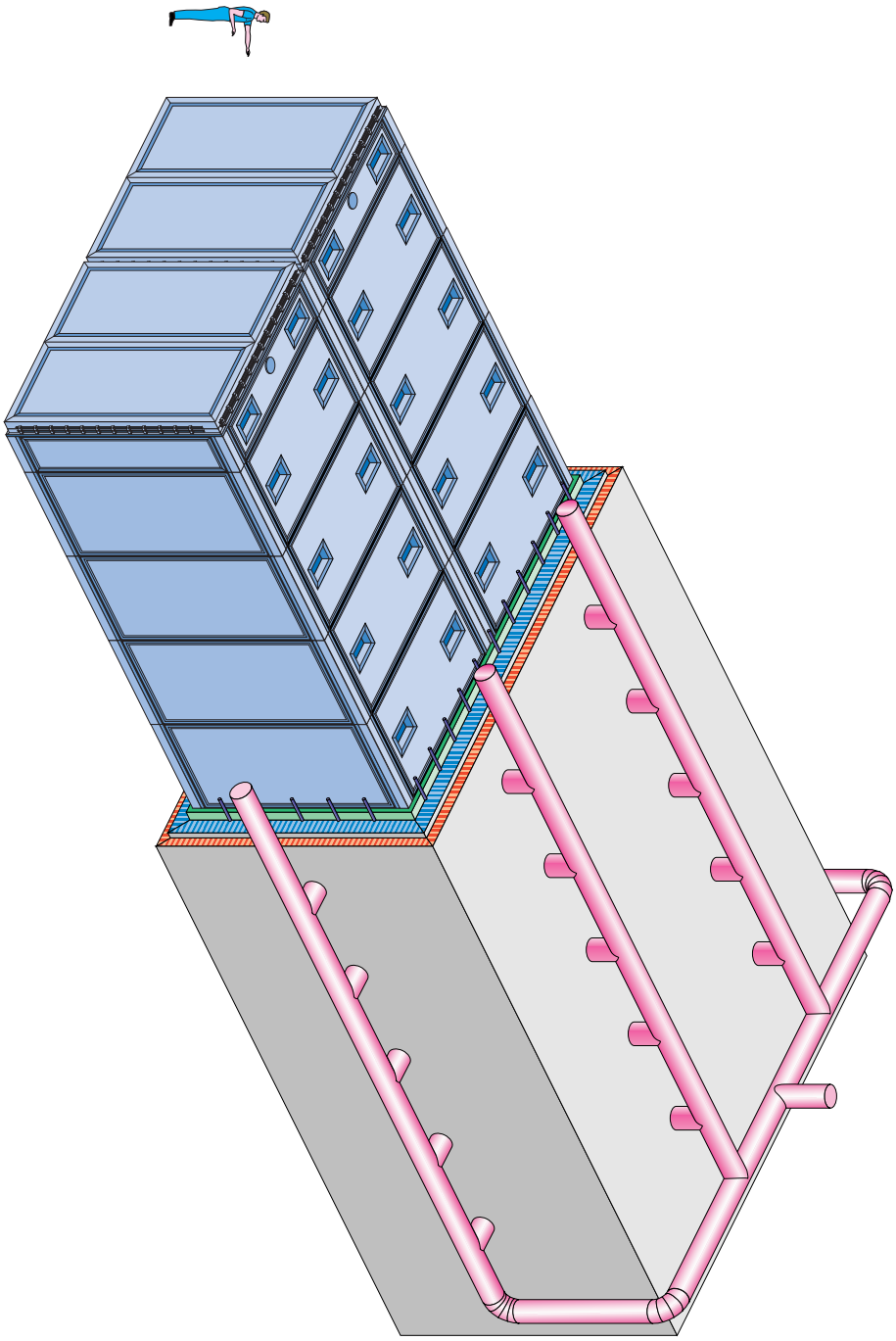

Figure 1: Schematic view of the ICARUS $T600$ cryostat.

surrounded by a common insulation layer made of Nomex (aramid fiber pre-impregnated paper) honeycomb panels.

The cooling of the LAr containers is provided by a forced circulation of liquid Nitrogen ($LN_2$) inside aluminum pipes directly inserted into the aluminum honeycomb panels. $LN_2$ pressure and circulation speed are fixed in such a way to maintain the LAr at about 89 K (LAr equilibrium pressure $\approx$ 1.25 bar abs), with a maximum temperature non-uniformity into the LAr smaller than 1 $^0$C. Additional cooling is obtained by circulating $GN_2$, coming from the evaporation of $LN_2$ from the main cooling circuit, into an aluminum shield inserted in the middle of the insulation panels.

Inside each cryostat half-module the internal detector for imaging and calorimetric event reconstruction is installed. It consists of a large LAr TPC formed by a field shaping system and a wire chamber, with three readout planes, with 3 mm pitch and 3 mm distance among the planes. The first plane, facing the drift region, has horizontal wires, the other two have wires at $\pm 60^0$ from the horizontal direction. Each plane provides an independent view of the event. The geometrical redundancy allows for a fast 3D reconstruction by means of simple algorithms.

Signals from the wires are transported outside the LAr containers through a set of flanges located on top of the cryostat. Custom ultra-high vacuum tight feed-throughs (576 signals per flange) have been developed to this purpose.

The readout electronics boards are located on top of the cryostat, just in front of the signal flanges to minimize the input capacitance due to the cables. This electronics is the latest evolution of the traditional solution developed in the past years by the ICARUS collaboration and tested on many prototypes [3]. The front-end electronics chain is composed by:

1. low noise charge preamplifiers (based on B-CMOS technology);
2. analog multiplexers (8x);
3. commercial 40 MHz, 10 bit digitizers (FADC);
4. custom chip (DAEDALUS) for hit finding, zero-skipping (level-0 trigger);
5. level-1 trigger logic (localized signal multiplicity).

Additional electronics components are: circular memory buffers for continuous data recording with zero dead time; test circuits for signals calibration and routine checks on all the electronics components; HV distribution on the wires. Distributed intelligence (1 CPU per each crate/feedthroughs flange) provides higher level triggers (deposited energy, signal multiplicity), and a basic networking interface.

A brief review of the results achieved in 1999 concerning the activities related to the $T600$ construction is given in the following. For a more complete review and further details about the $T600$ module refer also to the 1996-1998 LNGS Annual Reports.

## 2.1 Cryogenics

According to our previous planning, the first $T600$ half-module was expected to be delivered in Pavia around October 1999, for the start up of the internal detector mechanics

assembly. The bottom part of the insulation with the relative supports for the dewar was installed and aligned in the assembly Hall in Pavia during August/September. The assembly of the first half-module by AIR LIQUIDE Italia, the main industrial counterpart for the realization of the cryogenic system, was completed in September. All the welds have been individually tested for helium tightness by pumping vacuum in the cryostat walls inter space.

Vacuum tests in the main volume started in October 1999. A mechanical instability, evidenced as an anomalous local deformation, at a residual pressure of about 100 mbar, was found on one of the aluminum panels of the vertical walls. After internal inspection of the panel, it was found a largely defective gluing of the aluminum honeycomb in correspondence of the external reinforcing frame, where the shear stresses are most important. Unfortunately this kind of defect cannot be identified with non-destructive methods (x-rays, ultrasound, etc.) therefore, in agreement with AIR LIQUIDE, we decided to proceed to the reinforcement of all the panels by adding aluminum plaques (10 mm thick) on the borders.

During the vacuum tests some defective welds were also found in correspondence of the special elements (aluminum fusion blocks) inserted in the bottom part of the dewar for the internal detector positioning and alignment. This was due to an anomalous content of silicon in the blocks (probably an intrusion occurred during the fusion process), which prevented a correct material penetration during the welding. This defect led to the decision to substitute the fusion blocks with standard laminated aluminum elements. All the reparations and substitutions are expected to be completed by mid February 2000. The delivery of the dewar is therefore now planned by the end of February 2000.

## 2.2 Internal Detector: mechanics construction and test

All the mechanical components of the sustaining structure and the wire chamber system for the first $T600$ half-module, assigned for the construction to the CINEL industry, have been successfully tested both for the correct dimensions and required precision and for the quality of the machine work and of the cleaning procedures. All the mechanical components have been delivered to the Pavia laboratory in the second half of 1999.

The mechanical components needed for the second semi-cryostat are currently under work and will be delivered in the first months of 2000.

The components of the field shaping system (HV cathode and race track system), assigned to the GALLI & MORELLI industry, have been partially tested and are currently under production and are expected to be delivered at the beginning of 2000.

The clean room (100,000 class) and the assembling ramp, described in details in the 1998 LNGS Annual Report, have been constructed and are ready to be utilized in the mounting of the mechanical parts of the internal detector.

The full-speed wiring of the nearly 60,000 wires for the wire chamber systems of the two half modules started in April 1999, after some months of tests and minor adjustments of the wiring and cleaning procedures. The mechanical tension of the wires is routinely tested in each 32 wire module to assure a constant quality of the wiring.

The typical week rate for the wiring is about 40 modules of 32 wires, including the cleaning and storage of the modules. By the end of 1999 about 2/3 of the modules for

the first half-module have been produced. At the current speed of the wiring procedure, all the modules needed for the two half modules will be finished by the first half of 2000.

## 2.3 High Voltage system

The high voltage to the field shaping system is provided by a custom HV feed-through. Two solutions have been studied and realized for the high voltage feed-through to be use in the $T600$ detector. The first solution is based on a coaxial geometry, electrically insulated by high vacuum. In the second solution, the electrical insulation is operated by ultra high molecular weight polyethylene (UHMW PE). Tests on the first solution pointed out its critical behavior for its use in a low noise context, mainly due to x-ray emission. The UHMW PE solution resulted much more safe, reliable and noiseless up the maximum voltage available (150 kV). After the completion of tests, the first PE insulated sample (1 m long) is going to be mounted on the $10m^3$ prototype at the LNGS (see section 3). At present, a series of four new feed-throughs, with improved design and increased length (1.3 m), is under production. Two of them will be mounted on the $T600$ module, the third is a spare and the forth will be used for tests at maximum voltage. Pieces for the first new feed-through are ready for assembling and test. A LabView interface for the HV power supply in use has been developed, for the remote control of a) switching ON/OFF, b) voltage ramp-UP/DOWN, and c) current limit setting.

## 2.4 Characterization of the DAQ system

At the end of 1998 the general layout of the DAQ system was frozen, after the approval of the prototype board performances. Immediately after this approval the production of the analogue ASIC's and digital ASIC's started. The analogue ASIC, in B-CMOS technology, houses two low noise amplifiers, while the digital ASIC, CMOS gate array technology, DAEDALUS, provides filtering and feature extraction on the digital data of 16 channels per unit. All those units are presently delivered and ready for mounting on electronics cards. Moreover, the construction of about 100 signal feed-throughs flanges (576 channels each) also started. Five prototype units are already available and they are used for tests on the existing detectors.

During 1999 the production of a first batch (about two thousand channels) of the elements composing the whole readout chain in their final version and the definition of the final parameters of the whole DAQ system for the $T600$ module have been to carried out.

In Figure 2 the three basic electronics modules of the readout chain are shown. 1) The small Decoupling Board (DB) receives 32 analogue signals from the chamber via the feed-through flange and passes them to the analogue board. It also provides biasing of the electrodes and distribution of test signals. It is housed in the back side of the VME-like crate that houses, in front, the analogue board. 2) The Analogue Board (V791 by CAEN) houses the amplifiers for 32 channels, based on the proprietary analogue BiCMOS VLSI (2 channels per chip) and provides the data conversion (10 bit) at 40MHz rate. The data are transmitted to the digital module via the cable connected to the front panel connector. 3) The Digital Board (V789 by CAEN), ARIANNA, has the two DAEDALUS

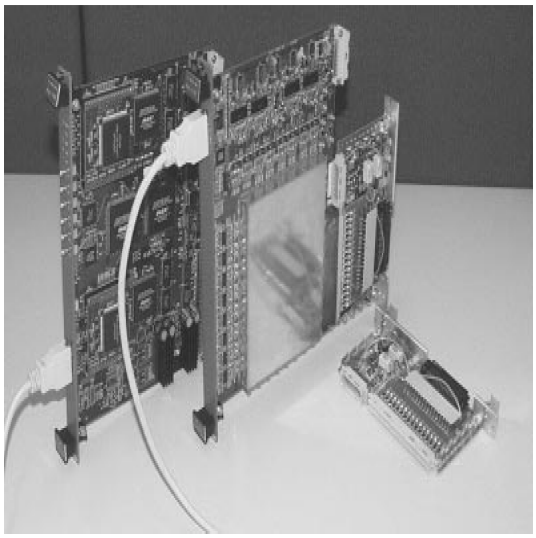

Figure 2: The three basic electronics modules of the ICARUS DAQ system. From left to right: the digital board (V789), the analogue board (V791) and the decoupling board.

VLSI chips, mounted on small piggy back PCBs. The board serves 32 channels and receives the digital data (multiplexed) via the small cable plugged in the front panel. The data out are available via the VME bus.

In the $T600$ the readout scheme is organized in units, each unit is made of a 30U Rack that houses the analogue crate (18 analogue modules), the digital crate (18 digital modules), the relative power supplies and their control and monitor. Each unit will serve 576 channels ($18 \times 32$) and will be mounted on top of the dewar close to each feed-through flange.

In order to test on real data the performance of the DAQ system we decided to ship a complete electronic rack to CERN and to connect it to the 50 liter LAr-TPC, exposed to the CERN neutrino beam in 1997 and 1998, whose characteristics in term of imaging detector are well studied. Aims of the test were multiple:

1) Optimisation of the signal shape and of the signal-to-noise ratio for the three signal configurations (one for each of the three wire planes, as described in Section 4.1). The sketch presented in Figure 3 clarifies this point.

2) Comparison of the "all-out" electronic front-end with the old solution, where the preamplifiers were immersed in LAr and directly connected to the readout wires.

3) Study of the self-triggering and zero-suppression capability of the DAEDALUS chip on real data. Integration in the DAQ system of a T=0 signal from scintillation light as trigger enabler.

4) Tuning of the DAQ software, on-line display and monitoring.

In order to perform these test in conditions as close as possible to the final layout of the $T600$ module, the 50 liter LAr-TPC was equipped with the actual components selected for the final $T600$ assembly. A three wire plane configuration was mounted (see Section 4.1). The cables connecting the wires to the feed-through were 2 meter long (as in the $T600$). The electric field in the drift volume was set to 500 V/cm. The voltages

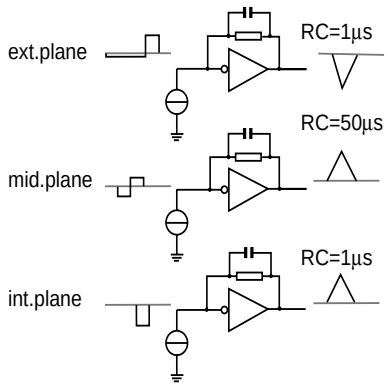


Figure 3: Sketch schematising the various signal configuration at the input of the reat-out chain. The approximative RC values needed to get similar outputs for all configurations are also indicated.

applied to the wire planes (0.V and ±400V.) were such to ensure complete transparency to the drifting electrons and were distributed, to the wire planes from the decoupling boards, through the signal cables.

A photomultiplier tube was placed in the Argon gas phase above the wire chamber looking into the drift volume, to provide a prompt scintillation signal. This was used either as global trigger (for the test of the front-end electronics) or as trigger enabler for the DAEDALUS chip. It was also recorded in the DAQ as T=O signal.

We performed a series of measurements, concentrating first on the short RC ("quasi-current") board that will equip the first induction plane and the collection plane and then of the long RC ("quasi-charge") board needed to equip the intermediate induction plane.

Measurements of the signal-to-noise ratio relative to the complete channel (Decoupling Board, Analogue Board, Digital Board), were previously obtained with a test pulse simulation of a minimum ionizing particle and using an input capacitance (replacing the detector readout electrodes and cabling) of 400 pF, rather larger than the capacitance of the real system. These measuremets provided respectively S/N=9.53 in "quasi-charge" mode, and S/N=13.1 in "quasi-current" mode. At CERN, the whole analogue part of both readout chains in the V791 boards went through a careful fine tuning that, after several iteration, allowed to find the best set of components matching the physics requirements (S/N <12, FWHM $\simeq 5\mu s$). Major modifications concerned the feedback RC of the preamplifiers as well as gain and bandwidth of the shaper.

A first preliminary version of the event builder has also been tested to verify the maximum sustainable rates and bandwidth. It performed within requirements (up to 1000 event fragments/s collected and delivered by the local cpu, equivalent to over 2 MB/s from crate to storage), although noise conditions before adjustment of the front-end shaping didn't allow to handle a fully DAEDALUS driven DAQ with reasonable low value thresholds. This is presently under evaluation with the modified V791 boards. The integration of a multi-crate layout is underway and will be installed at the LNGS during the $10m^3$ run foreseen from February 2000 (see Section 3.2).

# 3 $10m^3$ Module: tests and performances

A $10m^3$ prototype module has been designed and built by the AIR LIQUIDE Italia Industry to reproduce as close as possible the working conditions of the final $T600$ detector. The $10m^3$ LAr container is a parallelepiped box, 2.580 w x 1.000 l x 3.890 h $m^3$ (internal dimensions), made of aluminum honeycomb panels, 150 mm thick. The main cooling is provided by a forced circulation of pressurised $LN_2$ inside a circuit directly inserted into the aluminum panels of the LAr container. The container is surrounded by an insulation layer made of aramid fiber honeycomb panels with an intermediate aluminum shield, cooled by cold Nitrogen gas. According to our specifications, the circulation speed has to be such that the temperature of the LAr results to be uniform within one degree, to avoid relevant variations of the drift speed over the internal volume.

The top cover panel is removable to allow for the insertion of the internal detector (wire chamber module, sensors and monitors); the feedthroughs of the wire chamber, the feedthroughs of the sensors and the entry points of the main purification and recirculation systems are all located on the top cover. The prototype is equipped with:

1. a gas Argon (GAr) recirculation unit, containing a standard Oxisorb/Hydrosorb filter;

2. a LAr forced recirculation unit, using an immersed pump and containing a standard Oxisorb/Hydrosorb filter.

The prototype is also equipped with an automatic control and regulation system, identical to the one foreseen for the $T600$ module. The control system automatically regulates the various processes during the run (cooling process, pumps functionality, automatic valves opening and regulation, filling of dewars, etc..). It provides a schematic display of the prototype conditions, including the status of the various devices and the relevant cryogenic parameters (pressures, levels, temperatures of the $LN_2$ circuit). It also activates alarms in case of malfunctioning. An automatic logging of data on computer disk is dumped every 30 seconds.

Several types of sensors have been added to complete the equipment of the prototype (level meters, temperature and pressure probes, purity monitors, etc.).

A brief review of the activities of the Collaboration in 1999 concerning the $10m^3$ module is given in the following.

## 3.1 Cryogenic and purification test in Pavia

The cryogenic and purification systems of the $10m^3$ module (Figure 4) have been tested in Pavia during the period between February and July 1999.

The test programme aimed to the acquisition of data for the determination of the main features of the cryogenic and purification systems: vacuum tightness, cooldown slope, temperature gradients, purification and recirculation systems performances [4].

A wires chamber module, previously assembled and tested in 1998 [5], has been inserted in the cryostat. Some of the wires have been equipped with readout cables and connected to a $T600$ standard feedthrough flange.


Figure 4: Picture of the $10m^3$ prototype installed in the experimental hall in Pavia.

A vacuum tightness check to ensure good LAr purity has been performed, following a procedure defined in agreement with Air Liquide. The final vacuum level, after about 20 days of pumping using one of the four pumping station of the $T600$, was around $10^{-5}$ mbar. Considering the large dimensions of the cryostat this level has been judged as satisfactory. The pump down curve (see Figure 5) was almost perfectly compatible with the expected behavior from simulations used for dimensioning the pumping system for the $T600$ [6]. The analysis of the residual gasses inside the cryostat, from a mass spectrometer, showed that the gas composition was dominated by water ($\approx 60\%$), nitrogen ($\approx 30\%$) and oxygen ($\approx 10\%$) released by the plastic material of the cables. No significant percentages of other materials have been found, indicating that the adopted cleaning procedures are appropriate.

The start-up procedure of the cryogenic plant requires a well defined sequences of operations. The main goal of this test was to perform a check for a similar procedure to be applied with the $T600$ module. The first step was a pre-cooling phase of the system. During this phase, to avoid possible thermal stresses due to an abrupt injection of $LN_2$ into the cooling circuit, the cooling of the cryostat walls, down to about -30 $^o$C, was made using a dedicated device (pre-cooling unit: PCU), injecting a temperature controlled mixture of liquid and gas Nitrogen. During this phase, which lasted about 2 days (cooling speed $\approx$ -1$^o$C / hour), the cryostat was under vacuum and the internal temperatures decreased slowly to about 0$^o$C. The cryostat was then filled with purified GAr and continued the the pre-cooling. Due to the thermal exchange of the GAr, the internal temperature rapidly uniformed with the temperature of the walls. At about -60 $^o$C, we stopped the PCU

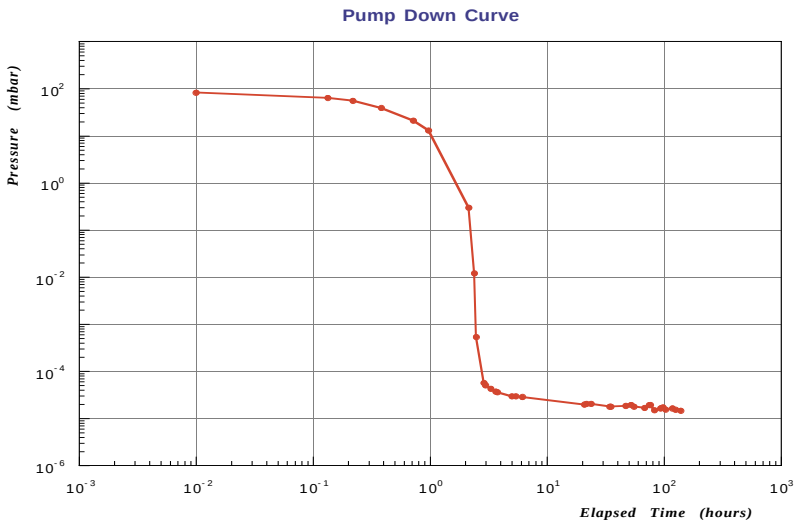


Figure 5: Pump down curve of the $10m^3$ module.

and started circulating $LN_2$, using the circulation pump. After other 2.5 days, when all the temperatures were below -150 $^o$C, we started filling the cryostat with purified LAr. The total filling time was about 36 hours. During all the cooling, according to our specifications, the internal temperatures maximum gradient never exceeded 40 $^o$C (see Figure 6a).

A position meter, installed on one of the three tensioning devices of the chambers module measured the total elongation of the compesating spring equipping the wires frame. The measured elongation was about 1.2 mm (Figure 6b), corresponding to about 200 grams of tension increase on the wires, about half of which was compensated by the tensioning device, as expected from previous tests [5]. This confirms the functionality of the variable geometry mechanics.

LAr purity was one of the main parameters to be checked during this test from measurement of the free electrons lifetime. Immediately after the LAr filling, the electrons lifetime was measured to be $200 \div 300$ $\mu s$. No significant degradation of the lifetime was observed in the four days following the filling. At this point we started the forced LAr recirculation with the immersed pump. The free electrons lifetime rapidly increased with a slope consistent with one volume (i.e. $10m^3$) recirculation time of about 40 hours. The final electrons lifetime, after about 4 days of recirculation, was measured between 2 ms-3 ms, at the sensitivity limit of our purity monitors. Reminding that the maximum drift time in the $T600$ module is of about 1 ms, we conclude that the required purity level has been reached. After the stop of the LAr recirculation we observed a decrease of the lifetime. We then turned on again the LAr pump and, after a sudden decrease [1], the lifetime restarted to increase with about the same time constant that we observed at the

[1]This behaviour is related to the particular configuration of the recircultion circuit, which allows concentration and stratification of the impurities inside the dewar housing the pump. As a consequence we decided to modify the circuit layout for the $T600$ to avoid this problem.

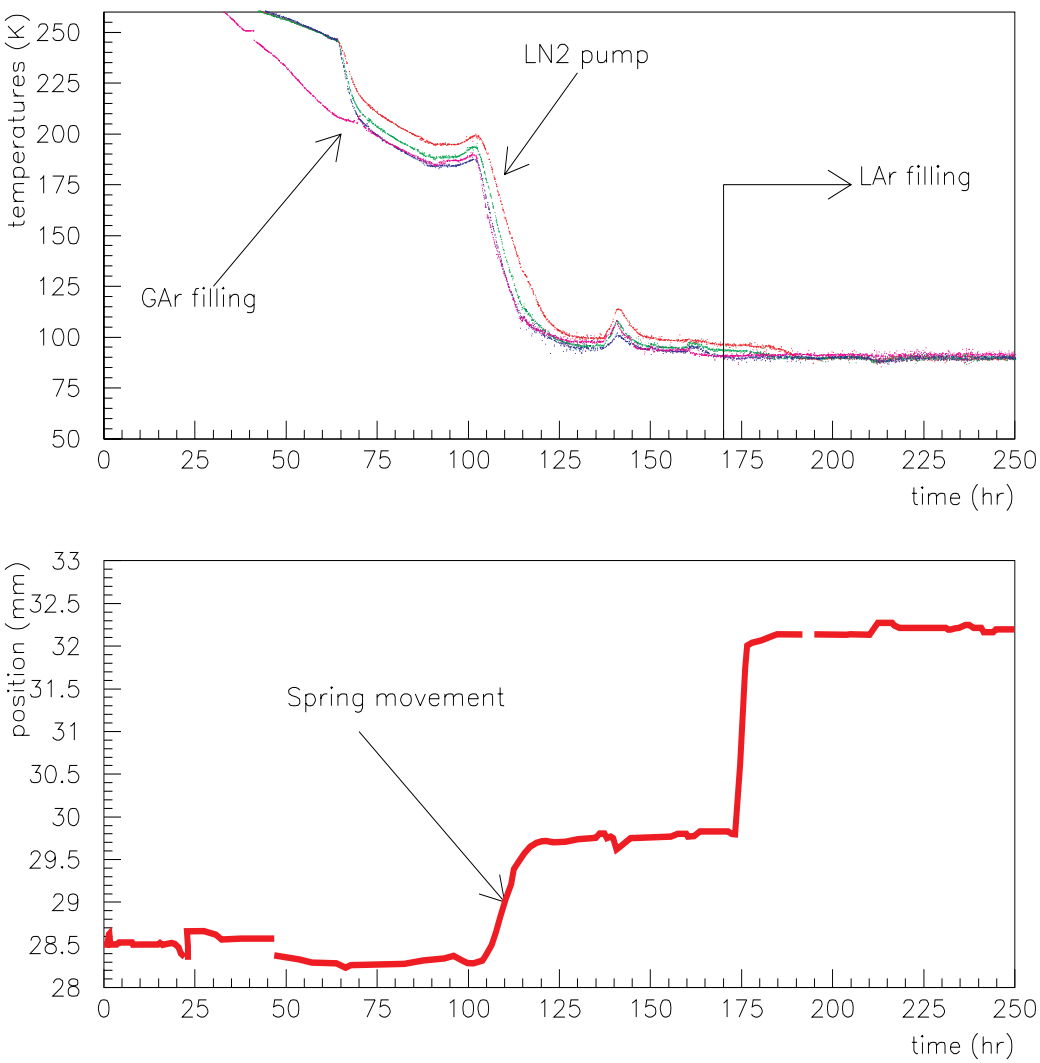


Figure 6: a) Cooldown curves measured on some of the temperature probes; b) the corresponding motion measured on the tensioning device is shown: the first ramp is the effect of the motion of the spring during the cooling in GAr, while the second is due to the capacitance increase of the instrument during the filling of LAr.

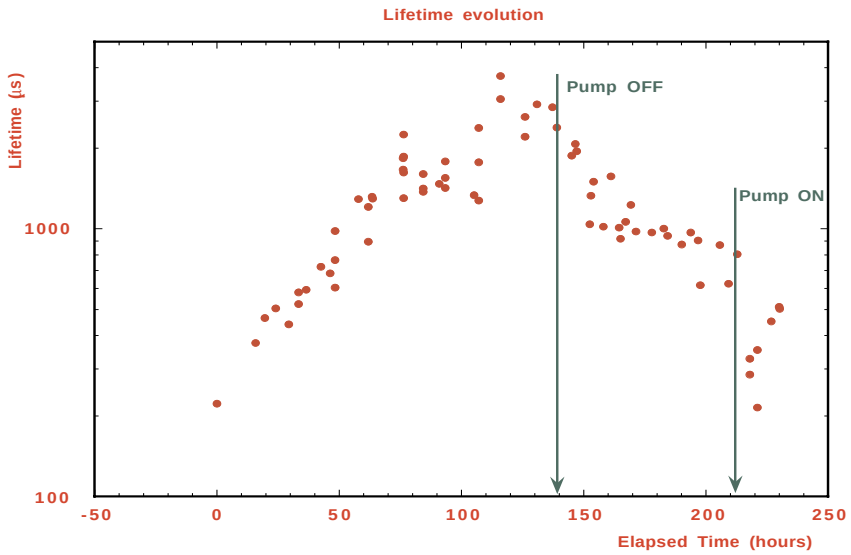


Figure 7: Free electrons lifetime evolution in the $10m^3$ module

beginning of the process, as shown in Figure 7.

Another basic parameter to be measured was the $LN_2$ consumption for cooling, which is related to several contributions: thermal inlet through the cryostat walls and consumption from various parts of the cooling circuit. A second, dedicated run in July 1999 has been performed to define these contributions. The measured thermal inlet was of 19-22 $W/m^2$, in agreement with the design value of 20 $W/m^2$, indicating that the insulation is performing as expected. Other significant contributions to the $LN_2$ consumption (about 1700 $LN_2$ litres per day) comes from the "services" (the $LN_2$ pump, transfer lines, flash evaporation, etc.). Optimisation of the circuit for the $T600$ is expected to reduce this contribution of about 25%.

The last issue of the Pavia test programme concerned the investigation of the noises induced by the cryogenic system on the wires chamber electronics. We were in particular interested to eventual microphonic noises induced by LAr boiling and/or convection, pumps vibrations, etc. To this purpose we connected to the feedthroughs flange a sample of channels corresponding to the longest wires of the chamber module. The wires were readout using our standard analog + digital boards followed by the hit finder/data reduction board [7, 8]. Low frequency noise (baseline fluctuations) was quite small (few ADC counts). No significant variations on the signals spectrum were observed by turning on and off the various devices of the cryogenic system (vacuum pumps, $LN_2$ pump, LAr pump, etc.). Also no effect was observed when the polarization field on the wires was turned on. We concluded therefore that, with the present configuration of the readout electronics, the noise, both high and low frequency, induced by the cryogenic and purification systems was negligible.

The successful operation of the $10m^3$ prototype during the two tests runs in Pavia concludes the R&D and prototyping phase concerning the cryogenics, purification and internal detector mechanics, in view of the $T600$ realization.

## 3.2 $10m^3$ module re-mounting at the LNGS and internal detector modifications

A further use of the $10m^3$ module as a full detector prototype has been considered highly useful to complete the development of the ICARUS $T600$ project and to explore technical upgrades or possible novel solutions for the multi-Kton detector design, presently under study for the future long baseline experiment. An extensive set of long term tests at LNGS has been planned, as discussed in [9]. The role of such proposed extension of the previous cryogenic test program of the $10m^3$ module is assesed by the following list:

- to provide a suitable facility for testing all the activity issues of the various ICARUS groups in real experimental $T600$-like conditions, before the final employ with the $T600$ module;
- to start-up interaction and cooperation with the local LNGS Technical Staff, assuring the growth of the necessary "in situ" expertise and technical support for the future ICARUS experimental activity.

An outside location of the $10m^3$ module was decided in order to guarantee an easier and more efficient use of the test facility compared to an underground site. Moreover, in principle, it also allows to extend the time window for further tests even after the arrival of $T600$ module at Gran Sasso. The operation of the $10m^3$ module required therefore an experimental area at the LNGS with the same kind of external facilities as at the Pavia workshop.

A $200m^2$ working area located at the *Hall di Montaggio* resulted compatible with the necessary specifications. It required only minor works, as a special concrete platform for the stocking dewars and and another one for the module itself. Transportation of the dismounted parts of the module and cryogenic system from Pavia to LNGS took place in August 1999.

In order to transform the $10m^3$ technical module into a full detector prototype a number of important modifications had to be performed on the internal detector. Namely, by adding a field shaping system (cathode and race-track) to the exsisting wire chamber frame, by equipping the module with a HV feed-through and by modifying the wire chamber layout in order to guarantee the electrical connection of the $\sim$ 2000 wires to the signal feed-through flanges. The field shaping system (cathode, Race-track rings and Vetronite supports) has been designed (from the corresponding $T600$ project, scaling its dimensions to fit the $10m^3$ dimensions) and entirely built in all components at the LNGS mechanical workshop.

The assembly has been completed in October 1999. All the wire modules (32 wires each) have been connected to dedicated printed circuits housing a 32 pins connector. 58 flat cable sets (32 channels each) with special connectors at both ends have been prepared and installed to bring the wire signals from the printed circuits to the 4 signals feed-through flanges mounted on special wayouts located on the top of the cryostat. All these components have been taken from the spare lot of the production series for the $T600$ module. Sensors and purity monitors, already used during the Pavia runs, have been tested, improved and re-installed. AIR LIQUIDE took care of improving the insulation

system in order to reduce the $LN_2$ consumption, following the indications from the Pavia tests.

Finally, in addition to the internal detector set-up described above, a number of features have been implemented, namely:

1. A number of PMT's tubes for UV scintillation light detection.
   UV light is copiously produced in LAr by ionizing events. Detection of the prompt UV light emission may provide a direct signal for the determination of the $T_o$ of the events. Several R&D studies have been performed to define the best solution for UV light collection. A solution with PMT's with $MgF_2$ windows, transparent to UV light, is straightforward, the main disadvantage is the cost. This kind of PMT's are produced in small sizes ($10cm$ diameter maximum) and an exceedingly large number is required for the necessary photocathode coverage for the $T600$. Standard PMT's with glass windows with a wavelength-shifter deposited on it may provide a suitable solution.
   The $10m^3$ represents an ideal volume where comparing the performance of PMT's of various kinds and possibly providing a proven solution to be implemented in the $T600$ module. Therefore we decided to mount an array of four PMT's, placed behind the wire chamber, equipped respectively with $MgF_2$ window (two PMTs) and with quartz window (one of which covered with a suitable wavelength-shifter).

2. A calorimetric readout system for one of the LAr non-imaging regions, located outside the drift volume.
   A calorimetric readout of the LAr volume outside the drift volume (the drift volume is defined by the internal dimensions of the field shaping system and closed at one end by the wire planes) is important to recover information about the energy deposition in these volumes from those events originating in the drift volume, where also imaging information is provided. The basic idea is that ionisation charges are produced everywhere in the $LAr$, obviously also outside the drift volume. Here we have a residual electric field produced by the race track shaping electrodes and by the cathode. Hence, ionisation electrons produced in these non-active regions are transported onto the detector walls (referenced to ground). Readout of these charges can be obtained simply by a set of electrodes (pads) placed close to the walls and eventually biased to a suitable potential.

   In details, the read-out scheme adopted for the $10m^3$ module is based on a set of 2 mm thick $\times$ 1 m $^2$ plane electrodes, placed closed to one of the inner walls, and segmented into 5 cm pads, each one connected to an amplifier. The pad electrodes have width and spacing from the walls adjusted in order to keep their capacitance of the order of 500 pF.

3. An external trigger system, made with two plastic scintillator arrays, with time coincidence logic, placed on two opposite sides of the external walls of the cryostat. This system should provide trigger signals for cosmic ray particles, crossing or stopping inside the sensitive LAr volumes.

The internal detector, completed by all the devices mentioned above, has been assembled by the end of October 1999 and immediately after inserted in the cryostat.

The cryogenic plant (insulation pannels, LAr and $LN_2$ circuits, etc.) was then re-mounted in the *Hall di Montaggio* in November 1999. During December 1999 all the preliminary tests have been succesfully performed. The start-up procedure will begin in January 2000.

# 4 LAr TPC prototypes: measurements and studies

During the year 1999 we exploited the liquid Argon imaging chambers available at CERN to study a number of open issues, concerning the detector characteristics and performance, that were important to finalise the design of the $T600$ module.

This activity concentrated on the following items: the optimisation of the front-end electronics for the three wire plane readout configuration, the detection of 140 cm drift ionisation tracks, the determination of the tracks direction by means of $\delta$-rays. In parallel, tests to study the properties of liquid Argon and liquid Xenon as Dark Matter detection media have been carried on.

A brief review of the results achieved in 1999 concerning the cited activities is given in the following.

## 4.1 Three wire plane readout test

In the readout chamber of the $T600$ module three wire planes are foreseen. The middle plane wires experience an induction current that changes sign as soon as the electrons cross the plane itself (bipolar signal).

We performed a test with the goals of studying the induction signal shape from the wires of the intermediate plane and verifying that the proposed configuration of the front-end electronics for this plane is adequate not only from the point of view of the signal to noise ratio but also from that of the low frequency noise and baseline fluctuations. The test has been performed using the 50 liter LAr-TPC chamber, which has the shape of a parallelepiped with top and bottom faces ($325 \times 325$ mm$^2$) acting as readout anode and cathode respectively, while the side faces, 47 cm long, supported the field shaping electrodes. The readout electrodes were two stainless steel wire planes with the wires running in orthogonal directions. The plane facing the drift volume worked in induction mode while the other was used to collect the drifting electrons. The plane separation was 4 mm, the wire pitch 2.54 mm and the wire diameter 100 $\mu m$. The total number of wires was 128 for each plane.

A third electrode plane (a metallised vetronite board) was added on top of the original readout structure at a distance of 4 mm from the collection wire plane. With a positive voltage applied between this plate and the collection plane, the drifting electrons cross the collection plane, which now works in induction mode as intermediate plane. With a negative voltage, electrons stop on the collection plane as in the original configuration of the LAr TPC.

The front-end electronics was mounted directly on the wire frame in order to reduce the input capacitance of the pre-amplifiers, which were originally designed to work immersed in Liquid Argon. A "quasi-current" configuration of the electronic chain was adopted

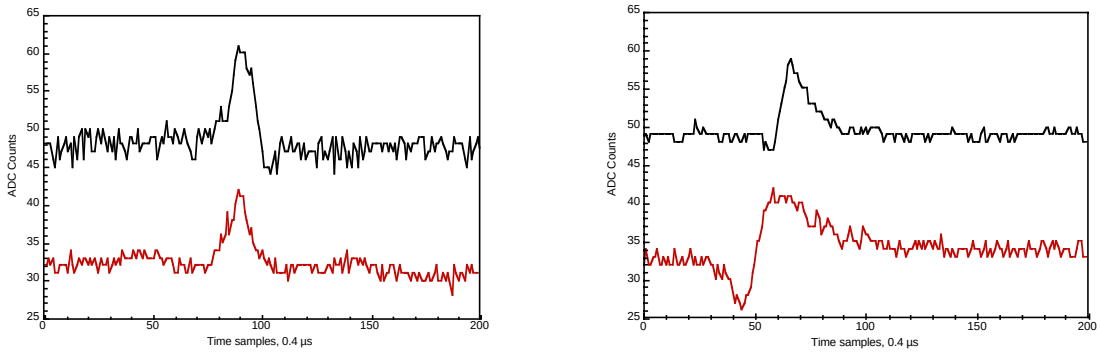


Figure 8: Left: Single wire signal on the intermediate plane read in charge mode; the top one is in collection mode and it is digitally differentiated for easier comparison, the bottom one is in induction mode. In collection mode 100 % of the electrons contribute to the signal pulse height while in induction mode only 80 % of the drifting charge is available. The signal rise-time and decay time are of the order of 4 $\mu s$ as expected. Right: As a comparison, two typical signals from the induction plane facing the drift volume (read in current mode) are shown. Pulse height and signal shape do not differ much from the those of the signal of the intermediate plane read in charge mode, except for the baseline variations due to the signal induced by the electrons approaching the wire plane.

with a RC constant of about 3 $\mu s$ for the induction plane. The electronics connected to the collection plane was switched to "charge mode" with a RC constant of about 100 $\mu s$. An electric field of 500 V/cm was applied in the drift volume. Cosmic ray muon tracks were collected and analysed.

A close look at a single wire signal on the intermediate plane (Figure 8-left) shows that in case of electron collection the signal is slightly higher than in the induction case. In fact in collection mode 100 % of the electrons contribute to the signal pulse height, while in induction mode only 80 % of the drifting charge is useful. The signal rise-time and decay time are of the order of 4 $\mu s$ in both cases.

This proves that the use of an approximate integrator, with a RC constant much larger than the typical pulse duration, is the correct solution for the front-end amplifier of the intermediate plane, because it allows to obtain signals very similar in shape and pulse height to those of the collection plane read in current mode.

As a comparison two typical signals from the induction plane facing the drift volume (read in current mode) are also shown in Figure 8-right. Pulse height and signal shapes do not differ much from those of the signal of the intermediate plane read in charge mode, except for the baseline variations. The r.m.s. noise level calculated on a window of 256 samples is about 0.7 ADC counts for the amplifiers working in current mode and 1.0 in charge mode. A 2.54 mm m.i.p. is expected to give a signal with a pulse height larger than 10-12 ADC counts; hence a signal-to-noise ratio for a m.i.p. close to 10 is also at reach for the intermediate plane wires [10].

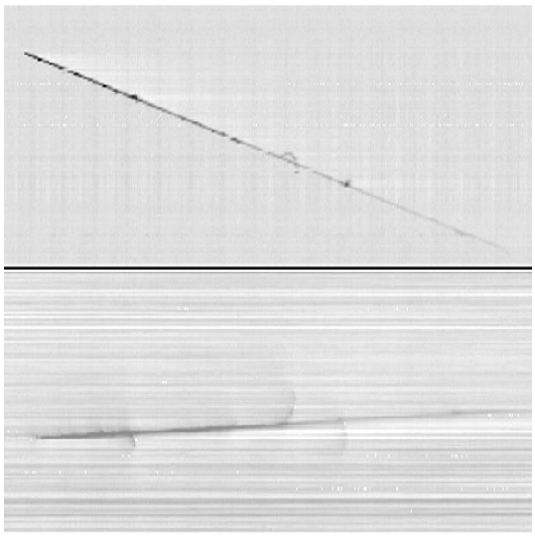

Figure 9: Muon tracks as seen in the 50 liter TPC with a drift of 140 cm, with an electric field of 500 V/cm. The top half of the figure shows the collection time-projection read in current mode, the bottom half is the induction time-projection read in charge mode; note the different baseline behaviour. The horizontal axis is the drift time (625 samples corresponding to 1 ms), the vertical is the wire numbering (128 wires in each view corresponding to 325 mm).

## 4.2 First observation of 140-cm drift ionising tracks

In the $T600$ module, an electron drift distance of 140 cm is foreseen. Up to now the longest drift path exploited in the R&D phase of the ICARUS experiment was only 50 cm. It was therefore important to perform a test with the drift increased to 140 cm. Among possible drawbacks due to the long electron drift path, we can cite the followings:

1. Distortions of the track pattern due to electric field non-uniformity, especially near the boundary of the TPC, where the field shaping electrodes are discontinuous. The field non uniformity can induce a local variation of the electron drift velocity, which in turn can produce a delay in the electron arrival times on the readout wires.

2. Degradation of the signal shape due to electron diffusion (longitudinal and transverse), which can spread out the drifting electron cloud. Being the induced signals read in "current" mode, this spread turns into a decrease of pulse height and increase of pulse duration with negative effect on the recognition of single pulses and on the separation of subsequent pulses.

Also for this test the 50 liter TPC was used, with a modified drift length increased to 140 cm simply using longer vetronite boards, supporting the field shaping electrodes. We took cosmic ray data (as an example, an events is shown in Figure 9) in stable conditions of electron lifetime (1 ms), with drift electric fields up to 500 V/cm.

It is worth noting that the full width half maximum of each pulse along the muon track (excepted those from where a delta-ray starts) was of the order of 4 $\mu s$, independently

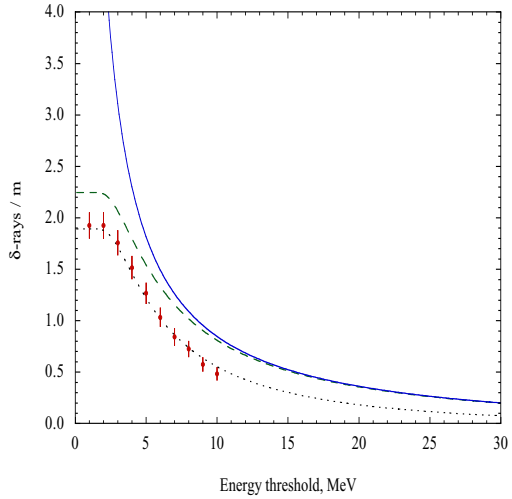


Figure 10: Experimental cumulative energy distribution of the $\delta$-rays (solid circles). The expectations are also plotted: the solid curve gives the rate with no selection cuts, the dashed line includes the kinematical and topological selection factors, the dotted one takes into account also the containment factor of the 50 liter LAr-TPC.

from the starting location of the free electron clouds. This implies that the thermal diffusion is negligible over full drift distance of 140 cm. Also the electric field distortions at the drift volume boundary do not affect appreciably the track direction [11].

## 4.3 Determination of m.i.p. tracks direction by means of $\delta$-ray

We exploited the crossing muon data, collected in the 50 liter LAr-TPC exposed to the CERN neutrino beam in 1997-1998, to investigate the possibility of identifying the direction of minimum ionizing particle tracks relying only on $\delta$-rays orientation.

Simple selection criteria, based on the topological separation of the $\delta$-rays from the parent track, allow identification and reconstruction $\delta$-rays down to very low energy (few MeV), with high efficiency and no misidentification of their direction, thanks to the fine grain spatial resolution of the LAr TPC.

These criteria were applied to the visual scanning of a sample of 320 crossing muon events, corresponding to 120 m of minimum ionizing particle track. The Monte Carlo prediction of two recognized $\delta$-rays per meter of track came out to be very well matched by the result of the scanning of the experimental data, as shown in Figure 10.

With the above analysis, we demonstrated experimentally that slightly more than two $\delta$-rays per meter of track can be fully reconstructed. This implies that the track direction identification cability can be very high: an efficiency of 99% is at reach considering only 2 m of track [12].

## 4.4 Study of nuclear recoils in liquid Xenon

In 1999 we concluded the analysis of the data of a test done with a liquid Xenon detector for Dark Matter search, exposed to a neutron beam to produce nuclear recoil events simulating those which would be generated by WIMP's elastic scattering.

The aim of the experiment was to measure directly the scintillation efficiency of nuclear recoil in the tens of KeV range and to compare it to that of natural radioactivity.

In the case of natural radioactivity, energy is deposited mostly by ionization and atomic excitation, detectable both as primary scintillation light and as free electrons when an electric field is applied through the LXe volume. In absence of electric field, electron-ion recombination strongly reduces the free-electron yield and proportionally increases the scintillation light yield.

In the case of nuclear recoil from neutrons or Dark Matter candidates, only a fraction of the energy loss goes into ionization and atomic excitation; moreover nearly all electron-ion pairs, produced by ionization, recombine because of the high ionization density, even in presence of a strong electric field; hence only primary scintillation light (from recombination and atomic de-excitation) is expected.

It follows that the relative scintillation efficiency, namely the ratio between the scintillation yield of nuclear recoil over the scintillation yield of electrons/gammas at zero electric field, is a good measurement of the nuclear recoil quenching factor, $f_A$, defined as the visible deposited energy over the true recoil energy. This is because in the case of electrons and gammas almost all the energy loss by ionization is converted into scintillation light through electron-ion ricombination.

The experiment was performed exposing a LXe detector to a neutron beam at the Legnaro National Laboratory. The scattered neutrons from the Xenon target were detected by neutron counters at some fixed angle to measure the actual energy transfer to Xenon nuclei. The energy of the incident neutron was selected by time of flight using the timing of the beam trigger, the Xenon scintillation light and the neutron counter signals. The quenching factor of LXe was thus obtained by comparing the LXe scintillation response to Xenon nuclear recoil of given energy with the LXe scintillation response to gamma rays of the same energy.

A detailed description of the experiment can be found elsewhere [13]. Here we want to point out the results of the data analysis.

The data collected in the experiment allowed calculating $f_A$ in the recoil energy range from 40 to $120 KeV$. It was evaluated to be about 20 %, as reported in Figure 11. These values of $f_A$ are consistent with the theoretical prediction proposed by Lindhard et al. As a comparison, the experimental and theoretical data for Silicon are also presented (in this case the free ionization charge has been used to determine the nuclear quenching factor).

# 5 Multi-Kton detector for LBL neutrinos: *ICANOE*

During 1999 we have submitted a proposal for a combined ICARUS and $N^O E$ [14] "general purpose" underground detector, *ICANOE*[15], to be located at the LNGS. The *ICANOE* main scientific goal is the one of elucidating in a comprehensive way the pattern of neutrino

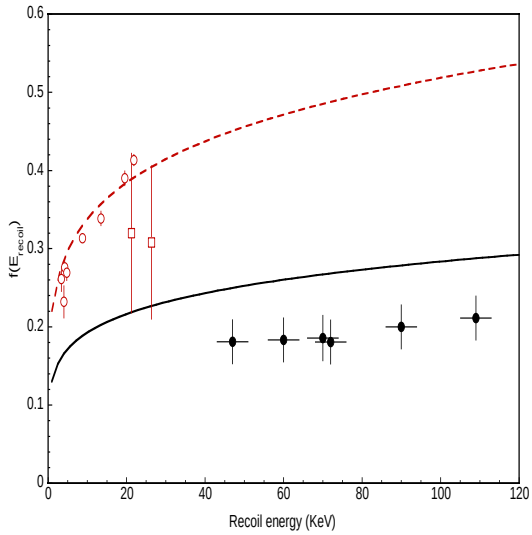


Figure 11: Relative scintillation efficiency in LXe as a function of the Xenon recoil energy. The full circles are the data from the present experiment, open circles and squares are data points from the Si experiment of Gerbier and Sattler respectively. The curve represents the calculation of Lindhard et al., dashed line for Si and continue for Xe.

masses and mixing. The experiment can simultaneously observe neutrinos from CERN beam (CNGS) and atmospheric neutrinos and adress searches for nucleon decays.

The *ICANOE* detector fruitfully merges the superior imaging quality of the ICARUS LAr detector (**liquid target**) with the high resolution full calorimetric containment of NOE[2], suitably upgraded to provide also magnetic analysis of muons (**solid target**).

The liquid target, which accomplishes simultaneously the two basic functions of target and detector, is able to provide high resolution, unbiased, three dimensional images of ionising events, and to provide accurate measurement of the basic kinematical properties of the particles of the event, including particle identification. The superior quality of the event vertex inspection and reconstruction of the liquid target is ideally complemented by the addition of the external calorimetric module capable of magnetic analysis of the muons escaping the LAr chamber. Bubble chambers have in fact often been very similarly complemented in the past by external identifiers. An iron muon tracking spectrometer would fulfill this job, but it would also introduce in between adjacent LAr volumes a blind region incapable of giving information on the energy and on the nature of the escaping particles. A sensitive magnetized calorimeter appears therefore as an ideal containment module to be interleaved between adjacent LAr volumes.

## 5.1 Outline of the *ICANOE* detector

The *ICANOE* layout is similar to that of a "classical" neutrino detector, segmented into almost independent **supermodules**. The layout of the apparatus can be summarized as follows:

- the **liquid target**, with extremely high resolution, dedicated to tracking, $dE/dx$

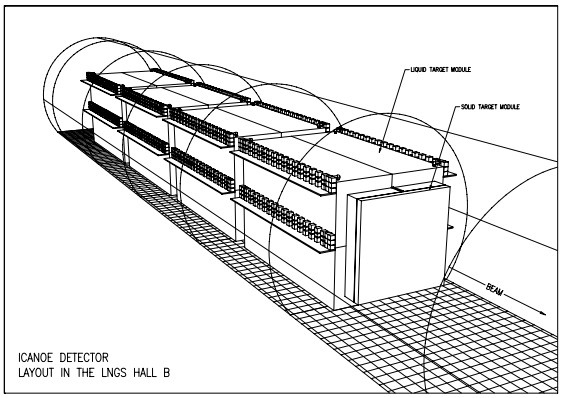


Figure 12: Perspective view of the baseline detector with 4 supermodules.

measurements, full e.m. calorimetry and hadronic calorimetry, where electrons and photons are identified and measured with extremely good precision and $\pi/\mu$, $K$ and $p$ separation is possible at low momenta;

- the **solid target**, with good e.m. and hadronic resolution, dedicated to calorimetry of the jet, and a magnetic field for measurement of the muon features (sign and momentum);

- The **supermodule**, obtained joining a liquid and solid module, which constitutes the basic module of an *expandable* apparatus. A supermodule behaves as a complete building block, capable of identifying and measuring electrons, photons, muons and hadrons produced in the events. The solid, high density sector reduces the transverse and longitudinal size of hadron shower, confining the event (apart from the muon) within the supermodule.

The *ICANOE SuperModule* is, according to the present design, composed by a liquid Argon module with $18 \times 11 \times 11$ m$^3$ of external dimensions and 1.4 kton (1.9 kton) of active (total) mass, and a magnetized calorimeter module, with $3 \times 9 \times 9$ m$^3$ of external dimensions and 0.8 kton of mass. At this stage, *four* SuperModules with a total length of the experiment of 82.5 m and a total active mass of 9.3 kton fully instrumented are being considered for the baseline option (Figure 12). Discussions and evolutions within the Collaboration and with the involved industries are still in progress; the *ICANOE* detector design will be completely defined during year 2000.

In the present configuration, the liquid target modules are horizontally and vertically split into four drift volumes "submodule". The drift distance is 4 m long, requiring a maximum applied high voltage of 200 kV. In this configuration each module is equipped with a unique HV power supply, a filter for residual ripple suppression, a HV 1-to-4 splitter, with resistive de-coupler, 6 HV cable segments, 4 HV feedthroughs. Each drift volume is contoured by a set of 80 field-shaping electrodes and a cathode. The cathode is connected to the HV feedthrough. The field-shaping electrodes are biased in voltage through resistive voltage dividers connecting the cathode to ground.

The calorimetric modules consist of planes of calorimetric units. Each plane is 9 m long and 9 m wide and is made of 180 units, each with 5×5 cm cross section. The units

have alternating orientation (horizontal and vertical) with respect to the beam direction. Each calorimeter plane contains 5 thin sheets of absorbers (5 mm thick iron sheet) and 5 planes of scintillating fibers (2 mm in diameter). A plane of tracking chambers follows each pair of horizontal and vertical calorimetric units.

## 5.2 Physics goals

The *ICANOE* detector is capable to achieve the full reconstruction of neutrino (and antineutrino) events of *any* flavor, and with an energy ranging from the tens of MeV to the tens of GeV, for the relevant physics analyses. No other combinations can provide such a rich spectrum of physical observations, including the systematic, on-line monitoring of the CNGS $\nu$-beam at the LNGS site. The unique lepton identification capabilities of *ICANOE* are really fundamental in tagging the neutrino flavor. In general, the oscillation pattern of the neutrinos may be complicated and involve a combination of $\nu_\mu \rightarrow \nu_\tau$, $\nu_\mu \rightarrow \nu_e$ and $\nu_\mu \rightarrow \nu_{sterile}$ transitions. In order to fully sort out the mixing matrix, unambiguous neutrino flavor identification is mandatory to distinguish $\tau$'s from $\nu_\tau$'s and electrons from $\nu_e$'s interactions. In other words, we stress the importance of constraining the oscillation scenarios by coupling appearance in several different channels and disappearance signatures.

The *ICANOE* sensitivity in the classic $(\sin^2 2\theta, \Delta m^2)$ plot is evidenced in Figure 13, for a data taking time of 4 years, with $4.5 \times 10^{19}$ pot at each year. We remark:

1. The recent results on atmospheric neutrinos ("A" and "B" of Figure 13) can be thoroughly explored by appearance and disappearance experiments. For the current central value, both CNGS and cosmic ray data will give independent and complementary measurements and they will provide a precise $(\sin^2 2\theta, \Delta m^2)$ determination.

2. In the mass range of LSND, the sensitivity is sufficient in order to solve definitely the puzzle.

3. At high masses of cosmological relevance for $\Delta m^2 <\approx 10$ eV$^2$, the sensitivity to $\nu_\mu \rightarrow \nu_\tau$ oscillations is better or equal to the one of CHORUS and NOMAD.

4. In the atmospheric neutrino events, one can approach a level of sensitivity sufficient to detect also the effect until now observed in solar neutrinos.

Since we can observe and unambiguously identify both $\nu_e$ and $\nu_\tau$ components, the full (3 x 3) mixing matrix can be explored. By itself, this is one of the main justifications for the choice of the detector's mass.

In the cosmic ray channel, all specific modes (electron, muon, NC) are equally well observed without detector biases and down to kinematical threshold. The CR-spectrum being rather poorly known, a confirmation of the SuperKamiokande result requires detecting both (1) the modulation in the muon channel and (2) the lack of effect of the electron channel. The consistency of the simultaneous observation of the $L/E$ phenomenon in as many modes as they are available is a powerful tool in separating genuine flavour oscillations from exotic scenarios. In some favourable conditions, the direct appearance of the

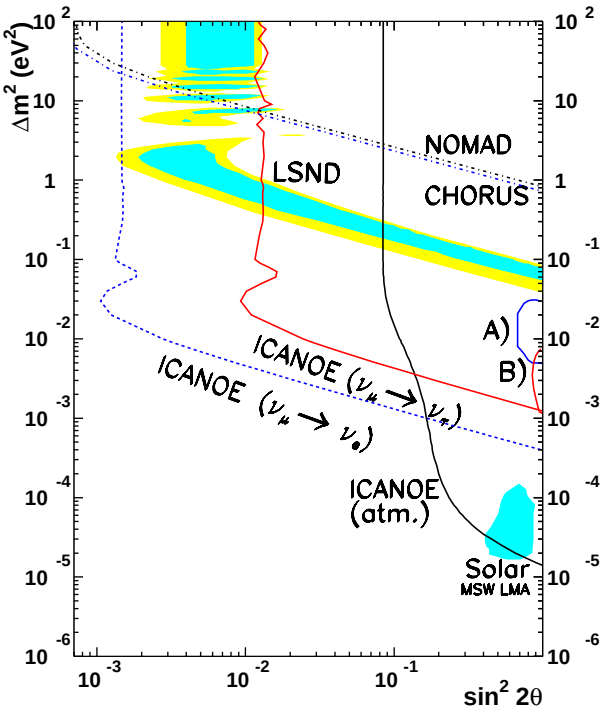


Figure 13: Overview of the status of the neutrino oscillations searches, displayed assuming two neutrino mixing schemes in the $(\sin^2 2\theta, \Delta m^2)$ plane. The 90%C.L. allowed regions obtained from the Kamiokande (resp. Superkamiokande) FC and PC samples are shown as A) (resp. B)). The 90% (resp. 99%C.L.) regions consistent with the LSND excess are shown as dark (resp. light) shaded areas in the upper region of the plane. The shaded area in the region $\Delta m^2 \approx 10^{-5}$ eV$^2$ represents the large angle MSW solution of the solar neutrino deficit. CHORUS and NOMAD 90%C.L. limits on $\nu_\mu \rightarrow \nu_\tau$ oscillations are visible in the upper $\Delta m^2$ region. The *ICANOE* sensitivities at 90%C.L. are indicated by three curves: the limit by direct observation of the atmospheric neutrinos ("*ICANOE* atm"); the direct tau appearance search at the CNGS ("*ICANOE* $\nu_\mu \rightarrow \nu_\tau$"); the direct electron appearance search at the CNGS ("*ICANOE* $\nu_\mu \rightarrow \nu_e$").

oscillated tau neutrino may be directly identified in the upgoing events, since even a few events will be highly significant.

While in atmospheric neutrinos, the knowledge of the sign of the muon is of little relevance, in the case of the CNGS is a powerful tool to verify the neutrino nature after oscillation path, excluding for instance oscillation channels into anti-neutrinos.

# 6 List of Publications

1. F. Sergiampietri, "Extending to 3 meters the drift length in the ICARUS 600 T detector", ICARUS-TM/99-01 (1999).

2. F.Arneodo et al., "Detection of scintillation light in coincidence with ionizing tracks

in a LAr TPC", submitted to Nucl. Instr. and Methods, March 1999.

3. F.Arneodo et al., "Neutron background measurements in the ICARUS area at the underground Gran Sasso Laboratory", submitted to Nuovo Cimento, March 1999.

4. ICARUS Collaboration, "Use of the ICARUS $10m^3$ module as detector prototype", ICARUS-TM/99-05 (1999).

5. ICARUS Collaboration, "Short report on performance evaluation of the ICARUS $10m^3$ Prototype", ICARUS-TM/99-09 (1999).

6. A. Ferrari and C. Rubbia, "Muon Momentum Determination by Multiple Scattering in Liquid Argon", ICARUS-TM/99-10 (1999).

7. A. Bueno and A. Rubbia, "Detecting the presence of $\mathrm{nu}_\tau$ in the atmospheric neutrino flux",ICARUS-TM/99-11 (1999).

8. F. Sergiampietri, "Layout of signal and calibration cables, flanges and crates for ICARUS 600T", ICARUS-TM/99-12 (1999).

9. M. Campanelli et al., "Three family oscillations from muons beams at very long baseline", ICARUS-TM/99-13.

10. Icarus Collaboration, "Scintillation Efficiency of Nuclear Recoil in Liquid Xenon", ICARUS-TM/99-14 (1999).

11. D. B. Cline, "Study of the HEP Neutrinos and the Vacuum Solar Neutrino Oscillations with the Icarus 600-Ton Detector", ICARUS-TM/99-15 (1999).

12. F. Sergiampietri, "About the thermal Insulation for the ICARUS Cryostat", ICARUS-TM/99-16 (1999).

13. ICARUS Collaboration, "Study of solar neutrinos with the 600-ton liquid Argon ICARUS detector", ICARUS-TM/99-17 (1999).

14. C. Carpanese et al., "A three-plane read-out test", ICARUS-TM/99-18 (1999).

15. C. Carpanese et al., "First tracks of 1.4 m length", ICARUS-TM/99-19 (1999).

16. C. Montanari et al., "Automatic monitoring and regulation for the Icarus cryogenic and purification system", ICARUS-TM/99-21 (1999).

17. G. Battistoni et al., "Determination of m.i.p. tracks direction by means of delta-rays", ICARUS-TM/99-23 (1999).

18. ICANOE Collaboration, "ICANOE: a proposal for a CERN-GS long baseline and atmospheric neutrino oscillation experiment", LNGS-P21/99 INFN/AE-99-17 CERN/SPSC 99-25 SPSC/P314

19. ICANOE Collaboration, "Addendum 1: Preliminary Technical Design & Cost Estimates", LNGS-P21/99-Add1, CERN/SPSC 99-39, SPSC/P314 Add.1

20. ICANOE Collaboration, "Addendum 2: Answers to Questions and Remarks Concerning the ICANOE project", LNGS-P21/99-Add2, CERN/SPSC 99-40, SPSC/P314 Add.2

# References


[1] The complete list of references can be found on the ICARUS Web page: *http://www.aquila.infn.it/icarus/.*

[2] The complete list of references can be found on the NOE Web page: *http://www.na.it/NOE/.*

[3] P. Benetti et al., Nucl. Instr. and Meth. A332 (1993) 395; P. Benetti et al., Nucl. Instr. and Meth. A333 (1993) 567; P. Benetti et al., Nucl. Instr. and Meth. A346 (1994) 550.

[4] ICARUS Collaboration, Short report on performance evaluation of the ICARUS 10m3 Prototype, ICARUS-TM/99-09 (1999).

[5] S. Bricola et al., Report on the 10 $m^3$ cryostat, ICARUS-TM/98-05 (1998).

[6] P. Benetti et al., Pumping system for the ICARUS 600 ton detector, ICARUS-TM/98-17 (1998).

[7] C. Carpanese et al., ARIANNA: the readout module for ICARUS, prototype version, ICARUS-TM/98-07 (1998).

[8] C. Carpanese et al., DEDALUS: a feature extractor for ICARUS signals, ICARUS-TM/98-08 (1998).

[9] ICARUS Collaboration, Use of the ICARUS 10 $m^3$ module as detector prototype, ICARUS- TM/99-05 (1999).

[10] C. Carpanese et al., A three-plane read-out test, ICARUS-TM/99-18 (1999).

[11] C. Carpanese et al., First tracks of 1.4 m length, ICARUS-TM/99-19 (1999), accepted for publication by NIM-A.

[12] G. Battistoni et al., Determination of m.i.p. tracks direction by means of delta-rays, ICARUS-TM/99-23 (1999), accepted for publication by NIM-A.

[13] ICARUS Collaboration, Scintillation Efficiency of Nuclear Recoil in Liquid Xenon, ICARUS-TM/99-14 (1999), accepted for publication by NIM-A.

[14] NOE Collaboration [Università di Napoli, Lebdev Institute (Moscow), Università di Lecce, Laboratori Nazionali del Gran Sasso, Università di Bari, Università della Calabria, Yerevan Physical Institute (Yerevan), Institute for High Energy Physiscs (Moscow), Institute of Nuclear Research (Moscow), Institute of Theoretical and Experimental Physics (Moscow)].

[15] F. Arneodo *et al.* [ICARUS and NOE Collab.], "ICANOE: Imaging and calorimetric neutrino oscillation experiment," LNGS-P21/99, INFN/AE-99-17, CERN/SPSC 99-25, SPSC/P314; LNGS-P21/99-ADD1, CERN/SPSC 99-39, SPSC/P314 Add.1; LNGS-P21/99-ADD2, CERN/SPSC 99-40, SPSC/P314 Add.2. Updated information can be found at *http://pcnometh4.cern.ch*.

# LUNA. Laboratory for Underground Nuclear Astrophysics

R. Bonetti[1], C. Broggini[2], H. Costantini[3] L. Campajola[4], P. Corvisiero[3], A. D'Onofrio[4], A. Formicola[4], G. Gervino[5], L. Gialanella[4,6], U. Greife[7], A. Gulielmetti[1], C. Gustavino[8], M. Junker[8], A. Kiss[9], P. Prati[3], V. Roca[4], C. Rolfs[6], M1. Romano[3], F. Schümann[6], F. Strieder[6], E. Somorjai[9], F. Terrasi[4], H.P. Trautvetter[6], S. Zavatarelli[4]

[1] Università di Milano, Dipartimento di Fisica and INFN, Milano
[2] INFN, Padova
[3] Università di Genova, Dipartimento di Fisica and INFN, Genova
[4] Università di Napoli, Dipartimento di Fisica and INFN, Napoli
[5] Politecnico di Torino, Dipartimento di Fisica and INFN, Torino
[6] Institut für Experimentalphysik III, Ruhr–Universität Bochum
[7]Colorado School of Mines, Golden, USA
[8] Laboratori Nazionali Gran Sasso, Assergi
[9] ATOMKI, Debrecen, Hungary

**Abstract**

The electron screening effect has been studied by measuring the cross section of the reaction D($^3$He,p)$^4$He at low energies using the 50 kV accelerator installed at LNGS. The work on the equipment which will be installed in the underground laboratories in June 2000 is in progress. It includes a new 400 kV accelerator, a BGO-summing detector, a new data acquisition system and a windowless target system. The reaction $^7$Be(p,$\gamma$)$^8$B has been reinvestigated at low energies considering for the first time the effect of recoil losses.

# 1 Introduction

The underground accelerator facility LUNA installed at the Laboratori Nazionali del Gran Sasso (LNGS), offers unique possibilities for the studies of nuclear reactions with low cross sections. At the moment it consists of a 50 kV accelerator [1]. A 400 kV accelerator is currently under construction and will be commissioned in September 2000. The accelerators are used to determine thermonuclear reactions of astrophysical interest in or near the range of stellar energies – called the Gamow Peak. As these energies are typically much lower than the Coulomb barrier, the measurements are hampered by exponentially dropping cross sections (see for example *LNGS Annual Report 1997, p. 106*) [2]. Typical cross sections in the Gamow peak are smaller than 1 fbarn. The reaction rate in a nuclear physics experiment involving such low cross sections is thus often less than one event per day. In consequence the studies of thermonuclear reactions in a laboratory at the earth's surface are hampered by the background induced in the detectors by cosmic rays.

Passive shielding around the detectors provides a reduction of gammas and neutrons from the environment, but it produces at the same time an increase of gammas and neutrons due to the cosmic-ray interactions in the shielding itself. A $4\pi$ active shielding can only partially reduce the problem of cosmic-ray activation. The best solution is to install an accelerator facility in a laboratory deep underground [3].

But still due to the extremely low counting rates mentioned above the experiments are very time consuming. Thus the facility must be very reliable and should not require a lot of maintenance.

# 2 Studies of Electron Screening at the LNGS

In order to interpret cross sections measurements at low energy correctly and to construct realistic stellar models good understanding of the electron screening effect is needed (see also *LNGS Annual Report 1997, p. 106* and [4]). For this reason the LUNA-collaboration has studied the reaction D($^3$He,p)$^4$He at the 50 kV accelerator at LNGS. The experiment

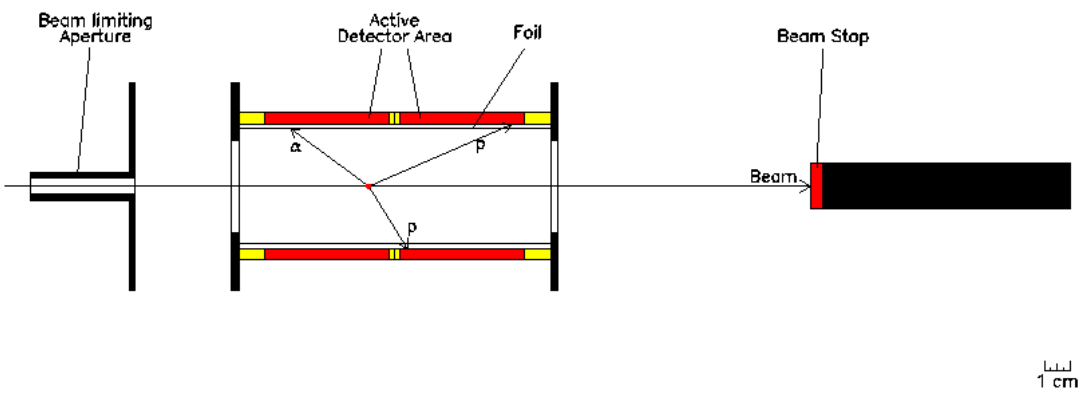


Figure 1: Schematic design of the new detector setup.

has been carried out reducing sources of systematic errors like energy loss and angle straggling [6] as much as possible. The 50 kV LUNA accelerator at LNGS delivered a $^3$He beam with energies $E_{\rm ext}$ between 25 keV and 12 keV in the laboratory system. The beam impinged on a windowless gas target. Target pressures $p$ of 0.1, 0.2 and 0.3 mbar were chosen for each energy $E_{\rm ext}$. The detector setup mounted in the target gas is shown in Figure 1. It consisted of eight 1000 $\mu$m thick silicon particle detectors with a surface of 5 cm x 5 cm each, which were covered by 1.5 $\mu$m Al foils.

As the beam lost part of its energy while passing the gas target, the effective beam energy $E$ in the center of mass system increases with decreasing target pressure at each energy $E_{\rm ext}$ and thus $E = E(p)$. Because of the exponential energy dependence of the cross section $\sigma(E)$ this pressure dependence is of particular importance for deriving the astrophysical $S$-Factor $S(E)$ from the cross section $\sigma(E)$ determined experimentially:

$$\sigma(E(p) = \frac{S(E)}{E} \exp\left(-31.27 Z_1 Z_2 \sqrt{\mu/E(p)}\right)$$

The lost energy has been determined in the past by applying the stopping power tables of Ziegler at al. [5].

However, the energy loss at low energies quoted in these tables rely on extrapolation and thus induce an additional uncertainty in the data analysis as pointed out by Langanke [6]. The data taking for this experiment has been finished in 1999, but the data analysis is still on the way. The results will be published in 2000.

# 3 The 400 kV accelerator at LNGS

In 1998 INFN has approved the funding for installing a new 400 kV accelerator in the underground laboratories of LNGS. The machine will be dedicated to Nuclear Astrophysics (see also *Annual Rep. 1997, p. 110*). The accelerator is actually under construction at High Voltage Engineering Europa B.V. (The Netherlands). The final drawings have been approved in December 1999.

At the same time the LNGS engineering devision is working on the experimental site. By the end of 1999 the building for the accelerator has been constructed at the exit of Hall A. The site will be ready to host the accelerator by May 14$^{\rm th}$ 2000. Figure 2 shows a sketch of the installation located at the exit of Hall A.

The first measurements to be carried out at the new accelerator will concentrate on the $^{14}$N(p,$\gamma$)$^{15}$O reaction, which is of interest for solar neutrino astrophysics as well as for the determination of the age of globular clusters. Extensive simulations have been carried out in order to design the target and the detection system. As a result the first step to investigate the reaction will be performed with a gas target located inside a massive BGO detector with a diameter of 21 cm a a length of 20 cm. A central bore-hole with a diameter of 6 cm will allow to place the target inside the detector. The detector will consist of six segments, each of which will be observed by two photomultipliers at either side of the detector. Figure 2 shows a sketch of the setup currently under construction at the INFN section of Genova.

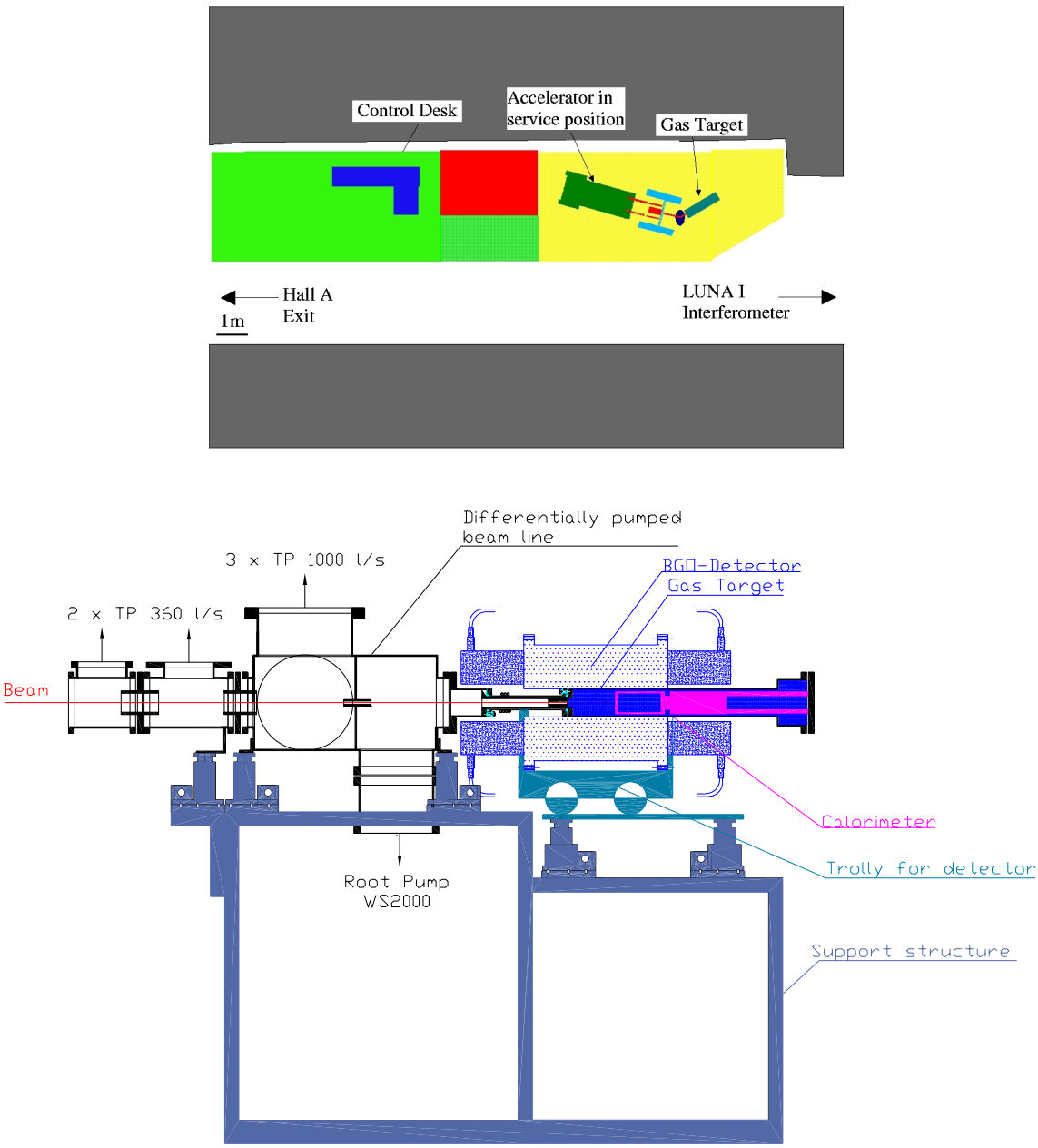


Figure 2: Top: Sketch of the LUNA II site for the 400 kV accelerator. Bottom: Schematic view of the new gas target with the BGO-summing detector.

For the acquisition system of LUNA II the new FAIR bus system developed by the LASS laboratory of the INFN Naples has been chosen. During 1999 the design of the LUNA version has been completed and all the hardware ordered, received and assembled.

The actual system configuration includes:

- 1 VME crate, FAIR version
- 6 CPU Motorola 68030
- 2 RAM disks
- 1 RAM module 64MB
- 1 SEGC and 1 SYSC VME modules
- 2 peak ADC 32 channels 12bits
- 1 TDC 32 channels
- 3 scalers 16 inputs
- 1 HP UNIX workstation

The system is presently under bench tests in Naples. The acquisition tasks run on the Motorola CPU under the operating system OS/9. The acquisition control and the on line monitoring software runs on the Unix workstation, linked to the VME bus.

# 4 Measurement of the $^{7}$Be(p,$\gamma$)$^{8}$B reaction with solid state targets

The absolute cross section $\sigma_{17}$(E) of the $^{7}$Be(p,$\gamma$)$^{8}$B reaction influences sensitively the calculated flux of high-energy neutrinos from the sun. Due to its importance for the solar-neutrino-puzzle, the cross section $\sigma_{17}$(E) should be known with adequate precision, i.e. to better than 5 % [7]. In order to reach this goal the LUNA–Collaboration has performed a new measurement of $\sigma_{17}$(E) at the Dynamitron Tandem Laboratorium in Bochum. This experiment includes for the first time measurements with Pt and Cu backings taking into consideration the possible influence of the recoil loss effect [8]. The $^{7}$Be nuclides were produced in a metallic Li sample via the $^{7}$Li(p,n)$^{7}$Be reaction using a 11.4 MeV proton beam (20$\mu$A) from the cyclotron of the ATOMKI. Using hot chemistry the activated samples were transformed into nearly pure $^{7}$Be. The 4 MV Dynamitron tandem accelerator at the Ruhr-Universitt Bochum provided a proton beam at $E_p$ = 0.3 to 3 MeV with a maximum current in the range of 10 $\mu$A. The cross section was determined from the yield of the $^{8}$B recoils, which was deduced from the $\beta$–delayed $\alpha$–decay of $^{8}$B ($T_{1/2}$ = 770 ms). The target was mounted on a rotating wheel, which moved the target between the beam irradiation position and the $^{8}$B–decay counting position (Si detector). The detector efficiency, the irradiation/counting-, and the transfer time–intervals were determined using a calibrated $\alpha$-source mounted in the target position. The beam current was measured in a Faraday cup mounted behind the target. The number of $^{7}$Be target nuclei was determined by measuring the $\gamma$–activity of the target. The measurements were carried out for targets both on Pt and Cu backing. Preliminary results (see figure 3) are

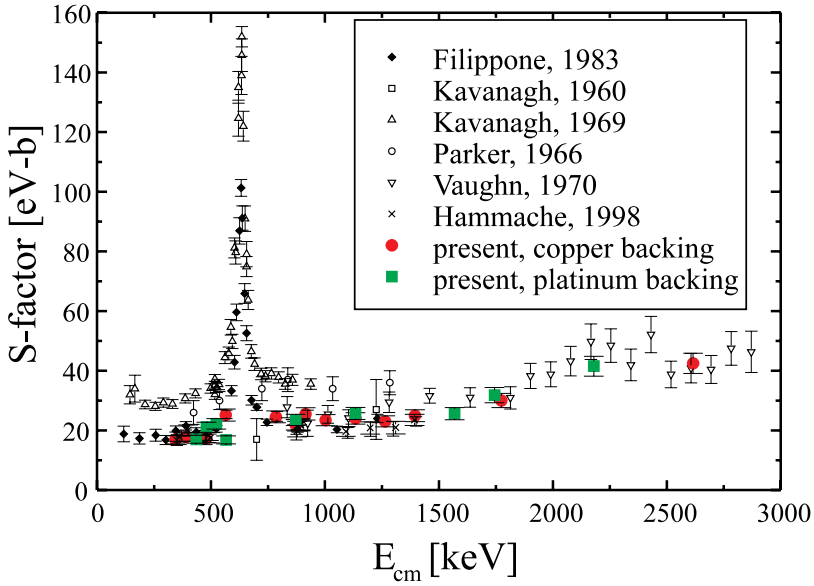


Figure 3: Preliminary result of the measurements on $^{7}$Be(p,$\gamma$)$^{8}$B of the LUNA-Collaboration shown with this literature data.

in good agreement with the measurement of Filippone et al. [9] and suggest that within the experimental errors there is no influence of the recoil loss effect.

# 5 Acknowledgements

The LUNA-Collaboration is indebted with the Director of LNGS for the hospitality and the support offered to this experiment. We would like to thank the LNGS engineering devision and all the technical staff of LNGS both for there help during the course of the running experiments and for the constructive collaboration in setting up the new LUNA II site in the underground laboratories.

# 6 Publications and Conferences

- The LUNA Collaboration, R. Bonetti et al., "First Measurement of the He3+He3–¿He4+2p Cross Section down to the Lower Edge of the Solar Gamow Peak", Phys.Rev.Lett. 82 (1999), 5205–5208;
- M. Junker, "Direct approches to nuclear cross sections at low energies", Invited talk at Workshop "Nuclear Reactions in Stars and in the Laboratory", 8.–19.02.1999, ECT*, Trento, Italy;
- P. Corvisiero, " Present and future work of the LUNA-Collaboration and their implications", Invited talk at Workshop "Nuclear Reactions in Stars and in the Laboratory", 8.–19.02.1999, ECT*, Trento, Italy;

- A. Guglielmetti, "Possible use of CR39 track detector for measuring the p+7Be cross section at low energies", Talk at Workshop "Nuclear Reactions in Stars and in the Laboratory", 8.–19.02.1999, ECT*, Trento, Italy;
- S. Zavatarelli "Gamma-detectors for nuclear reactions studies at low energies" Talk at Workshop "Nuclear Reactions in Stars and in the Laboratory", 8.–19.02.1999, ECT*, Trento, Italy;
- U. Greife, "Reaction Rate Measurements Relevant To The Solar Neutrino Problem (LUNA and NABONA)" invited Talk at 217$^{\text{th}}$ American Chemical Society Nuclear Chemistry Symposium, 21–22.03.1999, Anaheim, Ca, USA;
- F. Strieder, "Production of a $^{7}$Be solid target and measurement of the $^{7}$Be(p,$\gamma$)$^{8}$B reaction", Talk at 217$^{\text{th}}$ American Chemical Society Nuclear Chemistry Symposium, 21-22.03.1999, Anaheim, Ca, USA;
- C. Rolfs, "Modern quests in experimental nuclear astrophysics", Invited talk at ENPE99 21.–29.06.1999 Sevilla, Spain;
- G. Gervino, "Measurement of the $^{3}$He($^{3}$He,2p)$^{4}$He cross section down to the lower edge of the solar Gamow peak", Poster at the international workshop in "Experimental Nuclear Physics in Europe Facing the next millennium", ENPE99 Seville (Spain), 21–26.06 1999;
- C. Gustavino, "The LUNA nuclear astrophysics program", , Poster at the international workshop in "Experimental Nuclear Physics in Europe Facing the next millennium", ENPE99 Seville (Spain), 21–26.06. 1999;
- C. Rolfs, "Open quests in experimental nuclear astrophysics", Invited talk Invited talk at 10$^{\text{th}}$ International Symposium on Capture Gamma-Ray Spectroscopy and Related Topics in Santa Fe, NM, USA, 30.08–03.09.1999;
- M. Junker, "LUNA: An Underground Accelerator Facility for Nuclear Astrophysics", Invited talk at 10$^{\text{th}}$ International Symposium on Capture Gamma-Ray Spectroscopy and Related Topics in Santa Fe, NM, USA, 30.08–03.09.1999;
- F. Strieder, "Measurement of the $^{7}$Be(p,$\gamma$)$^{8}$B reaction with solid state targets", Poster at 10$^{\text{th}}$ International Symposium on Capture Gamma-Ray Spectroscopy and Related Topics in Santa Fe, NM, USA, 30.08–03.09.1999;
- C. Broggini, "Results from LUNA", Talk at Taup99, .09.1999, Paris, France;
- C. Rolfs, "Laboratory studies of astrophysical nuclear reactions", Invited talk Breit Centennial Symposium 29.–30.10. 1999, New Haven, Yale University, USA.

# References


[1] U. Greife et al., Nucl.Instr.Meth. **A350** (1994) 327;

[2] C. Rolfs and W.S. Rodney, Cauldrons in the Cosmos (University of Chicago press, 1988);

[3] G. Fiorentini, R. W. Kavanagh, and C. Rolfs, Zeitsch. Phys.**A350** (1995) 289;

[4] B. Ricci et al., Phys. Rev. **C52** (1995) 1095;

[5] J.F. Ziegler, SRIM Program, (C) 1984-2000, International Business Machines Corporation;

[6] K. Langanke et al., Phys.Lett. **B369** (1996) 211;

[7] J. N. Bahcall and M. H. Pinsonneault, Rev. Mod. Phys. **64**, 885 (1992).

[8] F. Strieder et al., Eur. Phys. J. A3, (1998) 1

[9] B. W. Filippone, et al., Phys. Rev. **C28**, 2222 (1983).

# LVD. Large Volume Detector

M.Aglietta[14], E.D.Alyea[7], P.Antonioli[1], G.Badino[14], G.Bari[1], M.Basile[1], V.S.Berezinsky[9], F.Bersani[1], M.Bertaina[14], R.Bertoni[14], G.Bruni[1], G.Cara Romeo[1], C.Castagnoli[14], A.Castellina[14], A.Chiavassa[14], J.A.Chinellato[3], L.Cifarelli[1,†], F.Cindolo[1], A.Contin[1], V.L.Dadykin[9], L.G.Dos Santos[3], R.I.Enikeev[9], W.Fulgione[14], P.Galeotti[14], P.Ghia[14], P.Giusti[1], F.Gomez[14], R.Granella[14], F.Grianti[1], G.Iacobucci[1], E.Kemp[3], F.F.Khalchukov[9], E.V.Korolkova[9], P.V.Korchaguin[9], V.B.Korchaguin[9], V.A.Kudryavtsev[9], M.Luvisetto[1], A.S.Malguin[9], T.Massam[1], N.Mengotti Silva[3], C.Morello[14], R.Nania[1], G.Navarra[14], L.Periale[14], A.Pesci[1], P.Picchi[14], I.A.Pless[8], V.G.Ryasny[9], O.G.Ryazhskaya[9], O.Saavedra[14], K.Saitoh[13], G.Sartorelli[1], M.Selvi[1], N.Taborgna[5], N.Takahashi[12], V.P.Talochkin[9], G.C.Trinchero[14], S.Tsuji[10], A.Turtelli[3], P.Vallania[14], S.Vernetto[14], C.Vigorito[14], L.Votano[4], T.Wada[10], R.Weinstein[6], M.Widgoff[2], V.F.Yakushev[9], I.Yamamoto[11], G.T.Zatsepin[9], A.Zichichi[1]

[1] *University of Bologna and INFN-Bologna, Italy*
[2] *Brown University, Providence, USA*
[3] *University of Campinas, Campinas, Brazil*
[4] *INFN-LNF, Frascati, Italy*
[5] *INFN-LNGS, Assergi, Italy*
[6] *University of Houston, Houston, USA*
[7] *Indiana University, Bloomington, USA*
[8] *Massachusetts Institute of Technology, Cambridge, USA*
[9] *Institute for Nuclear Research, Russian Academy of Sciences, Moscow, Russia*
[10] *Okayama University, Okayama, Japan*
[11] *Okayama University of Science, Okayama, Japan*
[12] *Hirosaki University, Hirosaki, Japan*
[13] *Ashikaga Institute of Technology, Ashikaga, Japan*
[14] *Institute of Cosmo-Geophysics, CNR, Torino, University of Torino and INFN-Torino, Italy*
[†] *now at University of Salerno and INFN-Salerno, Italy*

**Abstract**

The Large Volume Detector (LVD) in the Gran Sasso Underground Laboratory is a neutrino observatory mainly designed to study low energy neutrinos from gravitational stellar collapses. The experiment is sensitive to collapses in our Galaxy since June 1992, nowaday with a total scintillator mass of about 670 tons.

During 1999 the telescope continued the Galaxy monitoring searching for neutrino burst, with no positive results.

The third LVD tower has been nearly completed, 70% of new counters are already assembled and tested. In 2000 the telescope will run with a scintillator mass $M = 1kt$, and a new, up to date, DAQ system.

Results on Cosmic ray muons studies have been presented at the 1999 International Cosmic Ray Conference, they include muon astronomy and a measurement of the local muon induced neutron flux.

# 1 Introduction

The Large Volume Detector in the Gran Sasso underground Laboratory is a multipurpose detector consisting of a large volume of liquid scintillator interleaved with limited streamer tubes in a compact geometry.

A major purpose of the LVD experiment is to search for neutrinos from Gravitational Stellar Collapses (GSC) in our Galaxy [1].

Most theoretical models agree in predicting the total neutrino energy emitted as during the stellar collapse, the energy equipartition among the different neutrino flavours and the time duration of the neutrino burst. For any scintillator detector the bulk of events (about 90% of the total) is due to the capture reaction $\bar{\nu}_e p \rightarrow e^+ n$. The $e^+$ spectrum is determined by the temperature of the $\bar{\nu}_e$ neutrino-sphere.

Further, in LVD, about 5% of the events are due to neutral current interactions with $^{12}C$ which deexcites emitting a 15.1 MeV $\gamma$. The detector efficiency on detecting these signals has been evaluated. Because $\mu$ and $\tau$ neutrino-spheres are located deeper in the collapsing stellar core, and because of a temperature gradient, their energy spectra have higher temperatures as compared with the electron neutrino spectra. As a consequence more then 90% of the n.c. interactions with carbon nuclei are produced by $\nu_\mu$ and $\nu_\tau$. The ratio between the number of n.c. interactions to the total is related to the ratio between $\mu, \tau$ and $e$ neutrino-sphere temperatures.

Only 3% of events in LVD, are due to elastic scattering of all neutrino flavours with electrons, and less then 1% to c.c. interactions of $\nu_e$ and $\bar{\nu}_e$ with $^{12}C$ nuclei. These reactions could easily be separated by subsequent $\beta$ decay, but because of their relatively high thresholds ($> 15$ MeV) they are few. If energetic $\mu$ and $\tau$ neutrinos oscillate into electron neutrinos, the $\bar{\nu}_e$ spectrum will be distorced and the number of c.c. interaction will increase.

Among all existing detectors of neutrino from gravitational collapse, LVD has some peculiarities:

- LVD can operate at low energy thresholds as compared to $\check{C}$erenkov light detectors.

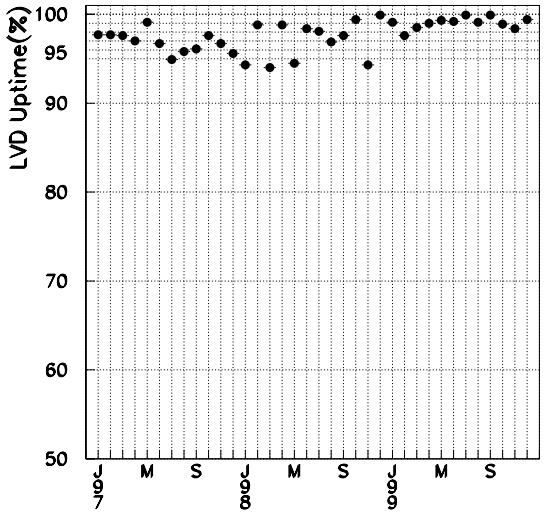


Figure 1: LVD monthly duty cicle since January 1997.

The detection of low energy neutrinos, of the order of a few MeV, gives the possibility to study objects emitting at low temperatures neutrino-sphere. When the collapsing star gives up into a black hole, models predict a sharp, low energy neutrino bounch, due to the strong gravitational and Doppler red shift.

- LVD can identify interacting $\bar{\nu}_e$ by the strong signature of the dominant reaction $\bar{\nu}_e p \rightarrow e^+ n$.

  The possibility of identify $\bar{\nu}_e$ interactions with protons by a stringent signature (and not simply by the absence of directionality as for light water Cherenkov detectors) gives us the chance to play with pure $\bar{\nu}_e$ energy spectrum and to separate the rare, but very interesting, charged and neutral current interactions with Carbon nuclei from the most common $\bar{\nu}_e$ interactions.

- LVD is extremely modular.

  Due to the extreme modularity of the detector, normal maintainance or calibration operations can be executed without stop data taking. Actually during last three years LVD has been observing the Galaxy searching for collapsing objects with an average duty cicle better than 97%. The monthly duty cicle of this period is shown in Fig.1.

# 2 The LVD detector

The LVD detector, operating since June 1992, has a modular structure that consists of aligned towers of 35 modules each. In any tower the scintillator / tracking modules are stacked in five columns.

Every module contains 8 liquid scintillation counters of dimensions $1.5 \times 1 \times 1\ m^3$ seen by three photomultipliers. The density of the scintillator is about $0.8\ g/cm^3$ and the energy resolution is about 15% for a 10 $MeV$ energy release, where for electrons it begins to be dominated by leakage effects in the counter.

The tracking system consists of L-shaped detectors for each module. Each element contains two staggered layers of 6.3 $m$ long limited streamer tubes. The bidimensional read-out is made by means of 4 $cm$ strips, parallel and perpendicular to the tubes, providing high detection efficiency and an angular resolution better than 4 milliradians.

In the search for neutrino bursts from GSC, the most important performances of LVD are the following:

- the information related to each signal is stored in a temporary memory buffer which is shared by 8 scintillator counters; This buffer can store up to 2 $10^5$ pulses, which corresponds to the signal from a "standard" supernova at a distance closer then 1 Kpc from the Earth.

- the total deadtime corresponds to a maximum detectable frequency (per counter) of 500 kHz; The read out procedure does not introduce any additional deadtime.

- the time of each event, relative to the U.T. time ( $\pm$ 1 $\mu$s from the Gran Sasso facility), is measured with an accuracy of $\pm$12.5 ns;

## 2.1 Upgrade of the detector during 1999

The scintillator production for tower 3 during 1999 has continued. By the end of the year over 70% of counters (200 out of 280) needed to complete tower 3 have been installed. The electronic installation is also in progress: first test data of tower 3 counters have been collected during November 1999. The completion of the installation is now planned by first semester of 2000. In this final setup the total LVD sensitive mass will reach 1 kt.

Since February 1999 a new motor generator system to protect the detector from short power supply black-outs and glitches has been installed. The upgrade on duty cycle has been significant: the total uptime since 1st March 1999 has raised to 99.2% (during 1998 the uptime was 98.1%).

The upgrade of the HV power supply system for the scintillator photomultipliers has been planned during 1999. The new system (based on CAEN SY527) will allow a more complete remote control of every channel and more flexible configuration with respect to the old one. It is running for test purposes on tower 3, it will be installed definitely during first semester of 2000.

A complete upgrade of the DAQ system has been also prepared during 1999. The current system, running since 1991, is based on CES PDP-11 Startburst for event read-out and an online VAX cluster ($\mu$VAX III and a VAXstation 4000/90). This obsolete system (in particular the Startburst is now out of production and the OpenVMS will be no longer supported by the INFN) will be replaced by VME PowerPC CPUs Motorola 2700 running LynxOS. The CAMAC bus will be then read-out through the CBD 8210 (a standard VME-CAMAC adapter provided by CES). An AlphaStation 255/233 running Digital Unix will complete the system for run control and monitoring tasks. The new system is under

test on tower 3 since November 1999. On the basis of the experience of these years, particular care has been taken designing the new system to ensure high modularity of the DAQ configuration and possibility to insert/remove counters or electronic modules from the read-out for normal maintenance without stopping the data taking. The complete phase-out of the old system is planned during first semester of 2000.

# 3 Results

## 3.1 Search for gravitational stellar collapse

At the 26th ICRC, we reported [2] on the results of the analysis of the period from $30^{th}$ April '97 to $15^{th}$ March '99. The time sequence of clustered single pulses is checked and compared with the expected one. Each cluster is defined by the multiplicity $m$ and the time duration $\Delta t$ ($\Delta t \leq 200\ s$). The corresponding Poisson probability is calculated on the basis of the current trigger rate and an imitation frequency ($F_{im}$) is obtained.

Since June 1992 no evidence for neutrino burst candidates has been found. On the basis of this data the upper limit at 90% c.l. on the rate of Gravitational Stellar Collapse in the Galaxy is 0.4 events $\cdot$ year$^{-1}$.

Since February 1999 the LVD joined the SNEWS (SuperNova Early Warning System) network [3]. This project, carried out by different neutrino telescopes searching for a burst from SuperNova (AMANDA, LVD, MACRO, SNO and SuperKamiokande are currently involved), intends to develop an early warning advise system to the astronomical comunity based on a multiple coincidence of burst candidates between the experiments. To build a redundant system and minimize network failures a second central server (the first one is at Kamioka) to collect the signals from different experiments has been setup at LNGS. Currently the project is in a test phase, during the year 2000 it is planned a test to synchronize different clocks.

## 3.2 Muon astronomy

We analysed the arrival directions of single muons detected by the first LVD tower from November, 1994 to January, 1998.

We used the shadowing of cosmic rays by the Moon to confirm the pointing accuracy of the LVD detector. The data used in the search for the shadow of the Moon included $1.85{\cdot}10^6$ muons. For every muon arrival time, right ascension (R.A.) and declination $\delta$ of the geocentric apparent position of the center of the Moon has been computed taking into account the corrections for parallax. The angle between muon direction and the position of the center of the Moon has been evaluated. We simulated the background events from the experimental zenith-azimuthal distribution of muons and the mean time between two consecutive muons observed by LVD run by run. Then the angle between background event and Moon position has been calculated. Fig. 2 shows the angular density $dN/d\Omega$ as a function of the angular distance from the center of the Moon. The observed deficit has a significance of 2.62 standard deviations (s.d.). This study confirms that the track reconstruction and pointing accuracy used to give previous results on muon intensity [4], muon astronomy [5] and search for prompt muon flux [6] have no serious systematic errors.

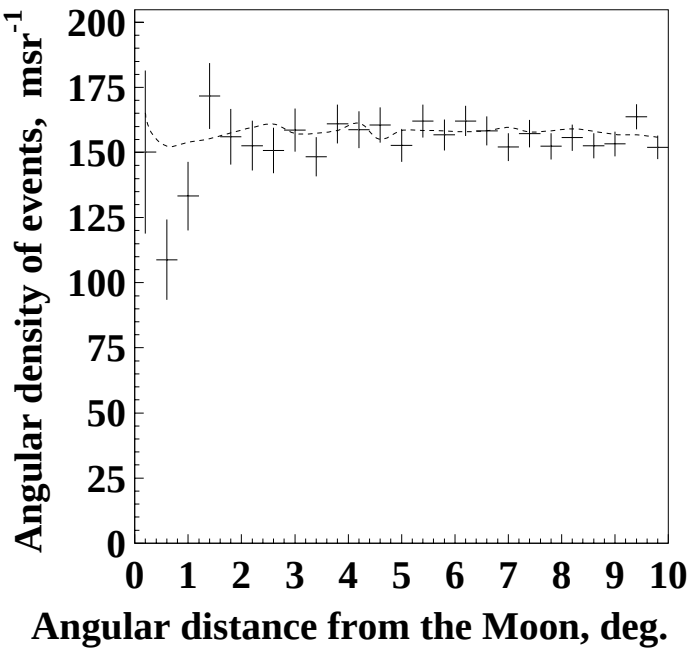


Figure 2: The angular density $dN/d\Omega$ as a function of the angular distance from the Moon; the distribution for the simulated background events is shown by dashed line.

To search for point sources of high energy photons we have analysed muons crossing the rock thickness greater than 3, 5 and 7 km w.e., which corresponds to the mean muon energies 1.6, 3.9 and 8.4 TeV at the surface, respectively.

The distribution of the data versus declination (after summing over R.A.) for three selected ranges of depth is presented in Figures 3a,b,c together with calculated background of atmospheric muons. The difference in the distributions for three depth ranges reflects different mountain structure for these regions at LVD site. Fig. 3d shows the distribution of the muon flux versus R.A. (summed over declination). The calculated background fits data for three analysed depth ranges rather well.

Within the three depth (muon energy) ranges selected to search for point sources of VHE gammas, no statistically significant excess of muons above the simulated background has been found from any angular cell on the sky and for all energy ranges included in the analysis procedure. We have not found either any enhancement of muon flux from the angular cells which include some known astrophysical sources. Updated limits (with respect to the ones published on 1997) have been reported [7],[8].

Finally, during 1997 Markarian 501 had a remarkable flaring activity and was the brightest source in the sky at TeV energies. We used LVD data to look at possible enhancement of observed muons above calculated background during the period of Mrk501 activity from iddle of March to the end of August, 1997. The results are presented in Table 1.

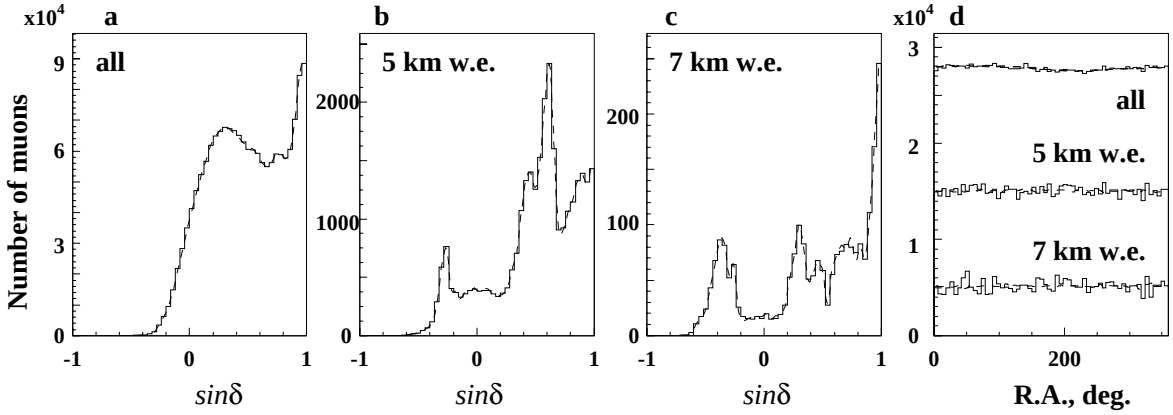


Figure 3: Distribution of muon events vs $\sin\delta$ (a,b,c) and R.A. (d) for three depth ranges analysed. The histograms are experimental data, dashed curves show simulated backgrounds from atmospheric muons initiated in hadronic showers. The histograms for the second and the third depth ranges in plot (d) were multiplied by factors of 15 and 66, respectively.

| Number of muons | all depths | $>$ 5 km w.e. | $>$ 7 km w.e. | $>$ 7 km w.e. after depth cut |
|---|---|---|---|---|
| Observed | 101 | 5 | 1 | 1 |
| Simulated | 95 | 5.1 | 0.4 | 0.3 |

Table 1: Number of events seen from Mrk501 at different depths compared with the expectations from c.r. background.

## 3.3 Neutron flux produced by cosmic-ray muons

The flux of muon-produced neutrons far away from the muon track may constitute a background for the underground detectors searching for rare events. The muon events collected by the first LVD tower from March, 1996, to February, 1998, (1.56 years of live time) were used to estimate the neutron flux at various distances from the muon track or muon-produced cascade.

All muon events were divided into two classes: i) 'muons' – single muon events, where a single muon track is reconstructed (small cascades cannot be excluded), and ii) 'cascades' – there is no clear single muon track but the energy release is high enough to indicate that at least one muon is present; such events may be due to either muon-induced cascades or multiple muons.

Each neutron ideally should generate two pulses: the first pulse above the HET is due to the recoil protons from $n-p$ elastic scattering (its amplitude is proportional to and even close to the neutron energy); the second pulse, above the LET in the time gate of about 1 ms is due to the 2.2 MeV gamma from neutron capture by a proton. The sequence of two pulses (one above the HET and one above the LET) was the signature of neutron detection.

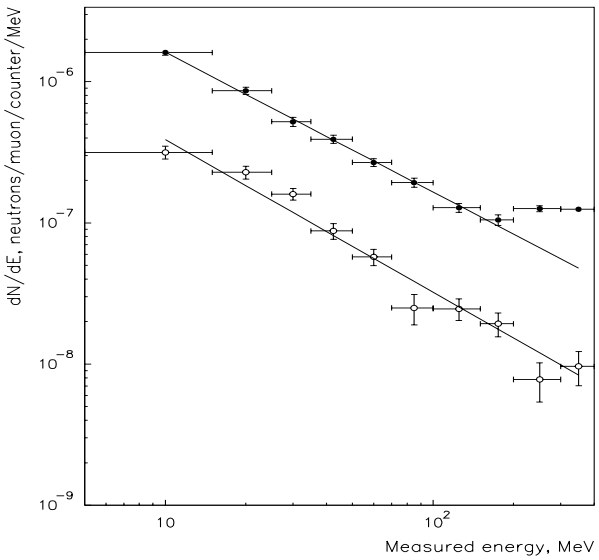


Figure 4: Neutron flux versus energy of HET pulses at $R > 1$ m (*filled circles*) and $R > 2$ m (*open circles*).

The energy of a trigger pulse in a counter can be attributed to the neutron kinetic energy if: 1) there is no energy loss neither of the muon nor of secondary particles (other than neutrons) in this particular counter; 2) all neutron kinetic energy is tranferred to protons inside this counter; 3) the energy deposited by a recoil proton is proportional to the pulse amplitude and this proportionality is the same as for electron pulses. Although these conditions are not strictly satisfied, we assume (at zero approximation) that the measured spectrum of HET pulses at large enough distances from the muon track corresponds to the neutron energy spectrum (near the point of neutron capture, within a sphere with a diameter of about 1 m). Such a spectrum is presented in Fig. 4 by filled circles for distances $R > 1$ m. Only statistical errors are shown.

The distance between the counter in which a neutron was detected and the muon track has been calculated. The neutron flux decreases by more than three orders of magnitude at distances more than 5 meters from muon track or cascade core. The average number of neutrons produced per muon per g/cm$^2$ of its path in the liquid scintillator is found to be $(1.5 \pm 0.4) \cdot 10^{-4}$ neutrons/(muon event)/(g/cm$^2$). Under the assumptions discussed the neutron differential energy spectrum in the kinetic energy range (5 – 400) MeV was found to follow a power law with exponent close to -1. These results have been presented to the 1999 ICRC [9][10].

## 3.4 GRB990705

On July $5^{th}$ 1999, 16:01:25 UT, a Gamma Ray Burst (GRB990705) has been detected by BeppoSAX from the direction of the outskirts of the Large Magellanic Clouds (GCN circular n.368). If the burst was indeed located in the LMC or its halo (or even closer),

a search for a neutrino signal coincident with, or just prior to the GRB event, would be very interesting.

At the time of GRB990705 LVD was regularly taking data with an active scintillator mass $M = 573$ ton.

On July $19^{th}$ 1999, the result of a preliminary analysis of the data recorded during 48 hours of data taking "near" July $5^{th}$ was reported by the LVD collaboration (GCN circular n.390 [11]). The absence of a neutrino signal, as expected from a gravitational stellar collapse in the Galaxy or Magellanic Clouds, correlated to the GRB990705 was established. A more careful analysis has been performed to search for weaker signals even preceding GRB990705 [12].

Some models suggest that gamma ray bursts are related to Supernova explosions. In this scenario the neutrino emission should be associated to the cooling of the collapsed object while photons should be emitted by narrow ultra-relativistic jets streaming along the rotational axis. Therefore the time gap between the two signals depends on the time necessary to transfer energy from the central engine, which emits thermal neutrino to the outer region transparent for high energy photons.

On the analogy of SN explosions modelling, where few hours are necessary to the shock to reach the star envelope and give rise to the sudden increase of luminosity, a similar time gap for the event under study has been assumed.

In addition one has to take into account a possible non zero neutrino mass. In the cosmologically allowed mass region ($m_\nu \leq 100\ eV$) and for a source in the LMC ($D \sim 50\ kpc$), the maximum delay for the neutrino signal should be: $\tau^{max} \simeq 250s$.

For these reasons the search has been extended up to 24 hours before the GRB time to 10 minutes after, for a total time $T = 1450\ min$ on three event classes, namely:

- class A: pulses with energy deposit $E_d \geq 7MeV$ ($M = 573\ ton$);
- class B: pulses with $E_d \geq 7MeV$ followed by at least one delayed low energy pulse in the same counter ($M = 573\ ton$);
- class C: pulses with $E_d \geq 4MeV$ detected by core scintillators followed by at least one delayed low energy pulse in the same counter ($M = 256\ ton$).

| | coincidence | | 24 hour preceding | |
|---|---|---|---|---|
| $\delta t$ [s] | $\int_0^{\delta t} dt \int_5^{\infty} \frac{d^2\phi_\nu}{dEdt}\sigma dE$ | $\int_0^{\delta t} dt \int_8^{\infty} \frac{d^2\phi_\nu}{dEdt}\sigma dE$ | $\int_0^{\delta t} dt \int_5^{\infty} \frac{d^2\phi_\nu}{dEdt}\sigma dE$ | $\int_0^{\delta t} dt \int_8^{\infty} \frac{d^2\phi_\nu}{dEdt}\sigma dE$ |
| 1 | $1.7 \cdot 10^{-31}$ | $4.3 \cdot 10^{-32}$ | $5.9 \cdot 10^{-31}$ | $1.9 \cdot 10^{-31}$ |
| 5 | $1.7 \cdot 10^{-31}$ | $4.3 \cdot 10^{-32}$ | $5.9 \cdot 10^{-31}$ | $2.4 \cdot 10^{-31}$ |
| 10 | $1.7 \cdot 10^{-31}$ | $4.3 \cdot 10^{-32}$ | $7.4 \cdot 10^{-31}$ | $2.8 \cdot 10^{-31}$ |
| 20 | $1.7 \cdot 10^{-31}$ | $7.5 \cdot 10^{-32}$ | $8.1 \cdot 10^{-31}$ | $3.5 \cdot 10^{-31}$ |
| 50 | $1.7 \cdot 10^{-31}$ | $8.6 \cdot 10^{-32}$ | $9.6 \cdot 10^{-31}$ | $5.2 \cdot 10^{-31}$ |
| 100 | $2.9 \cdot 10^{-31}$ | $8.6 \cdot 10^{-32}$ | $1.1 \cdot 10^{-30}$ | $6.0 \cdot 10^{-31}$ |

Table 2: Limits on the $\bar{\nu}_e$ time integrated flux (cross-section weighted).

The search for a signal in time coincidence with GRB990705 has been performed by comparing the number of observed signals inside time windows of different duration $\delta t$ centered on the GRB time, with the average number of signals expected from background. On the other hand in the 24 hours search, the interval of interest has been divided into $N_{\delta t} = 2 \cdot \frac{T}{\delta t}$ intervals of duration $\delta t$, each one starting at the middle of the previous one. The multiplicity distributions of clusters (number of events within each interval of duration $\delta t$) have been studied for $\delta t = 1, 5, 10, 20, 50$ and 100 seconds and compared with expectations from pure Poissonian fluctuations of the background as calculated by using the average event rate in 24 hours.

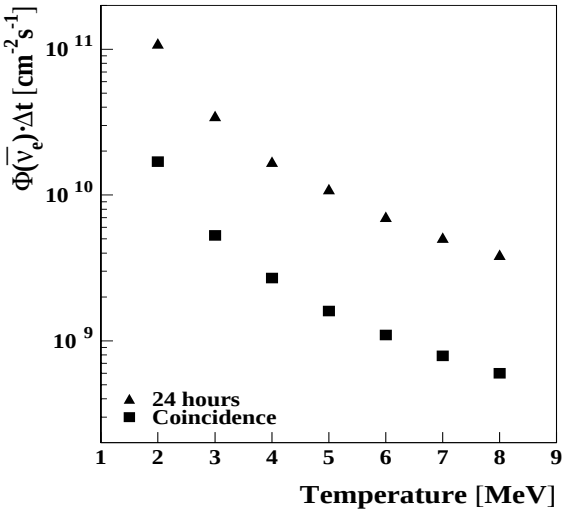


Figure 5: Upper limits to the time integrated $\bar{\nu}_e$ flux as a function of the $\bar{\nu}$ emission temperature, for $\Delta t \leq 10s$.

The agreement between data and expectations allows to state that there is no evidence for any detectable neutrino signal during this period.

In the absence of any information on the distance of the source and the emission spectra, we can express the results of the search in terms of upper limits to the time integrated flux cross-section product at the Earth: $\int dt \int \frac{d^2\phi}{dEdt}\sigma dE$. Those limits, reported in Table 2 at 90% c.l. for various $\delta t$, are expressed in number of interactions per target proton.

Any hypothesis on the $\bar{\nu}_e$ spectrum leads to a limit to the time integrated $\bar{\nu}_e$ flux at the Earth. Assuming, in analogy with the neutrino emitted by SN, a thermal $\bar{\nu}_e$ spectrum, the time integrated $\bar{\nu}_e$ flux, for burst duration $\delta t \leq 10$ $s$, is obtained as a function of the emission temperature $T[MeV]$ and the corresponding 90% $c.l.$ upper limits are shown in Fig. 5.

# References

[1] LVD Collaboration, Il Nuovo Cimento A105 (1992) 1793

[2] The LVD Collaboration, 26th ICRC Proceedings, "Search for neutrino burst from SN collapse with Large Volume Detector", HE 4.2.08, Vol. 2, 223 (Salt Lake City, USA, 1999)

[3] http://hep.bu.edu/ snnet/

[4] The LVD Collaboration, Phys. Rev. D, 58, 2005 (1998)

[5] The LVD Collaboration, 25th ICRC Proceedings, "Search for point sources with muons observed by LVD", HE 3.1.9, Vol. 6, 349 (Durban, South Africa,1997)

[6] The LVD Collaboration, Phys. Rev. D, 60, 112001 (1999)

[7] The LVD Collaboration, 26th ICRC Proceedings, "Muon astronomy with LVD detector", SH 3.2.40, Vol. 7, 222 (Salt Lake City, USA, 1999)

[8] The LVD Collaboration, hep-ex/9905048

[9] The LVD Collaboration, 26th ICRC Proceedings, "Measurement of the Neutron Flux Produced by Cosmic-Ray Muons with LVD at Gran Sasso ", HE 3.1.15, Vol. 2, 40 (Salt Lake City, USA, 1999)

[10] The LVD Collaboration, hep-ex/9905047

[11] http://lheawww.gsfc.nasa.gov/docs/gamcosray/legr/bacodine/ gcn3/390.gcn3

[12] The LVD Collaboration, INFN/AE-99/19

# MACRO. Monopole Astrophysics Cosmic Ray Observatory

M. Ambrosio[12], R. Antolini[7], G. Auriemma[14,a], D. Bakari[2,17], A. Baldini[13], G. C. Barbarino[12], B. C. Barish[4], G. Battistoni[6,b], R. Bellotti[1], C. Bemporad[13], P. Bernardini[10], H. Bilokon[6], V. Bisi[16], C. Bloise[6], C. Bower[8], M. Brigida[1], S. Bussino[18], F. Cafagna[1], M. Calicchio[1], D. Campana[12], M. Carboni[6], S. Cecchini[2,c], F. Cei[13], V. Chiarella[6], B. C. Choudhary[4], S. Coutu[11,m], G. De Cataldo[1], H. Dekhissi[2,17], C. De Marzo[1], I. De Mitri[10], J. Derkaoui[2,17], M. De Vincenzi[18], A. Di Credico[7], O. Erriquez[1], C. Favuzzi[1], G. Giacomelli[2], G. Giannini[13,e], N. Giglietto[1], M. Giorgini[2], M. Grassi[13], L. Gray[7], A. Grillo[7], F. Guarino[12], C. Gustavino[7], A. Habig[3], K. Hanson[11], R. Heinz[8], E. Iarocci[6,f], E. Katsavounidis[4], I. Katsavounidis[4], E. Kearns[3], H. Kim[4], S. Kyriazopoulou[4], E. Lamanna[14,o], C. Lane[5], D. S. Levin[11], P. Lipari[14], N. P. Longley[4,i], M. J. Longo[11], F. Loparco[1], F. Maaroufi[2,17], G. Mancarella[10], G. Mandrioli[2], S. Manzoor[2,n], A. Margiotta[2], A. Marini[6], D. Martello[10], A. Marzari-Chiesa[16], M. N. Mazziotta[1], D. G. Michael[4], S. Mikheyev[4,7,g], L. Miller[8,p], P. Monacelli[9], T. Montaruli[1], M. Monteno[16], S. Mufson[8], J. Musser[8], D. Nicolò [13,d], R. Nolty[4], C. Orth[3], G. Osteria[12], M. Ouchrif[2,17], O. Palamara[7], V. Patera[6,f], L. Patrizii[2], R. Pazzi[13], C. W. Peck[4], L. Perrone[10], S. Petrera[9], P. Pistilli[18], V. Popa[2,h], A. Rainò [1], J. Reynoldson[7], F. Ronga[6], C. Satriano[14,a], L. Satta[6,f], E. Scapparone[7], K. Scholberg[3], A. Sciubba[6,f], P. Serra[2], M. Sioli[2], G. Sirri[2], M. Sitta[16], P. Spinelli[1], M. Spinetti[6], M. Spurio[2], R. Steinberg[5], J. L. Stone[3], L. R. Sulak[3], A. Surdo[10], G. Tarlè [11], V. Togo[2], M. Vakili[15], E. Vilela[2], C. W. Walter[3,4], R. Webb[15]

1. Dipartimento di Fisica dell'Università di Bari and INFN, 70126 Bari, Italy
2. Dipartimento di Fisica dell'Università di Bologna and INFN, 40126 Bologna, Italy
3. Physics Department, Boston University, Boston, MA 02215, USA
4. California Institute of Technology, Pasadena, CA 91125, USA
5. Department of Physics, Drexel University, Philadelphia, PA 19104, USA
6. Laboratori Nazionali di Frascati dell'INFN, 00044 Frascati (Roma), Italy
7. Laboratori Nazionali del Gran Sasso dell'INFN, 67010 Assergi (L'Aquila), Italy
8. Depts. of Physics and of Astronomy, Indiana University, Bloomington, IN 47405, USA
9. Dipartimento di Fisica dell'Università dell'Aquila and INFN, 67100 L'Aquila, Italy
10. Dipartimento di Fisica dell'Università di Lecce and INFN, 73100 Lecce, Italy
11. Department of Physics, University of Michigan, Ann Arbor, MI 48109, USA
12. Dipartimento di Fisica dell'Università di Napoli and INFN, 80125 Napoli, Italy
13. Dipartimento di Fisica dell'Università di Pisa and INFN, 56010 Pisa, Italy
14. Dipartimento di Fisica dell'Università di Roma "La Sapienza" and INFN, 00185 Roma, Italy
15. Physics Department, Texas A&M University, College Station, TX 77843, USA
16. Dipartimento di Fisica Sperimentale dell'Università di Torino and INFN, 10125 Torino, Italy
17. L.P.T.P., Faculty of Sciences, University Mohamed I, B.P. 524 Oujda, Morocco
18. Dipartimento di Fisica dell'Università di Roma Tre and INFN Sezione Roma Tre, 00146 Roma, Italy
*a* Also Università della Basilicata, 85100 Potenza, Italy
*b* Also INFN Milano, 20133 Milano, Italy
*c* Also Istituto TESRE/CNR, 40129 Bologna, Italy
*d* Also Scuola Normale Superiore di Pisa, 56010 Pisa, Italy
*e* Also Università di Trieste and INFN, 34100 Trieste, Italy
*f* Also Dipartimento di Energetica, Università di Roma, 00185 Roma, Italy
*g* Also Institute for Nuclear Research, Russian Academy of Science, 117312 Moscow, Russia
*h* Also Institute for Space Sciences, 76900 Bucharest, Romania
*i* The Colorado College, Colorado Springs, CO 80903, USA
*l* Also INFN Catania, 95129 Catania, Italy
*m* Also Department of Physics, Pennsylvania State University, University Park, PA 16801, USA
*n* Also RPD, PINSTECH, P.O. Nilore, Islamabad, Pakistan
*o* Also Dipartimento di Fisica dell'Università della Calabria, Rende (Cosenza), Italy
*p* Also Department of Physics, James Madison University, Harrisonburg, VA 22807, USA

**Abstract**

The status of the MACRO detector is described and experimental results are presented on atmospheric neutrinos and neutrino oscillations, high energy neutrino astronomy, searches for WIMPs, search for low energy stellar gravitational collapse neutrinos, searches for magnetic monopoles, nuclearites and lightly ionizing particles, high energy downgoing muons, primary cosmic ray composition and shadowing of primary cosmic rays by the moon and the sun.

# 1 Introduction

MACRO is a large area multipurpose underground detector designed to search for rare events in the cosmic radiation. It has been optimized to look for the supermassive magnetic monopoles predicted by Grand Unified Theories (GUT) of the electroweak and strong interactions; it can also perform measurements in areas of astrophysics, nuclear, particle and cosmic ray physics. These include the study of atmospheric neutrinos and neutrino oscillations, high energy ($E_\nu \gtrsim 1$ GeV) neutrino astronomy, indirect searches for WIMPs, search for low energy ($E_\nu \gtrsim 7$ MeV) stellar collapse neutrinos, studies of various aspects of the high energy underground muon flux (which is an indirect tool to study the primary cosmic ray composition, origin and interactions), searches for fractionally charged particles and other rare particles that may exist in the cosmic radiation. The mean rock depth of the overburden is $\simeq 3700$ m.w.e., while the minimum is 3150 m.w.e. This defines the minimum muon energy at the surface at $\sim 1.3$ TeV in order to reach MACRO. The average residual energy and the muon flux at the MACRO depth are $\sim 310$ GeV and $\sim 1$ m$^{-2}$ h$^{-1}$, respectively. The detector has been built and equipped with electronics during the years $1988 - 1995$. It was completed in August 1995 and since the fall of 1995 it is running in its final configuration.

The 1999 highlights have been presented at the 1999 summer conferences (in particular at the 1999 ICRC in Salt Lake City); one of the main results is the evidence of an anomaly on atmospheric $\nu_\mu$ flux, which is suggestive of neutrino oscillations.

# 2 The Detector

The MACRO detector has a modular structure: it is divided into six sections referred to as supermodules. Each active part of one supermodule has a size of $12.6 \times 12 \times 9.3$ m$^3$ and comes with separate mechanical structure and electronics readout. The full detector has global dimensions of $76.5 \times 12 \times 9.3$ m$^3$ and provides a total acceptance to an isotropic flux of particles of $\sim 10,000$ m$^2$ sr. The total mass is $\simeq 5300$ t.

Redundancy and complementarity have been the primary goals in designing the experiment. Since no more than few magnetic monopoles can be expected, multiple signatures and ability to perform cross checks among various parts of the apparatus are important.

The detector is composed of three sub-detectors: liquid scintillation counters, limited streamer tubes and nuclear track detectors. Each one of them can be used in "stand-alone" and in "combined" mode. A general layout of the experiment is shown in Fig. 1.

Each supermodule contains 77 scintillation counters, divided into three horizontal planes (bottom, center, and top) and two vertical planes (east and west). The bottom and center horizontal planes, along with the lower seven scintillators of the east and west planes, occupy the lower section of each supermodule which is frequently referred to as the *lower* MACRO. The mass of the *lower* MACRO is $\simeq 4200$ t, mainly in the form of crushed Gran Sasso rock. The top and upper seven scintillators of the east and west planes occupy the upper section of the detector, often referred to as the *Attico*. The lower part of the north and south faces of the detector are covered by vertical walls with seven scintillation

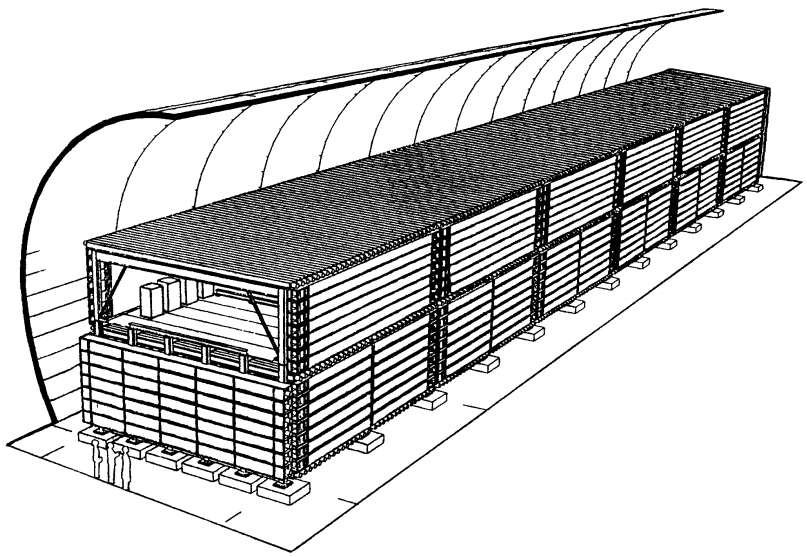

Figure 1: General layout of the MACRO detector installed in Hall B of the LNGS. Overall dimensions of the active part are $76.5 \times 12 \times 9.3$ m$^3$.

counters each. The upper parts of these faces are left open in order to allow access to the readout electronics. Each scintillation counter measures $12 \times 0.75 \times 0.26$ m$^3$. The active volume of horizontal scintillator counters is $11.2 \times 0.73 \times 0.19$ m$^3$, while for the vertical ones it measures $11.1 \times 0.22 \times 0.46$ m$^3$. All are filled with a mixture of mineral oil (96.4 %) and pseudocumene (3.6 %), with an additional 1.44 g/l of PPO and 1.44 mg/l of bis-MSB as wavelength shifters. The horizontal counters are seen by two 8″ phototubes (PMTs) and the vertical counters by one 8″ PMT at each end. Each PMT housing is equipped with a light collecting mirror. The total number of scintillators is 476 (294 horizontal and 182 vertical) with a total active mass of almost 600 tons. Minimum ionizing muons when crossing vertically the 19 cm of scintillator in a counter release $\simeq 34$ MeV of average energy and are measured with a timing and longitudinal position resolution of $\simeq 500$ ps and $\simeq 10$ cm, respectively.

The scintillation counters are equipped with specific triggers for rare particles, muons and low energy neutrinos from stellar gravitational collapses. The Slow Monopole Trigger (SMT) is sensitive to magnetic monopoles with velocities from about $10^{-4}c$ to $10^{-2}c$, the Fast Monopole Trigger (FMT) is sensitive to monopoles with velocities from about $5 \times 10^{-3}c$ to $5 \times 10^{-2}c$, the Lightly Ionizing Particle (LIP) trigger is sensitive to fractionally charged particles, the Energy Reconstruction Processor (ERP) and "CSPAM" are primarily muon triggers (but used also for relativistic monopoles) and finally the gravitational collapse neutrino triggers (the Pulse Height Recorder and Synchronous Encoder –PHRASE– and the ERP), optimized to trigger on bursts of low energy events in the liquid scintillator. The scintillator system is complemented by a 200 MHz wave form digitizing (WFD) system that is used in rare particle searches but also on any occasion where knowledge of the PMT waveform is useful.

The lower part of the detector contains ten horizontal planes of limited streamer tubes, the middle eight of which are interleaved by seven rock absorbers (total thickness

$\simeq 360$ g cm$^{-2}$). This arrangement sets a $\simeq 1$ GeV energy threshold for muons vertically crossing the lower part of the detector. In the *Attico* there are four horizontal streamer tube planes, two located above and two below the top scintillator layer. On each lateral wall six streamer tube planes sandwich the corresponding vertical scintillator plane (three streamer planes on each side). Each tube has a $3 \times 3$ cm$^2$ cross section and measures 12 m in length. The total number of tubes is 55,200 and are all filled with a gas mixture of $He$ (73 %) and n-pentane (27 %). They are equipped with 100 $\mu$ *Cu/Be* wires and stereo pickup strips at an angle of 26.5°. The intrinsic position and tracking resolutions of the streamer tube system are $\simeq 1$ cm and $\simeq 0.2°$, respectively. The overall angular resolution is limited to $\simeq 1°$ by the multiple scattering in the rock above the detector. The streamer tubes are read by 8-channel cards (one channel for each wire) which discriminate the signals and send the analog information (time development and total charge) to an ADC/TDC system (the QTP). The discriminated signals are used to form two different chains (Fast and Slow) of TTL pulses, which are the inputs for the streamer tube Fast and Slow Particle Triggers.

The nuclear track detector is deployed in three planes, horizontally in the center of the lower section and vertically on the East and North faces. The detector is divided in 18,126 individual modules, which can be individually extracted and changed upon need. Each module ($\sim 24.5 \times 24.5 \times 0.65$ cm$^3$ in size) is composed of three layers of CR39, three layers of Lexan and 1 mm Aluminium absorber to stop nuclear fragments.

In addition to the three detection elements already described, a Transition Radiation Detector (TRD) was installed in part of the *Attico*, right above the central horizontal scintillator plane of the main detector. It is composed of three individual modules (overall dimensions $6 \times 6 \times 2$ m$^3$) and it is made of 10 cm thick polyethylene foam radiators and proportional counters; each counter measures $6 \times 6 \times 600$ cm$^3$ and is filled with $Ar$ (90 %) and $CO_2$ (10 %). The TRD provides a measurement of the muon energy in the range of 100 GeV $< E <$ 930 GeV. Although the energy measurement with the TRD saturates at $\sim 930$ GeV, muons of higher energies can still be detected and counted.

# 3 Selected Physics Results

In 1999 five papers were published and in addition two were submitted for publication. The papers concerned the observation of the shadowing of primary cosmic rays by the moon [M1], the energy spectrum of underground muons measured with the Transition Radiation Detector [M2], the search for dark matter WIMP annihilations in the Earth and the Sun [M3], the measurement of the underground muon pair separation [M4], the search for nuclearites [M5]; the two papers submitted for publication concern a search for Lightly Ionizing Particles [M6] and the study of low energy atmospheric muon neutrinos [M7]. Several results appeared in preliminary form in 37 paper contributions that were published in various physics conference proceedings [M8, M44]. They concerned the study of high and low energy atmospheric neutrinos, high energy muon neutrino astronomy, rare particle searches, the observation of the sun shadow of high energy cosmic rays and the underground muon energy spectrum measured with the TRD.

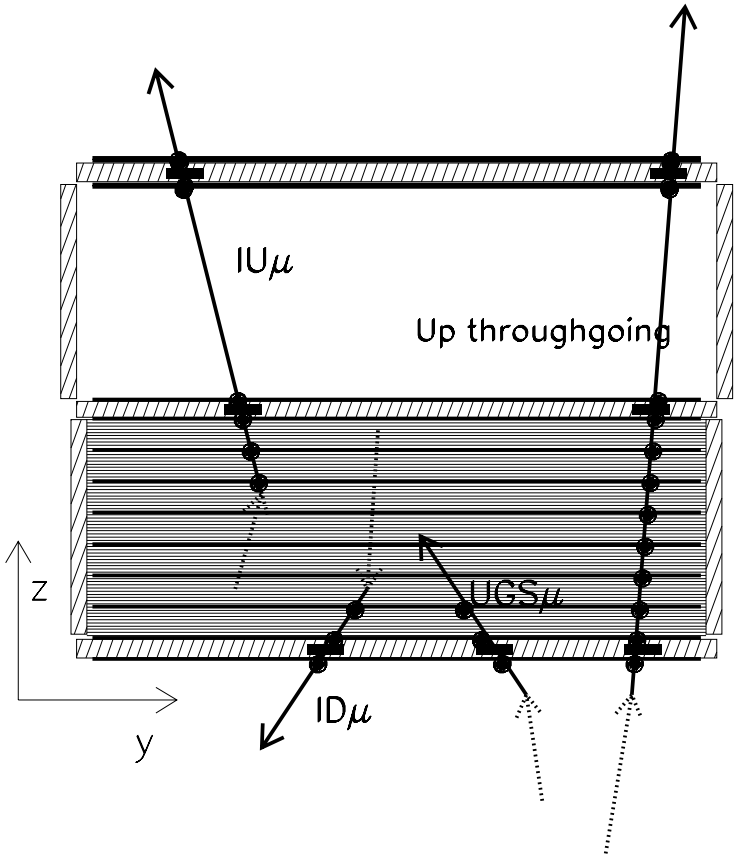


Figure 2: Sketch of different event topologies induced by $\nu_\mu$ interactions in or around MACRO. The stars represent scintillator hits. The track directions are measured by the streamer tubes; the time-of-flight of the muons can be measured for *Up Semicontained* and *Up throughgoing* events.

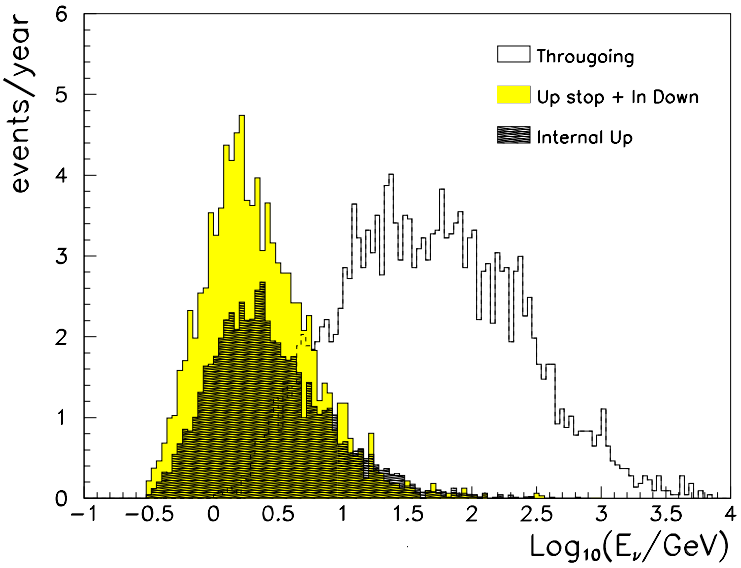


Figure 3: Distributions of the parent muon neutrino energy giving rise to the three different event topologies, upthroughgoing, up semicontained and upstopping plus down semicontained, with median neutrino energies of approximately 50, 4.2 and 3.5 GeV, respectively.

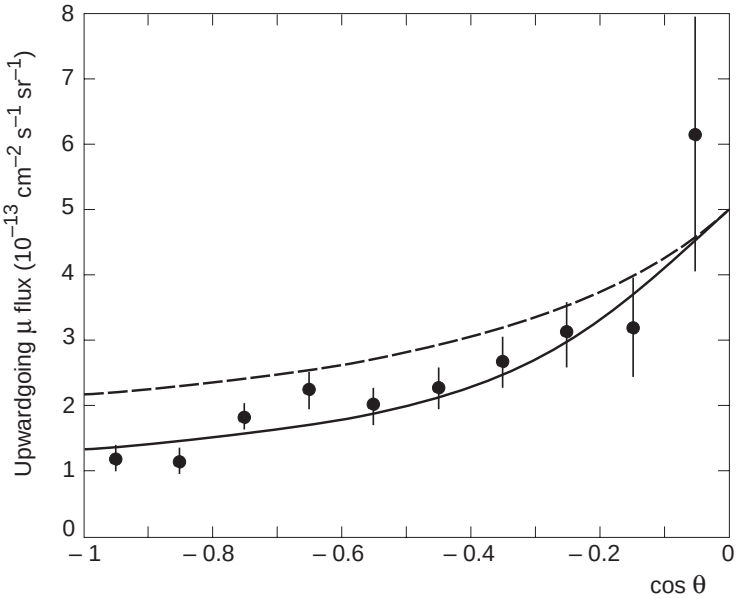


Figure 4: The black points are the measured flux of the up throughgoing muons with $E_\mu > 1$ GeV plotted vs. zenith angle $\theta$. The dashed line is the expectation for no oscillations; it has a 17 % scale uncertainty. The solid line is the prediction for an oscillated muon flux with maximum mixing and $\Delta m^2 = 0.0025$ eV$^2$.

## 3.1 Neutrino-induced Upward Going Muons

Upward going muons are identified using the streamer tube system (mainly for tracking) and the scintillator system (mainly for time-of-flight measurement). A rejection factor of at least $10^5$ is needed in order to separate the up-going muons from the large background coming from the down-going muons. Fig. 2 shows a sketch of the three different topologies of neutrino events analyzed until now: up throughgoing muons, semicontained upgoing muons and up stopping muons+semicontained downgoing muons. Fig. 3 shows the parent muon-neutrino energy spectra for the three event topologies, computed with Monte Carlo methods. The number of events measured and expected for the three topologies are given in Table 1.

The background on upgoing muons arising from downgoing muons interacting in the rock around MACRO and giving an upward going charged particle was studied in detail in [1]. This background is small at MACRO depths and when using a tracking system; it is large at lower depths and if no tracking system is present.

## 3.2 Upgoing $\mu$ fluxes. Neutrino oscillations

**Up-throughgoing muons**

The *up throughgoing muons* come from $\nu_\mu$ interactions in the rock below the detector; the $\nu_\mu$'s have a median energy $\overline{E}_\nu \sim$ 50 GeV. The muons ($E_\mu > 1$ GeV) cross the whole detector. The time information provided by the scintillation counters allows the determination of the direction (versus) by the time-of-flight (T.o.F.) method. The data

presented in Fig. 4 correspond to 1.38 live years (l.y.) with the first lower SM, 0.41 l.y. with the lower structure and 3.93 l.y. with the full detector. In 1997 and 1998 we studied a large number of possible systematic effects that could affect our mesurements. We have shown that no significant systematic problems exist in the detector or in the data analyses. One of the most significant checks was performed using only the scintillator system with the PHRASE Wave Form Digitizer, completely independent of the ERP system.

The measured data have been compared with Monte Carlo simulations. In the up throughgoing muon simulation the neutrino flux computed by the Bartol group is used. The cross sections for the neutrino interactions have been calculated using the GRV94 parton distribution set. The propagation of muons to the detector has been done using the energy loss calculation by Lohmann *et al.* [2]. The total theoretical uncertainty on the expected muon flux, adding in quadrature the errors from neutrino flux, cross section and muon propagation, is 17 %. Fig. 4 shows the zenith angle distribution of the measured flux of up throughgoing muons with energy greater than 1 GeV; the Monte Carlo expectation for no oscillations is shown as a dashed line, and for a $\nu_\mu \to \nu_\tau$ oscillated flux with $\sin^2 2\theta = 1$ and $\Delta m^2 = 0.0025$ eV$^2$ is shown by the solid line. The systematic uncertainty on the up throughgoing muon flux is mainly a scale error that doesn't change the shape of the angular distribution. The ratio of the observed number of events to the expectation without oscillations is $0.74 \pm 0.031_{stat} \pm 0.044_{sys} \pm 0.12_{theor}$ [M19, M30, 2, 3].

The shape of the angular distribution of Fig. 4 has been tested with the hypothesis of no oscillations, giving a $\chi^2$ of 22.9 for 8 degrees of freedom (probability of 0.35 %). Assuming $\nu_\mu \to \nu_\tau$ oscillations, the best $\chi^2$ in the physical region of the oscillation parameters is 12.5 for values of the parameters around $\Delta m^2 \simeq 0.0025$ eV$^2$ and $\sin^2 2\theta \simeq 1$.

To test oscillation hypotheses, the independent probabilities for obtaining the number of events observed and the angular distribution have been calculated for various parameter values. The value of $\Delta m^2$ suggested from the shape of the angular distribution is equal to the value needed to obtain the observed reduction in the number of events in the hypothesis of maximum mixing, see Fig. 5. Notice that for $\nu_\mu \to \nu_\tau$ oscillations the maximum probability is 36.3 %; the best parameters are $\Delta m^2 = 0.0025$ eV$^2$, $\sin^2 2\theta = 1$. The probability for no-oscillations is 0.36 %. The probability for $\nu_\mu \to \nu_{sterile}$ oscillations is 7%; combining these probability values with the measured ratio of horizontal/vertical muons (Fig. 7) we conclude that the $\nu_\mu \to \nu_{sterile}$ oscillations are disfavoured compared to $\nu_\mu \to \nu_\tau$.

Fig. 6 shows the confidence regions for $\nu_\mu \to \nu_\tau$ computed according to ref. [4].

**Low energy data.**

The *upgoing semicontained muons* come from $\nu_\mu$ interactions inside the lower apparatus. Since two scintillation counters are intercepted, the T.o.F. is applied to identify the upward going muons (Fig. 2). The average parent neutrino energy for these events is 4.2 GeV (see Fig. 3). If the atmospheric neutrino anomalies are the results of $\nu_\mu \to \nu_\tau$ oscillations with maximum mixing and $\Delta m^2$ between $10^{-3}$ and $10^{-2}$ eV$^2$ one expects a reduction of about a factor of two in the flux of these events, without any distortion in the shape of the angular distribution.

This is what is observed in Fig. 8a.

The *up stopping muons* are due to external $\nu_\mu$ interactions yielding upgoing muon tracks stopping in the detector; the *semicontained downgoing muons* are due to $\nu_\mu$ induced

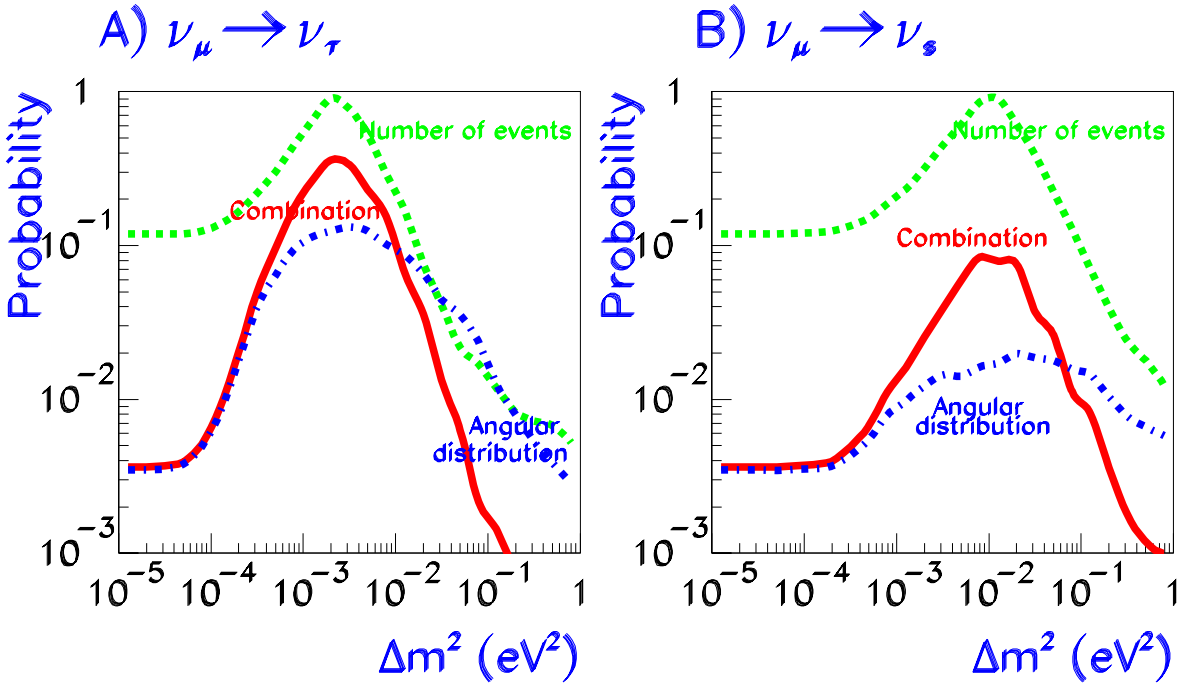


Figure 5: MACRO up-throughgoing muons. Probabilities for maximum mixing and (a) oscillations $\nu_\mu \rightarrow \nu_\tau$ or (b) oscillations $\nu_\mu \rightarrow$ sterile neutrino. The three lines correspond to the probability from the total number of events (dashed line), the probability from the chi-square of the angular distribution with data and prediction normalized (dotted line) and to the combination of the two independent probabilities (continous line).

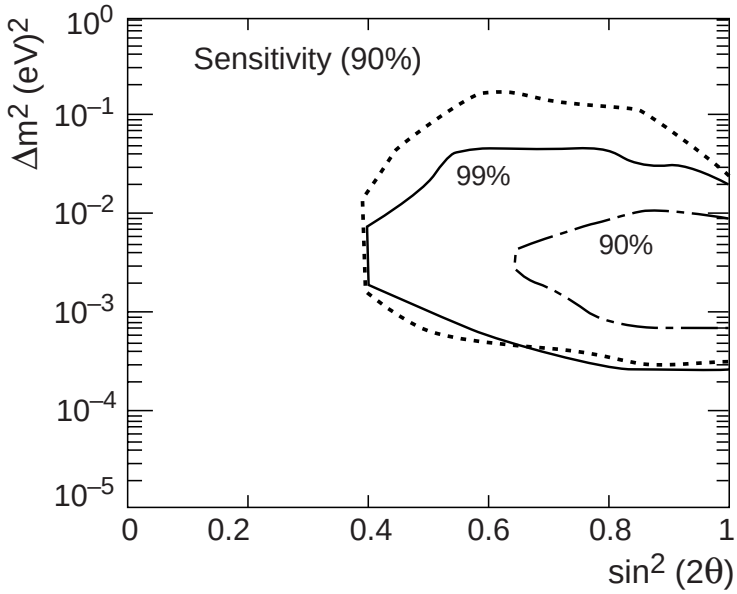


Figure 6: Confidence regions for $\nu_\mu \rightarrow \nu_\tau$ oscillations at the 90 % (dotted-dashed line) and 99 % (solid line) confidence levels calculated according to [4]. Since the best probability is outside the physical region the confidence interval regions are smaller than the one expected from the sensitivity of the experiment (dashed line).

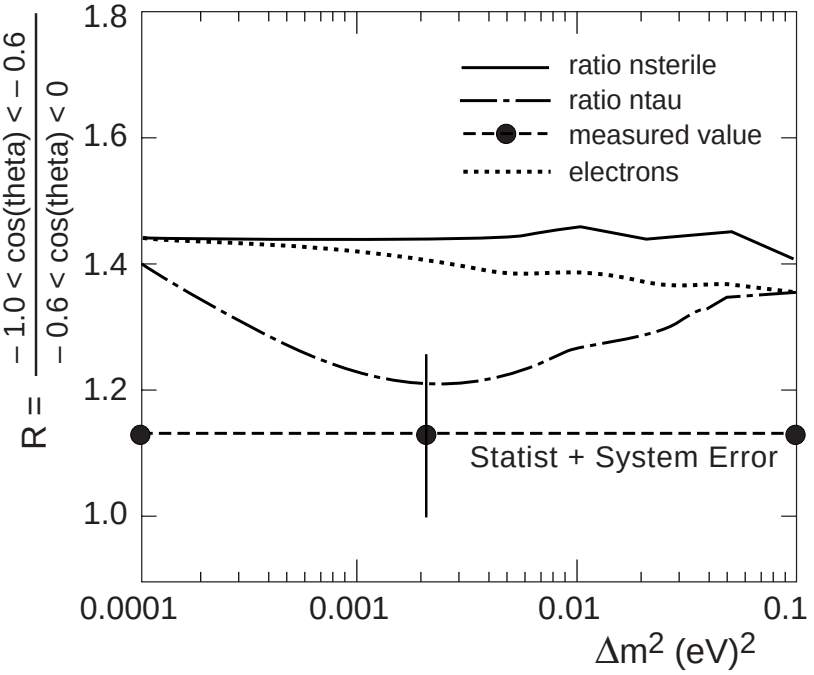


Figure 7: The ratio vertical/horizontal for upthroughgoing muons. The ratio is plotted at a $\Delta m^2$ around the minimum of $\chi^2$ for $\nu_\mu \to \nu_\tau$ oscillations [22].

downgoing tracks with vertex in the lower MACRO (Fig. 2). The events are found by means of topological criteria; the lack of time information prevents to distinguish the two sub samples. An almost equal number of up stopping and semicontained downgoing events is expected, and the average neutrino energy for these events is around 3.5 GeV (Fig. 3). In case of oscillations with the quoted parameters, a similar reduction in the flux of the up stopping events as the semicontained upgoing muons is expected. No reduction is instead expected for the semicontained downgoing events (coming from neutrinos having path lengths of $\sim 20\,\mathrm{km}$).

The MC simulation for the low energy data uses the Bartol neutrino flux and the neutrino low energy cross sections of ref. [5]. The number of events and the angular distributions are compared with the predictions in Table 1 and Fig. 8. The low energy data show a uniform deficit of the measured number of events over the whole angular distribution with respect to the predictions; there is good agreement with the predictions based on neutrino oscillations using the parameters obtained from the up throughgoing muon sample.

Using the double ratio $R = (Data/MC)_{IU}/(Data/MC)_{ID+UGS}$ between data and MC of the two low energy data sets, the theoretical uncertainties on neutrino flux and cross sections almost disappear (a residual 5 % uncertainty remains due to the small differences between the energy spectra of the two samples). The systematic uncertainty is reduced to about 5 %. The average value of the double ratio over the measured zenith angle distribution is $R \simeq 0.73$ (with a statistical uncertainty of about 0.12). $R = 1$ is expected in case of no oscillations, also assuming a reduction of the neutrino flux and neutrino cross

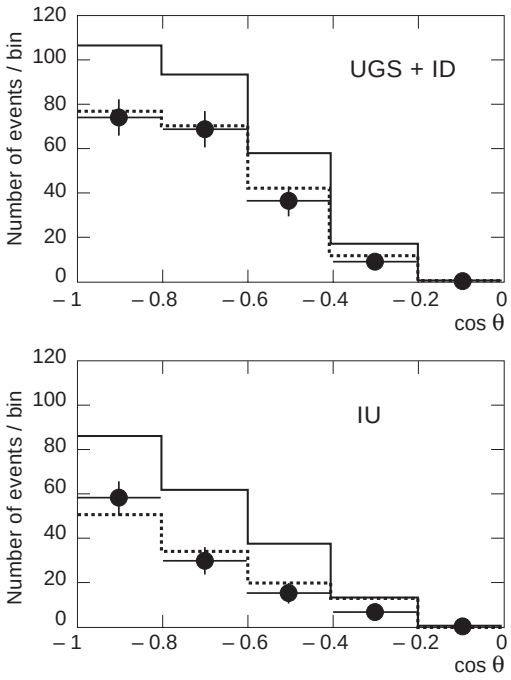


Figure 8: Measured and expected number of low energy muon neutrino events versus zenith angle; top graph: up stopping plus down semicontained; bottom graph: up semicontained. The solid lines are the predictions without oscillations; the dotted lines are the predictions assuming neutrino oscillations with the parameters suggested by the Up throughgoing sample.

| | Events selected | Predictions (Bartol flux) | | R = Data/MC |
|---|---|---|---|---|
| | | No oscill. | With oscill. | |
| Up throughgoing | 607 | 825 | 431 | $0.74 \pm 0.031_{st} \pm 0.044_{sys} \pm 0.12_{th}$ |
| Internal Up | 116 | 202 | 115 | $0.57 \pm 0.05_{st} \pm 0.06_{sys} \pm 0.14_{th}$ |
| Up Stop + In Down | 193 | 273 | 202 | $0.71 \pm 0.05_{st} \pm 0.07_{sys} \pm 0.18_{th}$ |

Table 1: Event summary for the MACRO neutrino flux analyses. The predicted numbers of events with oscillations are for maximum mixing and $\Delta m^2 = 0.0025$ eV$^2$. The ratios R = Data/MC are relative to MC expectations assuming no oscillations (column 3).

| Source | $\delta$ | Data $3^o$ | Backg $3^o$ | $\mu$-Flux limit 1 $cm^{-2}s^{-1}$ | $\mu$-Flux limit 2 $cm^{-2}s^{-1}$ | Prev. best $\mu$ limit $cm^{-2}s^{-1}$ | $\nu$-Flux limit $cm^{-2}s^{-1}$ |
|---|---|---|---|---|---|---|---|
| SMCX-1 | $-73.5^o$ | 3 | 1.87 | $0.60 \cdot 10^{-14}$ | $0.67 \cdot 10^{-14}$ | - | $0.19 \cdot 10^{-5}$ |
| SN1987A | $-69.3^o$ | 0 | 1.79 | $0.29 \cdot 10^{-14}$ | $0.16 \cdot 10^{-14}$ | $1.1 \cdot 10^{-14}$B | $0.09 \cdot 10^{-5}$ |
| Vela P | $-45.2^o$ | 1 | 1.40 | $0.56 \cdot 10^{-14}$ | $0.53 \cdot 10^{-14}$ | $0.78 \cdot 10^{-14}$I | $0.17 \cdot 10^{-5}$ |
| SN1006 | $-41.7^o$ | 1 | 1.21 | $0.58 \cdot 10^{-14}$ | $0.58 \cdot 10^{-14}$ | - | $0.18 \cdot 10^{-5}$ |
| Gal. Cen. | $-28.9^o$ | 0 | 0.86 | $0.48 \cdot 10^{-14}$ | $0.35 \cdot 10^{-14}$ | $0.95 \cdot 10^{-14}$B | $0.15 \cdot 10^{-5}$ |
| Kep1604 | $-21.5^o$ | 2 | 0.82 | $1.04 \cdot 10^{-14}$ | $1.15 \cdot 10^{-14}$ | - | $0.32 \cdot 10^{-5}$ |
| ScoXR-1 | $-15.6^o$ | 1 | 0.76 | $0.85 \cdot 10^{-14}$ | $0.90 \cdot 10^{-14}$ | $1.5 \cdot 10^{-14}$B | $0.26 \cdot 10^{-5}$ |
| Geminga | $18.3^o$ | 0 | 0.42 | $1.34 \cdot 10^{-14}$ | $1.17 \cdot 10^{-14}$ | $3.1 \cdot 10^{-14}$I | $0.41 \cdot 10^{-5}$ |
| Crab | $22.o^o$ | 1 | 0.40 | $2.22 \cdot 10^{-14}$ | $2.22 \cdot 10^{-14}$ | $2.6 \cdot 10^{-14}$B | $0.68 \cdot 10^{-5}$ |
| MRK501 | $38.8^o$ | 0 | 0.12 | $5.40 \cdot 10^{-14}$ | $5.44 \cdot 10^{-14}$ | - | $1.66 \cdot 10^{-5}$ |

Table 2: High energy neutrino astronomy: muon and neutrino flux limits (90 % c.l.) for selected sources calculated using the classical Poissonian method ($\mu$ flux limit 1) and the prescription in [4] ($\mu$ flux limit 2). Previous best limits: B is for Baksan, I is for IMB.

sections.

These data analyses were presented at many 1999 conferences [M8, M9, M13, M16, M19, M25, M30, M31, M39, M42, M43, 6], new results have been submitted for publication [M7], previous papers are quoted in ref. [2].

## 3.3 Search for Astrophysical Point Sources (High Energy Muon Neutrino Astronomy)

The excellent angular resolution of the MACRO detector allows a sensitive search for up-going muons produced by neutrinos coming from celestial sources, with a negligible atmospheric neutrino background. An excess of events was searched for around the positions of known sources in 3° (half width) angular bins. This value was chosen so as to take into account the angular smearing produced by the multiple scattering in the rock below the detector and by the energy-integrated angular distribution of the scattered muon, with respect to the neutrino direction. A total of 1100 events observed with MACRO until now was used in this search, see Fig. 9. No excess was observed and the 90 % c.l. limits on the neutrino fluxes from specific celestial sources are in the range of $\sim 10^{-14}$ cm$^{-2}$ s$^{-1}$, see Table 2; preliminary data were reported in the papers submitted to the 1999 conferences [M11, M12, M26, M28, M38, M39, 6].

We searched for time coincidences of our upgoing muons and $\gamma$-ray bursts as given in the BATSE 3B and 4B catalogues, for the period from April 91 to February 99 [M28]. No statistically significant time correlation was found.

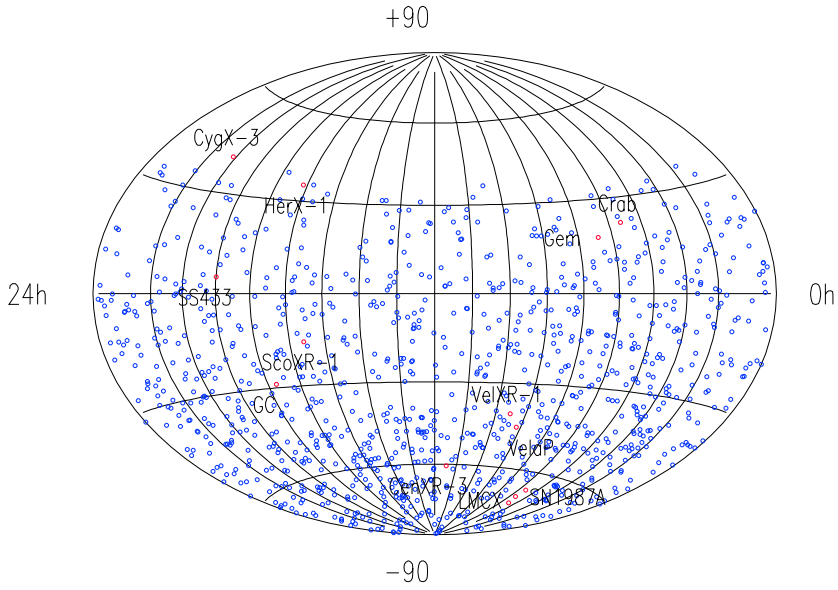


Figure 9: High energy neutrino astronomy. Upgoing muon distribution in equatorial coordinates (1100 events).

## 3.4 Indirect Search for WIMPs

Weakly Interacting Massive Particles (WIMPs) could be part of the galactic dark matter; WIMPs could be intercepted by celestial bodies, slowed down and trapped in their centers. WIMPs and anti-WIMPs could annihilate and yield up-throughgoing muons. WIMPs annihilating in these celestial bodies would produce neutrinos of GeV or TeV energy, in small angular windows around their centers. The 90 % c.l. MACRO limit for the flux from the Earth center is $0.8 \cdot 10^{-14}$ cm$^{-2}$ s$^{-1}$ for a 10° cone around the vertical. For the same cone searched for around the Sun direction, the limit is $\sim 1.4 \times 10^{-14}$ cm$^{-2}$ s$^{-1}$ [M35].

If the WIMPs are identified with the smallest mass neutralino, the MACRO limit may be used to constrain the stable neutralino mass, following the models of Bottino et al. [7], see Figures 10 [M35].

## 3.5 Magnetic Monopoles and Nuclearites

The search for magnetic monopoles (MM) is one of the main objectives of our experiment. Supermassive ($m \sim 10^{17}$ GeV) GUT monopoles are expected to have typical galactic velocities, $\sim 10^{-3}c$, if trapped in our Galaxy. MMs trapped in our solar system or in the supercluster of galaxies may travel with typical velocities of the order of $\sim 10^{-4}c$ and $\sim 10^{-2}c$, respectively. Monopoles in the presence of strong magnetic fields may reach higher velocities; intermediate mass monopoles could reach relativistic velocities.

The reference sensitivity level for a significant MM search is the Parker bound, the

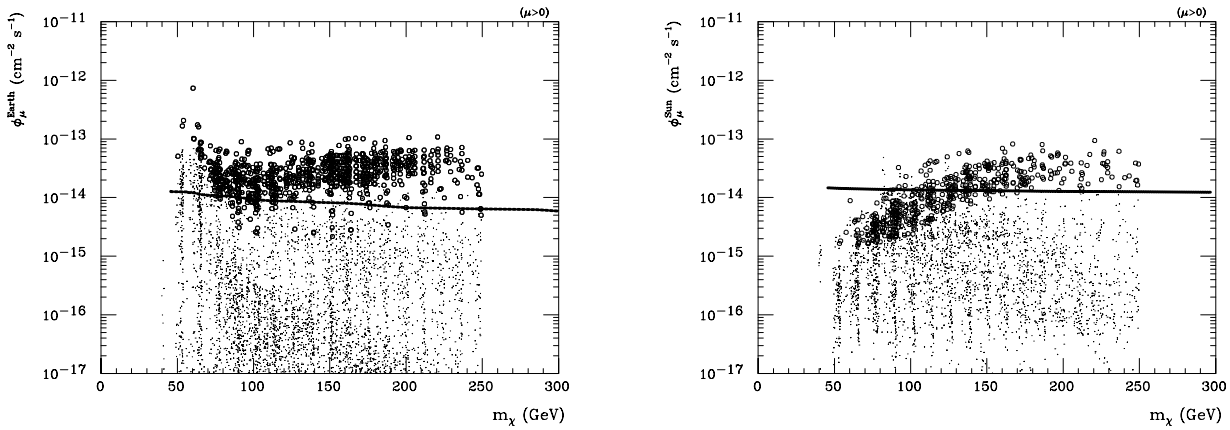


Figure 10: (a) Upward-going muon flux vs neutralino mass $m_\chi$ for ${E_\mu}^{th} = 1$ GeV from the Earth [M35]. Each dot is obtained varying model parameters. The solid line is the MACRO flux limit (90 % c.l.); the line for the no-oscillation hypothesis is essentially indistinguishable in the log scale from the one for the $\nu_\mu \to \nu_\tau$ oscillation hypothesis (it could be about two times lower). The open circles indicate models *excluded* by direct measurements (particularly the DAMA/NaI experiment [8]) and assume a local dark matter density of 0.5 GeV cm$^{-3}$. (b) The same as in (a) but for upward-going muons from the Sun [7, M35].

maximum monopole flux compatible with the survival of the galactic magnetic field. This limit is $\Phi \lesssim 10^{-15}$ cm$^{-2}$ s$^{-1}$ sr$^{-1}$, but it can be reduced by almost an order of magnitude when considering the survival of a small galactic magnetic field seed [6, 9]. Our experiment was designed to reach a flux sensitivity well below the Parker bound, in the MM velocity range of $4 \times 10^{-5} < \beta < 1$. The three MACRO sub-detectors have sensitivities in wide $\beta$-ranges, with overlapping regions; thus they allow multiple signatures of the same rare event candidate. No candidates were found in several years of data taking by any of the various subdetectors.

The limits set by different analyses were combined to obtain a global MACRO limit. For each $\beta$ value, the global time integrated acceptance was computed as the sum of the independent portions of each analysis. The MACRO limit is shown in Fig. 11 together with those set by other experiments [M20, M21, M32, M37], [6, 9].

The searches based on the scintillator and on the nuclear track subdetectors were also used to set new limits on the flux of cosmic ray nuclearites (strange quark matter), see Fig. 12, [M20, M32], [6].

Work is in progress in order to compute the energy losses of magnetic monopoles and dyons in the Earth and in the MACRO subdetectors for various particle masses and velocities [10]. This will allow a complete interpretation of all limits for monopoles of multiple charges, monopole composites as well as for monopoles of any given mass.

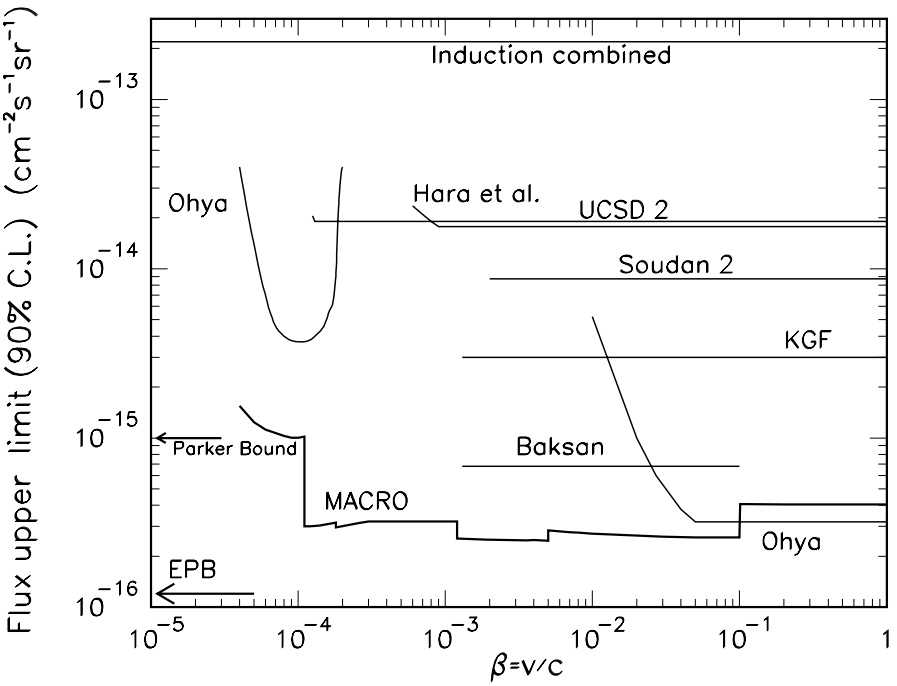


Figure 11: Magnetic monopole flux upper limits at the 90 % c.l. obtained by MACRO [M32] and other experiments [6, 9, 11, 12]. The limits apply to singly charged ($g = g_D$) monopoles assuming that catalysis cross sections are smaller than a few mb.

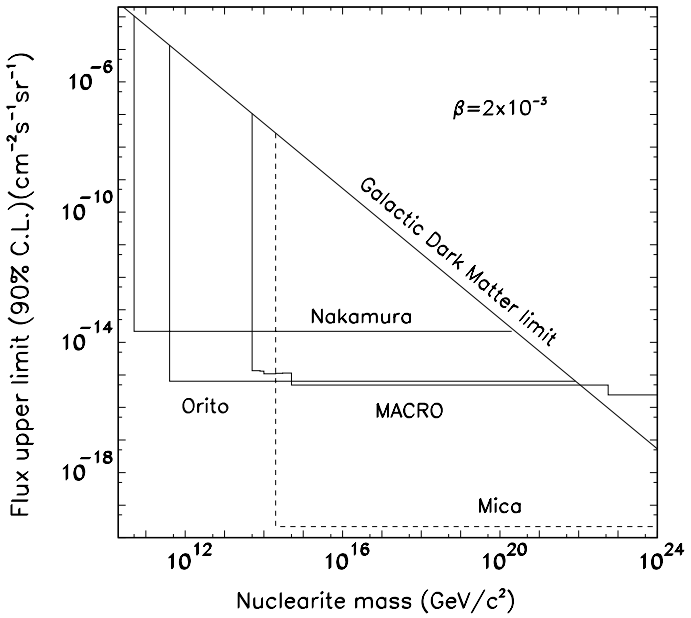


Figure 12: 90 % c.l. flux upper limits vs mass for nuclearites with $\beta = 2 \cdot 10^{-3}$ at ground level. Nuclearites of such velocity could have galactic or extragalactic origin. The MACRO direct limit (solid line) is shown along with the limits of Refs [11] (dashed line), [12] (dot-dashed line) and the indirect mica limits of Refs. [13], [14] (dotted line). The limit for nuclearite masses larger than $5 \cdot 10^{22}$ GeV c$^{-2}$ corresponds to an isotropic flux.

## 3.6 Neutrinos from Stellar Gravitational Collapses

A stellar gravitational collapse (GC) is expected to produce a large burst of all types of neutrinos and antineutrinos with energies of $7 - 30$ MeV and with a duration of $\sim 10$ s. The $\bar{\nu}_e$'s can be detected via the process $\bar{\nu}_e + p \rightarrow n + e^+$ in the liquid scintillator. About $100 \div 150$ $\bar{\nu}_e$ events should be detected in our scintillator for a stellar collapse at the center of our Galaxy.

We use two electronic systems for detecting $\bar{\nu}_e$'s from stellar gravitational collapses. The first system is based on the dedicated PHRASE trigger, the second one is based on the ERP trigger. Both systems have an energy threshold of $\sim 7$ MeV and record pulse shape, charge and timing informations. Immediately after a $> 7$ MeV trigger, the PHRASE system lowers its threshold to about 1 MeV, for a duration of 800 $\mu$s, in order to detect (with a $\simeq 25\,\%$ efficiency) the 2.2 MeV $\gamma$ released in the reaction $n + p \rightarrow d + \gamma_{2.2\ \mathrm{MeV}}$ induced by the neutron produced in the primary process.

A redundant supernova alarm system is in operation, alerting immediately the physicists on shift. We have defined a general procedure to alert the physics and astrophysics communities in case of an interesting alarm [15]. Finally, a procedure to link the various supernova observatories around the world (MACRO, SuperKamiokande, LVD, SNO and other neutrino observatories able to generate a prompt alarm) was set up.

The MACRO active mass is $\sim 580$ t; the live-time fraction in the last three years was $\simeq 97.5\,\%$. No stellar gravitational collapses were observed in our Galaxy since 1989.

## 3.7 Cosmic Ray Muons

The large area and acceptance ($\sim 10000\ m^2$ sr for an isotropic flux) of our detector allows to study many aspects of physics and astrophysics of cosmic ray muons. We have recorded $\sim 52.2 \times 10^6$ single muons and $\sim 3.2 \times 10^6$ multiple muons and we keep collecting them at the rate of $\simeq 18,000$/day.

**Intensity**

The underground muon intensity vs. rock thickness provides information on the high energy ($E \gtrsim 1.3$ TeV) atmospheric muon flux and on the all-particle primary cosmic ray spectrum. The results can be used to constrain the models on cosmic ray production and interaction. The analysis performed in 1995 covered the overburden range $2200 \div 7000$ hg/cm$^2$ [16]; a new analysis is under development to extend the results to larger rock thicknesses.

**Analysis of high multiplicity muon bundles**

The study of high multiplicity muon bundles can provide informations on the primary composition model and on the hadronic interaction features in the high energy region of primary spectrum. We have analyzed events reconstructed in the wire view of the detector with a multiplicity $N_{wire} \geq 8$, corresponding to a primary energy $E_{primary} \geq 1000$ TeV (the region above the "knee"). We have worked on a data sample consisting of 4893 events, for a total live time of 21622 h. A set of Monte Carlo productions has been performed, using different hadronic interaction models (DPMJET, QGSJET, SIBYLL, HEMAS, HDPM) interfaced to the HEMAS and CORSIKA shower propagation codes.

Each production is relative to 5528 h of MACRO live time. High multiplicity events have been analyzed using two different methods [23].

The first method is a study of muon correlations inside the bundle. We used the so called *correlation integral* analysis [24] to find out correlation of dynamical origin in the bundles. This tool is generally used in the study of physical systems with a multi-fractal behavior, e.g. systems generated by a cascade process. We found that the shower development in the atmosphere, being a typical cascade process, exhibits a self-similar behaviour. This feature has been used to extract informations on the primary composition model. In fact, since the cascade tree pattern in atmosphere is mainly determined by the number of "steps" in the tree formation, we expect a different behavior from light and heavy primaries originated cascades. For the same reason, the analysis should be less sensitive to the hadronic interaction model adopted in the simulations. The result of this analysis shows that, in the energy region above 1000 TeV, the composition model derived from the analysis of MACRO multiplicity distribution [25] is almost completely independent from the interaction model adopted.

The second method concerns the search for substructures ("clusters") inside muon bundles. This method of analysis, introduced in [26], has been extensively revised and improved. The search for clusters was performed by means of different software algorithms taken from the standard cluster analysis. This method is sensitive both to the hadronic interaction model and to the primary composition model. We proved that the dependence of the clustering from the composition model is a consequence of mathematical structure of the algorithm when applied to events with different average muon densities. On the other hand, the study of the muon clustering provided new information on the hadronic interaction model. When the primary composition model has been fixed (using the result of the first method), a particular choice of the bundle topology shows interesting connections with the early hadronic interaction features in the atmosphere: bundles with single muons well separated from the central core are produced with high probability in the fragmentation of hard partonic chains. The comparison between MACRO data and Monte Carlo simulations allowed to place severe constraints on the reliability of the interaction models adopted. Moreover, the same Monte Carlo study has shown that muon bundles with a central core and an isolated cluster with at least two muons are the result of random associations of peripheral muons. A combined analysis of this result with the study of the decoherence function for high multiplicity events has shown that the hadronic interaction model that better reproduces all the underground observables studied is the QGSJET model.

**Muon Astronomy**

In the past, some experiments have reported possible excesses of muons from the direction of known astrophysical sources, expecially Cyg X-3. Our data has not indicated any significant excess above the statistical background, both for steady dc fluxes and for modulated ac fluxes. For several sources (e.g. Cyg X-3, Vela Pulsar, etc.) our limits are the best existing. The data used for these analyses come from a long period of acquisition, from the first MACRO run (february 1989) until january 1999. After strict selection criteria we used 38.5 million single and double muons collected over 55248 h of live time [M14, M29]. The MACRO pointing precision was checked via the shadow of

the moon and the sun on primary cosmic rays, see below. The pointing resolution was checked with double muons, assuming they are parallel. The angle containing 68% of the events on a $\Delta\theta$ bin is $0.8^o$, which we take as our resolution.

*All sky d.c. survey.* The sky, in galactic coordinates, was divided into bins of equal solid angle, $\Delta\Omega = 2.1 \times 10^{-3} sr$, $\Delta\alpha = 3^o$, $\Delta sin\delta = 0.04$; they correspond to narrow cones of $1.5^o$ half angles. In order to remove edge effects, three other surveys were done, by shifting the map by one-half-bin in $\alpha$ (map 2), by one-half bin in sin$\delta$ (map 3) and with both $\alpha$ and sin$\delta$ shifted (map 4). For each solid angle bin we computed the deviation from the mean muon intensity after background subtraction in units of standard deviations

$$\sigma(i) = \frac{N_{obs}(i) - N_{exp}(i)}{\sqrt{N_{exp}(i)}}$$

where $N_{obs}(i)$ is the observed number of events in bin i and $N_{exp}$ is the number of events expected in that bin from the background simulation. No deviation was found and for the majority of the bins we obtain flux upper limits at the level of

$$\Phi_\mu{}^{steady}(95\%) \leq 5 \times 10^{-13} cm^{-2} s^{-1}. \qquad (1)$$

*Specific point-like d.c. sources.* For specific sources, Cyg X-3, Mrk421, Mrk501, we searched in a narrow cone ($1^o$ half angle) around the source direction. We obtain flux limits at the level of $(2-4) \times 10^{-13} cm^{-2} s^{-1}$. There is a small excess at the level of 2.0 $\sigma$ in the direction of Mrk501.

*Modulated a.c. search from Cyg X-3 and Her X-1.* No evidence for an excess was observed and the limits are $\Phi < 2 \times 10^{-13} cm^{-2} s^{-1}$.

*Search for bursting episodes.* Surface experiments reported several $\gamma$-bursts from celestial objects like Mrk421 and Mrk501. We therefore made a search for pulsed muon signals in a narrow window ($1^o$ half angle) around the location of these possible sources of very high energy photons. The bursting episodes of duration of $\sim 1$ day were studied with two different methods. In the first method we searched for daily excesses of muons above the background, also plotting cumulative excesses day by day. In the second one we computed day by day the quantity $-lg_{10}P$ where P is the probability to observe a burst at least as large as $N_{obs}$. We find some possible excesses for Mrk421 on the days 7/1/93, 14/2/95, 27/8/97, 5/12/98. These deserve further studies.

*Sidereal anisotropies.* A search for sidereal anisotropies (modulations in arrival times introduced by the galaxy's rotational motion through the extragalactic cosmic rays) is also in progress. The muon data sample is analyzed searching for periodic modulations. The amplitudes of the modulations are at the level of $\sim 0.2\,\%$. We are increasing the statistics and improving the systematics in order to obtain a significant result by adding a few more years of data to our current sample.

**Seasonal Variations**

Underground muons are produced by mesons decaying in flight in the upper atmosphere. The muon flux thus depends on the ratio between the decay and the interaction probability of the parent mesons, which is sensitive to the atmospheric density, and so, to

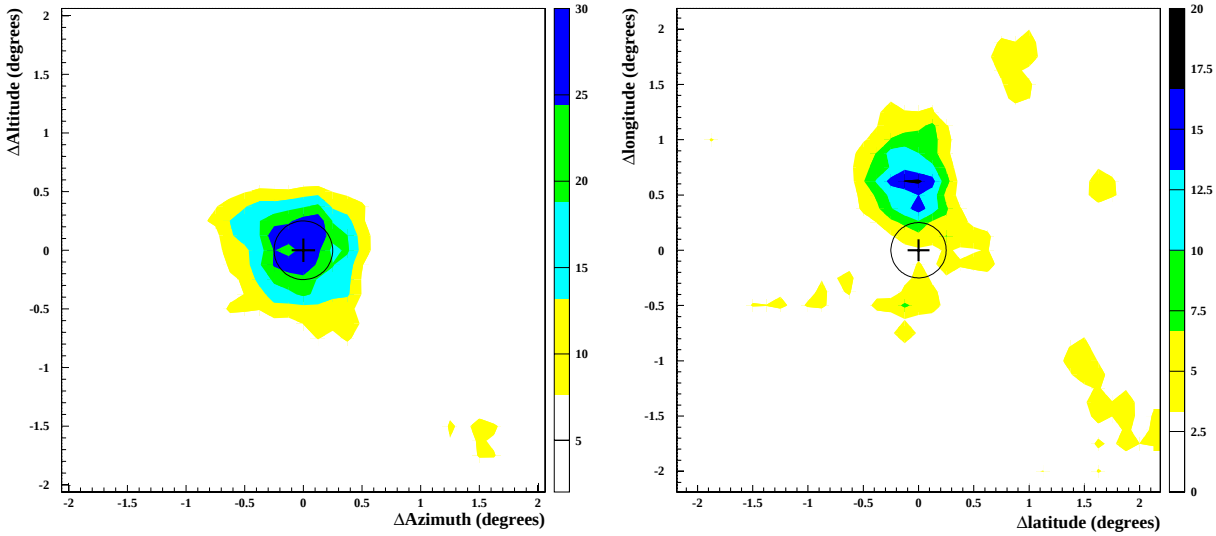


Figure 13: Moon and Sun shadows.(a) Two-dimensional distribution of the muon event density; the Moon is at (0,0). The various regions of increasing gray scale indicate various levels of deficit in percent. The darkest one corresponds to the maximum deficit. (b) Same analysis for the Sun direction.

its average temperature. The flux is expected to decrease in winter, when the temperature is lower and the atmosphere more dense, and to increase in summer. This correlation leads to variations at the level of 2 % to 3 %.
*Solar daily variations* are also under study.

**Moon and Sun Shadows of primary cosmic rays**

The pointing capability of MACRO was demonstrated by the observed "shadows" of the Moon and of the Sun, which produce a "shield" to the cosmic rays. We used a sample of $45 \times 10^6$ muons, looking at the bidimensional density of the events around the center of the Moon and of the Sun [17, M33]. In Fig. 13 we show two-dimensional plots of the significance of the muon deficit caused by the Moon and the Sun. For the Moon: we looked for events in a window $4.375^o \times 4.375^o$ centered on the Moon; the window was divided into $35 \times 35$ cells, each having dimensions of $0.125^o \times 0.125^o$ ($\Delta\Omega = 1.6 \times 10^{-2} deg^2$). The density of events is shown in a grey scale in a bidimensional plot in Fig. 13a. One observes an effect (a depletion of events) with a statistical significance of 5.5 $\sigma$. The observed slight displacement of the maximum deficit is consistent with the displacement of the primary protons due to the geomagnetic field. We have repeated the same analysis for muons in the Sun window, see Fig. 13b. The larger difference between the apparent Sun position and the observed muon density is due to the combined effect of the magnetic field of the Sun and of the geomagnetic field. The observed effect corresponds to a statistical significance of 4.2 $\sigma$.

**Photonuclear interactions of downgoing muons in the rock above MACRO**

The process was studied in detail and the frequency of such events relative to the number of downgoing single muons, $R_{\mu+h} = N_{\mu+h}/N_\mu$, was measured. The predictions of

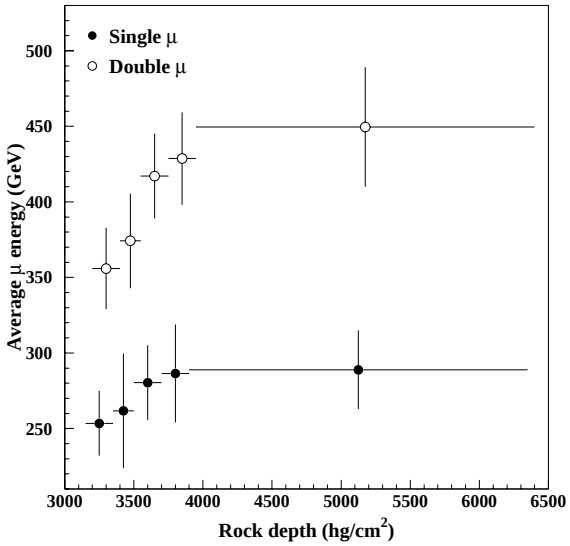


Figure 14: Average muon energy versus standard rock depth for single muons and for double muons [M34], see text.

the FLUKA Monte Carlo ($R_{\mu+h}(MC\,FLUKA) = (1.89 \pm 0.16_{stat} \pm 0.02_{syst}) \cdot 10^{-4}$) are in good agreement with the measured rates $R_{\mu+h}(DATA) = (1.91 \pm 0.05_{stat} \pm 0.03_{syst}) \cdot 10^{-4}$, while those of the hadronic interface of the GEANT code ($R_{\mu+h}(MC\,GEANT) = (1.31 \pm 0.14_{stat} \pm 0.02_{syst}) \cdot 10^{-5}$) are inadequate [M17].

## 3.8 Measurement of the Muon Energy with the TRD Detector

The underground differential energy spectrum of muons was measured by the TRD detector. The data were collected by the three TRD modules. We have analyzed two types of events: "single muons", i.e. single events in MACRO crossing a TRD module, and "double muons", i.e. double events in MACRO with only one muon crossing the TRD detector.The measurements refer to muons with energies $0.1 < E_\mu < 1$ TeV and for $E_\mu > 1$ TeV [M2, M34]. In order to evaluate the local muon energy spectrum, we must take into account the TRD response function, which induces some distortion of the "true" muon spectrum distribution. The "true" distribution can be extracted from the measured one by an unfolding procedure that yields good results only if the response of the detector is correctly understood. We have adopted an unfolding technique, developed according to Bayes' theorem, following the procedure described in [19]. Fig. 14 shows the average muon energy versus standard rock thickness for single and double muons. Systematic uncertainties are included in the error bars (they arise mainly from energy calibration uncertainties). The corrected average single muon energy is 272 $\pm 4_{stat}$ $\pm 33_{sys}$ GeV, while for double muons it is 398 $\pm 16_{stat}$ $\pm 39_{sys}$ GeV. Double muons are more energetic than single muons; this is in agreement with the predictions of interaction models of primary cosmic rays with the atmosphere.

## 3.9 EAS-TOP/MACRO Coincidences

The standard of data set coincidence events between EAS-TOP (located at Campo Imperatore) and MACRO includes the e.m. size on the surface and the correlated TeV muons detected underground ($N_e - N_\mu^{TeV}$: "2-fold coincidences") Up to the end of 1999, EAS-TOP and MACRO collected 22531 events of this kind, for a corresponding period of 756.17 days of live-time. The EAS-TOP and MACRO experiments have already presented analyses on part of these 2-fold coincidence data[27][28]. The analysis of these events was not easy because of the difficulty of separating hadronic physics from primary composition effects and of understanding the role played by fluctuations intrinsic in the detection technique. An increase in statistics is of limited help in this respect.

However, the strategy of performing multicomponent observations of extensive air showers and of analyzing a sample, although small, of individual events represents an effective response to meet these challenges. And this is indeed one of the aims of the collaboration of the EAS-TOP and MACRO experiments at the Gran Sasso laboratories. The main principles of the method are discussed elsewhere [29].

In the last year we started to analyze a new kind of coincidence events: they include data from the electromagnetic ($N_e$) and muon detectors ($N_\mu^{GeV} = N_\mu(E_\mu > 1GeV)$) of EAS-TOP and from the MACRO detector ($N_\mu^{TeV} = N_\mu(oE_\mu > 1.3\ TeV)$). These "3-fold" coincidence data are expected to provide a better discrimination of events produced by the heavy primary component, thus allowing a determination of the evolution of this fraction of primaries as a function of shower size. (Preliminary results in this area have also been presented [30] by the EAS-TOP and LVD Collaborations).

Events which are candidates for being originated by "very heavy" (iron-like) primaries are selected from their characteristics in the EAS-TOP ($N_e$) and MACRO ($N_\mu^{TeV}$). "Very heavy" primary candidates are selected from high TeV-muon multiplicities with a relatively low $N_e$. For these selected events, an analysis is then carried out using the $N_e - N_\mu^{GeV}$ data collected at the surface. In fact, the simulation described above has shown that, for fixed primary mass and energy, the fluctuations in the $GeV$ and $TeV$ muon numbers ($N_\mu^{GeV}$ and $N_\mu^{TeV}$) are uncorrelated. Therefore, the measured correlation is not connected with the shower development but to the EAS primaries.

The data analyzed in 1999 have been collected in 157 days of running time. A simulation study has been started and it makes use of the CORSIKA code as event generator. We describe the primary spectrum as the combination of five primary groups (from protons to Fe nuclei), and different interaction models can be considered. At present, we are considering the phenomenological model HDPM and the physical models QGSJET and DPMJET. The muon propagation in the rock is simulated by means of the MUSIC code [31], and the MACRO detector simulation is performed with GEANT. The full response of the detectors has been introduced.

The conversion from $N_e$ to the primary energy $E_0$ is obtained from the same Monte-Carlo simulation giving:

$$E_0 = \left(\frac{N_e}{\alpha_{30^o}}\right)^{1/\beta} \qquad (2)$$

where both $\alpha$ and $\beta$ depend on the mass number $A$ and on the interaction model.

¿From the simulation results we can estimate the contribution to the high muon multiplicity region from each mass group. We expect to be able to define experimental cuts in order to separate "light" (p, He) from "heavy" (N, Mg, Fe) primaries. Results of the analysis are expected within the first half of 2000.

As a further activity, the analysis of the coincidence between muon events detected in MACRO and the Cherenkov signal detected by the EAS-TOP Cherenkov telescope has now started. The number of MACRO candidate events under study is 57996, from a period including data taking in 1998. This analysis aims to study the dependence of TeV muon yield as a function of primary energy in a region (from few TeV to about 50 TeV) where protons largely dominate the primary spectrum. This will allow to place further constraints on the interaction models used in the MonteCarlo simulation.

# 4 Nuclear Track Detector Calibrations

We have continued the calibrations of the nuclear track detector CR39 with both slow and fast ions. In all measurements we have seen no deviation of its response from the restricted energy loss (REL) model. To complete the calibration, nuclear track detector stacks made of CR39 and Lexan foils, placed before and after various targets, were exposed to 158 A GeV $Pb^{82+}$ ions at the CERN-SPS and to 1 A GeV $Fe^{26+}$ ions at the BNL-AGS. In traversing the target, the beam ions produce nuclear fragments with $Z < 82$ and $Z < 26$ for the lead and iron beams, respectively, thus allowing a measurement of the response of the detector in a $Z$ regime most relevant to the detection of magnetic monopoles. We reported previously about the very good charge resolution of the detector in the range $83 > Z > 72$ (obtained by measurement of the etch-cone height) which complements its low threshold ($Z \sim 5$) and excellent resolution at low Z (by measurement of the cone base diameters).

Tests were made looking for a possible dependence of the CR39 response from its age, i.e. from the time elapsed between the date of production and the passage of the particle ("aging effects").
Two sets of samples, 0.8 y and 2.5 y old, respectively, were exposed in November 1994 to 158 A GeV $Pb^{82+}$ ions. For each detected nuclear fragment the reduced etch rate $p = v_T/v_B$ ($v_T$ and $v_B$ are the track and bulk etching rates, respectively) was computed and plotted in Fig. 15 vs REL. The lines represent the limits of the systematic uncertainties coming mainly from 1 standard deviation uncertainty on $v_B$. A more recent test was made by exposing CR39 samples 10y old to 1 A GeV$Fe^{26+}$ ions; the detector response is reported in Fig. 15. The results indicate that within experimental uncertainties, aging effects in the MACRO CR39 are negligible.
Until the end of december 1999, we etched and analyzed 265 $m^2$ of nuclear track detector in the search for magnetic monopoles and nuclearites. The 90% c.l. limit for an isotropic flux of monopoles with $\beta > 0.1$ is now at the level of 5.6 $10^{-16}$ $cm^{-2}s^{-1}sr^{-1}$ [M20, M21].

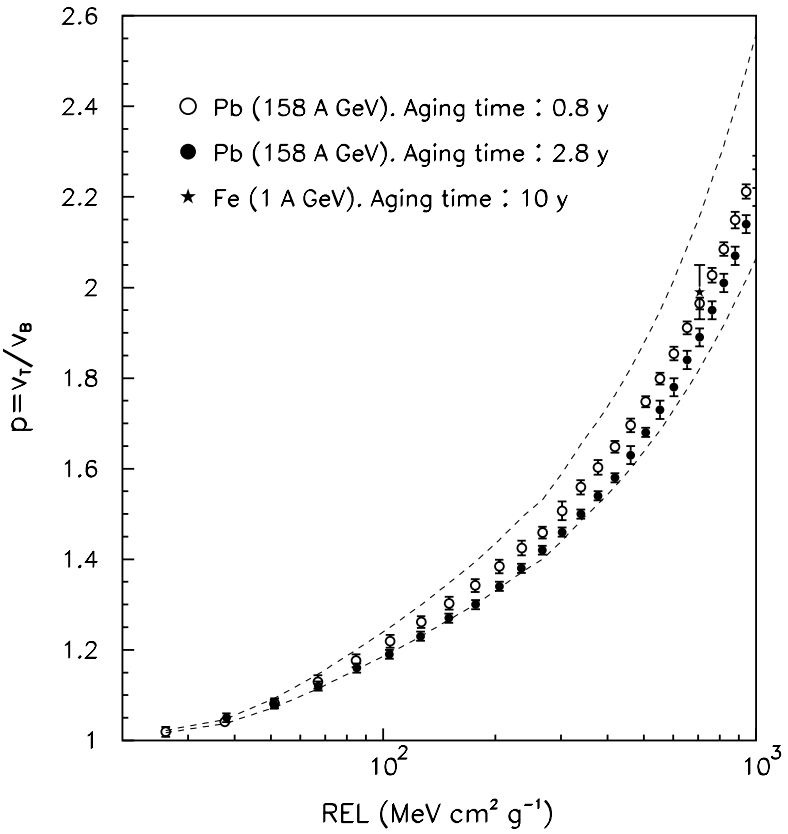


Figure 15: $p = v_T/v_B$ vs. REL for CR39 exposed to $Pb^{82+}$ ions of 158 A GeV and $Fe^{26+}$ ions of 1 A GeV at different times after production. This was done to estimate possible aging effects. The dashed lines indicate the systematic uncertainty arising mainly from fluctuations of the bulk etching rate $v_B$.

# 5 Conclusions

The MACRO detector is running smoothly in its final configuration. In 1999 we have extended most of our analyses and searches. We obtained important results on atmospheric neutrinos of high and low energies relevant to neutrino oscillations, more stringent limits on monopoles, nuclearites, WIMPs, astrophysical point sources, sidereal anisotropies, etc. Analyses sensitive to detector and Monte Carlo systematics have been refined and improved to yield solid results in many fields of high energy neutrino physics and astrophysics and of cosmic ray physics. No stellar gravitational collapse low energy neutrinos have been observed since 1989; our on-line monitor is now integrated in a world supernova watch system.

The present data rate for high energy muon neutrinos is (in parentheses we quote the number of available events as of December 1, 1999):
- Muon neutrinos for neutrino astronomy: 215 / yr ($\sim$ 1100);
- Up throughgoing muons: 140 / yr ($\sim$ 740);
- Semicontained muon events: 25 / yr ($\sim$ 138);
- Upstopping plus down semicontained: 45 / yr ($\sim$ 215).

These rates are approximate since they depend on the cuts used for the different analyses.

# 6 List of MACRO publications, conference proceedings and memos MACRO/PUBs during 1999


[M1] MACRO Collaboration, M. Ambrosio et al., "Observation of the shadowing of cosmic rays by the moon using a deep underground detector", Phys. Rev. D 59(1999)012003; INFN/AE **98/14** (1998) and hep-ex/9807006.

[M2] MACRO Collaboration, M. Ambrosio et al., "Measurement of the energy spectrum of underground muons at Gran Sasso with a Transition Radiation Detector", Astropart. Phys. **10** (1999) 11; INFN/AE **98/15** (1998) and hep-ex/9807009.

[M3] MACRO Collaboration, M. Ambrosio et al., "Limits on dark matter WIMPs using upward-going muons in the MACRO detector", Phys. Rev. D 60(1999)082002 and hep-ex/9812020.

[M4] MACRO Collaboration, M. Ambrosio et al., "High statistics measurement of the underground muon pair separation at Gran Sasso", Phys. Rev. D 60(1999)032001; INFN/AE **99/04** (1999) and hep-ex/9901027.

[M5] MACRO Collaboration, M. Ambrosio et al., "Nuclearite search with the MACRO detector at Gran Sasso", hep-ex/9904031, accepted by Eur. Phys. Jour.

[M6] MACRO Collaboration, M.Ambrosio et al., "A search for lightly ionizing particles with the MACRO detector", hep-ex/0002029, submitted to Phys. Rev. D.

[M7] MACRO Collaboration, M.Ambrosio et al., "Low energy atmospheric muon neutrinos in MACRO", hep-ex/0001044, submitted to Phys. Lett. B.

[M8] B. Nolty for the MACRO Collaboration, "Measurement of the neutrino induced semi-contained events in MACRO", hep-ex/9903030, DPF 99, American Physical Society Division of Particles and Fields, 5-9 January 1999, University of California, Los Angeles.

[M9] N.P.Longley for the MACRO Collaboration, "Neutrino-induced upward-going muons at MACRO", DPF 99, American Physical Society, Division of Particles and Fields 5-9 January 1999, University of California, Los Angeles.

[M10] D. Michael for the MACRO Collaboration,"Search for WIMPs with MACRO", DPF 99, American Physical Society, Division of Particles and Fields, 5-9 January 1999, University of California, Los Angeles.

[M11] D. Michael for the MACRO Collaboration,"Neutrino astronomy with MACRO" DPF 99, American Physical Society Division of Particles and Fields, 5-9 January 1999, University of California, Los Angeles

[M12] A. Di Credico for the MACRO Collaboration,"High-energy astrophysical neutrinos at MACRO", WIN99 (Capetown).

[M13] M. Spinetti for the MACRO Collaboration,"Atmospheric neutrino oscillation results with Macro at Gran Sasso", 8th Workshop on Neutrino Telescopes, Venice, 1999.

[M14] H. Dekhissi for the MACRO Collaboration,"Search for cosmic ray point sources", 8th UN/ESA Workshop on Basic Space Science: Scientific Exploration from Space, Mafraq, Jordan, 13-17 March 1999.

[M15] V. Popa for the MACRO Collaboration,"Search for magnetic monopoles and for nuclearites with the MACRO detector", 8th UN/ESA Workshop on Basic Space Science: Scientific Exploration from Space, Mafraq, Jordan, 13-17 March 1999.

[M16] D. Michael for the MACRO Collaboration,"Atmospheric neutrino results from MACRO", Moriond 99.

[M17] M. Sioli for the MACRO Collaboration, "Underground muon physics with the MACRO detector at Gran Sasso", First Arctic Workshop on Cosmic Ray Muons, Sodankyla, Finland, 24-29/04/1999.

[M18] M. Ouchrif for the MACRO Collaboration, "Q-balls in Underground Experiments", Sixth Topical Seminar on Neutrino and Astroparticle Physics, 17-21 May 1999, San Miniato (Italy).

[M19] M. Spurio for the MACRO Collaboration, "Neutrino Physics and Astrophysics with the MACRO Detector", Sixth Topical Seminar on Neutrino and Astroparticle Physics, 17-21 May 1999, San Miniato (Italy).

[M20] L. Patrizii for the MACRO Collaboration, "Search for massive rare particles with the MACRO detector at Gran Sasso", Sixth Topical Seminar on Neutrino and Astroparticle Physics, 17-21 May 1999, San Miniato (Italy).

[M21] M. Giorgini for the MACRO Collaboration, Search for magnetic monopoles with nuclear track detectors, Sixth Topical Seminar on Neutrino and Astroparticle Physics, 17-21 May 1999, San Miniato (Italy).

[M22] M. Sioli for the MACRO Collaboration,"Underground muon physics with the MACRO experiment, Sixth Topical Seminar on Neutrino and Astroparticle Physics, 17-21 May 1999, San Miniato (Italy).

[M23] E. Scapparone for the MACRO Collaboration, "Review of primary cosmic ray composition studies with underground detectors, Sixth Topical Seminar on Neutrino and Astroparticle Physics, 17-21 May 1999, San Miniato (Italy).

[M24] H. Dekhissi for the MACRO Collaboration, "Quelques resultats de l'experience MACRO", 6-10 July 1999, Summer School " Physique des hautes energie". Rabat-Morocco

[M25] P. Bernardini for the MACRO Collaboration,"Measurement of the atmospheric muon neutrinos with the MACRO detector", hep-ex/9906019, invited talk to "Les Rencontres de Physique de la Vallee d'Aoste", La Thuile (1999).

[M26] P. Bernardini for the MACRO Collaboration, "Neutrino astronomy and search for WIMPs with MACRO", TAUP99, Paris (1999).

[M27] M. Sitta for the MACRO Collaboration, "Search for magnetic monopoles with MACRO, TAUP99, Paris (1999).

[M28] T. Montaruli for the MACRO Collaboration, "MACRO as a telescope for neutrino astronomy", hep-ex/9905020, XXVI ICRC - Salt Lake City, Utah, USA, August 17-25, 1999.

[M29] C. Satriano for the MACRO Collaboration,"Search for steady, modulated and variable cosmic ray sources using underground muons in MACRO", XXVI ICRC - Salt Lake City, Utah, USA, August 17-25, 1999

[M30] F. Ronga for the MACRO Collaboration, "Neutrino oscillations at high energy by MACRO", XXVI ICRC - Salt Lake City, Utah, USA, August 17-25, 1999.

[M31] A. Surdo for the MACRO Collaboration, "Low energy atmospheric neutrino events in MACRO", XXVI ICRC - Salt Lake City, Utah, USA, August 17-25, 1999.

[M32] B.C. Choudhary for the MACRO Collaboration, "Search for magnetic monopoles with MACRO", hep-ex/9905023, XXVI ICRC - Salt Lake City, Utah, USA, August 17-25, 1999.

[M33] N. Giglietto for the MACRO Collaboration, "Moon and Sun shadowing observed by the MACRO detector", XXVI ICRC - Salt Lake City, Utah, USA, August 17-25, 1999.

[M34] M. N. Mazziotta for the MACRO Collaboration, "Transition Radiation Detector in MACRO", hep-ex/9905018, XXVI ICRC - Salt Lake City, Utah, USA, August 17-25, 1999.

[M35] T. Montaruli for the MACRO Collaboration, "Search for WIMPS using upward-going muons in MACRO", hep-ex/9905021, XXVI ICRC - Salt Lake City, Utah, USA, August 17-25, 1999.

[M36] M. Ouchrif for the MACRO Collaboration, "Energy Losses of Q-balls in Matter, Earth and Detectors", COSMO99, 27-2 September 1999 ICTP, Trieste (Italy).

[M37] M. Giorgini for the MACRO Collaboration, "Ricerca di monopoli magnetici con l'esperimento MACRO al Gran Sasso", LXXV Congresso Nazionale SIF, Pavia, Italy (1999).

[M38] L. Perrone for the MACRO Collaboration, "Neutrino astronomy and indirect search for WIMPS", LXXXV Congresso Nazionale SIF, Pavia, Italy (1999).

[M39] L. Perrone for the MACRO Collaboration, "High energy atmospheric neutrinos and oscillations", LXXXV Congresso Nazionale SIF, Pavia, Italy (1999).

[M40] E. Vilela for the MACRO Collaboration, "Search for magnetic monopoles and nuclearites with the MACRO nuclear track detector", Radiation Measurements 31(1999)605.

[M41] T. Montaruli for the MACRO Collaboration, "The MACRO detection of neutrinos, monopoles and indirect searches for WIMPs", Beyond the desert 99, Castle Ringberg, June 1999.

[M42] M. Spurio for the MACRO Collaboration, "Atmospheric neutrino oscillations in MACRO", PANIC99.

[M43] N. Longley for the MACRO Collaboration, " Atmospheric neutrinos at MACRO", Centennial APS meeting, Atlanta, Georgia.

[M44] S. Mufson for the MACRO Collaboration, "Recent results from the MACRO detector at Gran Sasso", Invited talk to High Energy Astrophysics Division Meeting of the America Astronomical Society, Charleston, South Carolina.

# 7 References

[1] MACRO Collaboration, M. Ambrosio et al., Astropart. Phys. 9(1998)105, hep-ex/9807032.

[2] MACRO Collaboration, M. Ambrosio et al., "Measurement of the atmospheric neutrino-induced upgoing muon flux using MACRO", Phys. Lett. **B434** (1998) 451, hep-ex/9807005; MACRO Collaboration, M. Ambrosio et al., "Atmospheric neutrino flux measurements using upgoing muons", Phys. Lett. **B357** (1995) 481.

[3] M. Spinetti, "Recenti risultati e prospettive dello studio dei neutrini atmosferici", 1998 Meeting of the Italian Physical Society (SIF); F. Ronga, "Atmospheric neutrinos", hep-ex/0001058.

[4] G. Feldman and R. Cousins, Phys. Rev. **D57** (1998) 3873.

[5] P. Lipari et al., Phys. Rev. Lett. **74** (1995) 384.

[6] G. Giacomelli, "Highlights in neutrino and astroparticle physics", Closing lecture at the 1999 S. Miniato Workshop, hep-ex/0001008.

[7] A. Bottino, N. Fornengo, F. Donato and S. Scopel (private communication). N. Fornengo, to appear in the Proceedings of the Ringberg Euroconference "New Trends in Neutrino Physics" (Ringberg Castle, Tegernsee, Germany, May 1998), edited by B. Kniel (World Scientific, Singapore).

[8] R. Bernabei et al., Phys. Lett. B **389** (1996)757.

[9] G. Giacomelli and L. Patrizii, "Magnetic monopoles", Lecture at the Fifth School on Particle Astrophysics, Trieste 29 June-10 July 1998, hep-ex/0002032, DFUB 98/30.

[10] J. Derkaoui et al., Astropart. Phys. **9** (1998) 173; "Energy losses of magnetic monopoles and dyons in scintillators, streamer tubes and nuclear track detectors", DFUB 98/13 (1998), to be published in Astrop. Phys.;

[11] S. Nakamura et al., Phys. Lett. **B263** (1991) 529.

[12] S. Orito et al., Phys. Rev. Lett. **66** (1991) 1951.

[13] P. B. Price, Phys. Rev. **D38** (1988) 3813.

[14] D. Ghosh and S. Chatterjea, Europhys. Lett. **12** (1990) 25.

[15] MACRO Collaboration, M. Ambrosio et al., "Real time supernova neutrino burst detection with MACRO", Astropart. Phys. 8 (1998) 123.

[16] MACRO Collaboration, M. Ambrosio et al., "Vertical muon intensity measured with MACRO at the Gran Sasso laboratory", Phys. Rev. **D52** (1995) 3793.

[17] MACRO Collaboration, M. Ambrosio et al., "Observation of the shadowing of cosmic rays by the moon using a deep underground detector", Phys. Rev. **D59** (1999)012003.

[18] G. Battistoni and E. Scapparone, "Hint of $\mu+n \rightarrow \mu+n+\mu^+ +\mu^-$ process observation with the MACRO detector at Gran Sasso", hep-ex/990218, ISVHECRI, Gran Sasso (1998)

[19] MACRO Collaboration, M. Ambrosio et al., "Measurement of the energy spectrum of underground muons at Gran Sasso with a transition radiation detector", Astropart. Phys. 10 (1999) 11, hep-ex/9807009.

[20] M. Aglietta et al., N.I.M. **A336** (1993) 310.

[21] MACRO Coll.,"Annual Report 1996 - Laboratori Nazionali del Gran Sasso"; P. Serra et al., "Total charge changing cross section of 158 A GeV *Pb* ions in different targets with nuclear track detectors", proceedings of the XXV ICRC Conference, Durban (South Africa), 28 july - 8 August 1997 and DFUB **10/97** (1997)

[22] F. Ronga,"Review on atmospheric neutrinos", invited talk to TAUP99, Paris (1999).

[23] M. Sioli, *A new approach to the study of high energy muon bundles with the MACRO detector at Gran Sasso*, Tesi di Dottorato, Universitá di Bologna (2000).

[24] P. Lipa, P. Carruthers, H.C. Eggers and B. Buschbeck, Phys. Lett. **285B** (1992) 300.

[25] MACRO Collaboration, M. Ambrosio *et al.*, Phys. Rev. **D56** (1997) 1418.

[26] G. Battistoni *et al.*, LNGS-95-09 (1995); G. Battistoni *et al.*, in *Proceedings of the XXIV Int. Cosmic Ray Conf.*, Roma, Italy, 1995, ed. N. Iucci *et al.*, Arti Grafiche Editoriali, Urbino, (1995), Vol. 1, p. 508.

[27] EAS-TOP and MACRO Collaborations, Nucl. Phys. B35(1994), 257.

[28] EAS-TOP and MACRO Collaborations, Nucl. Phys. B48(1996), 450.

[29] EAS-TOP Collaboration, Nucl. Phys. B54B(1997), 263.

[30] EAS-TOP and LVD Collaborations, Proc. 25th ICRC, Durban (South Africa), 1997.

[31] Antonioli P. *et al.* 1997, Proc. 25th ICRC, Durban (South Africa), 1997.

# MIBETA. A cryogenic experiment on double beta decay and search for rare event

A. Alessandrello[a], C. Arpesella[b], C. Brofferio[a],
C. Bucci[b], C. Cattadori[a], D.V.Camin[a], O. Cremonesi[a],
E. Fiorini[a], A. Giuliani[a], A. Nucciotti[a], M. Pavan[a],
A. Peruzzi[c], G. Pessina[a], S. Pirro[a], E. Previtali[a],
C. Pobes[b], M. Vanzini[a], L. Zanotti[a]

[a] Dipartimento di Fisica dell'Università di Milano e INFN, Sezione di Milano
[b] Laboratori Nazionali del Gran Sasso dell' INFN
[c] Laboratory of Nuclear and High Energy Physics, University of Zaragoza

## 1 The experimental apparatus

The experimental apparatus used by the group in the Gran Sasso Underground Laboratory consists of two dilution refrigerators operating in Hall A and C . The former has a power of 1000 microwatt at 100 mK , the second a power of 200 microwatt at the same temperature. Both have been made with previously tested low radioactivity materials and are equipped with helium liquefier , which provides a substantial recovery of the Helium and also prevents Helium contamination in the tunnel atmosphere. We would like to point out that this instrumentation represents the largest underground cryogenic facility in the world. In addition the group is carrying on continuous measurements of radioactive contamination in the Low Radioactivity Laboratory, where two of the large Ge detectors have been installed by the group itself. The dilution refrigerator operating in Hall A contains an array of 20 crystals of $TeO_2$ of $3 \times 3 \times 6$ cm$^3$ each for a total mass of almost 7 kg, by far the largest cryogenic mass operating underground. The dilution refrigerator in Hall C is mainly used for Research and Development for the recently approved and funded CUORICINO experiment. It has been operated with various arrays of crystals of $TeO_2$ of $\times 5 \times 5$ cm$^3$ each, which, with a mass of about 750 g each represent the largest thermal detector operated underground.

## 2 Aim of the experiments

One of the main object of the experiments being and going to be carried out with our cryogenic apparatuses in the Gran Sasso Laboratory is the searce for double beta decay of $^{130}$Te both in the lepton conserving two neutrino and in the lepton non conserving neutrinoless channel. The former one is allowed by the standard model of weak interactions, but a direct result on its lifetime would solve a long standing problem arising from the data provided by geochemical experiments, which yield lifetimes in strong disagreement among themselves. For this reason two crystals of $^{130}TeO_2$ and two crystals of $^{128}TeO_2$ have been installed in the dilution refrigerator operating in Hall A, together with crystals of natural tellurium. Most of the interest of the group is however addressed to the neutrinoless double beta decay channel which would imply lepton number non-conservation and, indirectly, a non-zero neutrino mass. The Gran Unified Theories of fundamental interaction predict both these facts. This search is presently carried out with the 20 crystal arrays, but will proceed with the CUORICINO experiment based on an array of 54 crystals of $5 \times 5 \times 5$ cm$^3$ with a total mass of 42 kg. Aim of these cryogenic experiments is also search for other rare events, like those produced by direct interaction of WIMPS. The group has in fact proved that the efficiency (Quenching Factor) for nuclear recoils in our detector is constantly equal to one for energies ranging from 20 to 200 keV. Searches on seasonal modulation of WIMP interactions will be made possible by the CUORICINO set-up. Another important aim of the cryogenic experiments will be the study of a subdiurnal modulation of the signal induced in our detector by possible electromagnetic interactions of axions coming from the Sun. This electromagnetic signal would be in fact enhanced when the position of a crystal plane of our crystals will be under he Bragg angle with respect to the direction of propagation of these particles.

## 3 Results obteined in 1999

The dilution refrigerator operating in Hall A was not running at full time in this year, due to the unexpected failure of a pump and to difficulties in power and water supply which are unavoidable in an underground laboratory, but particularly dangerous in a cryogenic experiment. Still our result on the limit of the lifetime for two neutrinoless double beta decay is by three order superior than in any other direct experiments, and already "touchs" the geochemical results and theoretical predictions. Our negative result on neutrinoless double beta decay is the most stringent one in the world after the limit obtained on $^{76}$Ge by the Heidelberg-Moscow and IGEX experiments on the basis of most theoretical calculations. An intense activity was carried out with the dilution refrigerator operating in Hall C for research and development of large crystals in view of the CUORICINO experiment, and also in the low background laboratory. Among the most important results we would like to quote the energy resolution obtained with the 750 $TeO_2$ crystals which is now the same as that of Ge diodes for high energy gamma rays. For alpha particles of 5400 keV we have reached a FWHM resolution better than 4 keV, the best ever obtained in the world with any t ype of detector. The study of the radioactive contamination of the $TeO_2$ crystals, carried out in collaboration with the Shanghai Institute of Ceramics, has

shown that it is located mainly on the surface, and that is due mainly to alpha particles and nuclear recoils. A chemical treatment of the surfaces has decreased the peak intensity by an order of magnitude.

# 4 List of Publications


1. A. Alessandrello et al: Measure of low radioactive contaminations and nuclear recoil quenching factor using cryogenic particle detectors, Nucl.Phys.B (Proc.Suppl) 70 (1999) 96

2. E. Fiorini: Double Beta Decay, Invited paper to Neutrino Telescope (Venice, February 23-27, 1999) Ed. By M. Baldo Ceolin (in the press)

3. E.Fiorini: Weak interaction searches with cryogenic detectors, Invited Talk to LTD8, Dalfsen (The Netherlands) , August 16-20, 1999, NIM A (in press)

4. S. Pirro: Present status of MI-BETA cryogenic experiment and preliminary results for CUORICINO , Talk to LTD8, Dalfsen (The Netherlands) , August 16-20, 1999, NIM A (in press)

5. A. ALESSANDRELLO et al : A massive thermal detector for alpha and gamma spectroscopy, NIM A (in the press)

6. A. Alessandrello et al: Toward the CUORE project, Presented to the H.E. Phys. Conf. (Tampere, Finland , July 1999) to be published in the Proceedings

7. A. Alessandrello et al: The first towards CUORE: CUORICINO a 54 thermal detector array to search for rare events, Presented to TAUP 1999 (Paris Sept.1999) to be published on Nucl.Phys. B

# THEORETICAL GROUP

R. Aloisio [b], Z. Berezhiani [a], V.Berezinsky[b],
P. Chardonnet [c], G. Di Carlo[d], M. Gianotti [b],
A. F. Grillo[a], M. Marchesini [g], F. Vissani[a]

[a] Laboratori Nazionali del Gran Sasso, Assergi L' Aquila, Italy
[a] Physics Department, University of L' Aquila, Italy
[b] LAPP, Annecy, France
[c] Laboratori Nazionali di Frascati, Italy
[d] Physics Department, University of Zaragoza, Spain
[e] Bochum University, Germany
[f] Bologna University, Italy

**Abstract**

The activity of the group has concerned research in two main areas: Astroparticle Physics and Cosmology, and Lattice Gauge Theory. During 1999 there has been an increase of the components of the group. Moreover, the group is now officially a member of Commission IV of INFN.

## 1 Astroparticle Physics

The activity of V.Berezinsky, in collaboration with M.Kachelriess (postdoc from Bochum University, Germany, until March 1999), F. Vissani (from September 1999), P.Chardonnet (LAPP,France from September 1999), M.Marchesini (student of Bologna University) and visitors B.Hnatyk (Lviv University, Ukraine) and S.Grigorieva (Institute for Nuclear Research, Moscow) concerned research in Astroparticle Physics. The group worked in close collaboration with A.Vilenkin (Tufts University, USA), with P.Blasi (now at the Fermi National Laboratory), with Ferrara group (G.Fiorentini et al), and with M.Lissia (Cagliari University)

**Scientific work**

The main field of the work is astroparticle physics, including solar neutrinos, ultra high energy cosmic rays, topological defects and relativistic astrophysics. From several works finished in 1999 two following results can be singled out.

V.Berezinsky and A.Vilenkin have shown that Topological Defects in the mirror matter can produce the large fluxes of high energy neutrinos, not being limited by usual cosmological and astrophysical constraints. (hep-ph/9908257).

V.Berezinsky, G.Fiorentini and M.Lissia have analyzed the time variation of neutrino signal in vacuum oscillation solution with high energy excess (HEE VO), which was earlier suggested by them. The predicted time variation is in a good agreement with the data of GALLEX, Homestake and Superkamiokande, though time-independent signal statistically is not excluded. (hep-ph/9904259, to be published in Astrop.Phys.)

**Participation in Conferences**

V. Berezinsky presented the invited talks in 1999 at TAUP-99 (Paris), Neutrino Telescopes (Venice), COSMO-99 (Trieste), Non-Accelerator New Physics (Dubna) and Particles in Astrophysics and Cosmology (Valencia). F.Vissani gave invited talk at the DAFNE workshop (Frascati).

**Journal and Proceedings publications**

1. V.Berezinsky and A.Mikhailov, Anisotropy of Ultra High Energy Cosmic Rays in the Dark Matter halo models. Phys. Lett. B 449 (1999) 237.

2. V.Berezinsky, Ultra High Energy Cosmic Rays. Nucl.Phys. B (Proc. Suppl.) 70 (1999) 419.

3. V.Berezinsky, M.Kachelriess and A.Vilenkin, Ultra High Energy Cosmic Rays from Decaying Relic Particles. Nucl. Phys. B (Proc. Suppl) 70 (1999) 500

4. V.Berezinsky, Ultra High Energy Cosmic Rays from Cosmological Relics. Nucl. Phys. B (Proc. Suppl) 75A (1999) 119.

5. V.Berezinsky, Solar Neutrino Oscillations. Proc. of 8th Int. Workshop on Neutrino Telescopes (ed. M. Baldo Ceolin) (1999) 91.

6. S.Dugal and F.Vissani, Proposal to Look for Up/Down Asymmetry in Atmospheric Neutrinos Beyound Multy-GeV Region. Phys. Lett. B 469 (1999) 171.

**Preprints**

1. V.Berezinsky and A.Vilenkin, Very High Energy Neutrinos from Hidden- sector Topological Defects hep-ph/9908257

2. V.Berezinsky, G.Fiorentini and M.Lissia, Vacuum Oscillations and Excess of High Energy Neutrinos Observed in Superkamiokande. hep-ph/9904259, to be published in Astrop. Phys.

3. V.Berezinsky, G.Fiorentini and M.Lissia, Solar Neutrino Fluxes with arbitrary He3 mixing astro-ph/9902222, to be published in Phys.Rev. D

4. V.Berezinsky, Oscillation Solutions to Solar Neutrino Problem. hep-ph/9904259 (to be published in Proc. Texas Symposium 1999

5.A.Datta, B.Mukhopadhyaya, and F.Vissani, Tevatron Signatures of an R-parity Violating Supersymmetric Theory hep-ph/9910296

The research activity of Z. Berezhiani and M. Gianotti was devoted to investigation of quark and lepton mass and mixing structure in supersymmetric theories of grand unification. It was demonstrated that in the frames of the SU(5) model one can naturally obtain large neutrino mixing angles needeed for explanation of the atmospheric neutrino anomaly while the quark mixing angles are small.

It was also analyzed the flavour puzzles in the models with TeV scale quantum gravity and large extra dimensions. It is generically very difficult to suppress at the sufficient level various flavour non-diagonal operators cutoff by order TeV scale. Several possibilities involving the horizontal symmetry were designed.

Yet another part of research was devoted to physics of light pseudo-Goldstone bosons and their astrophysical implications. In particular, it was suggested an cosmological gamma ray bursts via the emission of heavy (with mass order MeV) axion-like particles which can be emitted by collapsing compact objects with large luminosities and then decay at distances about 1000 km, giving rise to hot ultrarelativistic plasma, the fireball. Such an axion is within the reach of the future reactor experiments. It was also shown that if Majoron exists with the lepton number breaking scale below 300 GeV, then the oscillating neutrino flux could give rise to long range classical fields which could be observable due to their impact on supernova neutrino signal.

**Publications**

1) Zurab Berezhiani, Alessandro Drago, Gamma ray bursts via emission of axion-like particles.
DFAQ-TH-99-05 (Nov 1999) 15p. hep-ph/9911333. Accepted in Phys. Lett. B

2) Luis Bento, Zurab Berezhiani, Classical Nambu-Goldstone fields.
CFNUL-99-02 (Aug 1999) 10p. hep-ph/9908211. Phys. Rev. D, in press.

3) Z. Berezhiani, Exotic mechanisms for neutrino masses.
In "Trento 1998, Lepton and baryon number violation", Ed. H.V. Klapdor-Kleingrothaus, Bristol Publishing, 1999, pp. 147-172.

5) Zurab Berezhiani, Anna Rossi, Towards a Grand Unified picture for neutrino and quark mixings.
DFAQ-99-TH-01 (May 1999) 6p. hep-ph/9907397. Nucl. Phys. B (Proc. Suppl.), in press

6) Zurab Berezhiani, Anna Rossi, Grand Unified textures for neutrino and quark mixings. JHEP 9903 (1999) 002.

7) Zurab Berezhiani, Gia Dvali, Flavor violation in theories with Tev scale Quantum Gravity.
Phys. Lett. B450 (1999) 24.

# 2 Lattice Gauge Theories

The study of the properties of Quantum ChromoDynamics (QCD), in particular at non zero baryonic density, can provide in principle an ab initio calculation of nuclear and particle properties and processes of relevance to Cosmology, Astrophysics and to Heavy

Ions experiments. such as the equation of state of nuclear matter and the relevant critical properties. This kind of study is extremely difficult from a numerical point of view, due to the complex nature of the fermionic action in SU(3) that does not allow the use of standard simulation techniques.

In this framework, A.F. Grillo, R. Aloisio in collaboration with G. Di Carlo (LNF), V. Azcoiti and A. Galante (University of Zaragoza) have studied the model in two (unphysical) cases, more affordable from a numerical point of view. In the first the gauge group is still SU(3), but heavy quark are considered, in the second the color symmetry group has been reduced to SU(2) (two colors QCD) without limitations on quark masses.

In heavy quark limit signals of a deconfining (first order) phase transition at small density and near to the zero density critical temperature have been obtained [1]. This transition, expected on general grounds within phenomenological models, has never been seen before; previous results, instead, obtained using approximations or simplified models, casted doubts on its real existance.

For two colors QCD results have been obtained in light quark regime [2,4]; especially interesting is the study of diquark condensate formation at high density and zero temperature. This phenomenon, expected in the frame of theories based on similarity with the standard description of the superconducting phase of ordinary matter (BCS), has been studied in the strong coupling limit using a technique formerly developed for the analysis of chiral transition in noncompact QED. This technique, via the study of susceptibility, i.e. derivative of the order parameter, allows to avoid potentially harmful extrapolations procedures, making particularly clear the numerical analysis of the formation of the condensate [3].

The current situation of the results of three colors theory in the infinite gauge coupling limit [2,4], has been critically re-examined, raising strong doubts on the robusteness of the signal of strong first order phase transition obtained, in 1989, using the MDP (Monomer-Dimer-Polymer) algorithm. The existence of this transition could be considered as one of the few universally accepted results of numerical simulations of finite density QCD up to now, and the MDP as the only algorithm effective, in the strong coupling regime, to produce sensible results.

**Publications**

1. R. Aloisio, V. Azcoiti, G. Di Carlo, A. Galante, A.F. Grillo, "Finite density Fat QCD" DFTUZ 99/05,hep-lat-9903004, Phys. Rev. D (Rapid Comm.), in press.

**Proceedings**

3. R. Aloisio, V. Azcoiti, G. Di Carlo, A. Galante, A.F. Grillo; Strongly Coupled QCD at Finite Baryon Density
LATTICE99, hep-lat/9909120.

# TRIS
# A Measurement of the Spectral Index of the Galactic Diffuse Emission

R. Baselli[b], G. Boella[a], P. Buratti[b], F. Cavaliere[b], A. de Lucia[a], M. Gervasi[a], A. Passerini[a], D. Restifo[b], G. Sironi[a], D. Spiga[b], M. Zannoni[a]

[a] Physics Dept. G.Occhialini and GIFCO unit - Università di Milano-Bicocca - Italy
[b] Physics Department - Università degli Studi di Milano - Italy

**Abstract**

TRIS is a set of three absolute radiometers we use to measure the absolute temperature of the sky at three frequencies: 600 MHz, 820 MHz and 2.5 GHz. Final goal of this experiment is a measurement of the temperature of the Cosmic Microwave Background, Relic of the Big Bang, with an accuracy of 200 mK looking for deviations from a Planckian frequency distribution in the frequency region close to 1 GHz where spectral distortions are expected. An essential step toward this end is the evaluation of the contribution of the Galactic diffusion emission to the total signal. Here we present a measurement of the galactic spectral index.

## 1 Introduction

TRIS is an experiment which has been set up to measure the absolute temperature $T_{3K}$ of the Cosmic Microwave Background, Relic of the Big Bang, in the frequency region close to 1 GHz where deviations from a Planck frequency distribution of that radiation is expected ([1]). The frequency at which this distortion occurs can be used to evaluate the Universe baryon density $\Omega_b$.

To get $T_{3K}$ one measures $T_{sky}$, the absolute brightness temperature of the sky, and subtract the foreground contributions, $T_{Gal}$ (Galactic diffuse emission), and $T_{ex}$ (blend of unresolved extragalactic sources):

$$T_{3K} = T_{sky}(\alpha, \delta, \nu) - T_{Gal}(\alpha, \delta, \nu) - T_{ex}(\alpha, \delta, \nu) \quad (1)$$

where $\alpha$ and $\delta$ are the celestial coordinates (*right ascension* and *declination*) of the region of sky which is observed.

$T_{3K}$ and $T_{ex}$ have isotropic spatial distribution while $T_{Gal}$ is higly anisotropic. The frequency spectrum of $T_{Gal}$ is a power law

$$T_{Gal}(\nu, \alpha, \delta) = K(\alpha, \delta)\nu^{-\gamma(\alpha,\delta)} \tag{2}$$

At the frequencies $\nu$ of TRIS, 600 MHz, 820 MHz and 2.5 GHz, $T_{Gal}$ is comparable or even greater than $T_{3K}$ but is poorly known ([7]), therefore TRIS must include direct measurements of $T_{Gal}$ and its spectral index $\gamma$ ([6]).

Here we report a measurement of $\gamma$ between 408 MHz and 820 MHz made using TRIS data at 820 MHz and data in literature at 408 MHz.

# 2 Observation

The antennae of TRIS when aimed at the zenith receive signals from a declination $\delta$ equal to the latitude of the site where observations are made (Campo Imperatore latitude $= 42^\circ\ 27'$, longitude $= 13^\circ\ 35'\ E$). As the time goes on the right ascension $\alpha$ of the region of sky at the zenith varies and in a day the antenna beam covers the complete strip of sky of constant declination $\delta = 42^\circ$ with right ascension $\alpha$ variable between $0^\circ$ and $360^\circ$ ($0^h,\ 24^h$). A 24 h plot of the system output versus time gives therefore a profile of $T_{sky}$ versus $\alpha$. We call this profile *drift scan*.

Because of the difference between solar and sidereal time, $23^h\ 56^m$ are sufficient to cover the entire strip at constant $\delta$, therefore every day a region of sky arrive at zenith about 4 minute sooner than the day before and a source visible at daytime on a given day, six months later will be visible at nighttime.

This effect is used by TRIS to synthesize 24 h profiles made only with data collected at nighttime, when the sun does not disturb observation and when radio interferences induced by human activities are minimum.

## 2.1 820 MHz data

In 1999 the 820 MHz radiometer run almost continuously and collected more than 100 profiles regularly distributed between January and October. To combine them a program has been prepared which: i) cuts data collected between sunrise and sunset or when the system is disturbed by bad weather conditions or radionterferences; ii) combines clean profiles adjusting gain and offsets; iii) evaluates the average profile. Preparing and tuning the program was time consuming but produced a general purpose tool we can use to synthesize data collected by TRIS at different times ([2]).

The 820 MHz profile made with data collected in 1999 is shown in fig. 1. The accuracy of the profile (temperature variations) is about 10 mK. The zero level of the absolute scale of temperature at present is still poorly defined ($\pm 10$ K). In fact it had to be measured in October 1999 when absolute calibrations of the system were planned. However we were forced to postpone the complete program of calibration, because of a leakage in the vacuum tank of the liquid helium dewar we use for that purpose, and measured only the system sensitivity. The dewar has now been repaired and absolute calibrations are planned in late spring 2000, as soon as the road to Campo Imperatore will be reopened.

The accuracy we expect to reach on the the zero level of the temperature scale of $T_{sky}$ is $\pm 50$ mK. However as it will appear in the following, the accuracy of the zero level does not affect the accuracy we reach in evaluating the spectral index $\gamma$.

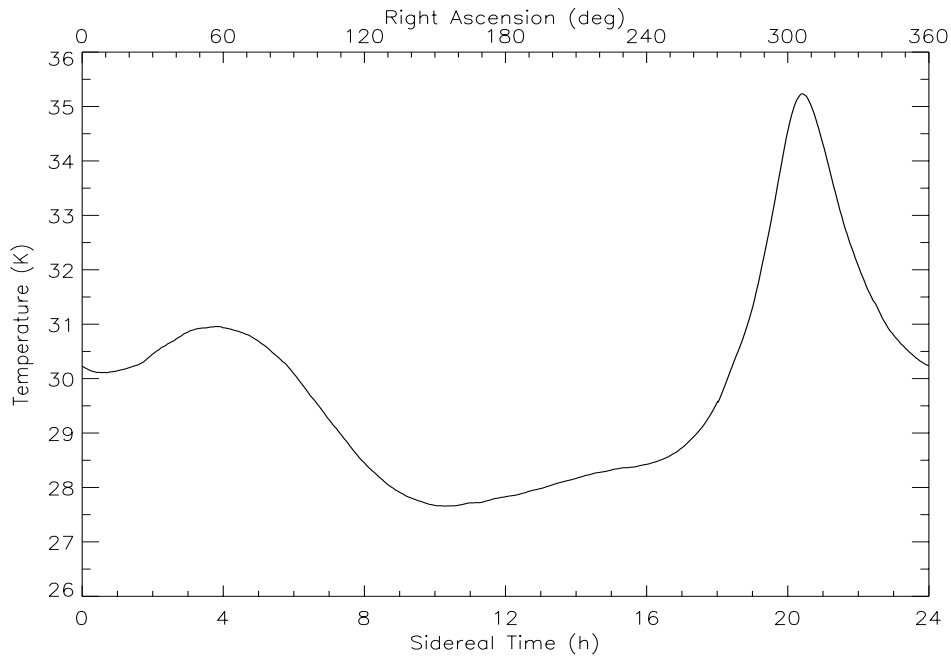


Figure 1: The synthesized profile of $T_{sky}$ at 820 MHz, $\delta = 42°$

## 2.2 600 MHz and 2.5 GHz Data

The radiometers at 600 MHz and 2.5 GHz are now collecting data respectively since October 1999 and January 2000. The data collected so far indicate that both system work regularly, therefore by the end of 2000 we expect to be able to synthesize profiles of $T_{sky}$ at 600 MHz and 2.5 GHz ($\delta = 42°$) with the the same level of accuracy we got at 820 MHz.

## 2.3 408 MHz data

The only complete set of data on $T_{sky}$ available in literature is the map produced by Haslam et al. ([3]) at 408 MHz. It has accuracies respectively of 10% on temperature variations and $\pm 3$ K on the zero of the absolute scale of temperature. The Haslam map is one of the few maps in literature which covers completely the sky therefore it is widely used as a reference in spite of its limited accuracy. We scaled it to the angular resolution of the antennae of TRIS and worked out the profile of $T_{sky}$ versus $\alpha$ for $\delta = 42°$ at 408 MHz (see fig. 2).

# 3 The T-T Plot method of analysis

The T-T plot method of analysis was suggested by Turtle et al. ([4]) in 1963. It allows to evaluate the spectral index of the galactic emission $\gamma$ comparing two profiles of $T_{sky}$ measured at the same declination $\delta$ at two frequencies $\nu_1$ and $\nu_2$.

From eq(1) and eq(2) we have

$$T_{sky}(\alpha, \delta, \nu_1) = T_{3K}(\nu_1) + T_{ex}(\nu_1) + T_{Gal}(\alpha, \delta, \nu_1) \tag{3}$$

$$T_{sky}(\alpha, \delta, \nu_2) = T_{3K}(\nu_2) + T_{ex}(\nu_2) + T_{Gal}(\alpha, \delta, \nu_2) \tag{4}$$

$$n_{12} = T_{Gal}(\alpha, \delta, \nu_1)/T_{Gal}(\alpha, \delta, \nu_2) = (\nu_1/\nu_2)^{-\gamma(\nu_1,\nu_2)} \tag{5}$$

Simple calculations give

$$T_{sky}(\alpha, \delta, \nu_2) = n_{12}\ T_{sky}(\alpha, \delta, \nu_1) + const. \tag{6}$$

Therefore a plot of $T_{sky}(\nu_2)$ measured at different positions versus $T_{sky}(\nu_1)$ measured at the same positions is a straight line of slope $n_{12}$ from which the spectral index $\gamma(\nu_1, \nu_2))$ between $\nu_1$ and $\nu 2$ follows.

Fig. 3 is a plot of profiles measured 820 MHz against the extrapolated 408 MHz profiles. It clearly shows a linear correlation and a weighted best fit gives

$$n(408, 820) = 0.15 \pm 0.01$$

$$\gamma(408, 820) = 2.67 \pm 0.26$$

The large error bar, comparable to the error bars associated to similar results so far published (for a discussion see [5], [7] and references therein), is essentially due to uncertainty of the temperature variations of the 408 MHz Haslam map, which is at least an order of magnitude larger than the measured and expected uncertainties of TRIS data. When we will work out $\gamma$ using only TRIS data we expect an improvement of an order of magnitude on the final accuracy of $n_{12}$ and $\gamma$, sufficient ([6]) to get $T_{Gal}$ and $T_{3K}$ with accuracies respectively of 50 mK and 200 mK.

# 4 Conclusions

We checked the capability of TRIS of working out the Galactic contributions to $T_{sky}$ with accuracy sufficient to extract $T_{3K}$ at three frequencies close to 1 GHz and detect deviations from a Planckian spectrum if the amplitude of these deviations is at least 200 mK.

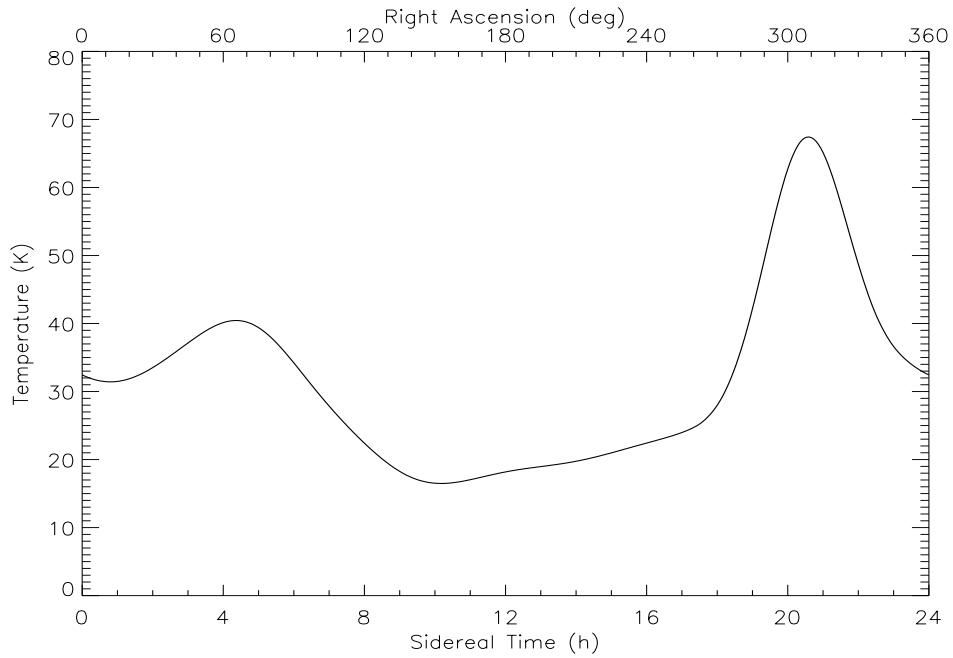


Figure 2: 408 MHz profile of $T_{sky}$ versus $\alpha$ at $\delta = 42°$ extrapolated from the map of Haslam et al.

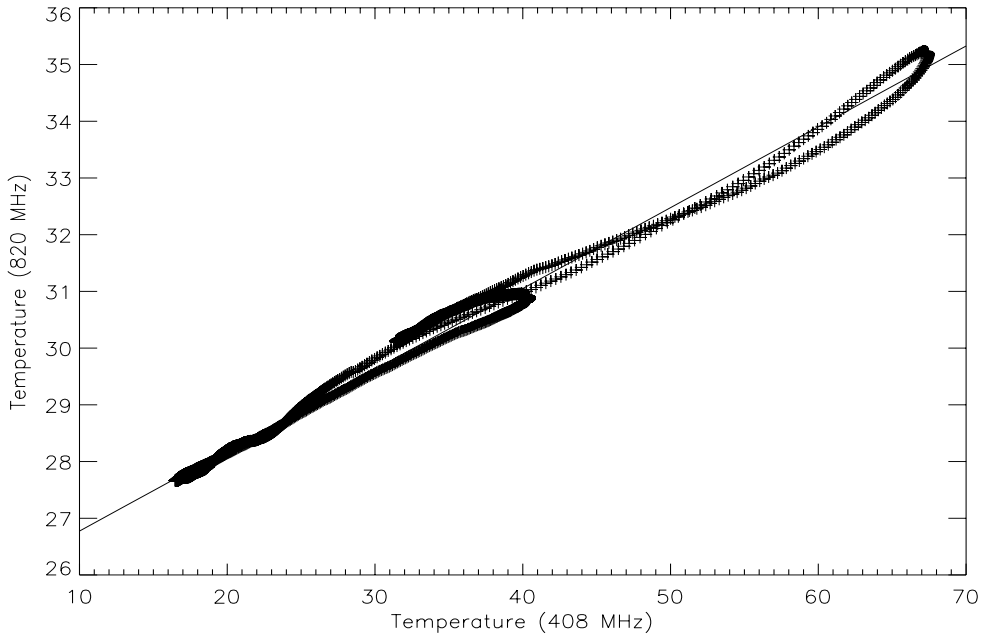


Figure 3: T-T plot of $T_{sky}$ measured by TRIS at 820 MHz against $T_{sky}$ at 408 extrapolated from the map of Haslam et al. for $\delta = 42°$ and $(0^h \leq \alpha \leq 24^h)$

**Acknowledgments**

This work has been supported by MURTS, CNR and PNRA.

# 5 List of Publications

1. M.Gervasi, G.Boella, F.Cavaliere, A.Passerini, M.Saglimbeni, R. Sgrò, G.Sironi, M.Tucci, A.Vaccari, M.Zannoni 1999: Search for Cosmic Microwave Polarization

   Proc. 3 K Cosmology Euroconference - Rome October 1998

   AIP Conf. Proc. 476, 154

2. M.Zannoni, G.Boella, G.Bonelli, F.Cavaliere, M.Gervasi, A.Lagostina, A.Passerini, G.Sironi, A.vaccari 1999: TRIS EXPERIMENT: a search for spectral distortions in the CMB spectrum close to 1 GHz

   Proc. 3 K Cosmology Euroconference - Rome October 1998

   AIP Conf. Proc. 476, 165

3. S. Cortiglioni, S. Cecchini, E. Carretti, M. Orsini, R. Fabbri, G. Boella, G. Sironi, J. Monari, A. Orfei, R. Tascone, U. Pisani, K.W. Ng, L. Nicastro, L. Popa, I.A. Strukov, M.V. Sazhin 1999 : The SPOrt Project: An Experimental Overview

   Proc. 3 K Cosmology Euroconference - Rome October 1998

   AIP Conf. Proc. 476, 186

4. R. Fabbri, S. Cortiglioni, S. Cecchini, M. Orsini, E. Carretti, G. Boella, G. Sironi, J. Monari, A. Orfei, R. Tascone, U. Pisani, K.W. Ng, L. Nicastro, L. Popa, I.A. Strukov, M.V. Sazhin 1999: The SPOrt Project: Cosmological and Astrophysical Goals

   Proc. 3 K Cosmology Euroconference - Rome October 1998

   AIP Conf. Proc. 476, 194

5. S.Cortiglioni, S.Cecchini, M.Orsini, G.Boella, M.Gervasi, G.Sironi, R.Fabbri, J.Monari, A.Orfei, K.W.Ng, L.Nicastro, U.Pisani, R.Tascone, L. Popa, I.A.Strukov 1999: The SPOrt Mission on Issa

   Space Technology and Application International FORUM 1999 ( STAIF '99), AIP Conf. Proc. 420, 294

6. G. Sironi 1999: The frequency spectrum of the Cosmic Microwave Background

   New Ast. Rev. 43, 243

7. G. Sironi 1999: Polarization of the Cosmic Microwave Background: the Milano Polarimeter Experiment

   New Ast. Rev. 43, 263

8. M.V. Sazhin, G. Sironi 1999: Degradation of the signal in measurements of polarization and anisotropy of the Cosmic Microwave Background

   New Ast. 4, 215

# References


[1] C.Burigana et al. 1991: ApJ 379, 1

[2] R.Baselli 1999: Tesi di Laurea in Fisica - Università degli Studi di Milano

[3] H.Haslam et al. 1982: A.A. Suppl.Ser. 47, 1

[4] A.J. Turtle et al. 1963: MNRAS 126,405

[5] G. De Amici et al. 1994: Ap. Space Sci. 214, 151

[6] M. Zannoni et al. 1998: AIP Conf. Proc. 476, 165

[7] G. Sironi et al. 1998: AIP Conf. Proc. 476, 149

# GIGS. The Interferometric Station at LNGS

Antonella Amoruso[a,c], Luca Crescentini[b,d], Roberto Scarpa[a,c]

[a] Dip.to di Fisica Univ. dell'Aquila, L'Aquila - Italy
[b] Dip.to di Scienze della Terra, Univ. di Camerino, Camerino (MC) - Italy
[c] INFN - Gruppo collegato dell'Aquila , L'Aquila - Italy
[d] INFN - LNGS, L'Aquila - Italy

**Abstract**

The activity during 1999 consisted of data analysis and refinement of its seismological implications, and technical improvement of the interferometers.

## 1 Research Activity

From a scientific point of view, during 1999 we performed a deeper analysis of the slow strain events occurred during 1997. A typical example is shown in the following Figure. As already mentioned in the 1998 Report, many clustered slow earthquakes were recorded for the first time during 1997 and never occurred during 1998.

The rise times of such events range from tens to thousands of seconds, and the seismic moment scales with the square root of the rise time.

This scaling law contrasts with the conservative assumption of constant rupture velocity in fault modeling and is consistent with the occurrence of a diffusion process. To explain the observed scaling law, we considered a one-dimensional array of slider blocks connected by springs. Slipping is resisted by a dynamic friction proportional to the slip rate, which is a simple example of velocity-strengthening friction. Slip propagation between adjacent blocks is the equivalent of the rupture propagation. Under reasonable simplifications, slipping is governed by the same Fourier equation as heat diffusion in a slab. The time evolution of the seismic moment (proportional to the integral of the slip over the fault) is given by the time evolution of the integral of the temperature (see following Figure, upper part) and is very similar to the signals recorded by the interferometer.

The scaling law is consistent with previous observations of slow earthquakes attributed to a slow slip propagation. Although the diffusion equation does not allow us to precisely define the velocity of the slip propagation, the point of maximum slip rate (previous Figure, lower part) propagates like the rupture in one of the events of a slow earthquake sequence observed in California in 1992.

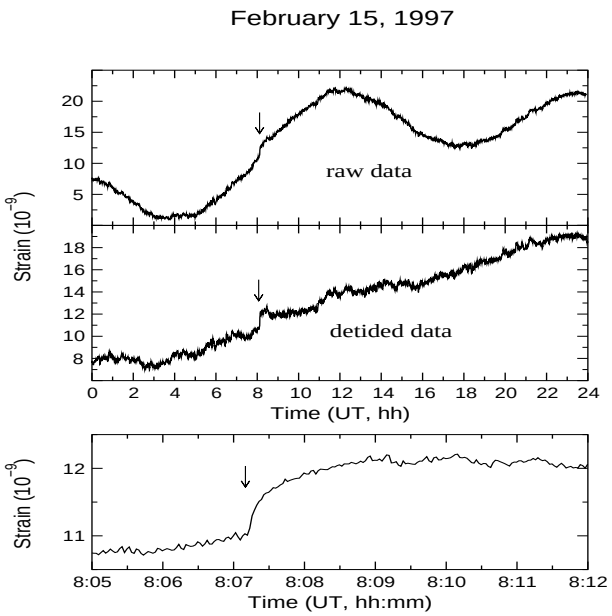


Figure 1: Slow earthquake recorded by the Gran Sasso underground geodetic interferometer on February 15th, 1997. The two upper plots show a whole day of data resampled every 20 seconds, before and after removing tides. The slow earthquake is indicated by the arrow.

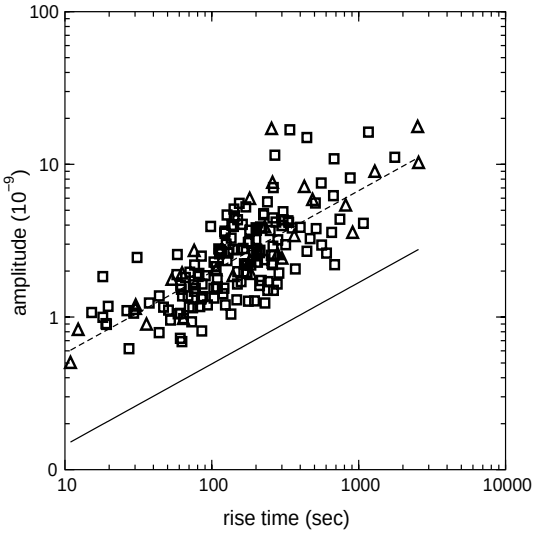


Figure 2: Amplitude (in $10^{-9}$strain units) vs rise time of the slow earthquakes recorded from February 1st, 1996, to September 9th, 1997.

During 1999 a second interferometer has been built. To shortly summarize, from May 1994 to October 1995 a first Michelson interferometer, monitoring the extension of a 90-m long baseline (azimuth N66E) approximately perpendicular to the Apennines, had worked. Because laser frequency fluctuations can give spurious signals whose amplitude depends on the difference in length between the two arms of the interferometer, from December 1995 to October 1999 the interferometer worked in an equal-arm configuration, using a 90-m long baseline (azimuth N24W) as reference arm. One component of shear strain was measured. Two independent interferometers are now at work. The former measures the extension of a 90-m long baseline (azimuth N66E) approximately perpendicular to the Apennines, the latter measures the extension of a 90-m long baseline (azimuth N24W) approximately parallel to the Apennines.

They monitor the extension of two 90-m long baselines, using two 20-cm long arms as reference. The electro-optical set-up has already been described in previous LNGS reports and is the same for the two interferometers, which share a single laser source. The difference between the two measurements gives one component of shear strain, unaffected by laser frequency fluctuations (see power spectral densities shown in the following Figure).

The previous Figure proves that the two measuremets are highly coherent in a wide spectral range. Environmetal parameters such as air pressure can generate deformation. Their effects are under study in order to discriminate different "error sources" in the measurements.

As soon as more data are available, possible differences between the Apenninic and the anti-Apenninic directions would appear: it would be the first experimental evidence of the tectonic regime actually acting in the Apennines.

# 2 Conclusions

Scientific and technical work performed during 1999 relates both to a more accurate analysis of previuos data and to the availability of new mesurements along two independent directions. It shows that the study of such fenomena is plenty of consequences both in a better understanding of fault dynamics and in identifying the tectonic regime actually acting in the Apennines.

# 3 List of Publications


1. Amoruso, A., and L. Crescentini, "Coseismic and aseismic strain offsets recorded by the Gran Sasso strainmeter," Phys. Chem. Earth, **24,** 101-104 (1999).

2. Amoruso, A., L. Crescentini, and R. Scarpa, "Removing tidal and atmospheric effects from Earth deformation measurements", XXIV General Assembly EGS, The Hague, 19-23 April, 1999.

3. Crescentini, L., "Are slow earthquakes so unusual? The case of the swarm recorded at Gran Sasso in 1997", 15th Course of the International School of Geophysics "Problems in Geophysics for the next millennium", Erice, 7-16 July, 1999.

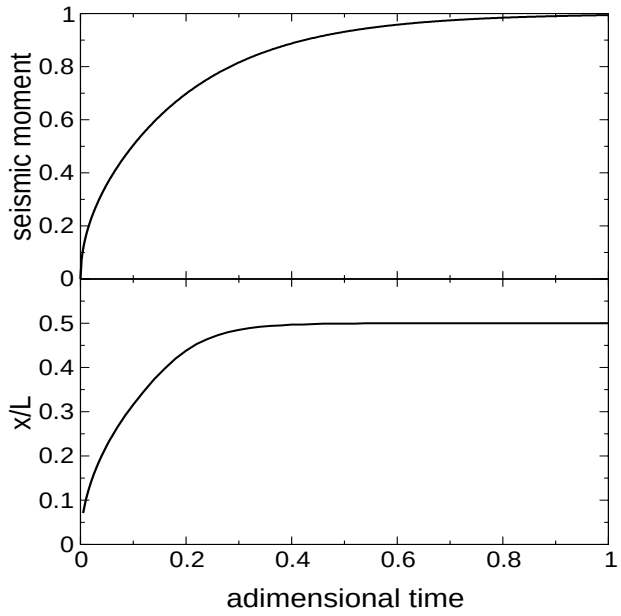


Figure 3: Time evolution for the 1D fault model described in the text. Upper plot: seismic moment; lower plot: position of the point of istantaneous maximum slip rate.

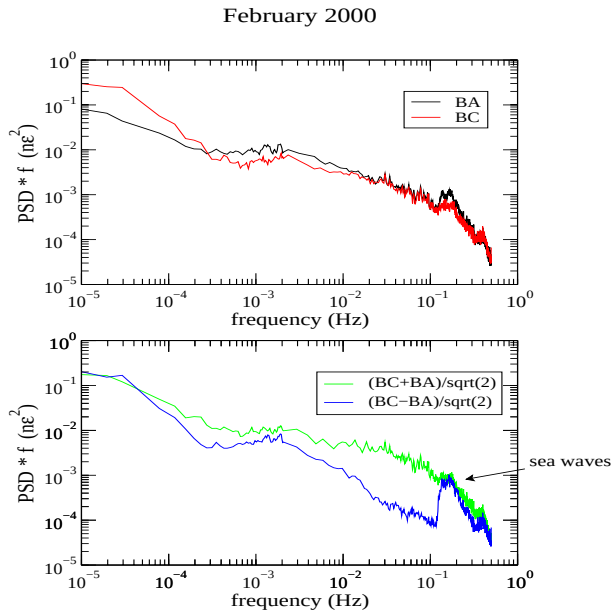


Figure 4: Power spectral densities of measurements along A-B and B-C directions.

4. Crescentini, L., “Strumenti a larga banda e dinamica per il monitoraggio delle deformazioni del suolo”, XVIII Convegno Nazionale GNGTS, 1999.

5. Amoruso, A., L. Crescentini, and R. Scarpa, “Semi-automatic analysis of unusual strain records”, AGU Fall Meeting, 1999.

6. Crescentini, L., A. Amoruso, and R. Scarpa, “Constraints on slow earthquakes dynamics from a swarm in central Italy”, Science, **286**, 2132-2134

# Tectonic deformation events and local seismicity in the Gran Sasso area of the central Apennines (1999)

Vittorio Sgrigna

Dipartimento di Fisica "E. Amaldi", Università Roma Tre, Via della Vasca Navale, 84, I-00146 Roma, Italy.

**Abstract**
Geophysical equipment and investigations at LNGS concerning deformation phenomena of seismotectonic interest are described, and ground tilt results obtained in 1999 are reported.

## 1 Introduction

Investigations concerning deformation events of tectonic interest, detected at three sites of the LNGS are carried out and correlated to earthquakes. Observations deal with the possibility to study the time and space of earthquake occurrence by the study of rock microfracturing process which takes place in the preparation focal area during the preseismic period.

Such process gives rise to a nonelastic rock behaviour (dilatancy) in which volumetric strain increases relative to what would be expected from the elasticity. At the LNGS, the intermediate-term volumetric strain increase, involved in the thrust and deep fault systems of the Gran Sasso chain, is studied by continuous ground tilt measurements.

Tiltmeters are also installed at the Gran Sasso area, outside the LNGS, for a better investigation of the above-mentioned phenomena of tectonic interest.

## 2 Results

Results obtained at LNGS and in the surrounding area during 1999, are summarized in the following sections.

## 2.1 Investigations in the Gran Sasso area

We have shown that new seismological data from the Latium-Abruzzi carbonate platform, which includes the Gran Sasso chain, fit a block tectonic modelling previously proposed for this area on the basis of structural and paleomagnetic evidences [1]. A migration of earthquake foci has been also observed. Velocity values are similar to those obtained in other seismic regions ($\approx 0.1 cm/s$), demostrating the slow propagation of a stress-strain field in such areas [2].

Aquifer-induced seismicity has also been revealed in the Gran Sasso area [3]. On this occasion it was observed that a sudden increase in the groundwater level changes, superimposed to the normal seasonal cyclic variations, triggered small earthquakes of the region.

## 2.2 Investigations in the LNGS

### 2.2.1 Experimental apparatus

The experimental apparatus consists of three tiltmeters realised at the Department of Physics of our University [4]. The tilt sensors consist of two-component-horizontal-pendulum tiltmeters with Zöllner bifilar suspension. They have been made using super Invar. The analog detecting system is constituted by an infrared laser beam and a 1024 photodiodes linear array of 0.5 inch long. The resolution is of $0.05 \mu rad$. A digital aquisition system allows the tilt data to be collected hourly.

### 2.2.2 Ground tilt

A 2-D model for slow crust movements, including creep-related tilt and strain precursors of earthquakes, has been proposed [2]. The model describes the earthquake preparation through the rheological properties of viscoelastic fault gouge (separating rigid crustal blocks) studied by constitutive equations of Standard Linear Solid.

Ground tilt variations have been correlated to the Umbria-Marches seismic sequence of 1997-1998. Figure 1 shows the aseismic creep strain (GRS) observed at LNGS which revealed to be precursor of the above-mentioned seismic sequence. Results of similar quality have been obtained at Peschiera (PES) tilt site (fig. 2). Such creep strains resulted also to be shifted in time between them, indicating a possible slow propagation ($\approx 1 cm/s$) of the preseismic tilt field generated in the Umbria preparation focal area. Figures 3 and 4 show the best fitting of the creep functions of figures 1 and 2, carried out on the basis of the viscoelastic Kelvin-Voigt model.

All these results have been reported to the 1999 AGU Fall Meeting of the American Geophysical Union [5], [6].

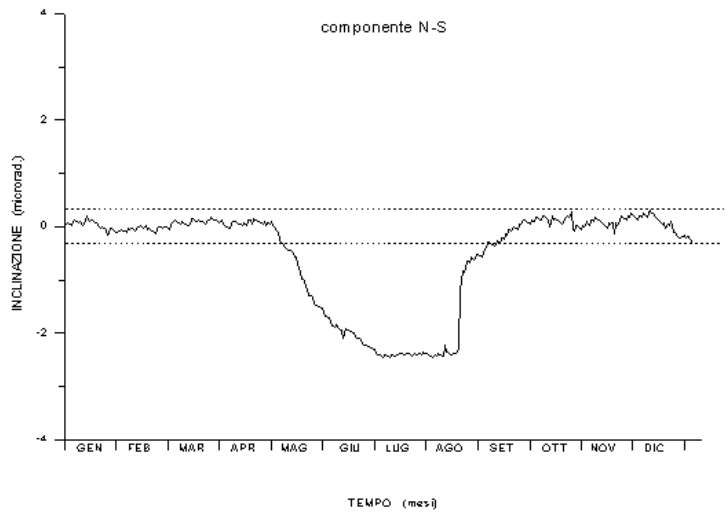


Figure 1: Aseismic creep strain observed at LNGS prior to the Marche–Abruzzi seismic sequence.

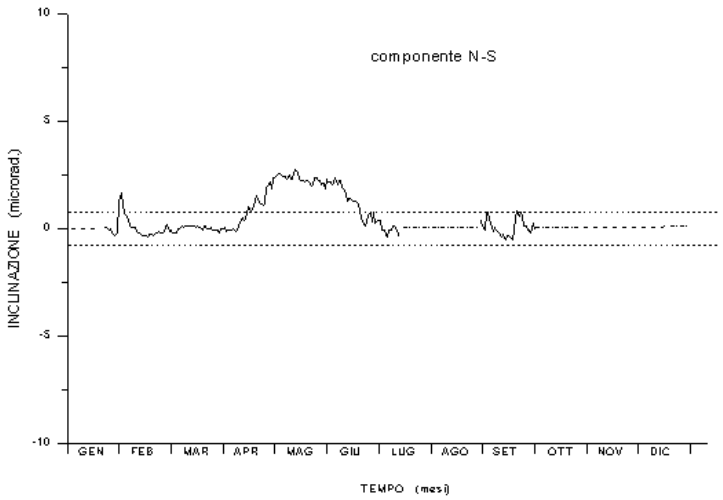


Figure 2: Aseismic creep strain obtained at Peschiera (PES) tilt site prior to the Marche–Abruzzi seismic sequence.

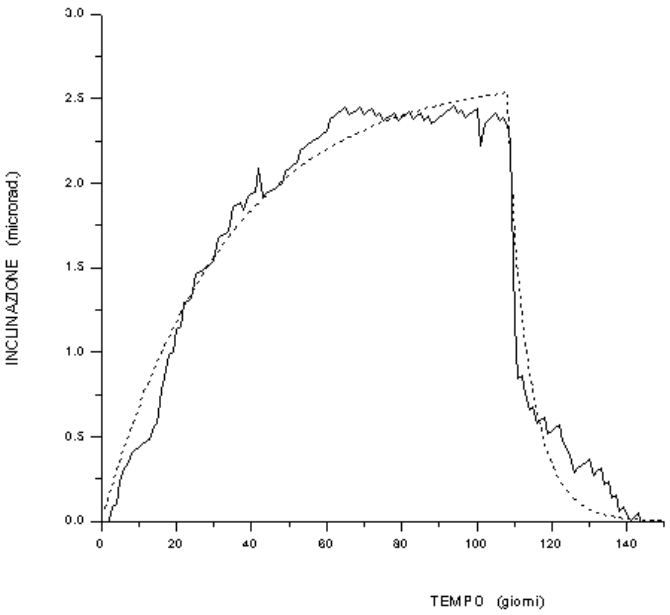


Figure 3: Best fitting of the creep function of figure 1.

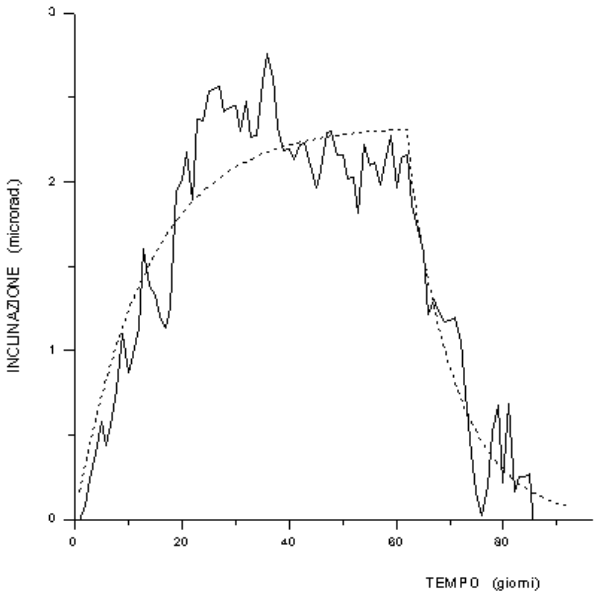


Figure 4: Best fitting of the creep function of figure 2.

# 3 Conclusions

Experimental and theoretical results at LNGS obtained during 1999, as well as the ongoing investigations, reveal a good agreement between geodynamic, rheological, and seismological data. These correlations are also confirmed by similar investigations carried out in the Gran sasso area of the carbonate platform and in particular in the PES tilt site.

# References


[1] Bella, F., M. Caputo, G. Della Monica, A. Lisi, W. Plastino, R. Scandone, and V. Sgrigna, 1998. *Crustal blocks and seismicity in the central Apennines*, Nuovo Cimento, **21C**, 597-607.

[2] Bella, F., M. Caputo, G. Della Monica, W. Plastino, V. Sgrigna, Yu. P. Vaveluk, and T.B. Yanovskaya, 1998.*A 2-D model for tilt and strain fields associated to earthquakes in crustal block structures*, Phys. Earth and Planet. Int., **106**, 155-164.

[3] Bella, F., P.F. Biagi, M. Caputo, E. Cozzi, G. Della Monica, A. Ermini, W. Plastino, and V. Sgrigna, 1998. *Aquifer-induced seismicity in the central Apennines (Italy)*, Pure Appl. Geophys., **153**, 179-194.

[4] Bella, F., P.F. Biagi, G. Della Monica, A. Ermini, and V. Sgrigna, 1998. *A horizontal pendulum tiltmeter with digital recording system*, Nuovo Cimento, **12C**, 799-809.

[5] Malvezzi, V., F. Bella, G. Della Monica, D. Zilpimiani, and V. Sgrigna, 1999. *Creep-related tilt precursors and rheological behavior of crustal block boundaries*, EOS Trans. T12B-10, AGU vol. **80**, n.46, pag. F934.

[6] Sgrigna, V., M. Caputo, V. Malvezzi, T. B. Yanovskaya, 1999. *A numerical 2-D model for crustal block dynamics in seismic regions*, EOS Trans. T12B-09, AGU vol. **80**, n. 46, pag. F934.

# **LSS.** Liquid Scintillation Spectrometry Radon time series analysis at LNGS, I

Francesco Bella and Wolfango Plastino

Department of Physics, University Roma Tre, Via della Vasca Navale, 84, Roma (Italy)

**Abstract**

Geophysical and geochemical investigations concerning deformation events of tectonic interest at the underground laboratory of Gran Sasso have been carried out and possible correlations with local seismicity are also investigated.

We have planned and realized an automatic multiparametric equipment (water temperature, electrical conductivity, pH, $^{222}$Rn) and from the May 1996 we performs automatic measurements with a discrete sampling (T=12 h) of the groundwater collected in the interferometric region.

The spike-like events observed in the geochemical parameters are related to local seismicity and Umbria -Marche seismic sequence (1997-1998).

## 1 Introduction

Temporal variations of the radon content in groundwater have been demonstrated to correlate with the variations in stress in rock associated with the seismicity; crustal gas-fluxes along active faults or the transport of the radon from its origin to the surface through microfractures are possible sources. [1], [2]

Moreover, the nontectonic environmentals factors are also related to radon variations. [3]

Then, the geological and hydrogeological setting and the meteorological characteristic of the measurement site and the chemical-physical property of the groundwater are very important to discriminate the source of the radon variations.

The Gran Sasso massif (central Apennines, Italy) is a tectonic unit formed by a overturned anticline-syncline structure characterized by a overthrust line sloping 40° S along NE direction over clay-marly sandstones and is formed by a double chain separated by deep trenches and with deep depressions at the boundaries. The hydrogeological system including the Gran Sasso chain has a total area of 2164 km² and it can absorb 714 mm of annual effective infiltration and can give back 49 m³/s as mean discharge. The Gran Sasso massif is carachterized by a very large and deep karst aquifer consisting of a series of minor aquifers separated by the main structural discontinuties with values of permeability $k$ up to $10^{-4}$ m/s. [4]

In the measurement site the rock is prevalently composed by detrital limestones and, in particular, the interferometric region has crossed by the overthrust fault which separate the limestones from the dolomite rocks.

# 2 Results

The multiparametric equipment consists of a system for water geochemical analysis and gases extraction dissolved in groundwater. [5]

The trends of the geochemical parameters monitored during the period from May, 1996 to June, 1999 are shown in figure 1.

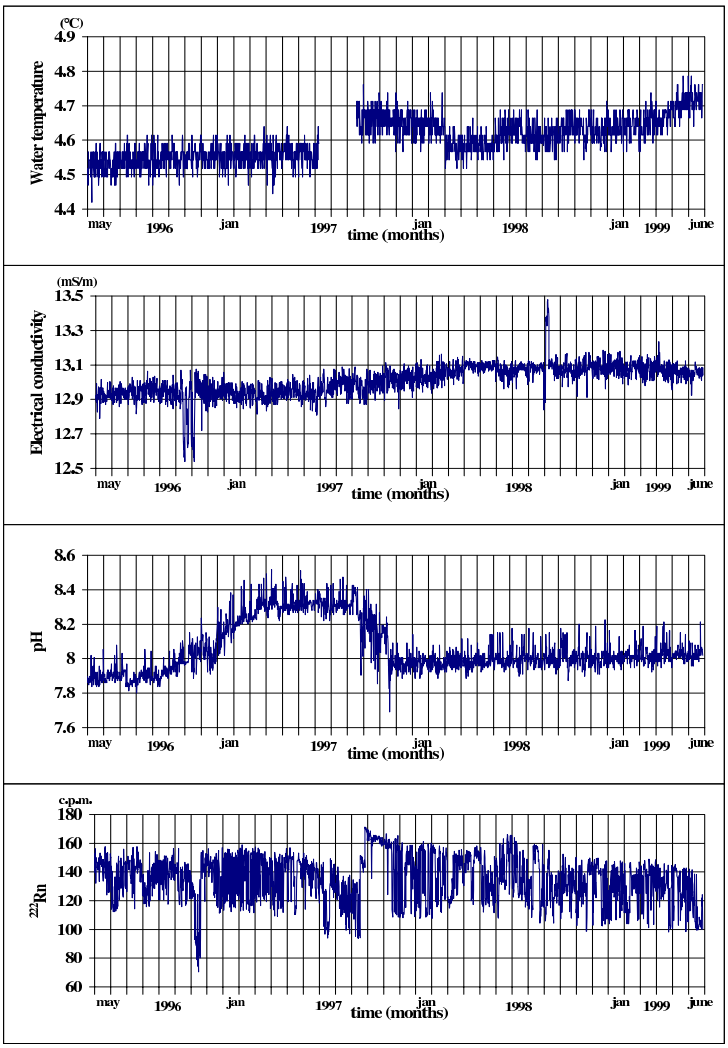


fig.1. The trends of the geochemical parameters monitored during the period from May, 1996 to June, 1999.

The data of the water temperature sensor from July, 1997 to September, 1997 are not supplied because of the breakdown between the thermocouple output and the analogic input channel.

From the analysis of the raw data my be observed: the water temperature is carach-

terized by a maximum excursion of 0.2 °C; the electrical conductivity has a small range of variability of the order of 0.2 mS/m but two spike-like events occurred respectively in October, 1996 and September, 1998; the pH during the period from January, 1997 to August, 1997 increases of 0.4 pH unit and then decreases to the initial value in November, 1997; a spike-like event of the radon content in groundwater in November, 1996 has occurred. Besides, the mean value of the $^{222}$Rn from May, 1997 to September, 1997 decreases and then rises ($15^{th}$ September, 1997) till November, 1997.

The trends of the setting parameters monitored during the period from May, 1996 to June, 1999 are shown in figure 2.

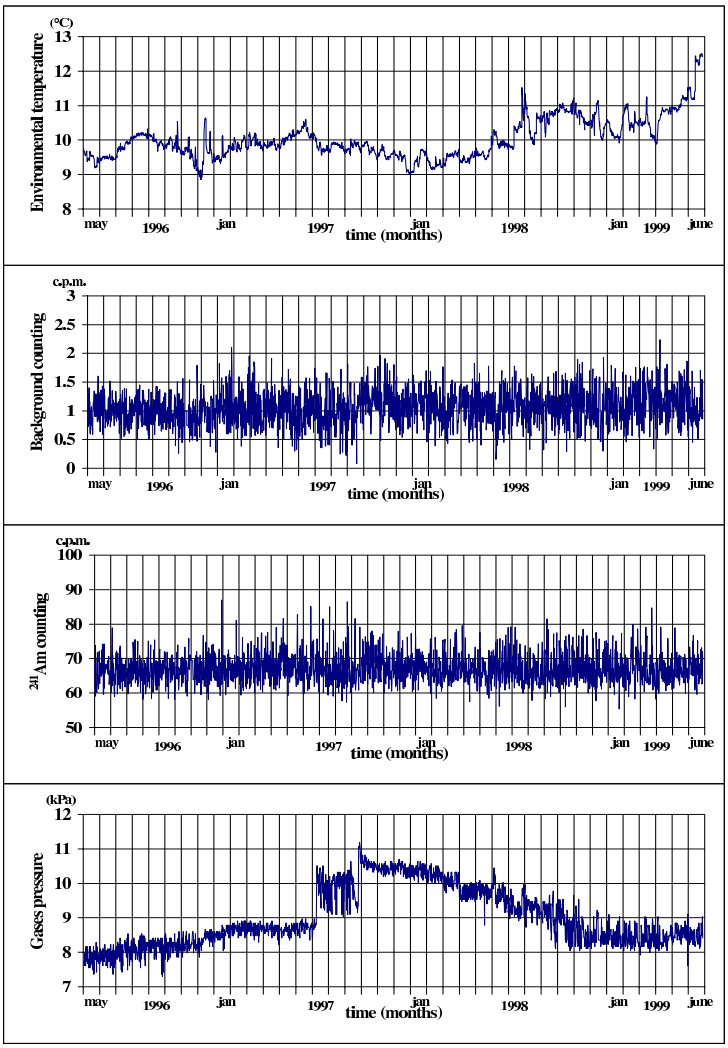


fig.2. The trends of the setting parameters monitored during the period from May, 1996 to June, 1999.

The environmental temperature shows a periodic component with T=180 days and some spikes due to the ventilation activity inside the underground laboratory.

The background and $^{241}$Am counting monitored before each measurement seem to point out respectively a good stability and reliability of the detecting system.

The gases pressure monitored in the counting cell shows two abrupt rises: the first in July, 1997 ($\cong$ 1.5 kPa) and the second in September, 1997 ($\cong$ 2 kPa). Then, the pressure

value decreases to the initial value in September, 1998.

# 3 Discussion

The occurrence probability of hydrogeochemical *anomalies* is computed by means of parametric time series approach. First, in order to avoid the influence of external noise, a preliminary filtering of the geochemical data from the meteo-climatic, stratum and tide is performed. Then an autoregressive linear model to describe the residual time series is selected. The final result is a white noise series with presumed *anomalies* that are identified when the modulus is grater than 3 times the estimated standard deviation. [6]

The residual time series of the electrical conductivity, pH, $^{222}$Rn and $\varepsilon$ Dobrovolsky's parameter during the period from May, 1996 to June, 1999 are shown in figure 3.

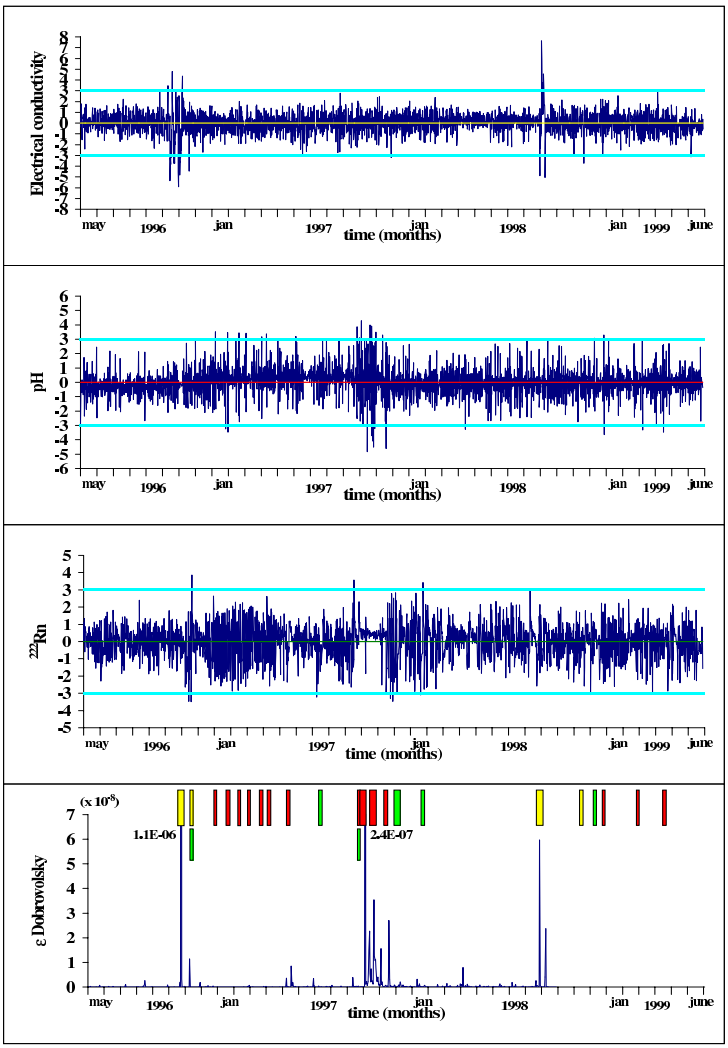


fig.3. The residual time series of electrical conductivity, pH, $^{222}$Rn and $\varepsilon$ Dobrovolsky's parameter during the period from May, 1996 to June, 1999.

The $\varepsilon$ Dobrovolsky's parameter [7] is computed by means of the seismic events of I.N.G.V. (National Institute of Geophysics and Volcanology) and Seismic Digital Net-

work of the central Abruzzo catalogues recorded within a distance of 100 km from the measurement site and available from May, 1996 to September, 1998. We have considered an inferior limit of $\varepsilon$ equal to $0.1 \cdot 10^{-8}$.

Fifteen *anomalies* in the electrical conductivity, twenty-six in the pH and ten in $^{222}$Rn series have been detected. Using the $\varepsilon$ Dobrovolsky's parameter thirteen seismic events potentially related to the detected *anomalies* have been identified. Particularly, seven events are related to the Umbria-Marche seismic sequence started the $26^{th}$ September, 1997, $M_D$=5.6, d=80 km and the other six events are shared out as follows: a) three related to earthquake occurred the $20^{th}$ October, 1996, $M_D$=2.0, d=1 km; b) one the $5^{th}$ November, 1996, $M_D$=3.2, d=23 km; c) one the $15^{th}$ August, 1998, $M_D$=4.6, d=40 km; d) one the $5^{th}$ September, 1998, $M_D$=3.3, d=13 km.

Comparison between earthquakes time series ($\varepsilon$ parameter) and alert period suggest by the occurrence of electrical conductivity (yellow), pH (red) and $^{222}$Rn (green) *anomalies* are also reported. The geochemical parameters seem to point out pre-co-post seismic carachteristic.

# 4 Conclusion

The radon time series analysis seem to point out the likely correlation between the spike-like events in the geochemical parameters and the local seismicity and Umbria-Marche seismic sequence (1997-1998). Nevertheless, the long term variations of pH and radon content in groundwater, during 1997, are also important and probably related to a local compressive process.

# 5 Acknowledgments

The authors wish to thank Prof. Alessandro Bettini for the his kind collaboration and the Dr. Raffaele Adinolfi Falcone, Dr. Alfredo Fulgenzi, Mr. Massimiliano De Deo, Mr. Nicola Massimiani, Mr. Nando Polidoro, Mr. Fabrizio Torelli of the L.N.G.S. and Mr. Fabio Basti, Mr. Antonio Miriametro of the University of Rome "La Sapienza" for the useful and precious assistance. The authors are grateful to Dr. Domenico Giambuzzi and Mr. Maurizio Faragalli of the Azienda Speciale Acquedotto del Ruzzo for the data provided.

# References

[1] Hauksson, E., 1981, *Radon content of groundwater as an earthquake precursor: evaluation of worldwide data and physical basis*, J. Geophys. Res., 86, 9397-9410.

[2] Qureshi, A.A., Manzoor, S., Qureshi, I.E., Molzahn, D. and H.A. Khan, 1993, *Radon measurements for use in earthquake prediction and location of geological faults in Pakistan*, Proceedings of the Second Workshop on Radon Monitoring in Radioprotection, Environmental and/or Earth Sciences, Trieste, 25 November - 6 December, 1991, World Scientific Publishing Co. Pte. Ltd., Singapore, 532-535.

[3] Shapiro, M.H., Rice, A., Mendenhall, M.H., Melvin,, D. and T.A. Tombrello, 1984/1985, *Recognition of environmentally caused variations in radon time series*, Pure and Appl. Geophys., 122, 309-326.

[4] A.N.A.S.-COGEFAR, 1979, *Gran Sasso-Il traforo autostradale.*

[5] Bella, F., Azzi, C., Bella, R., Della Monica, G., Plastino, W., Scandone, R. and V. Sgrigna, 1998, *Tectonic deformation events and local seismicity in the Gran Sasso area of the central Apennines*, L.N.G.S. Annual Report 1997, 169-178.

[6] Box, G.E.P. and Jenkins, G.M., 1976, *Time series analysis forecasting and control*, Holden Day, Oakland, California.

[7] Dobrovolsky, I.P., Zubkov, S.I. and V.I. Miachkin, 1979, *Estimation of the size of earthquake preparation zones*, Pure and Appl. Geophys., 117, 1025-1044.

# Radon time series analysis at LNGS, II

Francesco Bella and Wolfango Plastino

Department of Physics, University Roma Tre, Via della Vasca Navale, 84, Roma (Italy)

**Abstract**

Measurements of the radon contamination in groundwater and air with a discrete sampling (T=12 h) have been performed at the underground laboratory of Gran Sasso to study local deformation process.

From March, 1998 to June, 1999 the time series analysis are carried out. The data have emphasized that the simultaneous monitoring of these parameters may be a useful tool to discriminate the local volumetric strain events from the superficial one. Moreover, the radon time series analysis has shown the correlation between the spike-like events in the *ratio parameter* and the local seismicity.

## 1 Introduction

Radon variations related to deformation process of tectonic interest generally have been investigated by radon monitoring in air or groundwater. [1], [2]

We have considered the opportunity to perform simultaneous measurements of the radon content in air and groundwater to discriminate possible local volumetric strain events from the superficial one and study the migration process of this radioisotope.

The measurement site is located in the interferometric region that has crossed by the overthrust fault which separate the limestones from the dolomite rocks. In particular, the analysis have been carried out inside the box where is located the radon groundwater station of the University Roma Tre and the possible effects due to the underground laboratory ventilation have been reduced.

Radon in air has been monitored by the GAMMADATA ATMOS $12_{DPX}$ based on the pulse-counting ionization chamber technology. The air flow through the active chamber volume (0.6 l) was 1.0 l/min and the upper detection limit of the instrument was 100 kBq/m$^3$. [3]

Radon content in groundwater has been monitored by a multiparametric equipment based on the alpha scintillation technique. [4]

The measurements have been recorded with a discrete sampling (T=12 h).

# 2 Results

The trends of the radon content in groundwater and air monitored during the period from March, 1998 to June, 1999 are shown in figure 1. The systematic errors are checked by background and efficiency of the detecting system measurements, the statistical errors are related to the standard deviation of the data integrated on the time interval of thirty minutes. [3], [4]

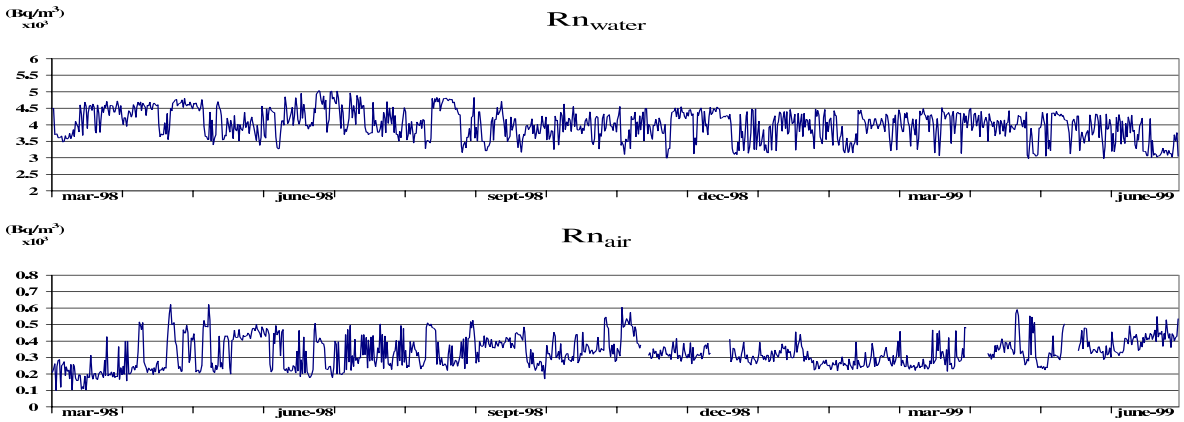


fig.1. The trends of the radon content in groundwater and air monitored during the period from March, 1998 to June, 1999.

From the analysis of raw data may be observed that the mean value of radon in air is $\cong$ 8% of radon in water. The cross-correlation analysis has shown that radon content in groundwater and air was inversly related (r=0.2) with a temporal shift of one day.

The *ratio parameter* ( $^{222}\mathrm{Rn}_{water}/\ ^{222}\mathrm{Rn}_{air}$) is also reported in figure 2.

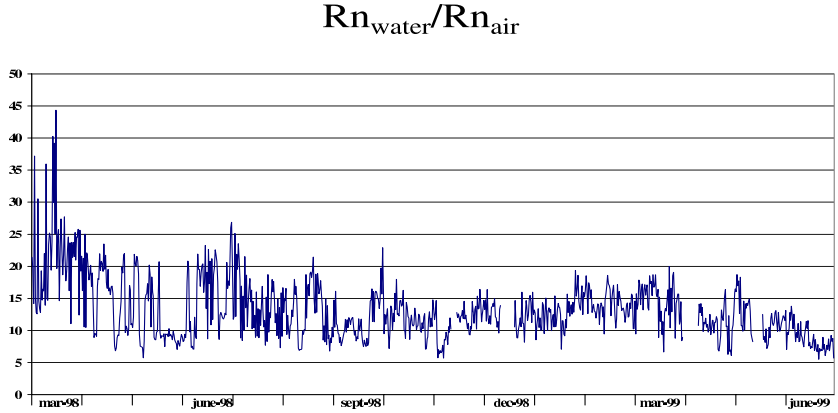


fig.2. The ratio of radon content in groundwater and air during the period from March, 1998 to June, 1999.

# 3 Discussion

An autoregressive linear model to describe the radon time series has been selected after that a filtering of the data from the meteo-climatic, stratum and tide has been performed. [5]

The $\varepsilon$ Dobrovolsky's parameter [6] is computed in an area of 100 km of radius from the measurement site [5].

The residual time series of radon content in groundwater, air and the *ratio parameter* during the period from March, 1998 to June, 1999 are shown in figure 3.

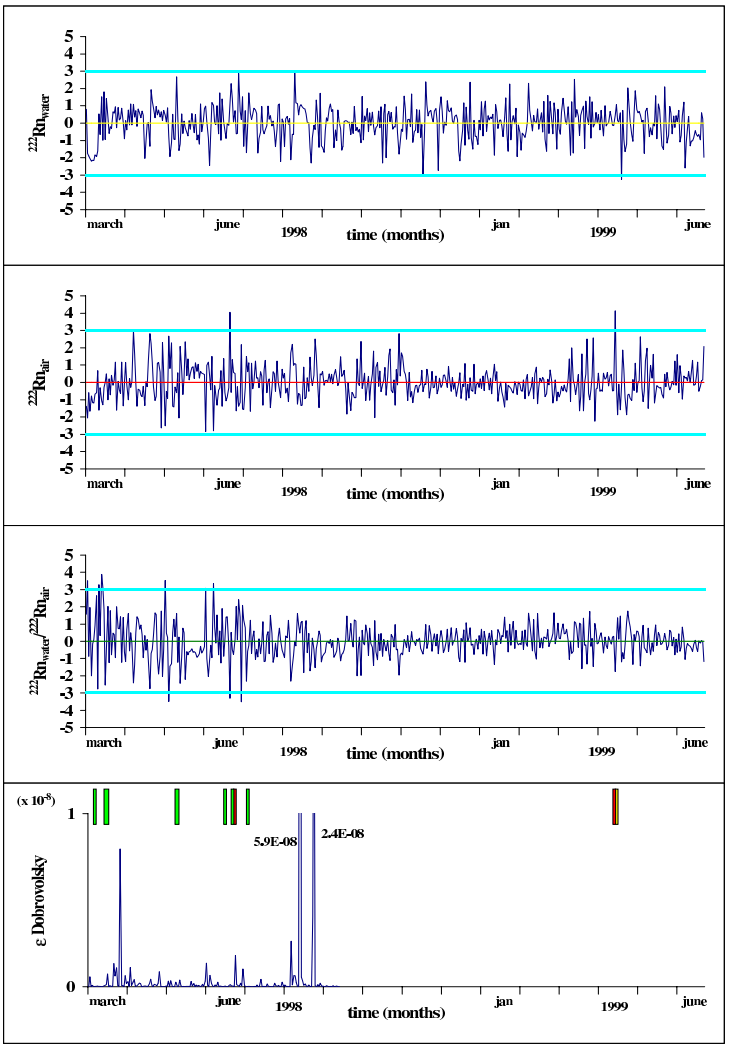


fig. 3. The residual time series of $^{222}\mathrm{Rn}_{water}$, $^{222}\mathrm{Rn}_{air}$, $^{222}\mathrm{Rn}_{water}/^{222}\mathrm{Rn}_{air}$ and $\varepsilon$Dobrovolsky's parameter during the period from March, 1998 to June, 1999.

Six *anomalies* [5] in the *ratio parameter*, two in the radon in air and one in the radon in groundwater have been detected. Particularly, five *anomalies* detected in the *ratio parameter* seem to emphasize pre-co seismic characteristic and are related to following earthquakes: a) $26^{th}$ March, 1998, $M_D$=4.7, d=90 km; b) $25^{th}$ June, 1998, $M_D$=3.1, d=80 km.

In figure 3 is also reported the comparison between $\varepsilon$ Dobrovolsky's parameter and alert period suggest by the occurrence of $^{222}Rn_{water}$ (yellow), $^{222}Rn_{air}$ (red) and $^{222}Rn_{water}/^{222}Rn_{air}$ (green) *anomalies*.

The simultaneous monitoring of radon content in groundwater and air in this test site have emphasized that the *ratio parameter* is another useful tool to study the possible correlations between the radon variations and the local deformation process.

# 4 Conclusion

The radon time series analysis detected at the underground laboratory has shown the correlation between the *ratio parameter* variations and local seismicity. This new technique may be a useful tool to analyze the radon variations related to deformation process of tectonic interest because allows a better resolution respect to only radon in air or groundwater monitoring.

Nevertheless, the spatial-temporal dynamic of the radon and relationship between the local volumetric strain events and superficial one may be better defined only by a network of measurement sites.

# 5 Acknowledgments

The authors wish to thank Prof. Alessandro Bettini for the his kind collaboration and Dr. Cristina Arpesella, Dr. Raffaele Adinolfi Falcone, Dr. Alfredo Fulgenzi, Mr. Massimiliano De Deo, Mr. Nicola Massimiani, Mr. Nando Polidoro, Mr. Fabrizio Torelli of the L.N.G.S. and Mr. Fabio Basti and Mr. Antonio Miriametro of the University of Rome "La Sapienza" for the useful and precious assistance. The authors are grateful to Dr. Domenico Giambuzzi and Mr. Maurizio Faragalli of the Azienda Speciale Acquedotto del Ruzzo for the data provided.

# References

[1] Papastefanou, C., Manolopoulou, M., Stoulos S. and Ioannidou A., *Measurements of radon exhalation from the ground for earthquake prediction studies*, 1995, Gas Geochemistry, Science Reviews, 317-323.

[2] Surbeck, H., *Radon as tool in hydrogeology: obstacles and prospects*, 1997, Rare Gas Geochemistry: Applications in Earth & Environmental Sciences, H.S. Virk Editor, Guru Nanak Dev University, Amritsar, 69-77.

[3] ATMOS $12_{DPX}$ Manual reference, GAMMADATA Matteknik AB, Sweden.

[4] Bella, F., Azzi, C., Bella, R., Della Monica, G., Plastino, W., Scandone, R. and V. Sgrigna, 1998, *Tectonic deformation events and local seismicity in the Gran Sasso area of the central Apennines*, L.N.G.S. Annual Report 1997, 169-178.

[5] Plastino, W. and F. Bella, *Radon time series analysis at the Laboratori Nazionali del Gran Sasso I*, in this issue.

[6] Dobrovolsky, I.P., Zubkov, S.I. and V.I. Miachkin, 1979, *Estimation of the size of earthquake preparation zones*, Pure and Appl. Geophys., 117, 1025-1044.

# Radiocarbon measurements by liquid scintillation spectrometry

F. Bella[a], P. Bartolomei[b], W. Plastino[a]

[a]Department of Physics, University Roma Tre, via della Vasca Navale, 84, I-00146 Roma (Italy)

[b]E.N.E.A., Radiocarbon Laboratory, via dei Colli, 16, I-40136 Bologna (Italy)

**Abstract**

Radiocarbon measurements by ultra low background scintillation spectrometer have been performed at the underground laboratory of Gran Sasso and radiocarbon laboratory of E.N.E.A.-Bologna to study the efficiency and background variations related to measurement sites.

The data indicates a background reduction of approximtely 65% at the underground laboratory compared to surface one, with no differences in the efficiency.

The cosmic noise reduction observed at the laboratory of Gran Sasso makes it possible to perform high precision radiocarbon measurements and extend the present maximum dating limit from 59000 BP to 69000 BP.

## 1 Introduction

The radiocarbon dating is very important tool in many fields of research such as geophysics, geochemistry, environment physics and archeology. [1], [2]

In the liquid scintillation counting technique the scintillation solvent is benzene ($C_6H_6$) because of its excellent light transmission properties and the high chemical conversion yield of sample C to benzene.

The principal difficulties related to high precision radiocarbon measurements are: a) quenching factor due to benzene synthesis; b) background due prevalently to cosmic noise. [3]

Then, we have settled two ultra low background scintillation spectrometers 1220 Quantulus Wallac [4], respectively at the E.N.E.A. radiocarbon laboratory and underground laboratory of Gran Sasso to study the background and efficiency variations related to measurement sites and the possibility to perform high precision radiocarbon dating.

The same configuration setup, i.e. the same centre of gravity of the radiocarbon spectrum (SQP(I)= 410±1) was obtained in both instruments.

# 2 Results.

Many different background and modern strandards have been realized:

*background* - two set of seven teflon vials with capacity ranging from 1 ml to 7 ml have been filled with pure analytical benzene;

*modern* - two set of seven teflon vials with the same capacity have been filled with pure analytical benzene enriched of radiocarbon obtaining the same activity as the standard sucrouse ANU (modern/sucrose ANU=1.0866).

For each of these standards, spectra were obtained for forty one hour periods.

The radiocarbon spectra recorded at the surface and underground laboratory for the H5A vial (modern standard of 5 ml) and for the L5A vial (background standard of 5 ml) are shown respectively in figure 1 and 2.

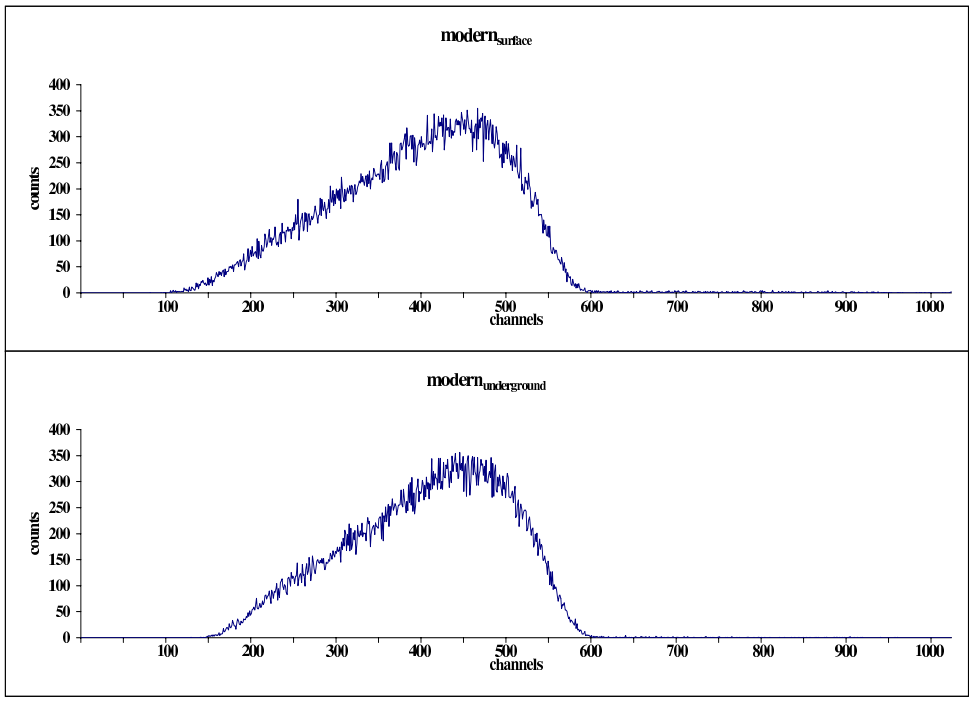


fig.1. The radiocarbon spectra of the H5A vial recorded at the surface (E.N.E.A.-Bologna) and underground (L.N.G.S.) laboratories.

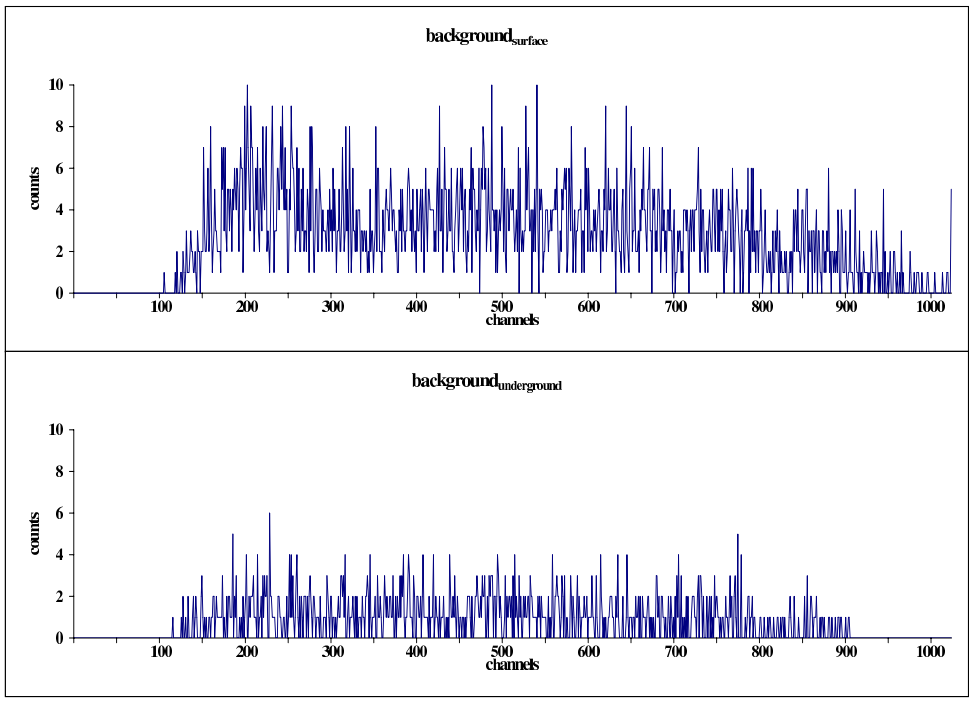


fig.2. The radiocarbon spectra of the L5A vial recorded at the surface (E.N.E.A.-Bologna) and underground (L.N.G.S.) laboratories.

A background reduction $\cong$ 65% at the underground laboratory respect to surface one may be observed.

# 3 Discussion

The statistics of the measurements shown in figures 1 and 2 in the radiocarbon spectrum soft window (5-650 channels) has been performed and the results are shown in table 1.

| | background (c.p.m.) | error | modern (c.p.m.) | error | efficiency | fM |
|---|---|---|---|---|---|---|
| surface | 0.8 | 0.02 | 68.47 | 0.42 | 73% | 62 |
| underground | 0.28 | 0.01 | 66.66 | 0.34 | 72% | 520 |

table 1. The statistics of the L5A and H5A vials measurements at the surface (E.N.E.A.-Bologna) and underground laboratories (L.N.G.S.).

The efficiency variations between the measurement sites is $\cong$ 1%.

The same efficiency in the both spectrometers is probably due to the photomultipliers characteristics.

Nevertheless, the cosmic noise reduction monitored at the underground laboratory is a useful tool to perform high precision radiocarbon measurements and extend the maximum dating limit. The dating limits for each vials have been calculated and are shown in table 2.

| vial (ml) | surface background (c.p.m.) | underground background (c.p.m.) | surface dating limit (BP) | underground dating limit (BP) |
|---|---|---|---|---|
| **1** | **0.36** | **0.13** | **45700** | **57400** |
| **2** | **0.47** | **0.16** | **50700** | **62000** |
| **3** | **0.58** | **0.20** | **53500** | **64300** |
| **4** | **0.70** | **0.24** | **55200** | **66000** |
| **5** | **0.80** | **0.28** | **56600** | **67100** |
| **6** | **0.92** | **0.31** | **57700** | **68200** |
| **7** | **1.03** | **0.35** | **58700** | **69000** |

table 2. The dating limits for each vials monitored at the surface (E.N.E.A.-Bologna) and underground laboratories (L.N.G.S.).

Moreover, the measurements carried out at the Gran Sasso have emphasized a better counting stability respect to the surface laboratory.

# 4 Conclusion

The measurements performed at the underground laboratory of Gran Sasso respect to the surface laboratory of E.N.E.A.-Bologna have emphasized a background reduction and no gain in the efficiency. Then, high precision radiocarbon dating may be performed at the L.N.G.S. and the possibility to extend the dating limit is also available.

# 5 Acknowledgments

The authors wish to thank Prof. Alessandro Bettini for the his kind collaboration and Dr. Lauri Kaihola, Mr. Pekka Makinen and Mr. Vincenzo Morelli of the Wallac and Dr. Raffaele Adinolfi Falcone, Dr. Alfredo Fulgenzi, Mr. Massimiliano De Deo, Mr. Nicola Massimiani, Mr. Nando Polidoro, Mr. Fabrizio Torelli of the L.N.G.S for the useful and precious assistance.

# References

[1] Gorsdorf, J., Dreyer, G. and U. Hartung, 1998, *New $^{14}C$ dating of the archaic royal necropolis Umm el-Qaab at Abydos (Egypt)*, Radiocarbon, 40, 1, 641-648.

[2] Bartolomei, P., Cini, S., Galli, M., Giampieri, R., Mongardi, C. and A. Salomoni, 1995, *Solar flare particle effects and seasonal radiocarbon variations in tree rings of the northern and southern emispheres*, Radiocarbon, 37, 2, 593-599.

[3] Mc Cormac, F.G., 1992, *Liquid scintillation counter characterization, optimization and benzene purity correction*, Radiocarbon, 34, 1, 37-45.

[4] Kojola, H., Polach, H., Nurmi, J., Oikari, T. and E. Soini, 1984, *High resolution low-level liquid scintillation beta-spectrometer*, Int. J. Appl. Rad. Isot., 35, 949-952.

# LNGS-EXP 20/99
# Measurement of the Radon concentration in the water from the Gran Sasso fault

A. Bassignani[a], G. Colombo[a], L. Degli Esposti[b], R. Fresca Fantoni[a], G. Giacomelli[b], G. Maltoni[b], G. Mandrioli[b], M. Mascoli[a], F. Materazzi[a], L. Patrizii[b], G. Sirri[b,c] and D. Ugolotti[b]

[a] Eni S.p.A. Agip Division, Radiation Protection Department, San Donato Milanese
[b] Dipartimento di Fisica dell'Università di Bologna and INFN, Bologna
[c] INFN, Laboratori Nazionali del Gran Sasso, Assergi

**Abstract**

We describe an equipment designed to monitor the $^{222}$Rn concentration in the water from the fault in the interferometric area of the underground Gran Sasso laboratory.

The water is directly collected from the fracturated rock and the radon gas is extracted from the water by nitrogen bubbling. The detector is a silver activated zinc sulfide scintillator located into an electrostatic chamber of 5 liter volume, where short half-life radon daughters are collected.

The main goal of the experiment is to investigate possible correlations between variations in the radon concentration in the water and various seismic phenomena.

The apparatus is remotely controlled via Internet; tests and measurements may be displayed on web pages.

## 1 Introduction

Radon emissions from ground waters and in air are being monitored by several experiments with the aim of studying possible correlations between radon concentration variations and seismic phenomena [1-5].

We have developed and implemented an automatic instrument for monitoring the radon concentration in groundwater. Since the middle of 1999 this apparatus is collecting test data in the interferometric tunnel of the underground Gran Sasso laboratory, near the fault. The fault is one of most important phenomena of the Gran Sasso Massif.

The apparatus may be considered to complement other instruments that are monitoring seismic activities in the underground laboratory: a geodetic interferometer [6], tiltmeters and the apparatus for groundwater analysis of the University of Roma Tre [7].

During 1999 we made measurements with a sampling rate of 2 measurements per day in order to test the detector and to establish the best conditions for the measurements.

# 2 The apparatus

A photograph of the apparatus is shown in Fig. 1; it consists of three sections: the system for the extraction of radon from water, the detecting system and the data acquisition and control system.

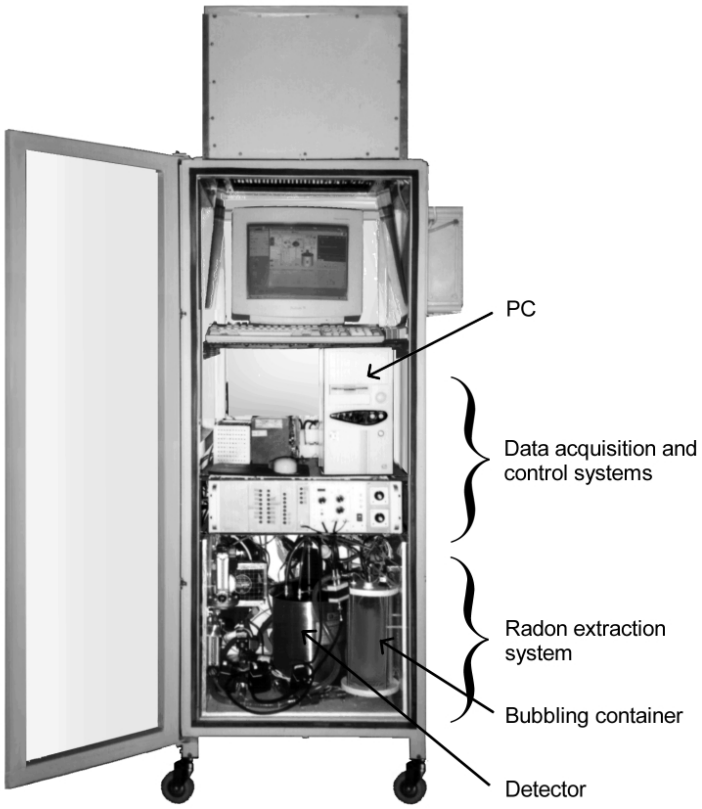


Figure 1: *Photograph of the apparatus for monitoring the radon concentration in the Gran Sasso groundwater from the fault.*

## 2.1 Radon extraction system

The layout of the extraction system is shown in Fig. 2. The system is located in the bottom part of the photograph in Fig. 1.

The process starts by flushing the radon extraction system with nitrogen gas (at this time the valves V1, V11, V3, V4, V10 are opened); immediately after, the measurement

of background counting is started. Then a sample of 1.9 liters of water collected directly from the rock fault is pumped into the bubbler.

Radon gas is then extracted from water by nitrogen bubbling. The bubbling circuit includes the bubbler, the drying system, the detector chamber, the air flow sensor, the air pump and the valves V3, V4, V9, V11.

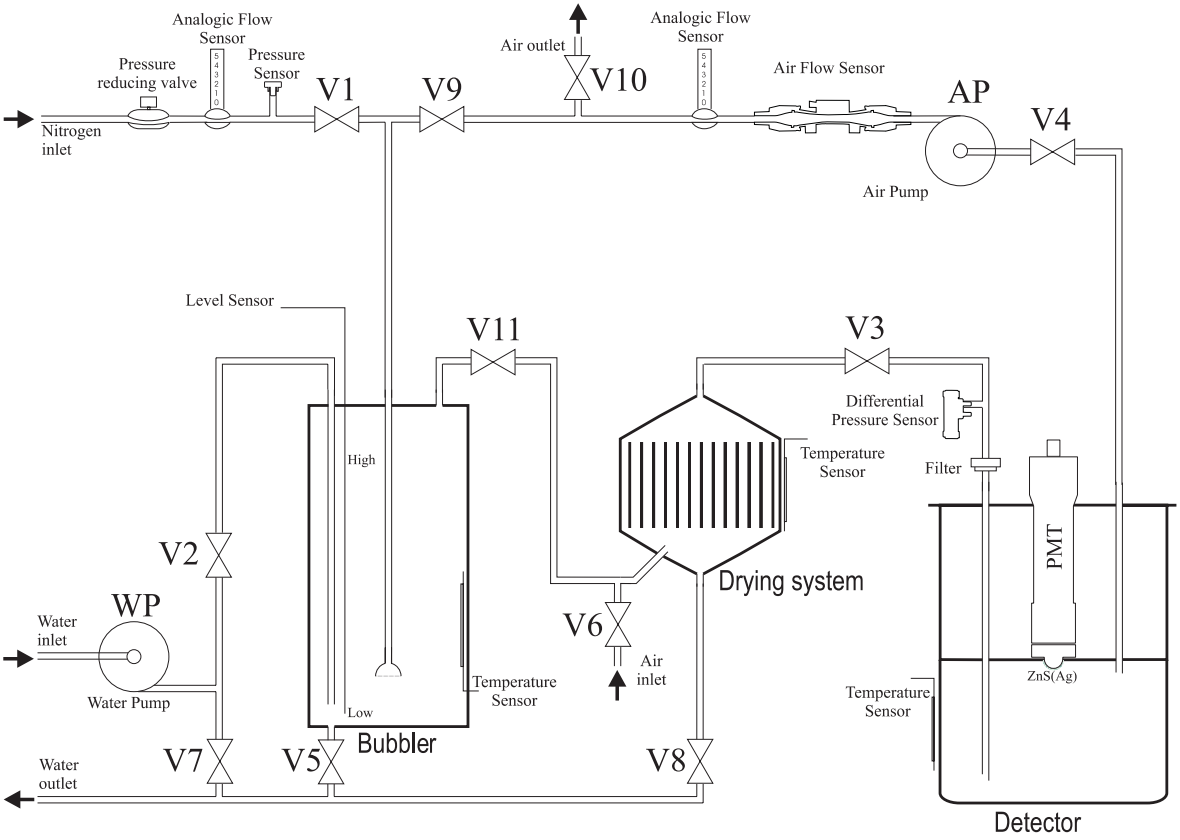


Figure 2: *Layout of the radon extraction system.*

At the end of the extraction the radon concentration in the bubbling gas and in the water are in equilibrium and distributed according to the Henry's law [8].

After radon extraction all valves are closed and radon counting is started. At the end of counting, the water is pumped out, and the process restarts.

## 2.2 Detection system

A scheme of the detecting system is shown in Fig. 3. The detector is a Pylon mod. PMT-EL, which is a silver activated zinc sulfide scintillator ZnS(Ag) located in an electrostatic chamber of 5 litres volume.

The scintillator is covered by an aluminized mylar foil that acts as cathode of the electrostatic chamber and collects the positively charged radon daughters. A power supply polarizes the chamber creating a potential difference of 1000 volts.

$^{222}$Rn in the nitrogen gas pumped inside the detector decays in $^{218}$Po , which is attracted to the negatively charged aluminium cathode. $^{218}$Po decays in $^{214}$Bi , which in turn decays in $^{214}$Pb and then in $^{214}$Po , as shown below:

$$\underset{3.82\ \text{d}}{^{222}\text{Rn}} \overset{\alpha}{\Longrightarrow} \underset{3.05\ \text{min}}{^{218}\text{Po}} \overset{\alpha}{\Longrightarrow} \underset{26.8\ \text{min}}{^{214}\text{Pb}} \overset{\beta}{\longrightarrow} \underset{19.7\ \text{min}}{^{214}\text{Bi}} \overset{\beta}{\longrightarrow} \underset{164\ \mu\text{s}}{^{214}\text{Po}} \overset{\alpha}{\Longrightarrow} {}^{210}\text{Pb}$$

(the time intervals quoted above are half-lives $t_{1/2}$). $^{222}$Rn , $^{218}$Po and $^{214}$Po emit alpha particles; a fraction of these particles impacts the scintillator and produces light pulses that are transmitted through the light pipe to the photomultiplier (PMT). The electric pulse produced by the PMT is amplified and sent to the data acquisition system (Fig. 3,a).

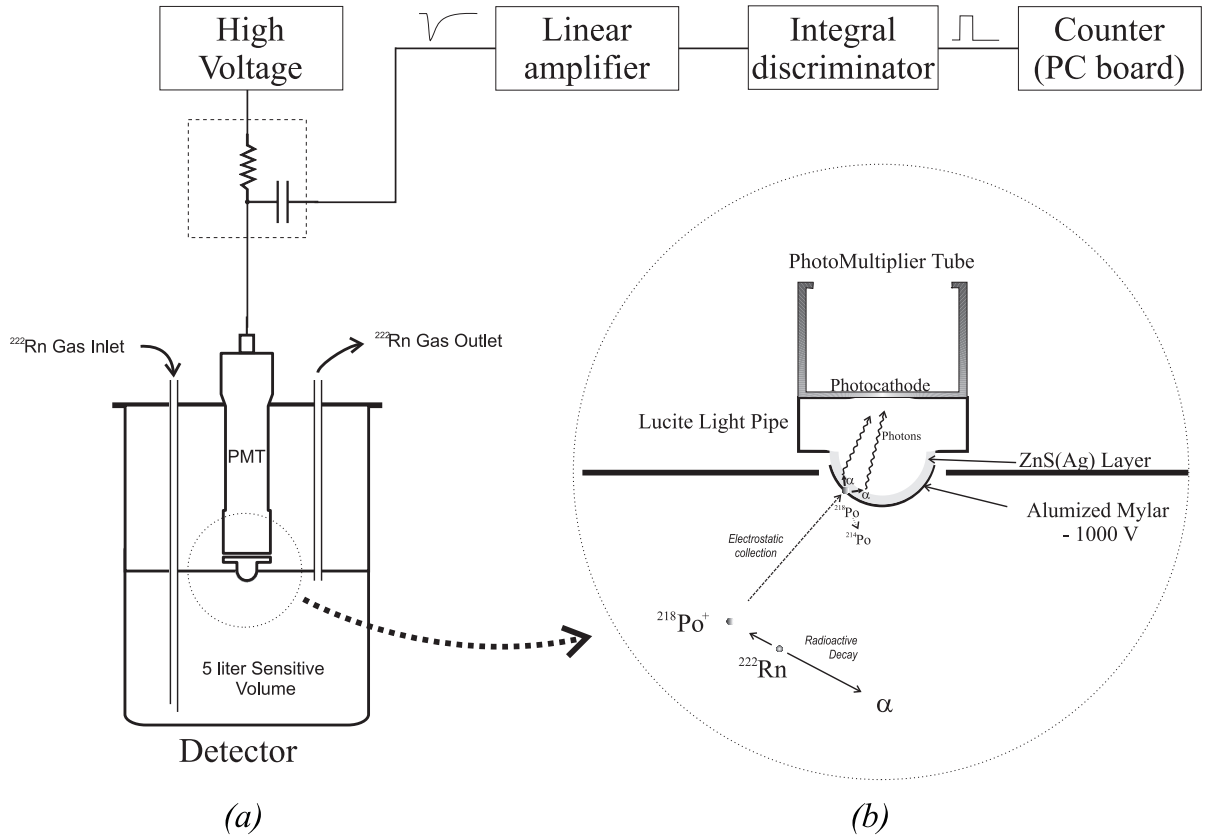


Figure 3: *(a) Scheme of the detection system; (b) scheme of the collection of radon daughters.*

## 2.3 Data acquisition system

The control process and the data acquisition is performed by a PC with a Pentium processor and two I/O interface boards. The system is located above the crate in the

rack of Fig. 1.

The control and data acquisition systems allow to control the various devices, such as the water pump, the air pump, the electrovalves and the Peltier cells placed in the drying system; at the same time it monitors the water level in the bubbler, the pressure in the nitrogen gas system, the air flow and the pressure in the circuit, the temperatures of different devices and finally the radon counting.

The computer is remotely controlled via Internet; the tests and the measurements may be displayed on web pages.

# 3 Preliminary results

An example of the measurements of the background and of the radon concentration performed over a 10 hour period are shown in Fig. 4.

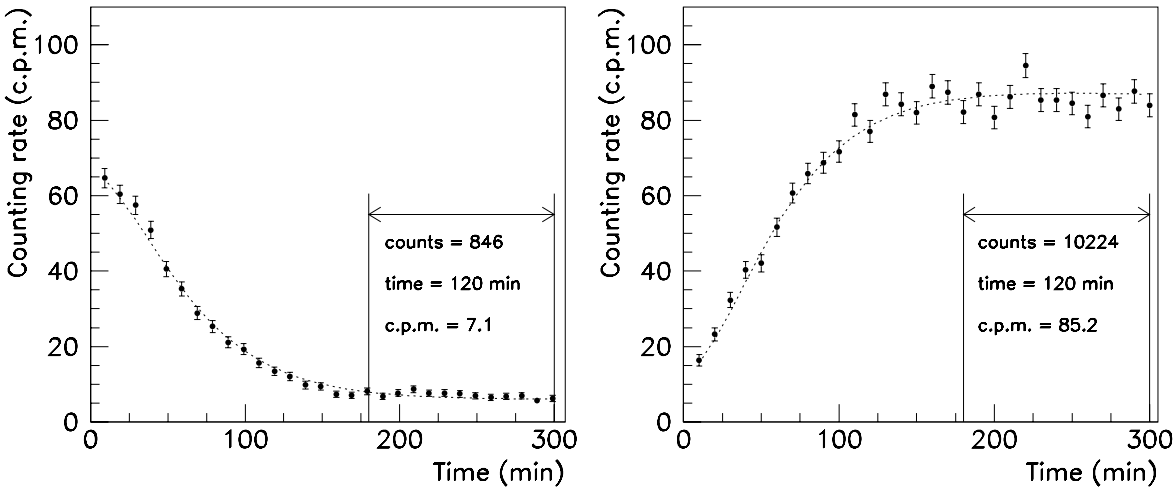


Figure 4: *Measurements of the background (a) and of the radon concentration (b) performed each over a 5 hour period. Each point corresponds to a data taking period of 10'. The final counting rate of background and of radon concentration may be obtained from a fit of the data over 300 minutes or simply taking the average rates from 180' to 300'.*

Even if the aim of this experiment is to monitor the variations of the radon concentration, an absolute calibration of the detector has been performed by cross-calibration with another instrument (Genitron Alphaguard).

At equilibrium the calibration factor of the detector is $\varepsilon = (4.5 \pm 0.5) \cdot 10^{-2}$ cpm Bq$^{-1}$ m$^3$. The Minimum Detectable Activity ($MDA$) of the gas sample into the elettrostatic chamber, when background and radon are counted each for about 300 minutes, is $\simeq 16$ Bq m$^{-3}$.

A preliminary plot of the radon concentration and of the background for the period July-Aug 1999 is shown in Fig. 5. Notice that the background is significantly smaller than

the signal rate. Notice also that there are only slow variations of the radon concentration rates.

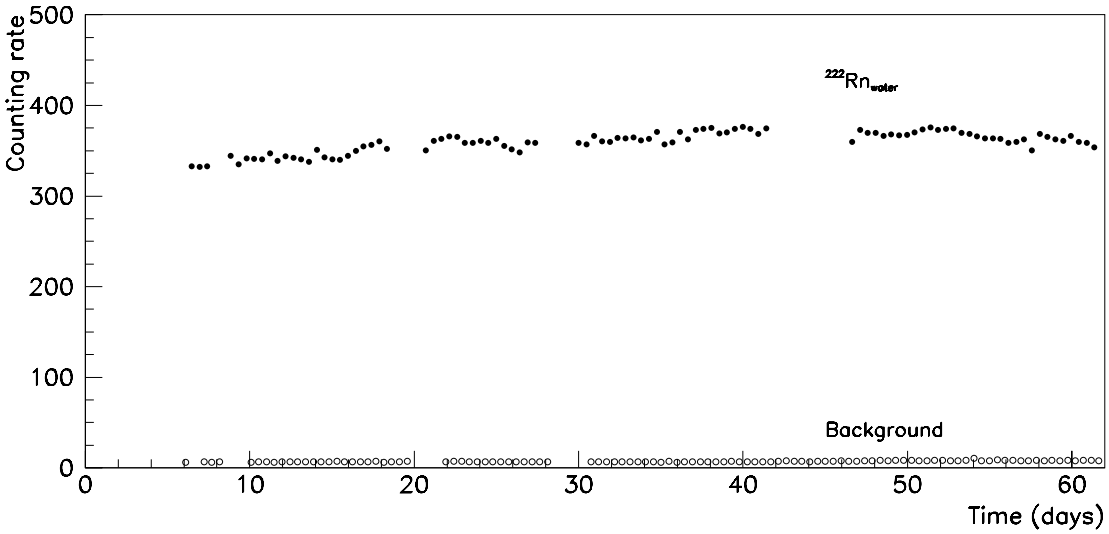


Figure 5: *Counting rate (in arbitrary units) of the radon concentration and of the background for the period July-August 1999*

# 4 Conclusions

An apparatus for monitoring the radon concentration in the water from the Gran Sasso fault has been designed and implemented. The extraction technique and the detector allow to obtain a good process reproducibility and good count ratio between radon and background.

Several improvements are in progress. In order to improve the stability of radon extraction and of the detection efficiency, a new air-conditioning system will be installed in the hut. A new system for collecting water will be designed in order to minimize radon exchange phenomena between air and water. Finally monitoring of other important parameters such as the humidity in the electrostatic chamber and the pH and electric conductivity of the water will be implemented.

# References

[1] M. Noguchi and H. Wakita, A method for Continous Measurement of Radon in Groundwater for Earthquake Prediction, Jou. Geoph. Res. 82 (1977) 1353.

[2] Chi-Yu King, Radon monitoring for Earthquake Prediction in China, Earthq. Predict. Res. 3 (1985) 47.

[3] A.A. Qureshi et al., Radon measurements for use in earthquake prediction and location of geological faults in Pakistan, Proc. of 2nd Workshop on Radon Monitoring in Radioprotection, Trieste (1991) 532.

[4] N. Matsumoto, Regression Analysis for anomalous changes of ground water level due to earthquakes, Geoph. Res. Lett. 19 (1992) 1193.

[5] U. Facchini et al. , Study on Radon Emission in a fault located in the Bergamasc Prealps, Atti Colloquio scientifico sulla protezione sismica (1993).

[6] A. Amoruso et al., GIGS, the Geophysical Interferometer at Gran Sasso, LNGS Annual Report 1997 and 1998.

[7] F. Bella et al., Tectonic deformation events and local seismicity in the Gran Sasso area of the Central Apennines, LNGS Annual Report 1997 and 1998.

[8] H. Faul, Nuclear geology, John Wiley and Sons, New York (1954).

# PULEX-2
## Biological Experiment

F. Amicarelli[d], F. Antonelli[a], C. Ara[d], M. Balata[e], M. Belli[a,c], M.P. Cerú[d], S. Colafarina[d], L. Conti Devirgliis[d], A. De Marco[d], A. Falgiani[e], S. Nisi[e], B. Pruiti[d], O. Sapora[b,c], L. Satta[f], G. Simone[a,c], E. Sorrentino[a,c], M.A. Tabocchini[a,c]

[a] Physics Laboratory, Istituto Superiore di Sanità
[b] Comparative Toxicology and Ecotoxycology Laboratory, Istituto Superiore di Sanità
[c] INFN-Gr.coll.Sanità
[d] Department of Basic and Applied Biology, L'Aquila University
[e] Service of Chemistry,
Cryogenic and Chemical plants of the INFN-Gran Sasso National Laboratory
[f] Energetics Department, Rome University "La Sapienza"

**Abstract**

The PULEX-2 experiment represents an interdisciplinary research that exploit the unique opportunity offered by the Gran Sasso National Laboratory of a well equipped low background radiation environment. Mammalian cells were cultured in parallel at the LNGS underground Laboratory, where a cell culture facility has been especially set up, and at the Istituto Superiore di Sanità, in the presence of standard radiation background. Both cultures were grown for up to about 360 generations and periodically tested to check for the onset of metabolic changes and different sensitivity to genotoxic damage caused by ionizing and UV radiation, as well as by chemical agents. These tests include measurements of enzyme activities protecting from oxidative cell damage, induction of apoptosis and mutation.

## 1 Introduction

The Gran Sasso National Laboratory (LNGS) which is an excellent shielding against cosmic rays and neutrons, offers a unique opportunity for investigating the effects of a low background radiation environment on living organisms. It is well known that the background radiation represented an important factor involved in biological evolution. Natural selection has promoted the development and the maintenance of biochemical/biological defense mechanisms against damage by radiation as well as other genotoxic agents. In the

last fifteen years adaptive response has been reported for different organisms and different biological end-points showing that cells pre-exposed to low doses of radiation or chemical mutagenic agents can acquire resistance to subsequent exposure to moderate or high doses of the same agents [1]. In this framework, scarce data concern the adaptive effects after "cronic" exposure to very low doses and low dose rates such as those given by the natural radiation background. The interest in this kind of studies is twofold: for a better understanding of the basic mechanisms involved in the radio-adaptive response and for their relevance in radiation protection. For the latter purpose, the present regulations are based on the so-called linear-no-threshold theory, implying the additivity of the effects due to the exposures taken during the life span. The adaptive response casts doubts on the validity of such a model implying a non-linear dose-response relationship. Few years ago a first experiment (PULEX) performed on yeast cells cultured in the underground laboratory of the LNGS indicated that cells grown in a low background environment are less protected from DNA damage induced by methyl-methane sulfonate than cells grown in a "standard" environment, such that found at the Rome University [2]. At the present, a new experiment (PULEX-2) performed in the framework of a collaboration among LNGS, Università di Roma, Università dell' Aquila and Istituto Superiore di Sanità, is in progress to extend the previous observations to cultured mammalian cells. This time the "standard" environment was that found at the Physics Laboratory of the Istituto Superiore di Sanita', were the reference culture was maintained. Here we report the results obtained in 1999 after about 360 generations conditioning in low/"standard" radiation environment.

# 2 Material and Methods

V79 Chinese hamster fibroblasts were grown in E-MEM medium supplemented with antibiotics and foetal calf serum [3]. To minimize the sources of variability, all reagents and chemicals used throughout the entire experiment were from the same batches. Measurements of enzyme activities [4], apoptosis [5], gene expression [6] and mutation induction [tre] were periodically performed on both cultures. The fluence ratios between low and standard background radiation environments are $10^{-6}$ for cosmic rays and $10^{-3}$ for neutrons. Radon concentration and low energy gamma ray dose were continuously monitored during the experiment and their corresponding ratios were about $10^{-1}$ and $5\text{x}10^{-2}$.

# 3 Results and Discussion

The aim of the experiment was to investigate if the environmental radiation background might contribute to the maintenance or induction of mechanisms involved either in protection or in repair against the induction of DNA damage or in the expression of gene(s) known to be involved in apoptosis (programmed cell death). To this purpose, a cell culture laboratory has been set up at the LNGS, in the gallery connecting the main experimental halls for underground physics (low background radiation). This laboratory is arranged in a new barrack of 240cm $\times$ 700cm $\times$ 260cm(high) dimensions. The barrack is equipped with all the basic uses (electrical power, water, telephone, heating, etc). A laminar flow hood for biologic purposes, an incubator with CO2 atmosphere (placed in a metallic shield:

further protecion against radioactive background), a biological microscope, a cryiogenic dewar for keeping the cells and some other minor devices are the equipments being used for performing the underground activities of the experiment. In the barrack another shielding container is available in case it were desired to use an additional incubator. A ventilation piping supplies continuosly fresh air in the room, so that the Radon level is kept always at its minimum level. A Radon measuring instrument records the Radon concentration in the lab environment in function of the time. This underground laboratory was set up with the financial and manpower support of the LNGS. Cells deriving from the same culture, were grown in parallel at the ISS (standard background radiation) and at the LNGS, and periodically tested to check for the onset of changes in enzyme activities protecting from oxidative cell damage and for different sensitivity to genotoxic agents. Measurements of enzyme activities were performed for superoxide dismutase (SOD), catalase (CAT), Se-dependent and independent glutathione peroxidase, reductase and transferase (GSH-PX, GSSG-RX, GST). Cell response to genotoxic damage was studied after treatment with chemical and physical agents. Cycloheximide, a protein synthesis inhibitor, was used to induce apoptosis and for monitoring the expression of p53 and c-myc genes. Gamma rays and UV radiation, that induce different types of DNA damage, were used for studying mutation induction at the X-linked hypoxantine-guanine phosphorybosil transferase locus (hprt). The results until now obtained show that after about 360 generations conditioning in low/standard background radiation environment some changes occur for the activities of all tested enzymes. Moreover, cells grown in low radiation environment show increased apoptotic activity after induction with cycloheximide together with a higher expression of c-myc gene; on the contrary, p53 seems to be unchanged. For hprt mutation, cells cultured in the low radiation environment seem to be more sensitive to mutation induction, especially after UV exposure.

# 4 List of Publications


1. F.Antonelli, M.Belli, O.Sapora, G.Simone, E.Sorrentino, M.A.Tabocchini, F.Amicarelli, C.Ara, M.P.Cerú, S.Colafarina, L.Conti-Devirgiliis, A.De Marco, B.Pruiti, M.Balata, A.Falgian, S.Nisi, L.Satta. Radiation biophysics at the Gran Sasso Laboratory: influence of a low background radiation environmen t on the adaptive response of living cells. 6th International Workshop on Topics in Astroparticle and Underground Physics (TAUP), Paris, France, September 6-10, 1999. Nuclear Physics (in press)

2. F. Antonelli, M. Belli, G. Simone, E. Sorrentino, M.A. Tabocchini, O. Sapora, L. Conti Devirgiliis, M.P. Cerú, F. Amicarelli, C. Ara, B. Pruiti, M. Balata, A. Falgiani, S. Nisi, L. Satta. Influence of a low background radiation environmen t on the cell response to physical and chemical agents: the Pulex-2 experiment at the LNGS. VII Congresso Annuale della Società Italiana di Mutagenesi Ambientale (SIMA), Cortona, 6 - 8 ottobre 1999

# References


[1] United Nations Scientific Committee on the Effects of Atomic Radiation, Sources and Effects of Ionizing Radiation, Annex B. Adaptive responses to radiation in cells and organisms, UNSCEAR 1994.

[2] L. Satta et al., Mut. Res., 347 (1995) 129

[3] M. Belli et al., Int. J. Rad. Biol., 74 (1998) 501

[4] F.Amicarelli et al., BBA, Mol. Basis Dis., 1453/1 (1999) 105

[5] E.B. Thompson, Ann. Rev. Physiol., 60 (1998) 575

[6] J. Galea-Lauri, J. Immunol., 157 (1996) 4109

# INFN - LNGS

## Laboratori Nazionali del Gran Sasso

s.s. 17 bis km 18+910 - 67010 Assergi (AQ) Italy
Tel. +39 0862 4371 - Fax +39 0862 410795
E-mail address: document@lngs.infn.it

http://www.lngs.infn.it